SYNTHESIS AND CHARACTERIZATION OF QUERCETIN-BASED LINEAR AND CROSS-LINKED POLYMERS FOR ADVANCED ENGINEERING APPLICATIONS

A Dissertation

by

SAMANTHA LYNN KRISTUFEK

Submitted to the Office of Graduate and Professional Studies of
Texas A&M University
in partial fulfillment of the requirements for the degree of

DOCTOR OF PHILOSOPHY

Chair of Committee,	Karen L. Wooley
Committee Members,	Donald J. Darensbourg
	Duncan J. Maitland
	Daniel Romo
Head of Department,	Simon W. North

May 2017

Major Subject: Chemistry

ABSTRACT

We have a keen interest in the design, preparation and investigation of engineering polymers that are derived from renewable biofeedstock resources. Natural products allow for access to diverse structures and provide a variety functionalization groups, which lead to many routes for the design of monomers and their subsequent polymerizations. Quercetin and its derivatives are well-studied molecules with interesting bioactivities, making them ideal to be incorporated into the backbone of different types of polymers. Four systems of either linear polycarbonates or epoxy cross-linked networks have been synthesized and characterized extensively. First, the monomer 3,7,4'-tribenzylquercetin was synthesized followed by condensation polymerizations to afford linear polycarbonates of various molecular weights. The photophysical properties were examined and compared to the monomer, including the identification of uniquely-high levels fluorescence emission intensity and quantum yield. Upon further exploration of the mechanism for this unexpected fluorescence, aggregation-induced emission (AIE) was found to contribute to this photophysical phenomenon. The identified AIE properties were further utilized in a second system for the incorporation of quercetin segments into micelles. The copolymerization of two quercetin-based monomers followed by "clicking" on various grafting percentages of poly(ethylene glycol) afforded amphiphilic macromolecules. The quercetin-based macromolecules were assembled into micelles and found to be fluorescent and non-cytotoxic to various cell lines, therefore demonstrating potential for applications in drug delivery. In another system, after several unsuccessful attempts of synthesizing a

polycarbonate with a protected catechol moiety of quercetin, copolymerization of this monomer with a lysine-containing tripeptide was achieved. Deprotection of the polymer to afford catechol and amine moieties will open opportunities for these materials to be potentially applied as biomedical adhesives. In the final explored system, a 3,7,4'-trimethylquercetin diglycidyl ether-nadic methyl anhydride cross-linked network was synthesized and was shown to exhibit comparable thermal and mechanical properties to the diglycidyl ether of bisphenol A-nadic methyl anhydride networks. Overall these quercetin-based materials represent a new class of environmentally-friendly networks with potential for various engineering applications.

DEDICATION

To my family,

Dad (Richard), Mom (Rebecca), Dylan, Phillip and Tyler Kristufek

and

Khôi N. Văn

ACKNOWLEDGEMENTS

First, I would like to thank my Ph.D. advisor Professor Karen L. Wooley, for her invaluable guidance and support over the past five and half years during my graduate study at Texas A&M University. I learned a lot from her about science especially in the area of natural product-based materials as well as dedication, passion, writing, attentiveness to detail and time management. I greatly appreciated her patience over these years while I took the time to develop as an independent researcher to learn about synthetic chemistry, nanomaterials and polymer science. Her influence helped me to develop into the scientist that I am today and for that I am grateful. I will always consider her an important mentor.

I would also like to thank my committee members, Professor Donald Darensbourg, Professor Duncan Maitland and Professor Daniel Romo for their valuable and stimulating conversations that helped to further this dissertation. Specifically, I would like to thank Professor Darensbourg for the valuable conversations about polycarbonates. I would like to thank Professor Maitland for the collaboration in obtaining the mechanical data for the isosorbide-based cross-link networks. I would also like to thank Professor Romo for the use of the microwave reactor and chemicals.

I gratefully acknowledge the financial support from the National Science Foundation (CHE-1410272 and CHE-1610311) and the Welch Foundation (A-0001). Instrument use from the ILSB and use of the TAMU/LBMS and Dr. Yohannes Rezenom and Vanessa Santiago are acknowledged for obtaining the mass spectrometry spectra. The X-ray diffractometers, small angle scattering instrumentation and crystallographic

computing systems in the X-ray Diffraction Laboratory at the Department of Chemistry, Texas A&M University were purchased with funds provided by the National Science Foundation (CHE-9807975, CHE-007982 and CHE-0215838) and samples were run by Joseph H. Reibenspies.

This work would not have been possible without the help of the brilliant collaborators that I had the pleasure to work with over these years. I would like to thank Mr. Yi-Yun Timothy Tsao (calculations), Dr. Lu Su, Dr. Yingchao (cryo-TEM), Mr. Justin A. Smolden (solid state FLIM), Dr. Kevin A. Pollack (AFM), Dr. Amandine Noel, Dr. Tiffany P. Gustafson and Dr. Jeffery E. Raymond for all of their contributions on the quercetin-based fluorescent polycarbonates in Chapter II. I would like to thank Dr. Lu Su (TEM), Dr. Yingchao Chen and Ms. Sarosh Khan for all of their helps on the characterization of the quercetin-based micelles in Chapter III. I would like to thank Ms. Randinu Pulukkody (synthesis of two monomers and scale up of pre-monomer) for her assistance in synthesizing the protected quercetin small molecules and Dr. Rachel Letteri for teaching me about solid phase peptide synthesis and her help in synthesizing the peptide in Chapter IV. I am very grateful for the collaboration with Dr. Megan Robertson and her group, specifically, Dr. Guozhen Yang and Dr. Brian J. Rohde on the quercetin-based epoxy networks. I would also like to thank Dr. Lauren Link from Texas A&M University on the same project in Chapter V.

I would also like to thank all of the collaborators on the isosorbide project including Dr. Andrew Weems (tensile testing) and Dr. Duncan Maitland from Texas A&M University, Department of Bioengineering. Also, I would like to thank Mr. Tyler

Kristufek, Dr. Lauren A. Link, Ms. Sarosh Khan, Dr. Soon-Mi Lim, Dr. Alexander T. Lonnecker and Dr. Jeffery E. Raymond from the Wooley group.

I would also like to thank all the past and present members of the Wooley group, Mr. Ryan Allen, Dr. Yannick Borguet, Dr. Sangho Cho, Dr. Yingchao Chen, Mr. Daniel Dobbins, Ms. Mei Dong, Dr. Andrew Dove, Ms. Sussana Elkassih, Dr. Mahmoud Elsabahy, Dr. Jingwei Fan, Ms. Simcha Felder, Dr. Jeniree Flores, Dr. Marco Giles, Ms. Amelia Gonzales, Ms. Alexis Gooch, Dr. Tiffany Gustafson, Mr. Xun He, Dr. Gyu Seong Heo, Ms. Jesscia Huang, Dr. Ashley Jahnke, Ms. Nari Kang, Ms. Sarosh Khan, Mr. Chris Komatsu, Mr. Tyler Kristufek, Mr. Eric Leonhardt, Dr. Rachel Letteri, Dr. Ang Li, Mr. Richen Li, Dr. Soon-Mi Lim, Dr. Young Lim, Mr. Yen Nan Lin, Dr. Yun Lin, Dr. Lauren Link, Dr. Alex Lonnecker, Ms. Sherry Melton, Ms. Casey McDonald, Mr. Andy Moutray, Dr. Koichiro Mikami, Mr. Tan Nguyen, Dr. Amandine Noel, Dr. Adriana Pavia-Sanders, Ms. Randinu Pulukkody, Dr. Jennifer Summerhill, Mr. Shota, Osumi Dr. Kevin Pollack, Ms. Stephanie Pollack, Ms. Danielle Policarpio, Mr. Kenton Rauwerdink, Dr. Jeffery Raymond, Mr. Joel Russell, Dr. Sandani Samarajeewa, Dr. Kellie Seetho, Dr. Ritu Shrestha, Mr. Travis Smith, Mr. Justin Smolen, Ms. Yue Song, Ms. Jennifer Streff, Mr. Matthew Svach, Dr. Lu Su, Dr. Guorong Sun, Ms. Judy Taylor, Mr. Timothy Tsao, Mr. Bryan Tucker, Ms. Ginny Vance, Ms. Mariela Vasquez, Ms. Brooke Versaw, Mr. Kevin Wacker, Ms. Sarah Ward, Mr. Hai Wang, Mr. Ryan Zentay, Dr. Fuwu Zhang, Dr. Shiyi Zhang and Dr. Jiong Zou for being such great peers and making the lab environment so enjoyable to be in.

Finally, I would like to thank my family including my parents (Richard and Rebecca Kristufek) and my brothers (Dylan, Phillip and Tyler Kristufek) for their love and support during all of these years. Thank you to all of the wonderful friends I have met and will continue to treasure since my time at Texas A&M University. A very special thank you to Khôi Văn for the love, patience, support and help through all of these years especially during my rehabilitation and reintroduction into lab during our fourth year of schooling.

CONTRIBUTORS AND FUNDING SOURCES

In Chapter II, Mr. Yi-Yun Timothy Tsao performed the calculations, Dr. Lu Su and Dr. Yingchao performed the cryo-TEM experiments and Mr. Justin A. Smolden performed the solid state FLIM experiment. Dr. Kevin A. Pollack, Dr. Amandine Noel, Dr. Tiffany P. Gustafson and Dr. Jeffery E. Raymond also contributed to the work performed in this chapter. In Chapter III, Dr. Lu Su and Dr. Yingchao Chen performed the TEM experiments and Ms. Sarosh Khan performed the cell studies. Ms. Randinu Pulukkody synthesized two monomers and prepared more pre-monomer in Chapter IV. In collaboration with Dr. Megan Robertson and her group, specifically working with Dr. Guozhen Yang and Dr. Brian J. Rohde, the quercetin-based epoxy networks were designed and characterized thermally and mechanically. Dr. Lauren Link also assisted in some of the mechanical characterization of the epoxy networks. In the appendix, Mr. Tyler Kristufek synthesized the monomer and networks as well as performed some of the characterization. Tensile testing was performed by a collaborator, Dr. Andrew Weems from the laboratory of Dr. Duncan Maitland, Texas A&M University, Department of Bioengineering. Dr. Lauren A. Link performed mechanical testing and Ms. Sarosh Khan and Dr. Soon-Mi Lim performed the cell studies on this project. Dr. Alexander T. Lonnecker and Dr. Jeffery E. Raymond also contributed to this project.

This work was supported by the National Science Foundation (CHE-1410272 and CHE-1610311) and the Welch Foundation (A-0001). Instrument use from the ILSB and use of the TAMU/LBMS and Dr. Yohannes Rezenom and Vanessa Santiago are acknowledged for obtaining the mass spectrometry spectra. The X-ray diffractometers,

small angle scattering instrumentation and crystallographic computing systems in the X-ray Diffraction Laboratory at the Department of Chemistry, Texas A&M University were purchased with funds provided by the National Science Foundation (CHE-9807975, CHE-007982 and CHE-0215838) and the samples were run by Dr. Joseph H. Reibenspies.

NOMENCLATURE

AIE	Aggregation-induced emission
BPA	Bisphenol A
BPS	Bisphenol S
Đ	Polydispersity index
DA	Diels-Alder
DGEBA	Diglycidyl ether of bisphenol A
DGEBA-NMA	Diglycidyl ether of bisphenol A-nadic methyl anhydride
DCM	Dichloromethane
DMA	Dynamic mechanical analysis
DMF	*N*,*N*-dimethylformamide
DSC	Differential scanning calorimetric
ε'	Rubbery modulus
ε	Molar absorptivity coefficient
ESI-MS	Electrospray ionization- mass spectrometry
FLIM	Fluorescence-lifetime imaging microscopy
FTIR	Fourier transform infrared spectroscopy
GPC	Gel permeation chromatography
MeOH	Methanol
m.p.	Melting point
M_n	Number average molecule weight
MPLC	Medium Pressure Liquid Chromatography

M_w	Weight average molecule weight
MWCO	Molecular weight cut-off
Q-NMA	Quercetin-nadic methyl anhydride
NMA	Nadic methyl anhydride
NMR	Nuclear magnetic resonance
Φ	Quantum yield
PEG	Poly(ethylene glycol)
phr	Parts per hundred resin
R	Gas constant
RIR	restriction of intramolecular rotations
RIM	restriction of intramolecular motions
RIV	restriction of intramolecular vibrations
SEC	Size-exclusion chromatography
T	Temperature
T_g	Glass transition temperature
T_d	Decomposition temperature
TEM	Transmission electron microscopy
TCSPC	Time-correlated single-photon counting
TGA	Thermogravimetric analysis
TLC	Thin layer chromatography
TPE	Tetraphenylethylene

TABLE OF CONTENTS

Page

LIST OF SCHEMES

Page

LIST OF FIGURES

Page

LIST OF TABLES

Page

CHAPTER I

INTRODUCTION – EXPLORING THE TOOLBOX OF NATURAL PRODUCT-BASED COMPOUNDS TOWARDS POLYMERIC MATERIALS AND THEIR APPLICATIONS*

1.1 Natural Product-based Polymeric Materials

In what has been coined as the age of scalability in organic chemistry,[1] the development of scalable transformations for natural products and their derivatives are more important than ever in materials science. The practicality of using functionalized natural products for polymerization is more of a reality as syntheses and isolation techniques become more concise. The ever-expanding chemical toolbox of novel reactions is also powerful for monomer synthesis. Whether it is the synthesis of a natural product with inherent polymerizable groups from readily-available starting materials or the functionalization of an isolated compound, scalability is the key to creating sustainable society-enhancing polymeric materials. While this account focuses on the functionalization of naturally-derived compounds, introducing sustainability in the syntheses of polymeric materials encompasses a vast scope of topics including greener solvents[2] or catalyst design.[3-4]

Implementing the use of natural products for the replacement of petrochemical-based monomers has the potential to decrease the dependence on fossil fuels and

---

* Reprinted with permission from "Monomer design strategies to create natural product-based polymer materials" by Kristufek, S. L.; Wacker, K. T.; Tsao, Y. T.; Su, L.; Wooley, K. L. 2017. Natural Product Reports, DOI: 10.1039/C6NP00112B Copyright 2016 by The Royal Society of Chemistry.

increase the number of material applications of more renewable resources. One way of expanding the content of natural products in polymeric materials is through the incorporation of bio-based materials and their derivatives as the monomer units. Bio-based materials are defined by the ASTM: "a material is an organic material in which carbon is derived from a renewable resource *via* biological processes. Bio-based materials include all plant and animal mass derived from CO_2 recently fixed *via* photosynthesis, per definition of a renewable resource."[5] Specifically, the introduction of bio-based materials leads to the potential to remove some petrochemical-based components and take advantage of the renewability of natural products. There are several examples of naturally-sourced monomers currently on the market, such as Coca-Cola natural sourcing part of the poly(ethylene terephthalate) in plastic bottle production.[6] In another example, the naturally-derived compound, isosorbide, is being utilized by Mitsubishi Chemical[7] in polycarbonate materials. Both academic and industrial research have made great strides in the area of bio-based materials, however, the myriad natural products generate boundless directions for the synthesis of polymeric materials.

Beyond the replacement of petrochemical-based materials, the synthesis of novel materials from natural products has the potential to yield novel reactions/methodologies, and ultimately leads to materials with emergent, unforeseen properties. The sheer chemical, structural, and stereochemical diversity of natural products compared to petrochemicals from which polymers are synthesized greatly lends itself toward the development of these potentially new processes and materials from bio-based sources.

Designing bio-based monomers requires innovation to maintain high percentages of biomass in the materials, which can be introduced through developing new chemistry. For example, Hoye and co-workers explored the Diels-Alder (DA) reaction of itaconic anhydride with various furans through a study of the kinetic and thermodynamic properties of the reaction.[8] The compounds developed through this novel chemistry can later be utilized in the polymerizations of several different polymer classes.

Regardless of the rationalization for the use of natural products in materials science applications, each natural product is initially limited in its potential final application, as it only possesses the functionalities that are inherent to the compound. However, through synthetic organic chemistry, additional functionalities can be installed to afford a compound with vastly different structural and chemical functionalities for polymerization. In particular, the Wooley group has studied natural product-based compounds such as sugars and their derivatives,[9-12] quinic acid,[13-14] honokiol,[15] feurlic acid[16-18] and amino acids.[19-25] Numerous reviews have also recently discussed the incorporation of renewable resources in polymer science[26-31] that demonstrates the current extent of natural product-based materials.

Aromatic polymeric materials such as poly(bisphenol A carbonate), polyaramids, polystyrene, poly(ethylene terephthalate), among others are essential to our current way of life. While these materials are important, they are based on petrochemical resources and some such as poly(bisphenol A carbonate), have harmful side effects that occur upon degradation into the monomers.[32] Other commonly used polymeric materials are nondegradable which, leads to plastics in landfills[33] and the ocean.[34] Currently, there is

a strong investigation into using lignin-based monomers to replace the petrochemical derived monomers. Lignocellulose is one of the largest biomass sources in the world and is characterized by three main components: hemicellulose, cellulose, and lignin. Of these components, lignin is a polymer consisting of aromatic rings and aliphatic side chains.[35] To produce high-value compounds including monomers, numerous lignin valorization processes have been well-studied.[36-39] Depending on the source of the lignin, the structure varies,[40] therefore, different compounds can be isolated with diverse functionalities. Post-isolation, compounds and their derivatives, have the potential to be polymerized including small molecule aromatic compounds are important such as vanillin, ferulic acid, eugenol, creosol, and sinapyl alcohol derivatives.[28, 41-43] While the previously mentioned methods have been developed, many of these conditions have not been able to be scaled up for industrial production therefore other sources of aromatic natural product-based materials need to be investigated.

1.2 Aggregation-Induced Emission Materials and Their Applications

Aggregation-induced emission (AIE) is the photophysical phenomenon that occurs by aggregation of non-emissive luminogens was first reported by the Tang group in 2001.[44] A luminogen is a compound which only emits under certain conditions. The mechanism of emission in AIE materials is still under investigation but it has been proposed that restriction of intramolecular rotations (RIR), restriction of intramolecular vibrations (RIV) and restriction of intramolecular motions (RIM) are the main processes that are contribute to this phenomenon.[45] While many of the current AIE materials are based on tetraphenylethene, hexaphenylsilole and other similar compounds,[46] the field

has potential to explore other monomers especially natural product-based compounds and their applications.

AIEgen-based compounds have been applied to a broad set of applications including fingerprinting,[47-49] chemo/bio sensors[50-52] as well as a wide variety of other applications.[53] Polymers with side-chains and backbones of AIEgens have been synthesized and applied to explosives detection,[54-56]drug delivery[57-59] and other applications.[60] The investigation of novel polymeric materials with AIE properties is an important direction, especially from natural product-based monomers, because they have the potential to widen the breadth of applications specifically in the area of environmentally-friendly and biomedical applications.

1.3 Fluorescent Nanomaterials

Over the past few decades, there has been an increase in biomedical research based on nanomaterials. Nanomaterials have been studied as advanced drug delivery systems to increase solubility of a drug, target site specific delivery among numerous other benefits of these systems.[61] Nanomaterials such as nanoparticles, liposomes and micelles, is a broad field covering organic and inorganic materials, with different morphologies including spheres[61] and brushes[62] and are assembled utilizing various methods including self-assembly[63-64] and layer-by-layer assembly.[65] Additionally, these materials have the capability to be functionalized with dyes[66] and other labels[67] to assist in the understanding of how the materials act in biological systems. Another functionality that can be built into a drug delivery system to allow for clearance, are degradable systems. The Wooley group has studied degradable systems based on

polyphosphoester [68-71] and polycarbonates.[18, 72-73] Many of these systems are natural product-based drug delivery systems which allow for an environmentally benign or beneficial by-products. The diversity of nanomaterials allows for expansion of drug delivery systems to develop better theranostics materials.

Labeling methods of include covalent or physical absorption but if inefficient attachment or degradation occurs the fluorescent signal can change.[74] Polymers with inherent fluorescence is a common way to avoid the traditional labeling with fluorescent dyes post-polymerization. Drug delivery systems such as micelles and nanoparticles have recent been synthesized.[75-77] Many of the AIEgen-based drug delivery systems are utilized in chemo- or bio- sensors to stimuli such as pH,[58] endogenous hypochlorite,[78] horseradish peroxidase[79] and Hg^{2+} ions.[80] Although these systems allow for well characterized fluorescence emission, there are few examples of degradable systems with AIE properties.[81-83] A system with the combination of inherent fluorescence and degradability would be advantageous for drug delivery.

1.4 Medical Adhesives

Medical adhesives is a broad field including applications in surgical procedures,[84] wound healing,[85] brain-machine interfaces[86] among others. The diverse substrates with biomedical applications requires a different types of adhesives such as hydrogels[85] and cyanoacrylates.[87] A major challenge with biomedical adhesives is that they can cause damage from multiple applications or irritation from incompatibility.[88] Therefore, there is a need for more biocompatible medical adhesives.

Presently, mussel-inspired materials are being investigated as the next generation of medical adhesives.[89-91] It was discovered in 1981 that marine mussels are abundant in the amino acid, 3,4-dihydroxyphenylalanine. The amino acid was isolated and found to contribute to the adhesive properties.[92] Although catechols of various types have been studies for over 35 years, the mechanism of adhesion is not well understood.[93] In 2007, the Messersmith group investigated the mussel-inspired, dopamine-based materials of polydopamine for their excellent adhesive properties.[94] Dopamine is an aromatic compound with a catechol and short chain amine which interacts to form adhesive materials. Recently, the Waite, Israelachvili, and Butler groups investigated the adaptive synergy between lysine and 3,4-dihydroxyphenylalanine with respect to abundance and proximity of the functionalities. This study furthered the understanding of mussel-inspired adhesive materials.[95-96] The understanding of the corporative effect of the lysine and 3,4-dihydroxyphenylalanine indicates that multicomponent systems will be desirable to create optimal adhesive biomedical materials.

1.5 Epoxy Resins

Epoxy resins are a significant part of modern life. They are used in a large vary of commercially available including coatings, adhesive and bulk materials.[97] Epoxy resins are at least a two-component system with one of the monomers containing one or more oxirane group and the second component must contain a functionality that can ring-open the epoxy moiety (*i.e.* amine, phenol, alcohol, *etc*.).[98] The simplicity of the epoxy system allows for a multitude of compounds to be functionalized with an epoxide unit using the commercial available reagent, epichlorohydrin then cross-linked with

common cross-linkers. Alternatively, commonly utilized epoxidized monomers have the potential to be cross-linked with monomers that are designed to have nucleophilic moieties. These two methods lead to a multitude of combinations of materials to be synthesized and characterized.

A current trend in epoxy resins is to synthesize monomers from natural products. One of the most common monomers for epoxy resin synthesis is based on bis(4 - hydroxy phenylene) - 2,2 propane, commonly known as bisphenol A (BPA).[99] BPA has been shown to be an estrogen hormone disruptor and increase rates of cancer and obesity.[100-101] As a waste materials, BPA-based products are put into landfills and as the materials degrade they are introduced into terrestrial aquatic environments which can lead to ingestion by humans, causing related health conditions.[102] BPA is also synthesized from non-renewable petrochemical resources. Current commercially available replacements such as bisphenol S (BPS) have many of the same health and environmental concerns as BPA,[103-104] which makes it more important to consider other structural cores. When considering a natural product-based replacement for current materials it is important to retain the properties of the material of interest. For bisphenol A-based epoxy resins, thermal and mechanical are key properties to compare. Although there are several reviews of the abundance of natural products that have been explored as BPA replacements,[105-110] there is still a need to find a commercial replacement for these petrochemical-based.

1.6 Designing Natural Product-based Materials Utilizing Quercetin as a Platform

With an interest in diverse applications and the desire to design materials from natural products, molecules with the potential to be a platform are desired. The quintessence of this type of monomer design is the diverse inherent functionalities with the capability to introduce further functional groups for a large array of starting materials. Also, essential to monomer selection is a natural product that is either benign or has beneficial biological properties. Considering several criteria for natural product-based monomers, flavonoids which have well studied biological properties and functionalized groups, are good candidates for these purposes.

In particular, the natural polyphenolic compound, quercetin has had limited use in the backbone of polymeric materials. Aside from the studies within this dissertation, quercetin has been used in epoxy[111] and methacrylate[112] networks as well as biodegradable polymers.[113] Due to the bioactivity of quercetin, the polyphenolic compounds has been well studied while being conjugated to polymers,[114-115] imprinted within networks[116-118] and loaded into nanomaterials.[119-121] Quercetin is a well-studied compound for the prevention of cardiovascular and neurodegenerative diseases and cancer among other diseases.[122] Structurally, quercetin has five phenol groups that have different reactivities[123-124] which allows for multiple and/or diverse functionalization. The polyphenolic compound, quercetin will be discussed herein as a platform for synthesis of designer monomers and the assessment of properties for the intended applications.

CHAPTER II

AGGREGATION-INDUCED EMISSION PROPERTIES OF A POLYCARBONATE DESIGNED FROM THE RENEWABLE RESOURCE QUERCETIN

2.1 Overview

Engineering polymers derived from biorenewable feedstocks are of interest due to their reduced reliance on petrochemicals and their potential to degrade into environmentally benign and bioresorbable natural products. Quercetin, a polyphenolic compound found in many food sources, was functionalized regioselectively to allow for its incorporation into a well-defined linear polymer backbone that was observed to exhibit remarkable physical and optical properties. The monomer, 3,7,4′-tribenzyl quercetin, was prepared *via* a one-step benzylation, and then transformed into a novel polycarbonate, poly(3,7,4′-tribenzyl quercetin carbonate) by condensation polymerization with the carbonylation reagent, diphosgene. Polycarbonates with molecular weights of 8 and 13 kDa were determined to have glass transition temperatures (T_g) of 118 °C and 124 °C, respectively, by differential scanning calorimetry. Thermogravimetric analysis indicated that the polymers were thermally stable until *ca.* 250 °C. Poly(3,7,4′-tribenzyl quercetin carbonate) also expressed bright broad-band auto-fluorescence, with detectable emission from 370-600 nm. A thorough investigation was conducted, through molecular modeling, experimental fluorescence studies of model compounds and a study of the aggregation-induced emission properties, to explain the unexpected fluorescence. Overall, this poly(3,7,4′-tribenzyl quercetin

carbonate) system represents a novel class of environmentally-friendly polymers, which have potential applications as engineering materials with the possibility of extension to biomedical applications, where the additional unique characteristic of being an emissive, self-reporting polymer could allow for monitoring of materials under changing biological or environmental conditions.

2.2 Introduction

Designing polymeric materials with natural product components has become a widely studied topic of interest towards both more environmentally friendly materials and those with interesting emergent properties.[26, 28-29] While many studies focus on the replacement of petrochemical counterparts, an exhaustive study of the novel materials' properties imparted by naturally derived materials may elucidate advantageous properties not present in petrochemical-based materials. Recently studied examples of biomass-derived chemicals used in the design of natural product-based polymeric materials vary widely in structure and functionality, and include plant oils,[125] quinic acid,[13] lactide[70, 126-127] and glucose,[9, 128-129] among others.[130-131] However, there is a large diversity of potential polyphenolic feedstocks that have yet to be polymerized into a functional form.

Of the naturally occurring polyphenolic compounds, quercetin is one of the most commonly found in edible plants, for example teas and onions.[132] Advantages to the use of quercetin in the design of versatile polycarbonate-based materials include: its pharmacological benefits leading to decreased rates of illnesses such as inflammation,[133] cancer,[134] and neurodegenerative diseases;[135] the biocompatibility of quercetin and its

naturally occurring derivatives;[136-137] and its extensively-studied pharmacokinetics and pharmacodynamics in humans.[138-139] These properties have led to the encapsulation[140] and covalently conjugation[141] of quercetin with polymeric materials for medical applications; however, to the best of our knowledge, it has not yet been used directly in the synthesis of a polycarbonate.

Aggregation-induced emission (AIE) is among the interesting properties that have the potential to be studied post-polymerization of natural product-based materials. AIE is a termed that was coined in 2001 by Ben Zhong Tang to describe the photophysical process that occurs when a non-emissive luminogen emits from an aggregate formation.[53] Many macromolecular structures exhibit AIE properties upon incorporation of a luminogen as a side chain or in the polymer backbone,[60] although there are limited examples of luminogenic polycarbonate systems.[142] Polymeric materials with AIEgens have been studied towards applications in chemosensors[54-55] and bio-imaging,[143] among other various applications.[53] While compounds with AIE properties, such as tetraphenylethylene (TPE), have been extensively incorporated into polymeric materials,[54, 144-146] natural product based monomeric luminogens studies remain elusive.

This work presents the synthesis and extensive thermal and photophysical characterization of an innovative poly(3,7,4′-tribenzyl quercetin carbonate), synthesized by condensation polymerization of 3,7,4'-tribenzyl quercetin carbonate with the carbonylation reagent diphosgene to afford polymers with two different molecular weights. Model studies were performed with small molecules to elucidate the effects of

dimerization, substitution and carbonyl substitution on the emissivity of the polymer. To further understand the fluorescence properties that are observed upon polymerization of the quercetin carbonate, computational analysis of dimer formation of the polymers was performed. Additional fluorescence characterization of the polymers revealed aggregation-induction emission properties, where the fluorescence of the polymer increased upon the addition of methanol when the polycarbonate was dissolved in dichloromethane. Given the importance of materials that sense changes in biomedical, environmental and other applications,[147-148] the ability of poly(3,7,4′-tribenzyl quercetin carbonate) to serve as a self-reporting material suggests its great potential in a number of applications.

2.3 Experimental

Materials

Quercetin was purchased from Cayman Chemical or Stanford Chemical. Sodium carbonate, dimethylformamide (DMF, DriSolv) and dichloromethane (DCM, DriSolv) were purchased from EMD Millipore. Triethylamine and pyridine were purchased from Sigma-Aldrich and freshly distilled over CaH_2. Diphosgene was purchased from either Sigma-Aldrich or Alfa Aesar. Triphosgene, N,N,N',N'-tetramethylethylenediamine, iodomethane and phenyl chloroformate were purchased from Alfa Aesar. All reagents were used as received unless otherwise noted.

Characterization

^{1}H and ^{13}C NMR spectra were recorded on a Varian 500 MHz spectrometer interfaced to a UNIX computer using Mercury software. Monomers were purified by

Medium Pressure Liquid Chromatography (MPLC) using a CombiFlash R_f (Teledyne Isco). Chemical shifts were referenced to the solvent proton resonance. The DMF gel permeation chromatography (GPC) was conducted on a Waters Chromatography, Inc. (Milford, MA) system equipped with an isocratic pump model 1515, a differential refractometer model 2414, and a four-column set of 5 μm Guard (50 × 7.5 mm), Styragel HR 4 5 μm DMF (300 × 7.5 mm), Styragel HR 4E 5 μm DMF (300 × 7.5 mm), and Styragel HR 2 5 μm DMF (300 × 7.5 mm). The system was equilibrated at 70 °C in pre-filtered DMF containing 0.05 M LiBr, which served as polymer solvent and eluent (flow rate set to 1.00 mL/min). Polymer solutions were prepared at a concentration of *ca.* 5 mg/mL and an injection volume of 200 μL was used. Data collection and analysis were performed with Empower 2 v. 6.10.01.00 software (Waters, Inc.). The system was calibrated with S3 polystyrene standards (Polymer Laboratories, Amherst, MA) ranging from 615 to 442,800 Da. IR spectra were obtained on a Shimadzu IR Prestige Attenuated Total Reflectance Fourier-transform Infrared Spectrometer (ATR-FTIR). Spectra were analyzed using IRsolution software package (Shimadzu).

Differential scanning calorimetric (DSC) studies were performed on a DSC822^e (Mettler-Toledo), with a heating rate of 10 ºC/min to determine the melting point (m.p.) of the model compounds and the monomer as well as the glass transition (T_g) of the polymers. The T_g was taken as the midpoint of the inflection tangent upon the third heating scan. Thermogravimetric analysis was performed under Ar atmosphere using a model TGA/DSC 1 Star^e system (Mettler-Toledo), with a heating rate of 10 ºC/min. Measurements were analyzed using Star^e software version 10.00d (Mettler-Toledo).

Steady State Optical Spectroscopy

UV-Vis spectra were acquired on a UV-2550 spectrophotometer (Shimadzu). All steady-state emission, excitation and anisotropy spectra were obtained with a FluoroMax4 (Horiba) with automated polarizers. Measurements were taken in matched quartz cuvettes with path-lengths of 1 cm in DMF, DCM or DCM/MeOH mixtures.

Lifetime Spectroscopy

Time-correlated single-photon counting (TCSPC) was employed to obtain all solution-based fluorescence lifetime spectra. The measurements were done with a Fluorotime 100 fluorometer and a 405 nm solid state ps diode laser source (PicoQuant) in matched quartz 3.0 mL cells (VWR). Instrument response functions (IRF) were determined from the scatter signal from a solution of Ludox HS-40 colloidal silica (0.01% particles in water S3 wt/wt). Emission spectra were collected after passing through a 450 nm long pass filter and a single polarizer, with emission polarization controlled to vertical. For emission decay spectra, collection was obtained through a magic angle polarizer.

Fluorescence Lifetime Microscopy, FLIM

Fluorescence lifetime images of the solid polymers (8 kDa and 13 kDa) were acquired on an FV1000 Olympus confocal microscope equipped with a FLIM LSM upgrade kit (PicoQuant) using a 40x dry objective. A 405 nm femtosecond pulsed laser source (LDH-P-C-405B, PicoQuant) driven at a frequency of 20 MHz and a line-scan speed of 8 µs/pixel (512 x 512 pixel image size) was used as the excitation source, which was attenuated by neutral density filters to maintain a count rate below 1% bin

occupancy to avert count pile-up. A high-pass emission filter (FF01/482/35) was used to reduce scattered light artifacts. FLIM analysis, including fitting of the time-resolved fluorescence decay, was performed using SymphoTime 64 software (PicoQuant).

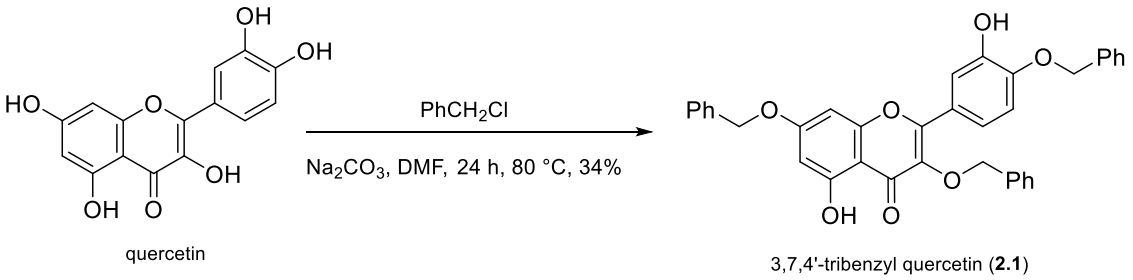

Figure 2.1 Synthesis of **2.1**.

Monomer synthesis, 3,4',7-tribenzylquercetin, **2.1**

The monomer was prepared by a procedure that was adapted from Hua *et al.*[149] A round bottom flask was charged with quercetin (20.0 g, 66.2 mmol), sodium carbonate (21.4 g, 202 mmol), benzyl chloride (23.8 mL, 207 mmol) and DMF (500 mL) under nitrogen. The reaction was stirred at 80 °C for 24 h and the DMF was then removed *in vacuo*, resulting in a brown solid crude product. Purification by Medium Pressure Liquid Chromatography (MPLC) eluted with 20% acetone in toluene, followed by recrystallization from toluene afforded **2.1** as a yellow solid (12.4 g, 32.7% yield, 3,7,4'-tribenzyl quercetin). ^{1}H NMR (DMSO-d_6, ppm, 500 MHz): δ 5.03 (s, 2H, -CH_2), 5.23 (s, 2H, -CH_2), 6.81 (d, *J* = 2.5 Hz, 1H, Ar), 6.49 (d, *J* = 2.5 Hz, 1H, Ar), 7.21-7.49 (m, 16H, Ar), 7.65 (dd, *J* = 2.3, 8.5 Hz, Ar, 1H,), 7.76 (d, *J* = 2 Hz, 1H, Ar), 9.50 (s, 1H, -OH), 12.69 (s, 1H, -OH). ^{13}C NMR (126 MHz, DMSO-d_6): δ 178.59, 164.62, 161.46,

156.85, 156.74, 149.66, 147.06, 137.25, 136.95, 136.55, 129.36, 129.00, 128.86, 128.66, 128.60, 128.56, 128.34, 128.32, 128.21, 125.77, 122.94, 121.00, 116.12, 113.80, 105.80, 98.94, 93.61, 73.82, 70.46, 70.15. FTIR (ATR) 3235, 3026, 2876, 1651, 1601, 1574, 1512, 1489, 1452, 1371, 1348, 1278, 1217, 1193, 1163, 1139, 1121, 1003, 954, 825, 802 cm^{-1}. HRMS (ESI+, *m/z*): $[M+H]^{+1}$ calculated for $C_{36}H_{28}O_7$, 573.1913, actual 573.1941. m.p. 151 °C Regiochemistry was confirmed by x-ray analysis (Figure S2.1)

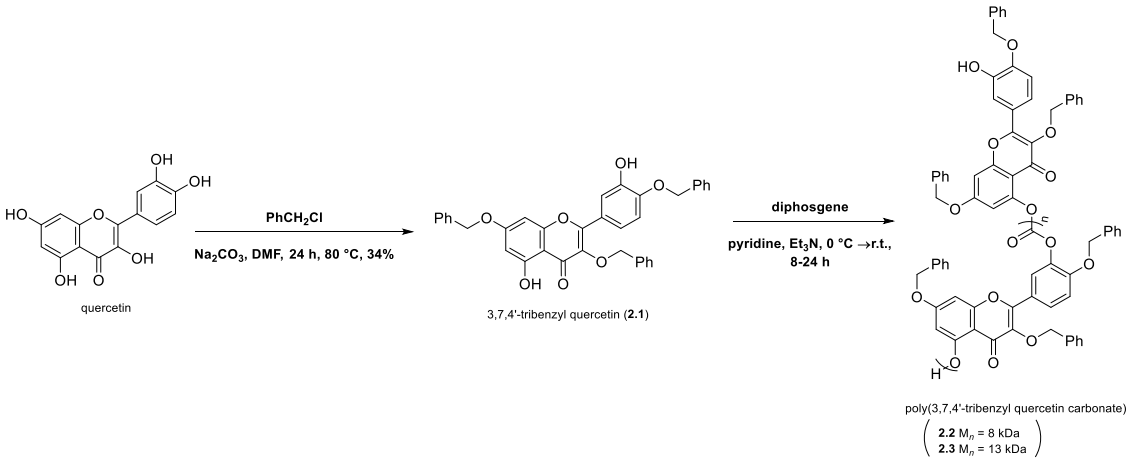

Figure 2.2 Synthesis of **2.2** and **2.3**.

Polymer synthesis, poly(3,7,4′-tribenzylquercetin carbonate) 8 kDa, **2.2**

In a Schlenk flask under N_2, 3,7,4′-tribenzyl quercetin (100 mg, 0.175 mmol), triethylamine (75 μL) and pyridine (0.42 mL) were combined. At 0 °C, diphosgene (12 μL, 0.100 mmol) was added dropwise. The solution was allowed to stir at room temperature for 8 h. The polymer product was isolated by diluting in DCM (7 mL) and washing with H_2O (10 mL x 2), followed by precipitation in cold methanol (40 mL x 2) and cold acetone (40 mL x 2), and dried *in vacuo* to afford the desired product, 3,7,4'-

tribenzyl quercetin polycarbonate. Yield: 65 mg ^{1}H NMR ($CDCl_3$, ppm, 500 MHz): δ 5.03-5.10 (br m, CH_2), 7.12-7.40 (br m, Ar), 7.80-7.89 (br m, Ar). ^{13}C NMR ($CDCl_3$, ppm, 125 MHz): δ 178.78, 173.18, 164.55, 162.45, 162.10, 157.41, 156.66, 155.36, 153.64, 152.14, 151.88, 150.87, 150.72, 150.64, 139.97, 139.46, 137.48, 136.39, 136.01, 135.90, 135.86, 135.78, 135.70, 135.28, 129.13, 129.08, 129.01, 128.85, 128.78, 128.70, 128.63, 128.49, 128.39, 128.36, 128.30, 128.21, 128.13, 127.69, 127.63, 127.46, 127.34, 127.07, 123.55, 123.40, 122.96, 122.79, 113.58, 111.76, 108.92, 106.19, 100.45, 98.74, 93.15, 74.41, 74.14, 70.87, 70.73, 70.46. FTIR (ATR): 3032, 2924, 2360, 1782, 1728, 1620, 1504, 1443, 1396, 1196, 995, 910, 818, 741, 694, 640 cm^{-1}. T_g = 119 °C. M_n = 8.3 kDa. PDI = 1.3.

Polymer Synthesis, poly(3,7,4′-tribenzylquercetin carbonate) 13 kDa, **2.3**

In a Schlenk flask under N_2, 3,7,4′-tribenzyl quercetin (100 mg, 0.175 mmol), triethylamine (75 μL) and pyridine (0.42 mL) were combined. At 0 °C, diphosgene (12 μL) was added dropwise. The solution was allowed to stir at room temperature for 24 h. The polymer product was isolated by diluting in DCM (7 mL) and washing with H_2O (10 mL x 2), followed by precipitation in cold methanol (40 mL x 2) and cold acetone (40 mL x 2), and dried *in vacuo* to afford the desired product, 3,7,4'-tribenzyl quercetin polycarbonate. Yield: 42.0 mg. ^{1}H NMR ($CDCl_3$, ppm, 500 MHz): δ 5.03-5.10 (br m, CH_2), 7.12-7.40 (br m, Ar), 7.80-7.89 (br m, Ar). ^{13}C NMR ($CDCl_3$, ppm, 125 MHz): δ 178.78, 173.18, 164.55, 162.45, 162.10, 157.41, 156.66, 155.36, 153.64, 152.14, 151.88, 150.87, 150.72, 150.64, 139.97, 139.46, 137.48, 136.39, 136.01, 135.90, 135.86, 135.78, 135.70, 135.28, 129.13, 129.08, 129.01, 128.85, 128.78, 128.70, 128.63, 128.49, 128.39,

128.36, 128.30, 128.21, 128.13, 127.69, 127.63, 127.46, 127.34, 127.07, 123.55, 123.40, 122.96, 122.79, 113.58, 111.76, 108.92, 106.19, 100.45, 98.74, 93.15, 74.41, 74.14, 70.87, 70.73, 70.46. FTIR (ATR) 3032, 2353, 1782, 1620, 1504, 1443, 1396, 1188, 1072, 995, 910, 818, 733, 694, 640 cm^{-1}. T_g = 123 °C. M_n = 12.7 kDa. PDI = 1.3

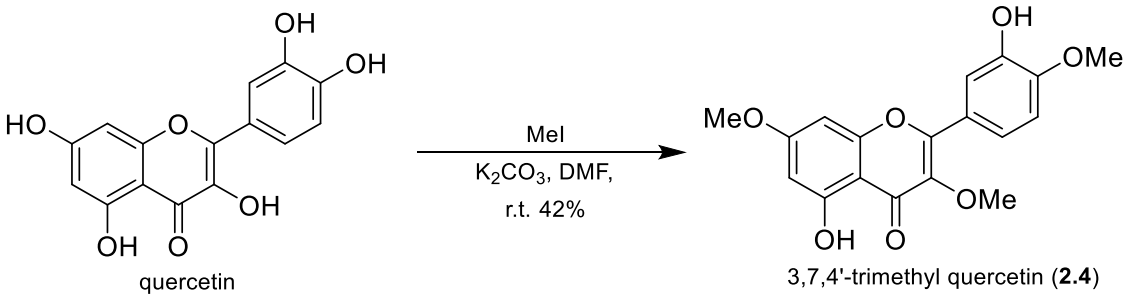

Scheme 2.1 Synthesis of **2.4**.

Synthesis of model compound, 3,7,4'-trimethylquercetin, **2.4**

The compound was prepared by a procedure adapted from Moalin et al.[150] A round bottom flask was charged with quercetin (20.0 g, 66.2 mmol), potassium carbonate (20.4 g, 148 mmol), methyl iodide (16.0 mL, 257 mmol) and DMF (500 mL) under nitrogen. The reaction was stirred at room temperature for 24 h and the DMF was then removed *in vacuo*, resulting in a brown solid product. The brown solid was purified by Medium Pressure Liquid Chromatography (MPLC) eluted with a 10% ethyl acetate in chloroform and recrystallized from chloroform to afford a yellow solid, 3,7,4'-trimethylquercetin (9.5 g, 42% yield). ^{1}H NMR (DMSO-d_6, ppm, 500 MHz): δ 12.65 (s, 1H, -OH), 9.44 (s, 1H, -OH), 7.59 – 7.55 (m, 2H, Ar), 7.11 (d, J = 8.4 Hz, 1H, Ar), 6.71 (d, J = 2.2 Hz, 1H, Ar), 6.37 (d, J = 2.2 Hz, 1H, Ar), 3.87 (s, 3H, -CH_3), 3.86 (s, 3H, -CH_3), 3.80 (s, 3H, -CH_3). ^{13}C NMR (DMSO-d_6, ppm, 125 MHz): δ 178.5, 165.5,

161.3, 156.7, 156.0, 150.7, 146.8, 138.6, 122.9, 120.8, 115.5, 112.2, 105.6, 98.2, 92.6, 60.2, 56.5, 56.1; FTIR (ATR) 3579-3140, 3047-3000, 3000-2847, 1643, 1597, 1196, 918, 895, 818, cm^{-1} HRMS (ESI+, m/z): $[M+H]^{+1}$ calculated for $[C_{18}H_{17}O_7]^+$, 345.0974, found 345.0970. m.p. 175 °C

Model monomer synthesis, 3'5-diphenyl-3,4',7-tribenzylquercetin carbonate, **2.5**

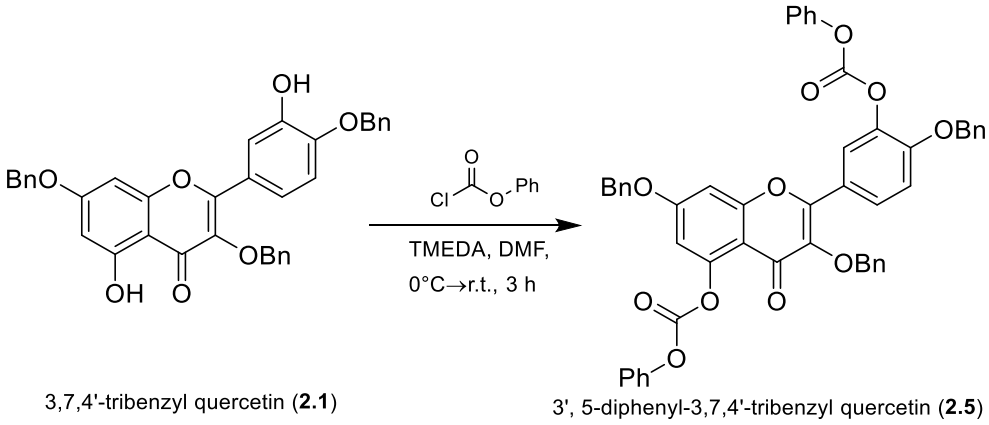

Scheme 2.2 Synthesis of **2.5**.

A round bottom flask was charged with 3,7,4′-tribenzyl quercetin (200 mg, 0.350 mmol), N,N,N',N'-tetramethylethylenediamine (108 μL, 0.723 mmol), and DMF (4 mL). The solution was cooled to 0 °C, followed by the addition of phenyl chloroformate (160 μL, 1.28 mmol) over 30 min. The solution was stirred for 3 h while warming to room temperature. The reaction was monitored by TLC, and upon completion the crude product was purified by MPLC (SiO_2, 0 to 40 % EtOAc in hexanes) to afford the model compound in quantitative yield as a yellow powder, 3',5-diphenyl-3,7,4'-tribenzylquercetin carbonate. ^1H NMR (DMSO-d_6, ppm, 500 MHz): δ 5.06 (s, 2H, -

CH_2), 5.32 (d, *J* = 8.5 Hz, 4H, -CH_2), 7.12 (app d, *J* = 1.1 Hz, 1H, Ar), 7.14 (app s, 1H, Ar), 7.17 (dd, *J* = 2.4, 0.8 Hz, 1H, Ar), 7.29-7.55 (m, 25H, Ar), 8.03-8.07 (m, 2H, Ar). ^{13}C NMR (DMSO-d_6, ppm, 125 MHz): δ 172.43, 162.29, 157.14, 153.13, 151.67, 150.97, 150.94, 150.85, 150.55, 149.43, 139.29, 138.83, 136.38, 136.09, 135.70, 129.88, 129.81, 129.22, 128.63, 128.62, 128.59, 128.38, 128.30, 128.24, 128.17, 127.80, 126.68, 126.54, 122.67, 122.27, 121.93, 121.23, 120.93, 114.14, 110.61, 108.51, 100.70, 73.29, 70.58, 70.36. FTIR (ATR) 3034, 2897, 1778 1722, 1614, 1601, 1593, 1510, 1495, 1456, 1438, 1390, 1290, 1225, 1190, 1178, 1144, 1082, 995, 964, 816, 750, 684 cm^{-1}. HRMS (ESI+, m/z): $[M+H]^{+1}$ calculated for $C_{50}H_{36}O_{11}$, 813.2336, actual 813.229. m.p. 155 °C

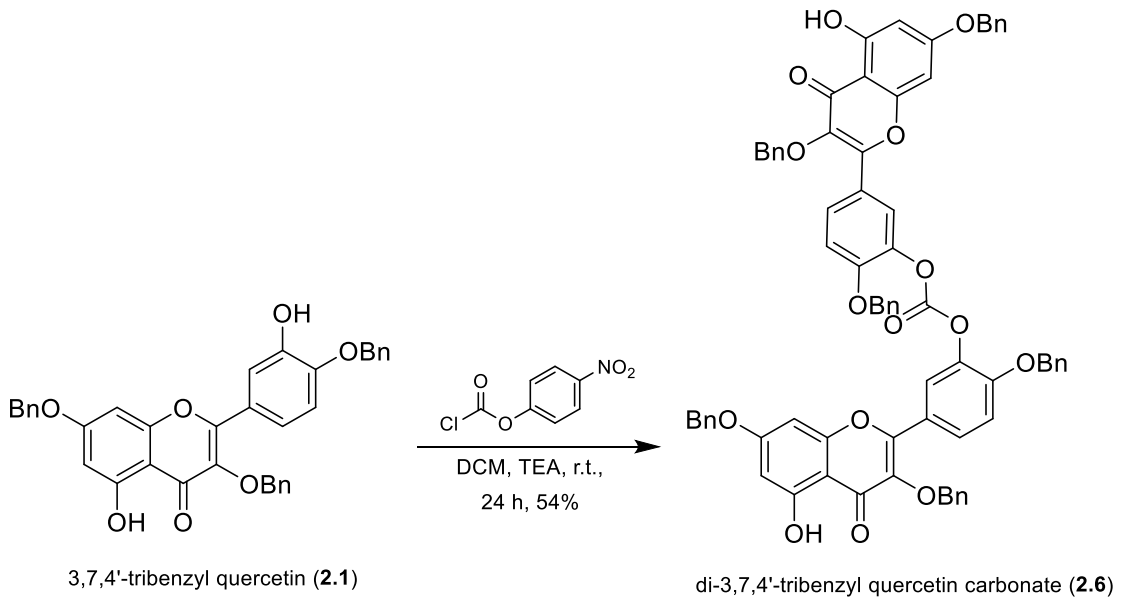

Scheme 2.3 Synthesis of **2.6**.

Dimer synthesis, **2.6**

In a round bottom flask 3,4',7-tribenzyl quercetin (499.5 mg, 0.8730 mmol), *p*-nitrophenyl chloroformate (88.2 mg, 0.4376 mmol) were combined in dichloromethane (2 mL). Triethylamine (0.18 mL, 1.29 mmol) was added dropwise to the solution. The reaction was allowed to occur over 24 h. The solvent was evaporated. The yellow solid was purified by Medium Pressure Liquid Chromatography (MPLC) eluted with a 100% DCM to afford the product as a yellow solid (275.9 mg, 54%). ^{1}H NMR (DMSO-d_6, ppm, 500 MHz): δ 5.03 (s, 2H, -CH_2), 5.23 (s, 2H, -CH_2), 6.81 (d, *J* = 2.5 Hz, 1H, Ar), 6.49 (d, *J* = 2.5 Hz, 1H, Ar), 7.21-7.49 (m, 16H, Ar), 7.65 (dd, *J* = 2.3, 8.5 Hz, Ar, 1H,), 7.76 (d, *J* = 2 Hz, 1H, Ar), 12.69 (s, 1H, -OH). FTIR (ATR) 3032, 2940, 2878, 2353, 1782, 1597, 1497, 1450, 1165, 1111, 995, 910, 810, 733, 694, 640 cm^{-1} m.p. 185 ºC

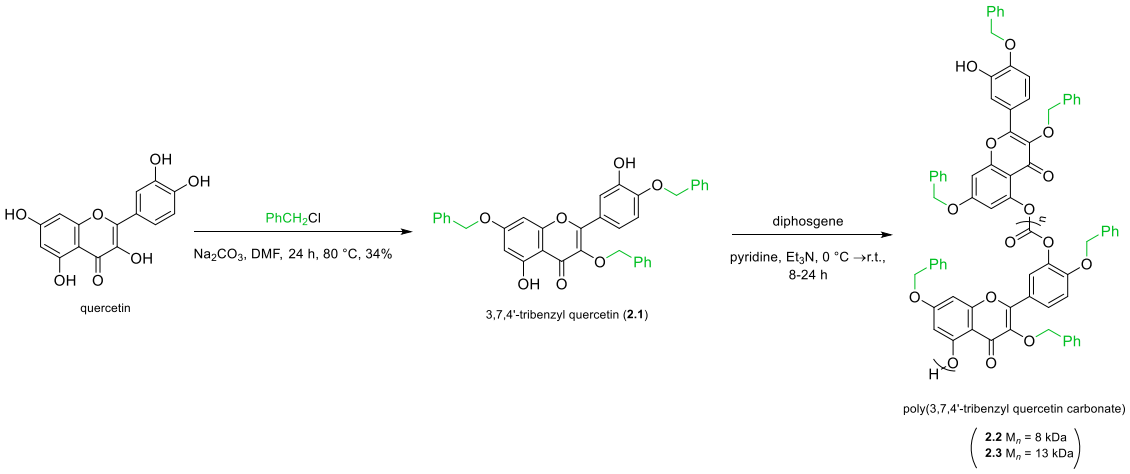

Scheme 2.4 Synthesis of the monomer 3,7,4'-tribenzylquercetin (**2.1**) and the polymer poly(3,7,4′-tribenzyl quercetin carbonate) (**2.2**-**2.3**).

2.4 Results and Discussion

Synthesis of poly(3,7,4′-tribenzylquercetin carbonate)s

The design of poly(3,7,4′-tribenzyl quercetin carbonate), begins with the selective synthesis of benzyl-protected quercetin, whereby the preferential substitution of the phenols occurs selectively as previously reported by Jurd *et al.*[124,123] Following the protection of the most reactive phenols 4, 7 and 3 to produce the monomer, 3,4',7-tribenzyl quercetin (**2.1**)[149] a condensation polymerization through phenols (3' and 5) was carried out to synthesize the polycarbonate poly(3,7,4′-tribenzyl quercetin carbonate) *via* reaction with phosgene generated *in situ* from the carbonylation reagent diphosgene (Scheme 2.1). Analysis by gel permeation chromatography (GPC) indicated the formation of polymer with M_n of 8 kDa or 13 kDa upon polymerization for 8 h or 24 h, respectively. The polymer repeated *ca*. 13-22 times depending on the molecular weight.

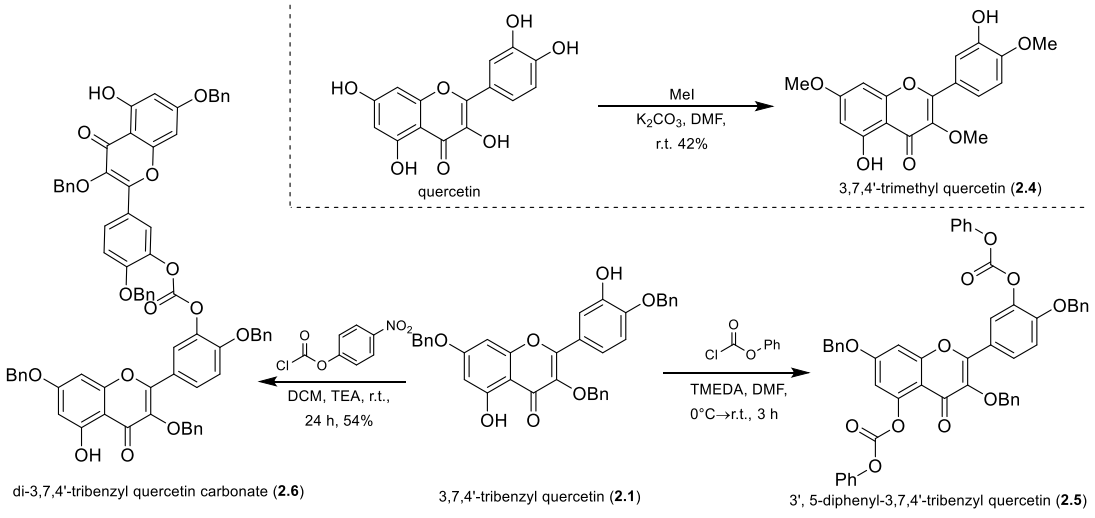

Scheme 2.5 Synthesis of model compounds for fluorescence studies.

Synthesis of model compounds for fluorescence analysis

Upon dissolution in DMF, strong autofluorescence was visualized by the naked eye from the poly(3,7,4′-tribenzylquercetin carbonate) system, but not from the monomer. To decouple the effect of carbonate substitution at the 3′ and 5 sites from the emission effects due to polymerization, the model compound 3'5-diphenyl-3,4',7-tribenzylquercetin carbonate was synthesized (Scheme 2.2). 3'5-diphenyl-3,4',7-tribenzylquercetin carbonate was prepared *via* a condensation reaction of 3,4',7-tribenzylquercetin with phenyl chloroformate under basic conditions. To understand the effect of the addition of the benzyl units to the monomer, a trimethylated quercetin compound (**2.4**) was synthesized as previously reported (Scheme 2.2).[151] Model compound **2.5** was synthesized to study the effect of dimerization within the polymer backbone. Taking advantage of the regioselectivity of the remaining phenols, **2.1** was allowed to react with *p*-nitrophenyl chloroformate to afford the regiospecific dimer (Scheme 2.2) in good yield. All model compounds were characterized by ^{1}H and ^{13}C NMR, MS and IR.

Thermal Analysis

Thermal transition temperatures and stabilities of the polymers were obtained by differential scanning calorimetry (DSC) and thermogravimetric analysis (TGA). The degradation temperatures, taken at 5% mass lost ($T_{d5\%}$), were determined to be 261 and 285 ºC for the 8 and 13 kDa quercetin polycarbonates, respectively. In comparison, the onset of breakdown for quercetin is 420 °C.[152] DSC scans revealed a T_g of 118 °C and 124 °C for the 8 and 13 kDa poly(3,7,4′-tribenzyl quercetin carbonate)s, respectively.

These transitions are comparable to that of poly(bisphenol A carbonate), which measured a T_g of 143°C.

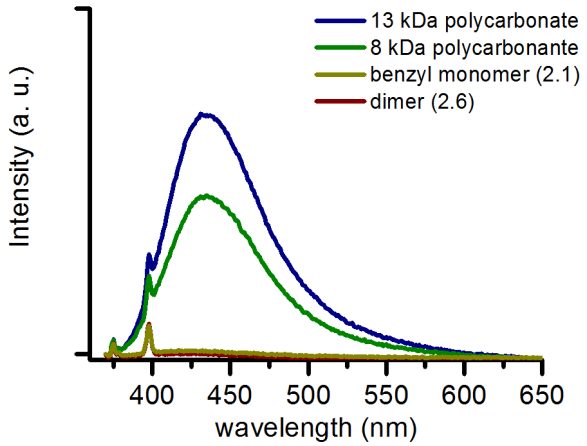

Figure 2.3 Emission spectra of the two different molecular weights of the polycarbonates and the small molecules, **2.1** and **2.6**.

Steady State Spectroscopy

Poly(3,7,4′-tribenzyl quercetin carbonate) expresses bright broad-band auto-fluorescence, visible by the eye at concentrations of less than 0.1 mg/mL. Steady state UV-vis and fluorescence spectroscopy were performed to assess the optical properties of this system. The absorbance was first measured, with log ε giving the same signal for

Table 2.1 Synthetic and thermal data for quercetin-based polycarbonates

	M_n (kDa)	**Đ**	**T_d (°C)**	**T_g (°C)**
2	8	1.6	261	118
3	13	1.3	285	124

the monomer and the polycarbonates, although the maxima were centered at 349 nm for the monomer and 330 nm for the polymers. Despite the similar absorbance properties of the monomer and polycarbonates, as seen in the emission spectra displayed in Figure 2.1, the polycarbonates fluoresce, while under the same conditions the monomer produced little emission. The synthesized model compounds also did not present a strong fluorescence under the conditions tested with the quercetin carbonate monomer and polymer.

Emission spectra from 350 nm excitation are presented for all species, and scaled relative to poly(3,7,4′-tribenzyl quercetin carbonate) to reflect the relative emissivities at similar subunit concentrations (1.67 x 10^{-5} M) and identical excitation-collection

Table 2.2 Photophysical properties of the quercetin-based polycarbonates.

	2.2	**2.3**
Abs_{max}	330	330
log ε	3.70	3.70
Fl_{max}[a]	424	425
Φ_{DMF}	0.83	0.87
Φ_{DCM}	0.38	0.41
$\Phi_{DCM/MeOH}$	0.65	0.97

[a]Fluorescence properties were taken at 1.67 x 10^{-5} M based on chromophore unit

regimes. Assessment of the quantum yield in the two solvents that the polycarbonates were apparently most soluble (DCM and DMF) showed low quantum yields (Table 2.1). The quantum yield was marginally higher for **2.3** than **2.2** for all solvent combinations. This result also indicates that the additional emission enhancement is associated with polymerization, though the exact mode of enhancement cannot be determined from emission intensity alone. In DMF, the quantum yield was twice as high as those measured in DCM. There was no notable fluorescence measured from the monomers or model compounds, therefore, the quantum yield was not recorded.

In an effort to further understand the fluorescence that resulted from polymerization, an aggregation-induced emission study was performed. The polymer was dissolved in DCM, followed by dilution with DCM and various volume percentages of methanol. Increasing the volume percentage of methanol from 0%-40% in increments of 10% resulted in an increase in fluorescence of 4.2 and 2.3 times for **2.2** and **2.3**, respectively at the corresponding emission maxima (Figure 2.2). In addition to the increase in intensity, the fluorescence peak broadened notably and the maximum of both **2.2** and **2.3** shifted from 424 to 433 nm upon increasing the volume percentage of methanol. The red shift is indicative of an increase in π-π stacking, possibly denoting an increase in aggregation of the polymer.

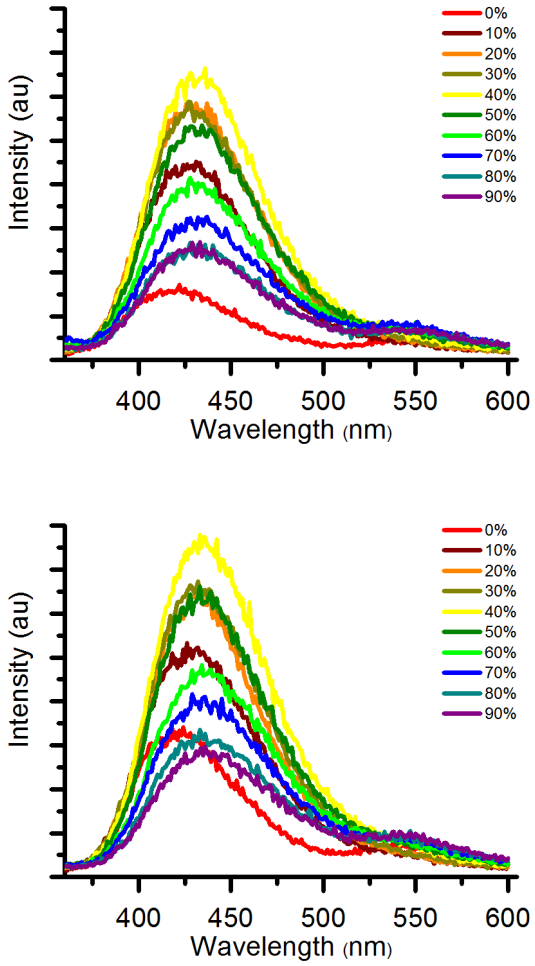

Figure 2.4 Aggregation induced emission study of the 8 kDa (top) and 13 kDa (bottom) polycarbonates.

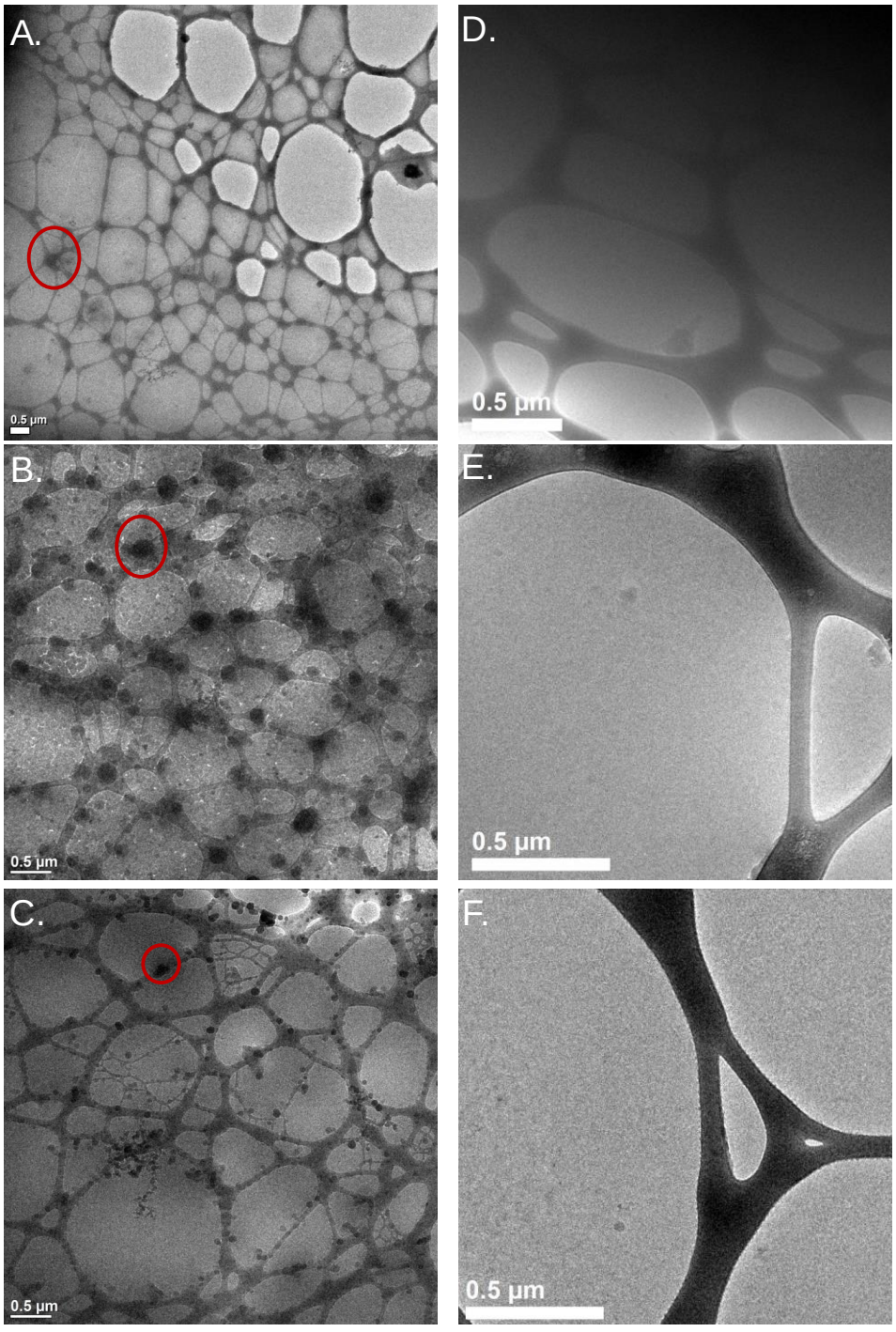

Figure 2.5 Cryo TEM images of polymer (**2.3**) in 0%, 20% and 40% solvent ratios of methanol in DCM (A-C) compared to the respective solvent ratios without polymers (D-F).

Preliminary results from cryo-TEM (Figure 2.3) images presented aggregation in the all tested solvent systems (0-40% methanol in DCM). This result further indicates the mechanism of fluorescence is through aggregation-induced emission. The quantum yield of both the polycarbonates were measured for the solvent combination yielding the highest fluorescence intensities (40:60 MeOH:DCM, Table 2.2). When the quantum yield of the quercetin-based polycarbonates in 40% methanol and DCM were compared to those measured in pure DCM, the quantum yields increased for both molecular weights, however **2.3** was determined to have a quantum yield that is 2.4 times higher. The addition of the poor solvent induces greater aggregation, resulting in closer molecular chains, which allows for an increase in fluorescence.

Aggregation-induced Emission Calculations

Upon the addition of methanol to the polycarbonate that is dissolved in dichloromethane, aggregation was induced, as observed in the cryo-TEM images. As aggregation occurred, the monomers were driven closer together, allowing for an increase in π-π stacking and a corresponding increase in fluorescence and add stabilization to the aggregate. To study effects of π-π stacking, it was important to consider that, when polymerized, the monomers can assemble in a tail-to-tail (**2.6**), head-to-head (**2.8**), or head-to-tail (**2.7**) or fashion, which was modeled using the two-layer ONIOM(M06-2X/6-31+G*:UFF) method to assist in explaining the aggregation-induced emission. Using the dimer for each regiochemistry, tail-to-tail (**2.6**), head-to-head (**2.7**) or tail-to-tail (**2.8**), the calculations showed that the π-π stacking had a strong

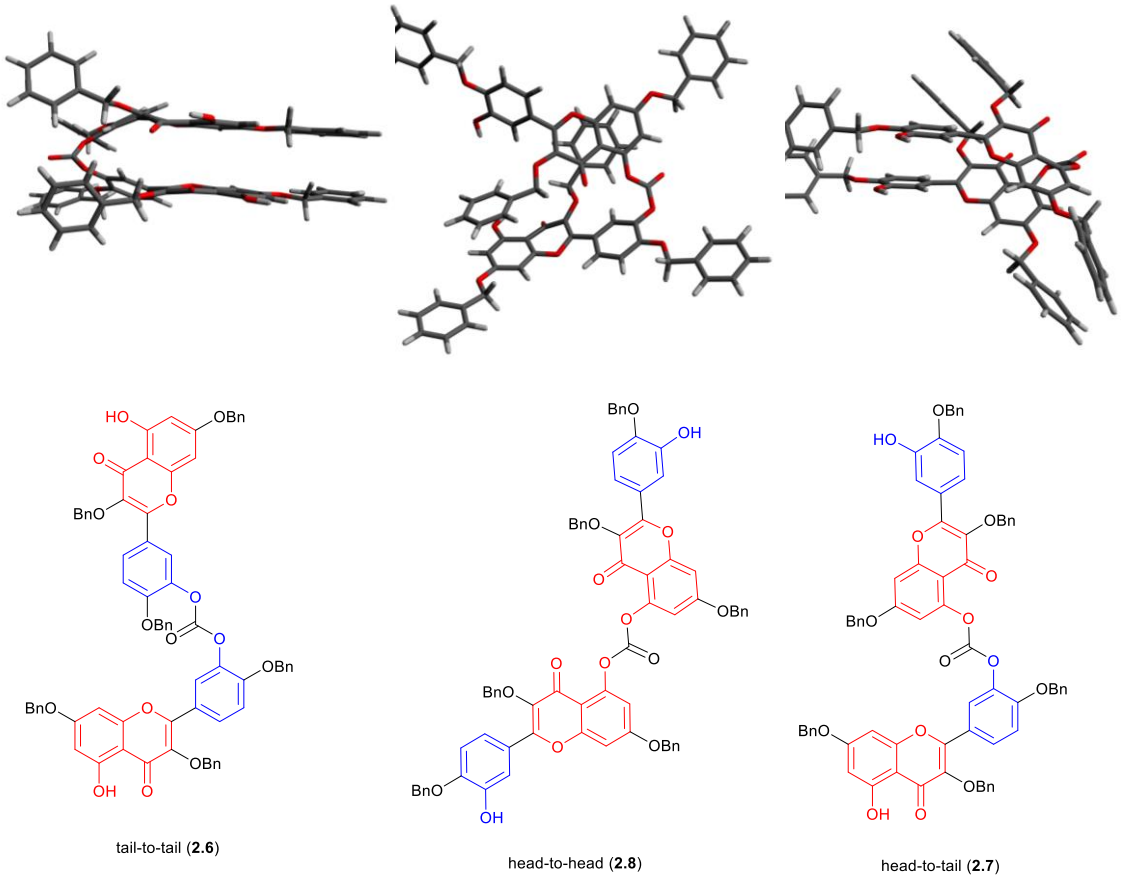

Figure 2.6 Structure and optimized geometry of the tail-to-tail (**2.6**), head-to-head (**2.7**) and head-to-tail (**2.8**) dimers of **2.1**.

dependence on the regiochemistry. Only the tail-to-tail configuration had the capability to π-π stack in the lowest energy conformation (0.44 kcal/mol) and was more stable than without the π-π stacking. The two benzopyran rings are horizontally off by 1.2 Å and have a vertical distance: 3.3 Å (Figure 2.4). Typical distance between π-π stacking is around 3.3–3.8 Å. In the lowest energy conformation for the head-to-tail dimer, the stacked conformation was found to be the more stable by 5.4 kcal/mol, but the two benzopyran rings are not aligned in parallel with a vertical distance outside of the range

of π-π stacking (2.7–4.2 Å). Unstacked conformation was found to be the most stable conformer for the head-to-head dimer, with no stacked conformation found as a local minimum. Condensation polymerization of the monomer does not have any control over the ratio of the regiochemistries in the polycarbonate, therefore; the mixture of regiochemistries, taken together with the model showing only the tail-to-tail configuration to yield energentically favorable π-π stacking, offers and explanation for explains the low quantum yields measured experimentally.

Solid State Fluorescence and Lifetime

While many fluorescent materials exhibit aggregation-induced quenching as a solid, AIEgens tend to exhibit a strong fluorescence.[53] The solid state allows for an increase in intermolecular interactions such as π-π stacking, therefore the solid state fluorescence of the polycarbonates was investigated. In these experiments, films were prepared by drop-casting a polymer solution (*ca.* 1 mg/mL) from DCM onto a glass slide then heated to 40 °C for 1 h to remove DCM. The films were excited with a 405 nm laser and exhibited a maximum centered at 540 nm (Figure 2.5) for both polycarbonates. The polycarbonate solid films emit strongly and uniformly, as observed in dark field and fluorescence micrographs. When compared to the dark field images, the fluorescence images showed the polymers to fluoresce in all regions of the film. When comparing the intensity of the films, **2.3** emitted more intensely than **2.2**.

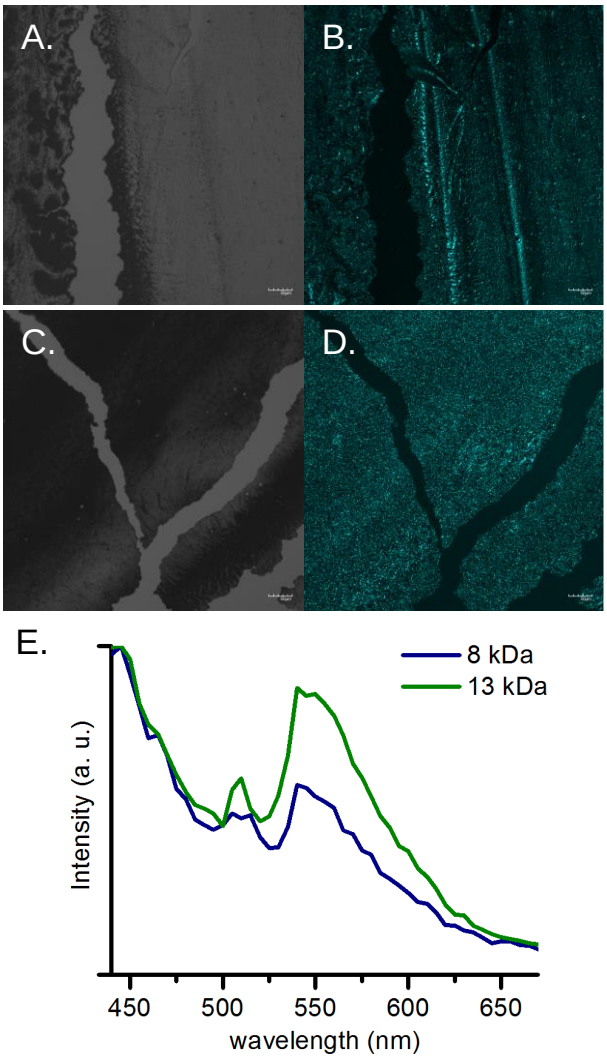

Figure 2.7 Dark field images (A and C) and fluorescent images (B and D) of film cast of **2.2** and **2.3**, respectively as well as the solid state fluorescence spectra of the films (E).

The lifetimes of the films were also measured from the same drop-casting method and measured by FLIM. The samples were imaged by repeatedly scanning frames until an average of 50 photon counts were measured per pixel. FLIM analysis in

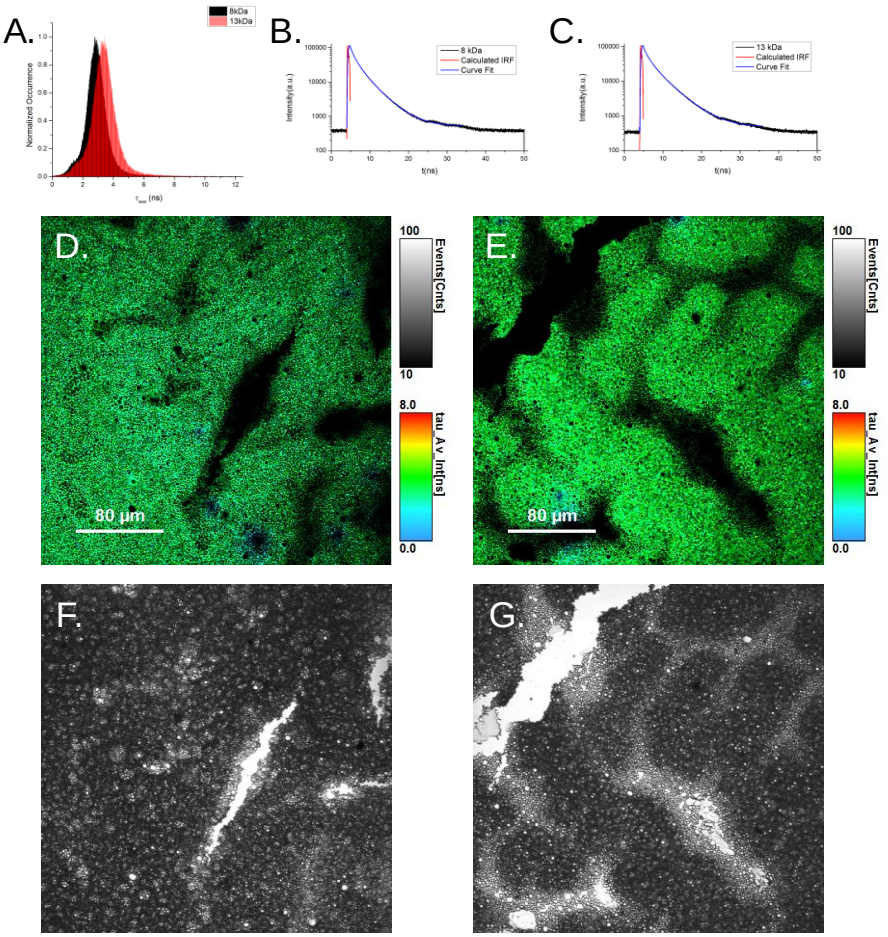

Figure 2.8 FLIM data of the fluorescence lifetime distributions (A), decay profiles (B-C), FLIM images (D-E) and dark field images (F-G.) of the reported polycarbonates.

SymphoTime revealed mono-modal fluorescence lifetime distributions over the entire fields of view (Figure 2.8A). The 13 kDa polymer (**2.3**) exhibited an average lifetime peak that was slightly higher than that of the 8 kDa polymer (**2.2**) (3.4 ns *vs.* 2.8 ns respectively). Curve fitting of the time-resolved lifetime decay profiles for both polymers (Figure 2.8B, C) identified three exponential lifetime parameters with similar associated lifetimes for both polycarbonates: $\tau_1 \approx 4.7$ ns, $\tau_2 \approx 1.7$ ns, and $\tau_3 \approx 0.5$ ns. The reconvolution curve fits were then computed pixel-by-pixel to generate the final FLIMs

(Figure 2.8). These FLIMs suggest a homogeneous distribution of the fluorescence lifetime over the surface of these polymers.

2.5 Conclusions

A natural product-based polycarbonate material, poly(3,7,4′-tribenzylquercetin carbonate) derived from quercetin, was synthesized. On polymerization, this system exhibited the fortuitous property of being highly auto-fluorescent. Comparisons with its monomer precursor and model compounds indicated that the properties were unique to the polymeric structure. Further exploration through experimental fluorescence studies and computation analysis of the properties indicated the fluorescence mechanism was aggregation-induced emission. Though the addition of a poor solvent to the polycarbonates, the emission increased *ca.* 2-4 times. Future work on this system and its derivatives will focus on applying the developed AIE polycarbonates towards familiar applications for these types of materials, such as an explosive detection or chemical sensing. Additionally, the natural product-based character of the materials suggests their potential in biomedical applications, such as biosensors.

CHAPTER III

FLAVONOID-BASED POLYCARBONATES APPLIED TOWARDS SELF-REPORTING, FLUORESCENT NANOSTRUCTURES FROM THE NATURAL PRODUCT QUERCETIN

3.1 Overview

The synthesis of fluorescent micelles from poly(3,7,4'-tribenzylquercetin-*co*-3,7,4'-tripropargylquercetin-*g*-polyethylene glycol) is reported herein. Two quercetin-based monomers were synthesized and copolymerized with a phosgene analogue to afford a polycarbonate. The propargyl moieties were functionalized with various percentages of polyethylene glycol. The thermal properties were compared and found to have a range of T_g and T_m values. The graft copolymers were then assembled into micelle structures. The micelles exhibited different sizes and fluorescent properties were dependent on the grafting density. The micelles were found to be noncytotoxic when compared to MC3T3 and SJSA cell lines. Overall, micelles with a natural product-based core and biocompatible hydrophobic block were developed and analyzed for their fluorescent and biocompatibility properties.

3.2 Introduction

There has been an increasing interest in polymeric nanostructures designed for biomedical application of drug delivery and diagnostic tools.[153] Well-designed materials are able to deliver cargo as well as incorporate beneficial properties such as labeling and/or target moieties.[61, 154] The monomeric unit within the backbone of polymeric

nanostructures is very broad and has, in recent past, been incorporating natural products into supramolecular architectures such as nanoparticles[155] and vesicles.[156] Building blocks such as sugars[10, 157-158] and ferulic acid[18] are some examples of natural products that have been included in polymeric architectures. Expansion of bio-based materials incorporated within supramolecular architectures will allow for drug delivery systems to expand the capabilities of the systems.

One important property in many polymeric nanostructures is fluorescence labeling for imaging in cells. Popular methods of labeling include covalent or physical absorption but if inefficient attachment occurs the fluorescent signal can differ.[74] Aggregation-induced emission (AIE) luminophores have the potential to avoid complicated labeling methods. AIE is the manifestation of emission from a non-emissive compound due to an aggregated state.[53] Through the assembly of various architectures of copolymers with AIEgens, in the backbone or as a side-chain, built in fluorescence can be "turned-on" resulting in fluorescent particles without a traditional dye.[159] The combination of properties from a natural product-based monomer with AIE properties would be advantageous as drug delivery vehicle.

This research entails the design and synthesis of a tunable micelle platform based on the natural product, quercetin. Quercetin-based monomers were synthesized and copolymerized with a phosgene analogue to afford a polycarbonate. Utilizing the propargylic functionalities installed on one of the quercetin monomers, an azide-alkyne Huisgen cycloaddition was performed with azide terminated PEG in different ratios to afford graft copolymers that were assembled into micelles. The size and emission of the

particles change with different grafting densities. Motivation for the synthesis of the natural product-based micelles were to design a material which has the potential to be a tunable, inherently fluorescent, biocompatible system for applications in drug delivery.

3.3 Experimental

Materials

Quercetin was purchased from Cayman Chemical or Stanford Chemical. Sodium carbonate, dimethylformamide (DMF, DriSolv) and dichloromethane (DCM, DriSolv) were purchased from EMD Millipore. Tetrahydrofuran was dried through solvent purification system (J. C. Meyer Solvent Systems, Inc., Laguna Beach, CA). Triethylamine and pyridine were purchased from Sigma-Aldrich and freshly distilled over CaH_2. Diphosgene was purchased from either Sigma-Aldrich or Alfa Aesar. α-Methoxy-ω-azido PEG-2k was purchased from RAPP POLYMERE (Tuebingen, Germany). Spectra/Por dialysis membranes (MWCO 12-14 kDa) were purchased from Spectrum Laboratories, Inc. (Rancho Dominguez, CA). Nanopure water (18 MΩ·cm) was acquired by means of a Milli-Q water filtration system, Millipore Corp. (Bedford, MA). All other reagents were purchased from Sigma-Aldrich. All reagents were used as received unless otherwise noted.

Characterization

^{1}H and ^{13}C NMR spectra were recorded on a Varian 500 MHz spectrometer interfaced to a UNIX computer using Mercury software. Monomers were purified by Medium Pressure Liquid Chromatography (MPLC) using a CombiFlash R_f (Teledyne Isco). Chemical shifts were referenced to the solvent proton resonance. The DMF gel

permeation chromatography (GPC) was conducted on a Waters Chromatography, Inc. (Milford, MA) system equipped with an isocratic pump model 1515, a differential refractometer model 2414, and a four-column set of 5 μm Guard (50 × 7.5 mm), Styragel HR 4 5 μm DMF (300 × 7.5 mm), Styragel HR 4E 5 μm DMF (300 × 7.5 mm), and Styragel HR 2 5 μm DMF (300 × 7.5 mm). The system was equilibrated at 70 °C in pre-filtered DMF containing 0.05 M LiBr, which served as polymer solvent and eluent (flow rate set to 1.00 mL/min). Polymer solutions were prepared at a concentration of *ca.* 5 mg/mL and an injection volume of 200 μL was used. Data collection and analysis were performed with Empower 2 v. 6.10.01.00 software (Waters, Inc.). The system was calibrated with S3 polystyrene standards (Polymer Laboratories, Amherst, MA) ranging from 615 to 442,800 Da. IR spectra were obtained on a Shimadzu IR Prestige Attenuated Total Reflectance Fourier-transform Infrared Spectrometer (ATR-FTIR). Spectra were analyzed using IRsolution software package (Shimadzu).

Differential scanning calorimetric (DSC) studies were performed on a DSC822^e (Mettler-Toledo), with a heating rate of 10 ºC/min to determine the melting point (m.p.) of the model compounds and the monomer as well as the glass transition (T_g) of the polymers. The T_g was taken as the midpoint of the inflection tangent upon the third heating scan. Thermogravimetric analysis was performed under Ar atmosphere using a model TGA/DSC 1 Star^e system (Mettler-Toledo), with a heating rate of 10 ºC/min. Measurements were analyzed using Star^e software version 10.00d (Mettler-Toledo).

All steady-state emission, excitation, and anisotropy spectra were obtained with a Horiba FluoroMax4 with automatic polarizers. Steady-state spectra were analyzed in

FluorEssence (Horiba, Kyoto, Japan) and in Origin 9.0 Pro (Origin Lab, Northampton, MA). Time-correlated single-photon counting (TCSPC) was employed to obtain all fluorescence lifetime and fluorescence anisotropy decay spectra. Measurements were achieved *via* a Fluorotime 100 fluorometer with a 640 nm solid-state picoseconds diode laser source (PicoQuant, West Springfield, MA) in matched quartz 0.7 mL cells (NSGPrecision Cells, Farmingdale, NY). Instrument response functions (IRF) were determined from the scattering signal with a solution of Ludox HS-40 colloidal silica (0.01% w/w particles in water). TCSPC analysis was performed on Fluorofit (PicoQuant) software and confirmed by tail-fitting in Origin 9 Pro. All fluorescence confocal microscopy was carried out on a FV1000 confocal microscope with an IX-81 inverted base (Olympus, Center Valley, PA) and PMT detectors. Dynamic light scattering (DLS) measurements were conducted using a Delsa Nano C (Beckman Coulter, Fullerton, CA) instrument equipped with a laser at 405 nm. Size measurements were made in nanopure water ($n = 1.3329$, $\eta = 0.890$ cP at 25 ± 1 °C). Scattered light was detected at a 165° angle and analyzed using a log correlator over 70 accumulations for a sample in a plastic cuvette (1 mL). The photomultiplier aperture and the attenuator were automatically adjusted to obtain a photon counting rate of *ca.* 10 kcps. Calculations of the particle size distribution and distribution averages were performed using CONTIN particle size distribution analysis routines. The peak averages of histograms from number distributions out of 70 accumulations were reported as the average diameters of the particles.

Transmission electron microscopy (TEM) images were collected on a JEOL 1200EX operating at 100 kV and micrographs were recorded at calibrated magnifications using a SIA-15C CCD camera. The samples as aqueous solutions (4 μL) were deposited onto carbon-coated copper grids, and after 1 min, the excess of the solution was quickly wicked away by a piece of filter paper. A drop of 1 wt% uranyl acetate was then added, and allowed to stand for 30 s before excess stain was wicked away. The grids were allowed to dry for serveral hours.

Synthesis

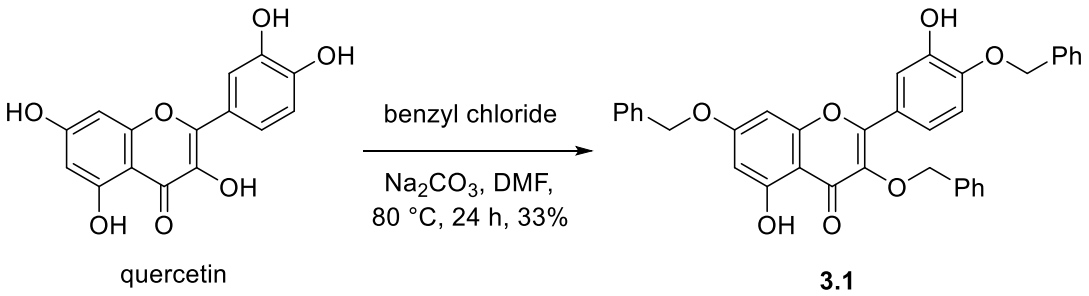

Scheme 3.1 Synthesis of **3.1**.

Synthesis 3,7,4'-tribenzylquercetin, **3.1**

The monomer was prepared by a procedure that was adapted from Hua *et al.*[149] A round bottom flask was charged with quercetin (20.0 g, 66.2 mmol), sodium carbonate (21.4 g, 202 mmol), benzyl chloride (23.8 mL, 207 mmol) and DMF (500 mL) under nitrogen. The reaction was stirred at 80 °C for 24 h and the DMF was then removed *in vacuo*, resulting in a brown solid product. The brown solid was purified by Medium Pressure Liquid Chromatography (MPLC) eluted with a 20% acetone in toluene, and recrystallized from toluene to afford a yellow solid (12.4 g, 32.7% yield, 3,7,4'-

tribenzylquercetin). ^{1}H NMR (DMSO-d_6, ppm): δ 5.03 (s, 2H, -CH_2), 5.23 (s, 2H, -CH_2), 6.81 (d, *J* = 2.5 Hz, 1H, Ar), 6.49 (d, *J* = 2.5 Hz, 1H, Ar), 7.21-7.49 (m, 16H, Ar), 7.65 (dd, *J* = 2.3, 8.5 Hz, Ar, 1H,), 7.76 (d, *J* = 2 Hz, 1H, Ar), 9.50 (s, 1H, -OH), 12.69 (s, 1H, -OH). ^{13}C NMR (126 MHz, DMSO-d_6): δ 178.59, 164.62, 161.46, 156.85, 156.74, 149.66, 147.06, 137.25, 136.95, 136.55, 129.36, 129.00, 128.86, 128.66, 128.60, 128.56, 128.34, 128.32, 128.21, 125.77, 122.94, 121.00, 116.12, 113.80, 105.80, 98.94, 93.61, 73.82, 70.46, 70.15. FTIR (ATR) 3235, 3026, 2876, 1651, 1601, 1574, 1512, 1489, 1452, 1371, 1348, 1278, 1217, 1193, 1163, 1139, 1121, 1003, 954, 825, 802 cm^{-1}. HRMS (ESI+, *m/z*): $[M+H]^{+1}$ calculated for $C_{36}H_{28}O_7$, 573.1913, actual 573.1941.

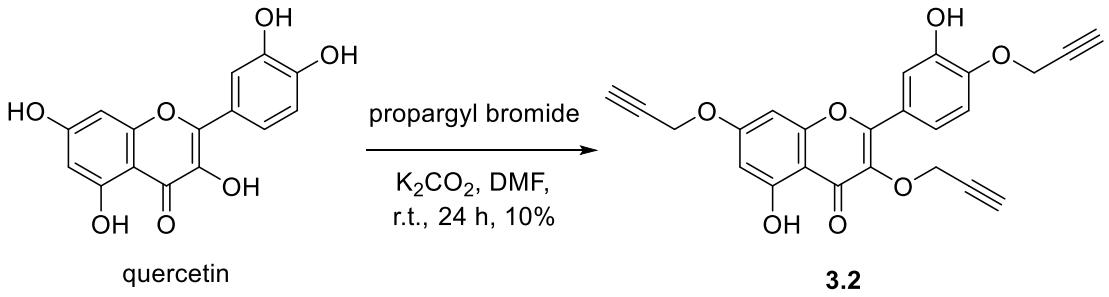

Scheme 3.2 Synthesis of **3.2**.

Synthesis 3,7,4'-tripropargylquercetin, **3.2**

A round bottom flask was charged with quercetin (1.00 g, 3.31 mmol), potassium carbonate (0.620 g, 4.49 mmol), and DMF (25 mL) under nitrogen. Propargyl bromide (80 wt% in toluene) (0.450 mL, 4.04 mmol) was added dropwise to the mixture. The reaction was stirred at room temperature for 24 h and the DMF was then removed *in vacuo*, resulting in a brown solid product. The brown solid was purified by Medium Pressure Liquid Chromatography (MPLC) eluted with a 20% acetone in hexanes to

afford a yellow solid, 3,7,4'-tripropargylquercetin (135 mg, 10% yield). ^{1}H NMR (500 MHz, DMSO-*d6*) δ 3.53 (s, 1H), 3.64 (s, 1H), 3.69 (s, 1H), 4.92 (d, *J* = 2.2 Hz, 4H), 4.96 (d, *J* = 2.3 Hz, 2H), 6.46 (d, *J* = 2.2 Hz, 1H), 6.80 (d, *J* = 2.2 Hz, 1H), 7.17 (d, *J* = 9.4 Hz, 1H), 7.61 (d, *J* = 1.8 Hz, 2H), 9.59 (s, 1H), 12.50 (s, 1H). ^{13}C NMR (126 MHz, dmso) δ 177.94, 163.08, 160.89, 156.52, 156.10, 148.14, 146.66, 135.65, 123.03, 120.54, 115.88, 113.69, 105.36, 98.57, 93.37, 79.54, 79.13, 79.03, 78.70, 78.55, 78.38, 58.99, 56.31, 56.01.

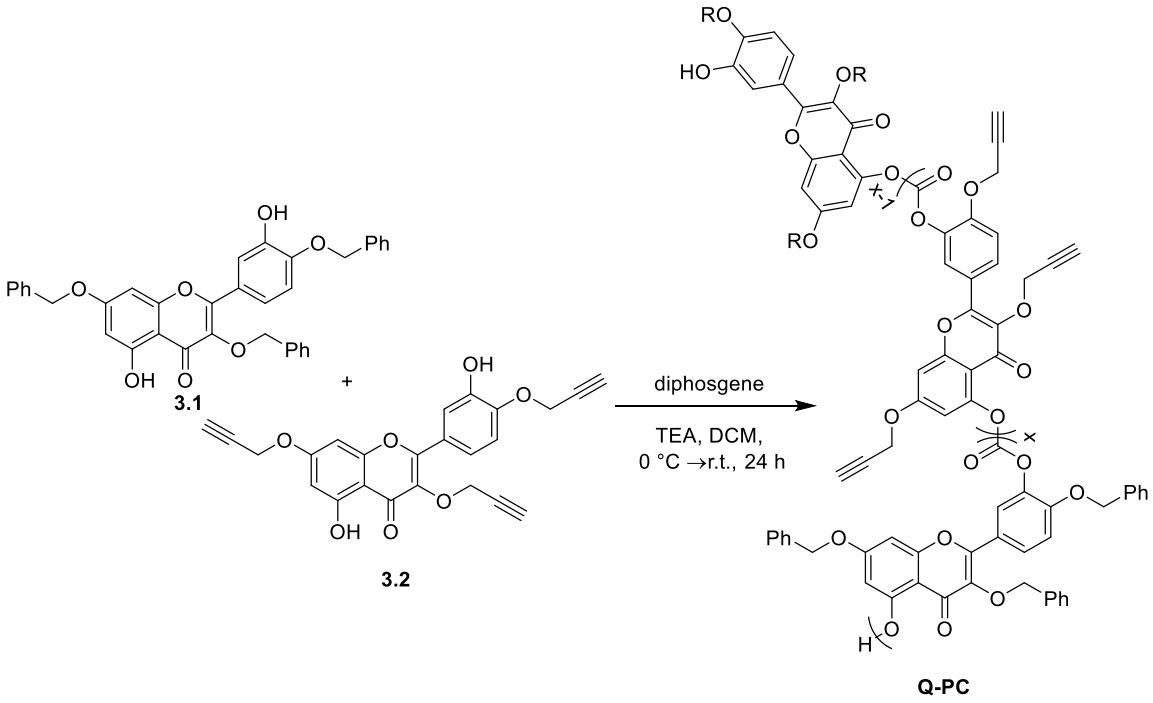

Scheme 3.3 Synthesis of polycarbonate, **Q-PC**.

Synthesis poly (3,7,4'-tribenzylquercetin-*co*-3,7,4'-tripropargylquercetin carbonate)

In a Schlenk flask under N_2, 3,7,4′-tribenzylquercetin (70.2 mg, 0.123 mmol), 3,7,4′-tripropargylquercetin, (21.2 mg, 0.0509 mmol), triethylamine (75.0 μL, 0.538 mmol) and DCM (0.84 mL) were combined. At 0 °C, diphosgene (11 μL, 0.092 mmol) was added dropwise. The solution was allowed to stir at room temperature for 24 h. The polymerization was quenched with saturated sodium bicarbonate solution. The polymer product was isolated by diluting in DCM (7 mL) and washing with H_2O (10 mL x 2) followed by precipitation in cold methanol (40 mL x 2) and cold acetone (40 mL x 2). The polymer was dried *in vacuo* to afford, poly(3,7,4′-tribenzylquercetin-*co*-3,7,4′-tripropargylquercetin carbonate). ^{1}H NMR (Chloroform-d, ppm, 500 MHz) δ 2.45 – 2.67 (m, 0.56H), 4.54 – 5.00 (m, 2.67H), 5.00 – 5.32 (m, 6.00H), 6.63 – 7.28 (m, 9.34H), 7.28 – 7.53 (m, 9.78H), 7.65 – 8.03 (m, 1.54H), 8.01 – 8.40 (m, 0.34H).GPC (DMF): M_n = 8.8 kDa, Đ = 1.4 Ratio: 10:4, Benzyl:Propargyl (calculated by NMR) T_d = 284 °C, T_g = 138 °C

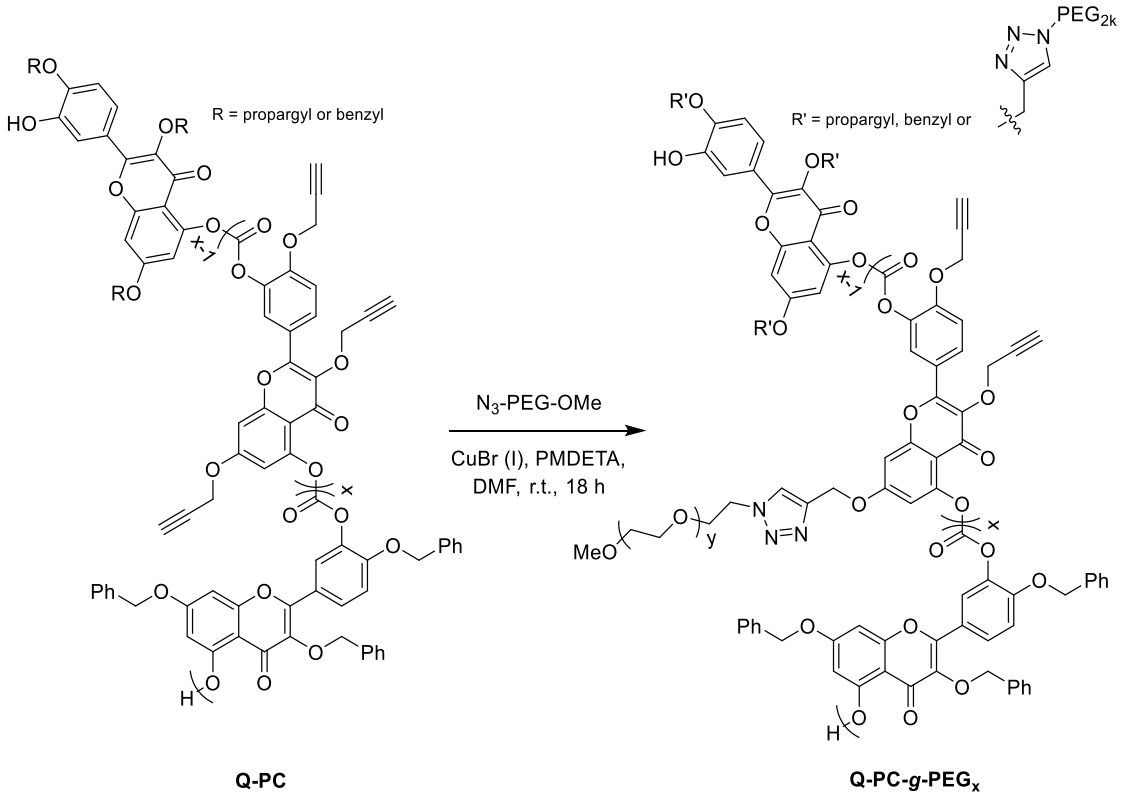

Scheme 3.4 Synthesis of the graft copolymers, **Q-PC-*g*-PEG$_x$**.

General procedure for the synthesis poly (3,7,4'-tribenzylquercetin-*co*-3,7,4'-tripropargylquercetin carbonate-*g*-poly ethylene glycol)

In a Schlenk flask, poly(3,7,4′-tribenzylquercetin-*co*-3,7,4′-propargylquercetin carbonate) (8.4 kDa, 50.0 mg), PEG (2 kDa, 50.1-230.0 mg), and PMDETA (25.0 µL, 0.120 mmol) were combined in DMF under N_2. The freeze-pump-thaw method was applied (x3) followed by the addition of CuBr (12.5 mg, 87.3 mmol) and another round of freeze-pump-thaw (x2). The reaction was allowed to occur over 18 h at r.t. A Sephadex column was used to remove the remaining CuBr. The solution was subsequently dialyzed against nanopure water with Chelex® 100 Resin for 1 d followed

by 2 d against pure nanopure water in presoaked dialysis tubing (MWCO *ca*. 12–14 kDa) for 1 d DMF and residual copper. The resultant polymer was dried by lyophilization to afford a yellow powder.

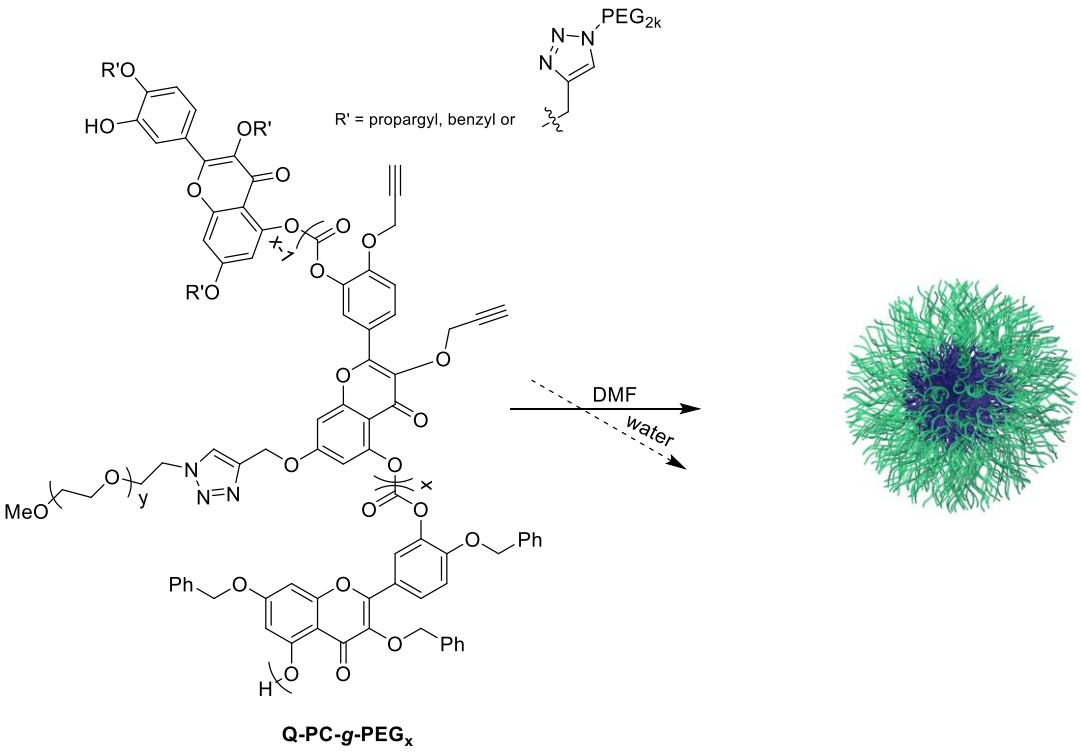

Scheme 3.5 Synthesis of micelles from the amphiphilic quercetin-based polymer

Synthesis of poly(3,7,4′-tribenzylquercetin-*co*-3,7,4′-propargylquercetin carbonate)-*g*-PEG_{2kDa} micelles

In a vial 10.0 mg of poly(3,7,4′-tribenzylquercetin-*co*-3,7,4′-tripropargylquercetin carbonate)-*g*-PEG_{2kDa} was dissolved in DMF (2.0 mL). Nanopure water (5.0 mL) was added over 30 min. The solution was subsequently dialyzed against

nanopure water in presoaked dialysis tubing (MWCO *ca.* 12–14 kDa) for 3 d to remove DMF. The solution was diluted to a concentration of 1 mg/mL for DLS measurements.

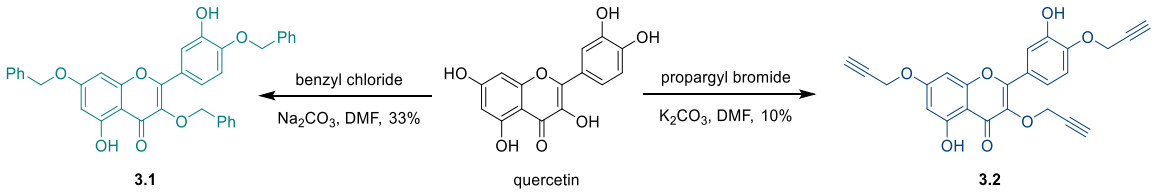

Scheme 3.6 The synthesis of the comonomers **3.1** and **3.2**.

3.4 Results and Discussion

Synthesis and Characterization of Monomers, Copolymers and Micelles

Building on the synthesis of the previously reported fluorescent, poly(3,7,4'-tribenzylquercetin carbonate), the assembly of micelles was attempted through the synthesis of an amphiphilic graph copolymer. To later incorporate a hydrophilic block, 3,7,4'-tripropargylquercetin was synthesized as a comonomer. Briefly, quercetin and potassium carbonate were dissolved in DMF under N_2. Propargyl bromide (80 wt% in toluene) was added dropwise and the reaction was allowed to proceed over 24 h. The solvent was removed *in vacuo* followed by purification by column chromatography to afford a yellow powder in poor isolated yield due to the difficult separation between the bi-, tri- and tetra- functionalized quercetin molecules.

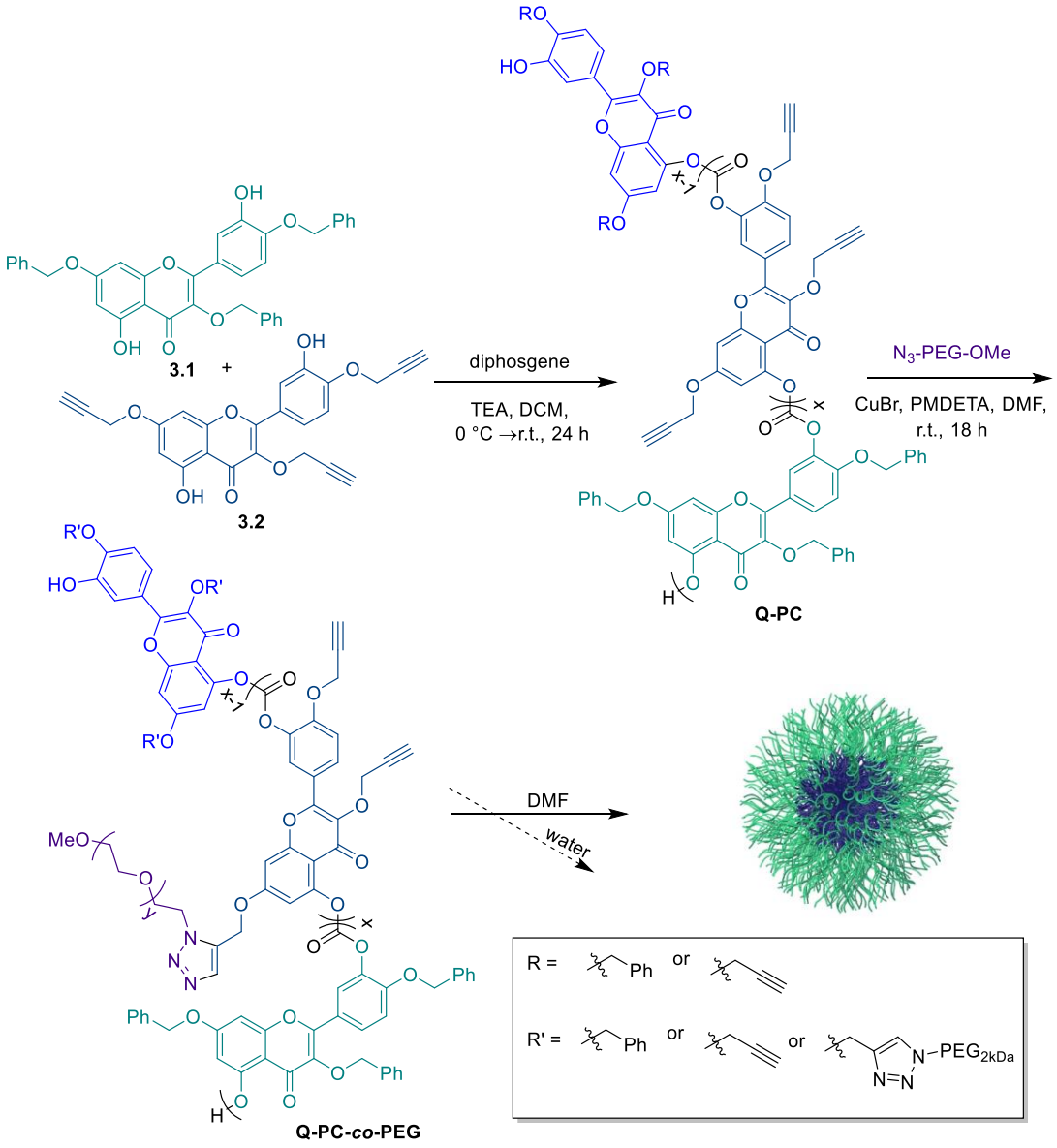

Scheme 3.7 Synthesis of **Q-PC**, grafting of PEG and self-assembly of the quercetin-based micelles.

With the two quercetin-based monomers in hand, copolymerization was attempted. Polymerization under conditions similar to the previously reported poly(3,7,4'-tribenzylquercetin carbonate), yielded low incorporation of **3.2** (Table 3.1, Entry 1). The general procedure, the two quercetin-based monomers in the desired ratio

were dissolved in a solvent (*i.e.* pyridine or DCM) under N_2. Triethylamine was added and the monomers were allowed to dissolve. The mixture was then cooled to 0 ºC followed by the dropwise addition of diphosgene. The reaction mixture was warmed to room temperature and allow to react for a predetermined amount of time. The reaction was quench by the addition of a saturated sodium bicarbonate solution (~3mL) followed by the addition of DCM to dissolve the resultant solids. An extraction of the biphasic mixture and wash of the organic layer followed. The organic layer was precipitated into cold methanol (3 x 40 mL) afforded the polymer as a yellow solid. Targeting 10% incorporation of **3.2**, resulted in ≥0.5 monomer per **3.1** which in less than one propargyl unit per polymer chain (Table 3.1, Entry 1). Increasing the reaction time or ratio of **3.2** to **3.1** resulted in similar results to the first attempted results (Table 3.1, Entries 2-3). Changing the solvent from pyridine to DCM considerably changed the ratio of the monomers to afford a 10:4 ratio of **3.1**:**3.2** incorporated into the polycarbonate (**Q-PC**) characterized by ^{1}H NMR, comparing the benzylic to propargylic protons as well as by comparing the benzylic to alkyne protons (Table 3.1, Entry 4). The polycarbonate was also characterized by ^{13}C NMR, SEC (DMF) and IR. The reaction was repeated several times and the products were combined to afford ~1 g of material for future studies.

Table 3.1 Effects of solvent on copolymerization of **3.1** and **3.2.**

Entry	Monomer Feed Ratio (3.1:3.2)	Monomer Added Ratio (3.1:3.2)	Time (h)	Solvent	M_n (kDa)	Đ
1	10:1	10:0.4	24	pyridine	10.0	1.5
2	10:1	10:0.5	72	pyridine	7.0	1.5
3	10:3	10:0.3	24	pyridine	9.0	1.5
4	10:3	10:4	24	DCM	8.8	1.4

Post-polymerization various ratios of poly(ethylene glycol) (2 kDa) were clicked onto the macromolecule using azide-alkyne chemistry to introduce a hydrophilic block for self-assembly. The ratios were calculated from the number of alkyne moieties per polymer using the M_n determined by SEC. Generally, **Q-PC**, PEG and PMDETA were dissolved in DMF under N_2 in a Schlenk flask. The mixture was submitted to freeze-pump-thaw three times followed by the addition of CuBr and an additional two freeze-pump-thaw. The reaction was allowed to occur over 18 h at room temperature. The product was purified through a Sephadex column followed by dialyzed against nanopure water with Chelex® 100 Resin for 1 d then pure nanopure water in presoaked for 2 d in dialysis tubing (MWCO *ca*. 12–14 kDa). The product was dried by lyophilization to obtain the product as a yellow powder. The addition of 20%, 40%, 60% and 80% of PEG resulted in growth of the polymer 13.2 kDa-29.1 kDa (**Q-PC-*g*-PEG$_x$** x = percent functionalization). Upon addition of 100% of the functional group, the molecular weight did not increase beyond the molecular weight for **Q-PC-*g*-PEG$_{80}$**. The PEG grafted polymers were then assembled into supramolecular architectures through the dissolution

of the polymer in DMF into nanopure water. The five macromolecules were compared through thermal, fluorescence and imaging analysis.

Table 3.2 Synthesis and characterization of the quercetin-based graft copolymers.

Sample	**M_n (kDa)**	**Đ**	**$T_{d5\%}$ (°C)**	**T_m (°C)**	**T_g (°C)**	**D_{TEM} (nm)**
Q-PC	8.8	1.37	268	-	134	-
Q-PC-*g*-PEG$_{20}$	13.2	1.24	291	42	163	-
Q-PC-*g*-PEG$_{40}$	18.3	1.24	325	45	71	200
Q-PC-*g*-PEG$_{60}$	25.7	1.13	330	46	70	40-70
Q-PC-*g*-PEG$_{80}$	29.1	1.15	329	48	65	20-30

Micelle Size Analysis

The sizes of the micelles were analyzed by transition scanning microscopy (TEM). Samples solutions for analysis by TEM were prepared at a concentration of 1.0 mg/mL. **Q-PC-*g*-PEG$_{20}$** and **Q-PC-*g*-PEG$_{40}$** did not require staining, however, **Q-PC-*g*-PEG$_{60}$** and **Q-PC-*g*-PEG$_{80}$** were stained with uranyl acetate. By TEM, **Q-PC-*g*-PEG$_{20}$** showed two types of nanostructures, one is the big micelle which is *ca.* 200-300 nm, the other is small micelles which formed the network (precipitation) (Figure 3.3A). The network structure did not occur with **Q-PC-*g*-PEG$_{40}$** but the micelles were large (*ca.* 200 nm). **Q-PC-*g*-PEG$_{60}$** and **Q-PC-*g*-PEG$_{80}$** presented considerably smaller micelles, 40-70 and 20-30nm, respectively.

Thermal Characterization

The graft copolymers were characterized thermally by thermal gravimetric analysis (TGA) and differential scanning calorimetry (DSC). The measurements were obtained of the powder prior to assembly for the **Q-PC-*g*-PEG$_x$** series. The degradation temperatures ($T_{d5\%}$) of the polymers of **Q-PC** and **Q-PC-*g*-PEG$_{20}$** were both <300 ºC. The PEG has seemingly protected the **Q-PC** as the grafting density increases and the degradation and the $T_{d5\%}$ increase by ~40 ºC (Table 3.2). The T_m increased slightly with increasing grafting density and the T_g initially increased upon the addition of PEG then steadily decreased as more PEG was added.

Photophysical Characterization

Using the weighted average molecular weight for each repeat unit of the **Q-PC** segment of the micelles, the photophysical properties were explored. The absorbance was measured at a concentration of 0.187 mM in nanopure water at 340 nm. The absorbance coefficients were calculated (Table 3.3). **Q-PC-*g*-PEG$_{20}$** had a high absorbance coefficient while **Q-PC-*g*-PEG$_{40}$**- **Q-PC-*g*-PEG$_{80}$** were similar.

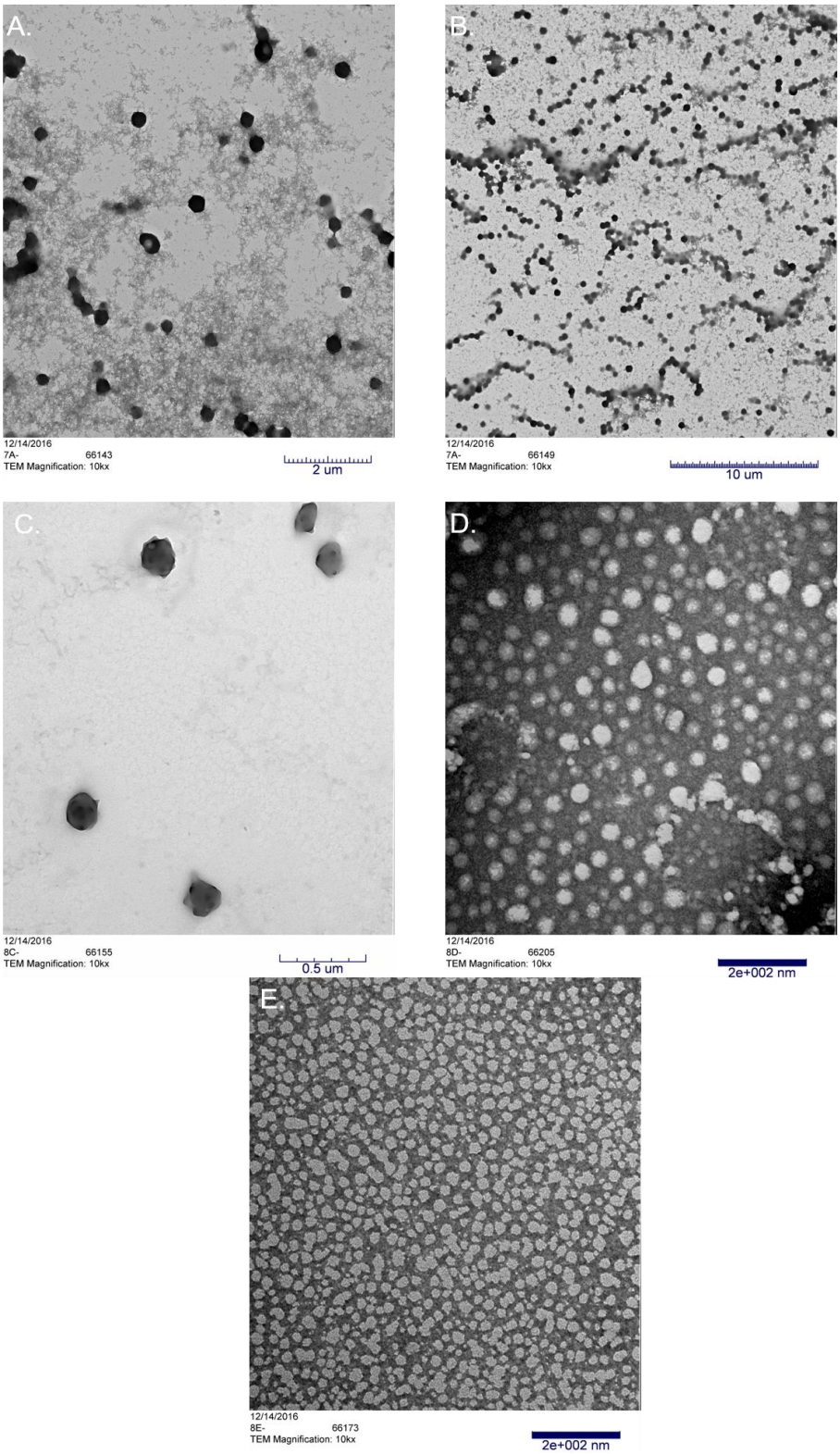

Figure 3.1 TEM images of various grafting densities of **Q-PC-*g*-PEG$_{20}$** (A and B), **Q-PC-*g*-PEG$_{40}$** (C), **Q-PC-*g*-PEG$_{60}$** (D) and **Q-PC-*g*-PEG$_{80}$** (E).

Table 3.3 Photophysical properties of the quercetin-based micelles.

Sample	log ε	λ_{em}^{max} (nm)	λ_{em}^{max2} (nm)
Q-PC-*g*-PEG$_{20}$	3.58	433	538
Q-PC-*g*-PEG$_{40}$	3.21	547	429
Q-PC-*g*-PEG$_{60}$	3.35	541	433
Q-PC-*g*-PEG$_{80}$	3.32	545	432

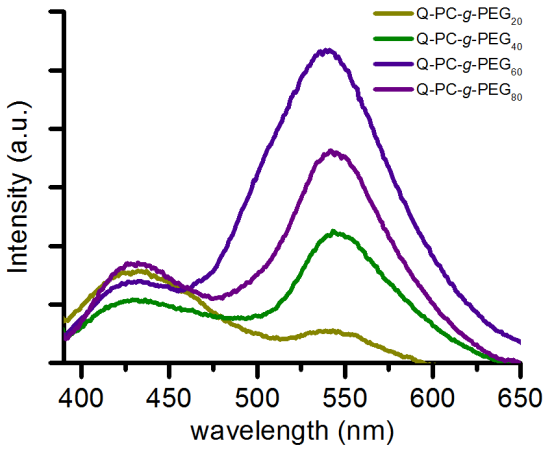

Figure 3.2 Emission spectra of the **Q-PC-*g*-PEG$_x$** micelles.

The fluorescence properties were evaluated at 0.0187 mM of chromophore in nanopure water. Emission was recorded at 340 nm. Although **Q-PC-*g*-PEG$_{20}$** did not assemble into micelles, it was soluble at the concentration which fluorescence was measured. It had an emission maximum of 433 nm and a shoulder centered at 538 nm. It is notable that there is a significant red shift in emission maximum (*ca.* 112 nm) on the

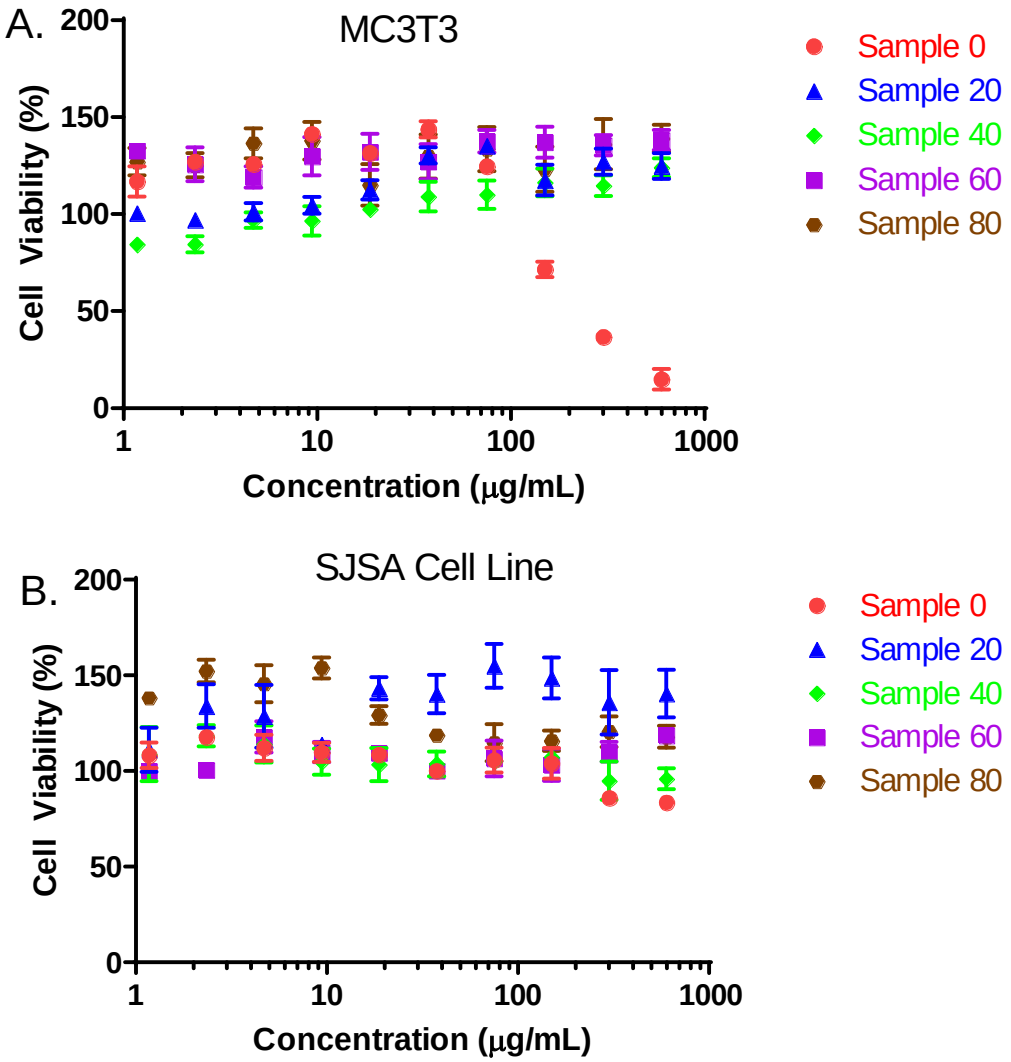

Figure 3.3 Cytotoxcitiy result of the quercetin-based polymers against MC3T3 and SJSA cells.

assembled micelles (Figure 3.1). The intensity increased from **Q-PC-*g*-PEG$_{40}$** to **Q-PC-*g*-PEG$_{60}$** and **Q-PC-*g*-PEG$_{80}$** decreased in intensity from **Q-PC-*g*-PEG$_{60}$**.

Cell Viability

With the intention of applying the quercetin-based micelles towards biomedical applications, a cytotoxicity study was performed against two cell lines. The MC3T3,

mouse healthy primary bone cells (preosteoblast) were tested with polymer concentrations of 1 ug/mL-1170 ug/mL. Although **Q-PC** showed cytotoxicity at concentrations of 600 μg/mL – 1170 μg/mL), **Q-PC-*g*-PEG$_{20}$** to **Q-PC-*g*-PEG$_{80}$** did not exhibit cytotoxicity in the measured concentration range (Figure 3.3). SJSA- The human osteosarcoma cancer cell line, SJSA was also tested against a polymer concentration range 1 μg/mL-1170 μg/mL. No cytotoxicity was observed for any of the synthesized polymers.

3.5 Conclusions

Overall, a series of quercetin-based micelles were synthesized. These macromolecular structures were compared by size as well as thermal and fluorescent properties. There was a decrease in size and T_g with an increase in grafting density. The cell viability was studied against MC3T3 and SJSA cell lines and the micellular structures were found to have no cytotoxicity in the measured range. The prepared micelles have the potential to be a self-reporting, drug delivery system.

CHAPTER IV

PROGRESS TOWARDS NATURAL PRODUCT-BASED, PLANT-DERIVED, MUSSEL-INSPIRED POLYCARBONATES FROM QUERCETIN AND LYSINE

4.1 Overview

The synthesis of poly(3',4'-diphenylmethylene ketal 3-propargyl quercetin-*co*-L-tyrosine-Nε-alloc-L-lysine-Fmoc-L-tyrosine methyl ester carbonate) is reported herein. With the goal of a quercetin-based polycarbonate with a free catechol, an initial survey of seven 3',4'-diphenylmethylene ketal 3-alkyl quercetin derivatives resulted in no homopolymerization. Upon consideration of beneficial comonomers, the addition of a lysine was proposed because it is important in the adhesive properties of mussel proteins. Retrosynthetic analysis of a tripeptide resulted in a synthetic route using a series of orthogonal protecting groups which included a protected lysine, the phenol groups of two tyrosines for copolymerization and a variety of protecting groups. Preliminary copolymerizations of the quercetin-based monomer with the tripeptide resulted in a polycarbonate with a molecular weight (M_n) of 10.9 kDa. Proposed deprotection of the resultant polycarbonate is anticipated to yield free lysines and catechols. Furthermore, the synthetic route developed herein is expected to be broadly applicable to generate tunable, biodegradable biomedical adhesives.

4.2 Introduction

Consequent to the discovery of adhesive properties in mussel, synthetic mussel-inspired materials have been widely studied. Initially, the Waite group found that adhesive mussel foot proteins contain a high quantity of 3,4-dihydroxyphenylalanine as well as lysine and 3- and 4-hydroxyproline.[92] Numerous subsequent studies have been performed correlating the presence of catechol groups (*ortho*-dihydroxybenzene) to adhesive properties of materials.[93] A transformative material in mussel-inspired adhesives was the synthesis of polydopamine[94] and the rapid production thereafter.[160] However, concerns such as oxidation[161] and incompatibility with biological substrates[162] among these materials has resulted in the continued search for adhesive materials with improved properties. Recent investigation into the catechol-lysine synergy showed that the presence of lysine in a scaffold alongside a catechol moiety greatly increases the adhesive properties of the materials.[95-96] Decreasing the complexity of mussel-inspired materials while integrating its key components is one strategy towards the establishment of synthetic materials that rival those found in nature.[163] Particularly, incorporation of lysine and catechol units have the potential to impart good adhesive properties to biomedical materials.

General surgical and wound-healing adhesives are based on non-natural and non-degradable cyanoacrylates, polyethylene glycol, and polyurethanes which have poor biocompatibility. Alternatively, bio-based adhesives, such as fibrin, gelatin, dextran and chitosan, are biocompatible, but lack good adhesive mechanical strength.[84] Bio-based adhesives also have the advantage of degradability, which allows for removal of the

material through a noninvasive method. In recent past, mussel-inspired materials have largely been applied as biomedical adhesives.[90-91, 164] In the interest of emulating advantageous properties of currently used bio-based adhesives, degradable systems utilizing natural products as the polymeric backbone, such as amino acid-based poly(ester urea) copolymers,[165] or biologically friendly materials, such as poly(ethylene glycol)[166] with catechol side-chains, have previously been synthesized. Many other natural product-based polymers have the potential to be used in adhesive materials, because upon degradation beneficial or binge products would be achieved.

Flavonoids are an underutilized class of natural product in polymer science. Many of these compounds have favorable biological properties including antioxidant, oncological therapeutic effects.[167] The general structure of flavonoids is a ($C_6C_3C_6$) core with a variety of functionalities incorporated, including a double bond and/or ketone on the heterocyclic rings and aromatic phenols.[168] The 3',4' catechol that occurs in compounds, such as quercetin, catechin and cyanidin have the potential be utilized as plant-derived mussel-inspired polymeric materials.

Herein, is described the synthesis of a quercetin and peptide-based polycarbonate. Initial investigation showed no evidence of homopolymerization for seven different synthesized 3',4'-diphenylmethylene ketal 3-alkyl quercetin monomers. When considering a beneficial comonomer, a protected tyrosine-lysine-tyrosine peptide was synthesized for copolymerization with a quercetin-based monomer. Preliminary results demonstrated the feasibility of the synthesis of the protected form of a quercetin-

based copolymer with a free catechol and a protected lysine unit, whereupon deprotection will allow for application as biomedical adhesives.

4.3 Experimental

Materials

Quercetin was purchased from Cayman Chemical or Stanford Chemical. Sodium carbonate, dimethylformamide (DMF, DriSolv) and dichloromethane (DCM, DriSolv) were purchased from EMD Millipore. Tetrahydrofuran was dried using a solvent purification system (J. C. Meyer Solvent Systems, Inc., Laguna Beach, CA). Triethylamine and pyridine were purchased from Sigma-Aldrich and freshly distilled over CaH_2. Diphosgene was purchased from either Sigma-Aldrich or Alfa Aesar. All other reagents were purchased from Chem-Impex International. All reagents were used as received unless otherwise noted.

Characterization

^{1}H and ^{13}C NMR spectra were recorded on a Varian 500 MHz spectrometer interfaced to a UNIX computer using VNMRj software. Monomers were purified by Medium Pressure Liquid Chromatography (MPLC) using a CombiFlash R_f (Teledyne Isco). Chemical shifts were referenced to the solvent proton resonance. The DMF gel permeation chromatography (GPC) was conducted on a Waters Chromatography, Inc. (Milford, MA) system equipped with an isocratic pump model 1515, a differential refractometer model 2414, and a four-column set of 5 μm Guard (50 × 7.5 mm), Styragel HR 4 5 μm DMF (300 × 7.5 mm), Styragel HR 4E 5 μm DMF (300 × 7.5 mm), and Styragel HR 2 5 μm DMF (300 × 7.5 mm).

The system was equilibrated at 70 °C in pre-filtered DMF containing 0.05 M LiBr, which served as polymer solvent and eluent (flow rate set to 1.00 mL/min). Polymer solutions were prepared at a concentration of *ca.* 5 mg/mL and an injection volume of 200 μL was used. Data collection and analysis were performed with Empower 2 v. 6.10.01.00 software (Waters, Inc.). The system was calibrated with S3 polystyrene standards (Polymer Laboratories, Amherst, MA) ranging from 615 to 442,800 Da. IR spectra were obtained on a Shimadzu IR Prestige Attenuated Total Reflectance Fourier-transform Infrared Spectrometer (ATR-FTIR). Spectra were analyzed using IRsolution software package (Shimadzu).

Differential scanning calorimetric (DSC) studies were performed on a DSC822^e (Mettler-Toledo), with a heating and cooling rate of 10 ºC/min to determine the melting point (m.p.) of the model compounds and the monomer, as well as the glass transition (T_g) of the polymers. The T_g was taken as the midpoint of the inflection tangent upon the third heating scan. Thermogravimetric analysis

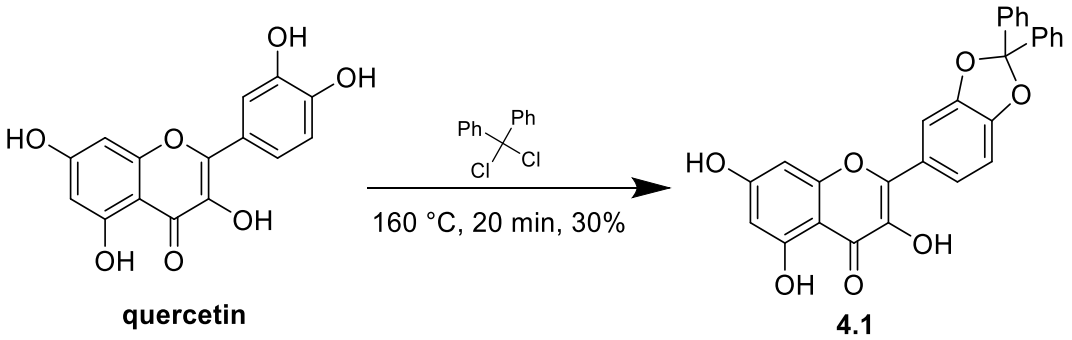

Scheme 4.1 Synthesis of **4.1**.

was performed under Ar atmosphere using a model TGA/DSC 1 Star^e system (Mettler-Toledo), with a heating rate of 10 ºC/min. Measurements were analyzed using Star^e software version 10.00d (Mettler-Toledo).

Synthesis 3',4'-diphenylmethylene ketal quercetin, **4.1**

Into a two-necked round bottom flask, quercetin (2.00 g, 6.62 mmol) and dichlorodiphenylmethane (3.40 mL, 19.1 mmol) were combined under N_2, and heated for 20 min at 160 ºC. After cooling, the mixture was quenched with acetone and filtered. The filtrate was concentrated and purified using column chromatography (acetone:hexanes 20:80). The crude product was recrystallized from chloroform and dried *in vacuo* to afford the desired product, 3',4'-diphenylmethylene ketal quercetin, **4.1** (0.30 g, 0.64 mmol, 30%). ^{1}H NMR (500 MHz, DMSO-d6) δ 12.38 (s, 1H), 10.84 (s, 1H), 9.66 (s, 1H), 7.85 – 7.79 (m, 2H), 7.60 – 7.54 (m, 4H), 7.50 – 7.41 (m, 6H), 7.22 (d, *J* = 8.3 Hz, 1H), 6.47 (d, *J* = 2.0 Hz, 1H), 6.20 (d, *J* = 2.1 Hz, 1H). 13C NMR (126 MHz, DMSO-d_6) δ 176.49, 164.61, 161.17, 156.69, 148.10, 147.14, 146.03, 139.86,

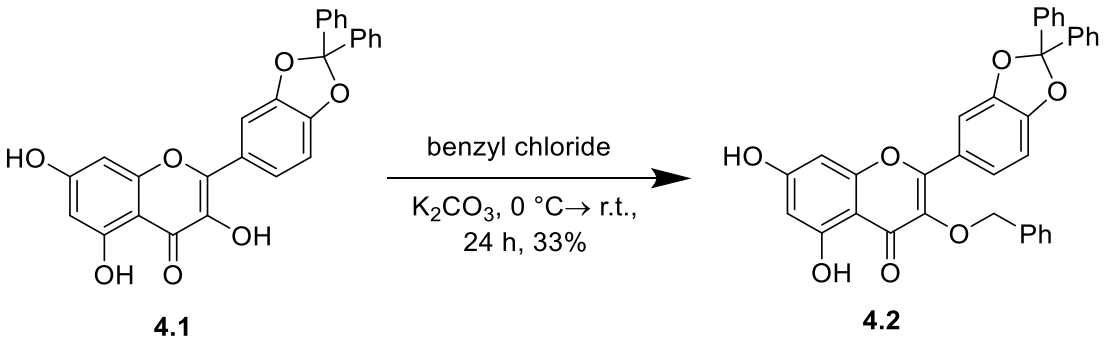

Scheme 4.2 Synthesis of **4.2**.

136.88, 129.95, 129.07, 126.24, 125.68, 123.51, 117.52, 109.30, 108.29, 103.58, 98.79, 94.11. Regiochemistry was confirmed by X-ray analysis (Figure S4.10)

Synthesis of 3',4'-diphenylmethylene ketal 3-benzylquercetin, **4.2**

In a round bottom flask, protected catechol quercetin, **4.1** (1.20 g, 2.58 mmol), K_2CO_3 (455 mg, 3.29 mmol), and DMF (36 mL) were combined under N_2. The reaction mixture was cooled to 0 °C, followed by the dropwise addition of benzyl chloride (0.290 mL, 2.44 mmol). The mixture was allowed to warm to room temperature over the next 24 h. The solvent was removed *in vacuo* and the resulting solid mixture was added to silica gel for a column chromatography using 30:70 ethyl acetate:hexanes. The solution was concentrated to a give yellow/orange powder (0.52 g, 33%). ^{1}H NMR (500 MHz, DMSO-d_6) δ 5.02 (s, 2H), 6.24 (d, J = 2.0 Hz, 1H), 6.46 (d, J = 2.0 Hz, 1H), 7.14 – 7.25 (m, 5H), 7.27 (d, J = 8.3 Hz, 1H), 7.44 – 7.60 (m, 12H), 10.91 (s, 1H), 12.64 (s, 1H).

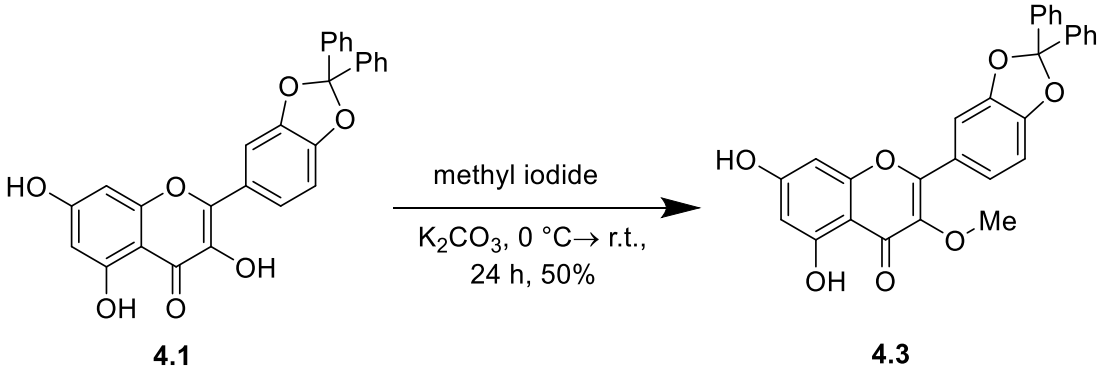

Scheme 4.3 Synthesis of **4.3**.

Synthesis of 3',4'-diphenylmethylene ketal 3-methyl quercetin, **4.3**

In a round bottom flask, protected catechol quercetin, **4.1** (1.00 g, 2.15 mmol), K_2CO_3 (444 mg, 3.22 mmol), and DMF (20 mL) were combined under N_2. The reaction mixture was cooled to 0 °C, followed by the dropwise addition of methyl iodide (0.130 mL, 2.01 mmol) in DMF (1.25 mL). The mixture was allowed to warm to room temperature over the next 24 h. The solvent was removed *in vacuo* and the resulting solid mixture was added to silica gel for column chromatography using 30:70 ethyl acetate:hexanes as the eluent. The solution was concentrated to give a yellow powder (0.52 g, 50%). ^{1}H NMR (500 MHz, Chloroform-*d*) δ 3.83 (s, 3H), 6.34 (d, *J* = 2.2 Hz, 1H), 6.44 (d, *J* = 2.1 Hz, 1H), 7.01 (d, *J* = 8.4 Hz, 1H), 7.38 – 7.44 (m, 6H), 7.58 – 7.63 (m, 4H), 7.67 (d, *J* = 1.8 Hz, 1H), 7.72 (dd, *J* = 8.3, 1.8 Hz, 1H).

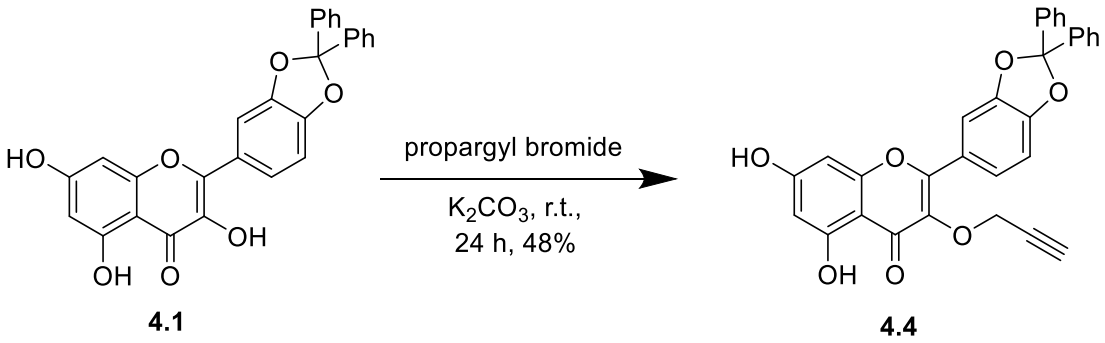

4.1 **4.4**

Scheme 4.4 Synthesis of **4.4**.

Synthesis of 3',4'-diphenylmethylene ketal 3-propargylquercetin, **4.4**

A mixture of **4.1**, propargyl bromide (48 µL, 0.54 mmol) and potassium carbonate (0.071 g, 0.524 mmol) were combined in DMF (4 mL) under N_2. The solution was allowed to stir at room temperature for 24 h. After removing excess solvent, the

mixture was diluted with ethyl acetate and extracted with water (20 mL). The combined ethyl acetate extracts were washed with water (20 mL), brine (20 mL) and dried over sodium sulfate. The product was purified by column chromatography to afford a yellow solid product with a 48% yield. ^{1}H NMR (500 MHz, Chloroform-*d*) δ 3.82 (d, *J* = 0.6 Hz, 3H), 6.33 (d, *J* = 2.4 Hz, 1H), 6.43 (d, *J* = 2.1 Hz, 1H), 6.99 (d, *J* = 8.4 Hz, 1H), 7.35 – 7.44 (m, 7H), 7.57 – 7.63 (m, 4H), 7.65 (d, *J* = 1.8 Hz, 1H), 7.70 (dd, *J* = 8.3, 1.8 Hz, 1H). 13C NMR (126 MHz, dmso) δ 178.19, 164.92, 161.64, 156.86, 155.91, 149.06, 147.14, 139.74, 136.01, 130.02, 129.11, 126.25, 124.71, 124.55, 117.82, 109.31, 109.21, 104.50, 99.33, 94.45, 79.94, 79.09, 59.58.

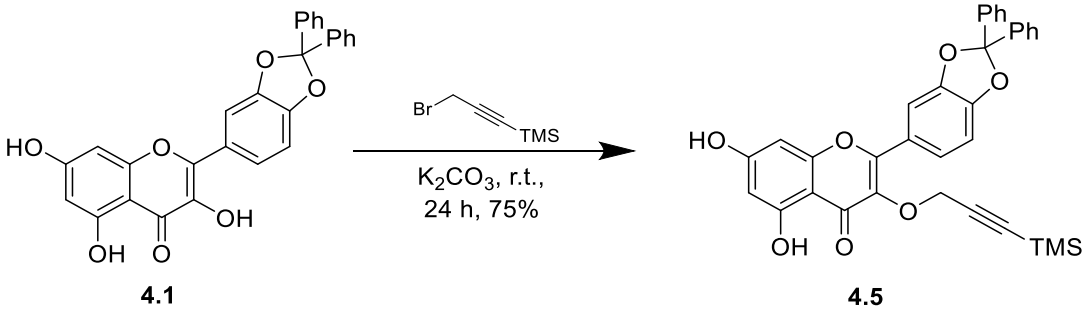

4.1 **4.5**

Scheme 4.5 Synthesis of **4.5**

Synthesis of 3',4'-diphenylmethylene ketal 3-TMS-propargylquercetin, **4.5**

A mixture of **4.1** (0.20 g, 0.43 mmol), (3-bromoprop-1-yn-1-yl)trimethylsilane (71 μL, 0.44 mmol) and potassium carbonate (0.071 g, 0.52 mmol) were combined in DMF (4.0 mL) under N_2. The solution was allowed to stir at room temperature for 24 h. After removing excess solvent, the mixture was diluted with ethyl acetate and extracted with water, brine and dried over sodium sulfate. Purification through a column resulted in a yellow gel-like product in 75% yield. ^{1}H NMR (300 MHz, Chloroform-*d*) δ -0.07

(d, *J* = 0.5 Hz, 9H), 2.20 (s, 1H), 4.86 (s, 2H), 6.31 (d, *J* = 2.2 Hz, 1H), 6.42 (d, *J* = 2.2 Hz, 1H), 6.99 (d, *J* = 8.3 Hz, 1H), 7.34 – 7.44 (m, 6H), 7.54 – 7.64 (m, 4H), 7.74 (d, *J* = 1.9 Hz, 1H), 7.78 (dd, *J* = 8.4, 0.5 Hz, 1H).

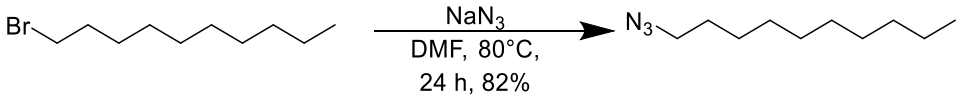

Scheme 4.6 Synthesis of azidodecane

Synthesis of azidodecane

A solution of bromodecane (1.106 g, 5.00 mmol) in DMF (20 mL) was treated with sodium azide (1.625 g, 25.00 mmol) under N_2 at 80 ºC for 24 h. The reaction mixture was cooled to room temperature followed by extraction with dichloromethane (2 x 10 mL). The combined organic layers were washed with water (20 mL) and brine (20 mL), dried over sodium sulfate and evaporated to afford an oil in 82% yield. ^{1}H NMR (300 MHz, Chloroform-*d*) δ 0.88 (t, *J* = 6.5 Hz, 3H), 1.21 – 1.37 (m, 14H), 1.60 (p, *J* = 7.0 Hz, 2H), 3.25 (t, *J* = 7.0 Hz, 2H).

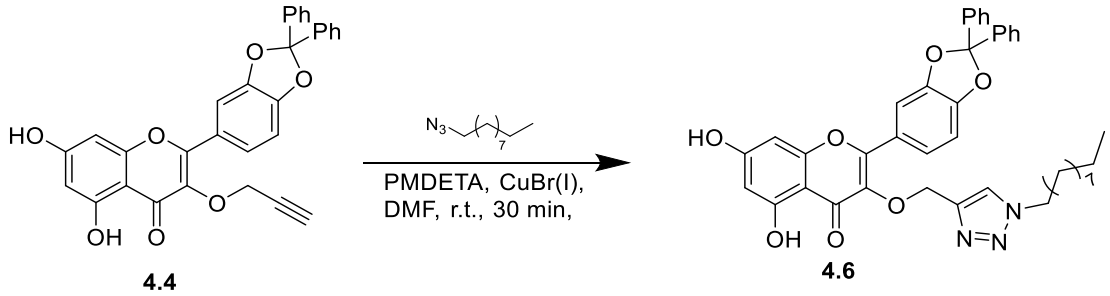

Scheme 4.7 Synthesis of **4.6**

Synthesis of 3',4'-diphenylmethylene ketal 3-decane triazole quercetin, **4.6**

A mixture of **4.4** (0.120 g, 0.239 mmol), azidodecane (0.0481 g, 0.263 mmol) and DMF (2 mL) were combined in a Schlenk flask under N_2. PMDETA (7.00 µL, 0.033mmol) was then added to the reaction mixture. The solution was degassed by freeze-pump-thaw cycles (x3), and CuBr (0.0034 g, 0.024 mmol) was added, followed by two more cycles of freeze-pump-thaw. The mixture was allowed to stir at room temperature for 30 min, then was diluted with dichloromethane (10 mL) and was extracted with water and brine (20 mL), followed by drying over sodium sulfate. The product was purified through a silica plug followed by column chromatography to afford a yellow solid product. ^{1}H NMR (Chloroform-*d*, ppm, 300 MHz) δ 0.92 (t, *J* = 6.2 Hz, 5H), 1.21 – 1.35 (m, 14H), 1.54 (p, *J* = 8.0, 7.4 Hz, 2H), 2.22 (d, *J* = 2.2 Hz, 1H), 3.75 (s, 2H), 6.09 (d, *J* = 2.1 Hz, 1H), 6.20 (s, 1H), 6.93 (d, *J* = 8.3 Hz, 1H), 7.14 (s, 1H), 7.45 – 7.52 (m, 6H), 7.64 – 7.74 (m, 4H) 11.16 (s, 1H), 12.47 (s, 1H).

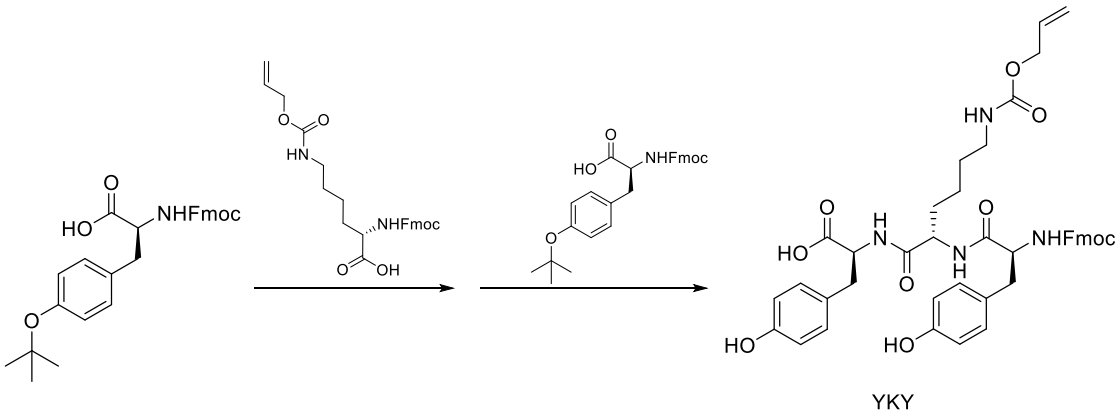

Scheme 4.8 Synthesis of YKY using solid phase peptide synthesis

Synthesis of **YKY**

The peptide, **YKY**, was synthesized according to procedures adopted from previously synthesized tripeptides.[169] ^{1}H NMR (DMSO-d_6, ppm, 500 MHz) δ 1.24 – 1.66 (m, 6H), 2.64 (t, J = 12.5 Hz, 1H), 2.75 – 3.03 (m, 5H), 4.07 – 4.52 (m, 8H), 5.13 (d, J = 9.6 Hz, 1H), 5.23 (d, J = 17.9 Hz, 1H), 5.87 (ddt, J = 16.1, 10.6, 5.5 Hz, 1H), 6.64 (dd, J = 8.0, 5.6 Hz, 4H), 7.00 (d, J = 8.1 Hz, 2H), 7.09 (d, J = 8.1 Hz, 2H), 7.13 (t, J = 6.3 Hz, 1H), 7.30 (dt, J = 14.4, 7.4 Hz, 2H), 7.40 (td, J = 7.5, 3.3 Hz, 2H), 7.53 (d, J = 8.6 Hz, 1H), 7.62 (t, J = 8.7 Hz, 2H), 7.87 (d, J = 7.6 Hz, 2H), 8.01 (dd, J = 16.8, 7.9 Hz, 2H), 9.19 (s, 2H).

Synthesis of **Me-YKY**

Using a procedure adopted from Slaughter and coworkers,[170] **YKY** (40.0 mg, 0.0514 mmol) was dissolved in MeOH:Toluene (3:2, 2 mL) under N_2. (Trimethylsilyl)diazomethane solution (0.10-0.015 mL) was added dropwise until the yellow color persisted. The solution was allowed to react for 30 min at r.t. followed by

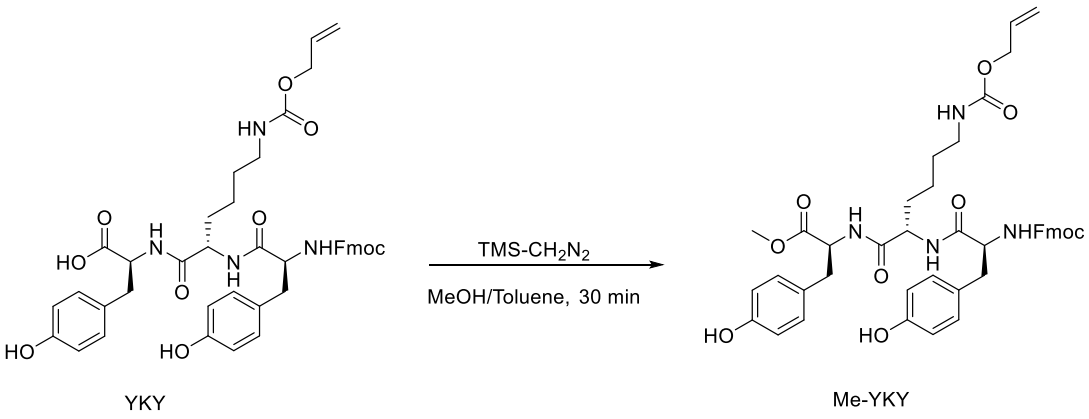

Scheme 4.9 Synthesis of **Me-YKY**

quenching with an aqueous solution of 10% acetic acid until the color dissipated. The solvent was removed *in vacuo* followed by dissolving in DCM (3 mL) and the product was washed with H_2O (3 x 5 mL). The organic layer was collected and dried over sodium sulfate and concentrated to afford the desired product in good yield as a white powder. Yield: 38.4 mg, 94.3% ^{1}H NMR (DMSO-d_6, ppm, 500 MHz) δ 1.31 (d, J = 63.0 Hz, 6H), 2.63 (t, J = 12.4 Hz, 1H), 2.85 – 3.00 (m, 5H), 3.56 (s, 3H), 4.14 – 4.49 (m, 8H), 5.13 (d, J = 10.5 Hz, 1H), 5.24 (d, J = 17.1 Hz, 1H), 5.87 (s, 1H), 6.64 (t, J = 9.1 Hz, 4H), 6.98 (d, J = 8.0 Hz, 2H), 7.02 – 7.20 (m, 3H), 7.30 (dd, J = 12.7, 7.4 Hz, 2H), 7.40 (t, J = 7.4 Hz, 2H), 7.51 (d, J = 8.5 Hz, 1H), 7.62 (t, J = 8.8 Hz, 2H), 7.92 (dd, J = 44.9, 7.9 Hz, 3H), 8.27 (d, J = 7.5 Hz, 1H), 9.18 (s, 2H).

4.4 Results and Discussion

Quercetin-based Monomer Design

With the goal of generating polymers with free catechol groups by post-polymerization modification, the first step towards synthesizing a monomer was the

protection of the catechol. Using adapted methods from a report by Rolando and co-workers,[171] quercetin was protected by formation of diphenylmethylene ketal **4.1**. Briefly, quercetin was mixed with α,α-dichlorodiphenylmethane and heated to 160 ºC for 20 min to afford the product in a 30% yield. The product was confirmed NMR, IR and MS. The regiochemistry was confirmed by X-ray crystallography (Figure S4.10). Considering the reactivity of the three remaining phenols on quercetin, the 3-phenol was next modified with various -R groups to create a library of monomers for attempted polymerization. The general synthesis of the monomers involved disosolution of **4.1** in DMF, followed by the addition of K_2CO_3. Under N_2, **4.1** was alkylated through the addition of R-X to the mixture, which was allowed to react for 24 h. All reactions were monitored by TLC.

Installation of different -R groups (Figure 4.10) was done systematically to attempt to produce a monomer capable of being copolymerized with a phosgene analogue to afford a polycarbonate. The rationale for the synthesis of **4.2** was two-fold; first, polycarbonates with benzyl protecting groups were previously synthesized, as in Chapter II and secondly, deprotection through hydrogenation is anticipated to be quantitative without reacting with any other installed functionality. Benzylation was performed under conditions previously used to synthesize 3,7,4'-tribenzylquecetin, except for the addition of one equivalent of benzyl chloride instead of three equivalents. Similar conditions previously used to synthesized 3,7,4'-trimethylquercetin were used, also with reduced equivalents of methyl iodide.[151] Methylation of the 3-phenol was designed to incorporate a permanent -R group which is smaller than the benzyl group,

therefore, the decrease in steric hindrance may allow for polymerization. Also, methylation of quercetin in Nature is common, and 3-methyl quercetin has been found in several sources, including Australian jelly bush honey (*Leptospermum polygalifolium*).[172] In addition to benzyl and methyl groups, a propargyl group was attached to the 3 position to add functionality for either further reactions of the monomer or post-polymerization modification. Compounds **4.5** and **4.6**, bearing an alkane and TMS-propargyl functional groups**,** were synthesized to attempt to increase the solubility of monomers for polymerization. Addition of the TMS group on **4.5** would also allow for propargyl group to be utilized post-polymerization upon deprotection. The final attempt to increase solubility was through a click-type azide−alkyne Huisgen cycloaddition reaction of **4.4** and azidodecane utalizing conditions from Chapter III. Azidodecane was prepared by the methods reported by the Delgado group.[173] Briefly, bromodecane was dissolved in DMF followed by the addition of sodium azide under N_2. The mixture was heated to 80 ºC for 24 h. After cooling, the product was extracted using dichloromethane and concentrated under reduced pressure to afford the product, azodecane, as a clear oil in 82% yield. The azide−alkyne Huisgen cycloaddition reaction of **4.4** and azidodecane was carried out in DMF under N_2, using PMDETA and CuBr as the catalyst and ligand, respectively. The product was purified by column chromatography to afford **4.6** as a yellow powder in good yield. All monomers were characterized by ^{1}H and ^{13}C NMR, ESI-MS, and FTIR. Monomers **4.1**-**4.6** failed to polymerize and resulted at most in a trimer, as determined by SEC eluting in DMF. Conditions utilized for polymerization of **4.1**, were non-phosgene conditions, attempting

to allow for the reaction of the more reactive phenols to polymerize with *p*-nitrophenyl chloromate.[174] General conditions for the polymerization of **4.2**-**4.6** involved dissolution of the monomer in either pyridine or DCM under N_2, followed by the addition of TEA. The mixture was cooled to 0 ºC, followed by the dropwise addition of diphosgene. The reaction mixture was warmed to room temperature and allowed to react for 24 h. Changing the protecting group from a diphenylmethylene ketal to other groups, such as an acetonide or boron-based protecting group in order to increase solubility failed afford the desired products. Copolymerization of the quercetin-based monomers with either naturally derived monomers (*i.e.* isosorbide, 1,4-butanediol, 3,7,4'-tribenzylqueretin, and 3,7,4'-trimethylqueretin) or biologically-friendly oligomers (*i.e.*, oligoethylene glycol) did not yield the desired result. It was then hypothesized that copolymerization with less sterically hindered phenolic groups may result in the desired polycarbonate. Therefore, new comonomers were desired for the construction of these polycarbonates that would (I) decrease steric hindrance of phenols and (II) retain benign or impart beneficial properties.

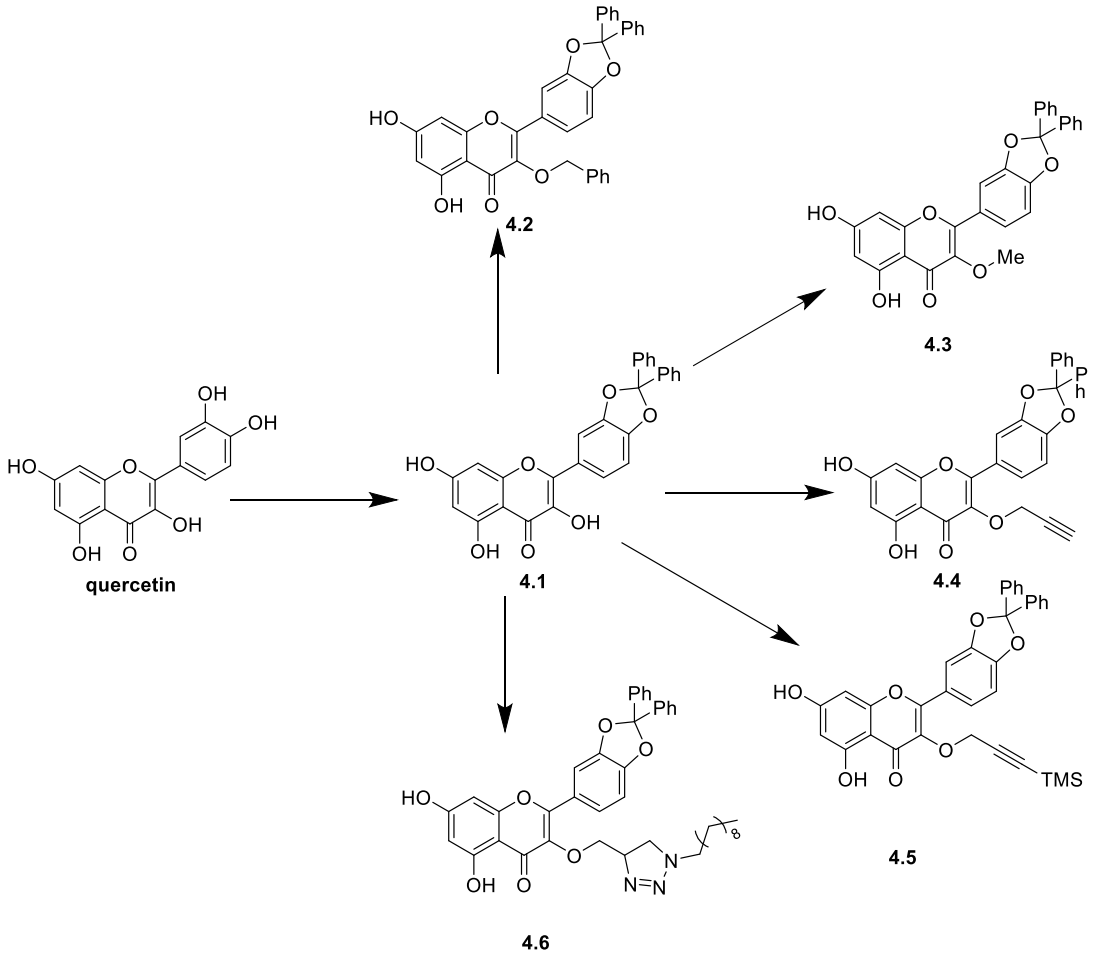

Scheme 4.10 Synthesis of quercetin-based monomers for attempted polymerization of polycarbonates**.**

Retrosynthetic Analysis of a Peptide-Based Monomer

In the design of a beneficial, non-sterically hindered comonomer, inspiration was drawn from mussel-inspired materials. Mussels contain the amino acid 3,4-dihydroxyphenylalanine, of which the catechol functionality contributes to their adhesive properties.[92] Mussel-inspired materials utilize 3,4-dihydroxyphenylalanine, dopamine or other catechol containing monomers to synthesize materials.[90-91, 93] Recently, there has been an emphasis on incorporating other functionalities into

synthetic materials that mimic the adhesive properties found in mussels.[95, 161] Lysine is one amino acid that has been found to enhance these properties. To incorporate lysine into the quercetin-based polycarbonate as part of the backbone of the polymer, solid phase peptide synthesis[169] was utilized to create a comonomer. Given the desired structural motif and the diverse functionalities to be introduced into the peptide-based monomers, the retrosynthesis in Scheme 4.9 was proposed utilizing a series of orthogonal protecting groups. These retrosynthetic manipulations led us from **4.7** to the advanced intermediate **4.7e**, for which synthesis by solid phase peptide synthesis required four synthetic steps. Cleavage from the Wang resin and deprotection of the t-butyl groups were expected occur in one synthetic step from **4.7d**. The strategic decisions made to synthesize **4.7c**-**4.7b** considered the orthogonal protecting groups needed for polymerization, namely to afford amines with different protecting groups. Equivalent protecting groups on both tyrosine units were expected to allow for a single deprotection under acidic conditions, therefore, **4.7d** and **4.7b** will both be synthesized from the same reagent, Fmoc-O-*tert*-butyl-L-tyrosine. While the t-butyl groups will be removed prior to polymerization, the alloc and Fmoc groups must be retained during polymerization to prevent reaction of the N-terminal and lysine amines with phosgene. Given that lysine will need a protecting group that is both acid and base stable, the synthesis of **4.7c** will use the reagent, Nα-Fmoc-Nε-Alloc-L-lysine. The final retrosynthetic step is to attach the starting material (Nα-Fmoc-L-butyl-tyrosine) to the resin by esterification to afford **4.7b** from **4.7a**.

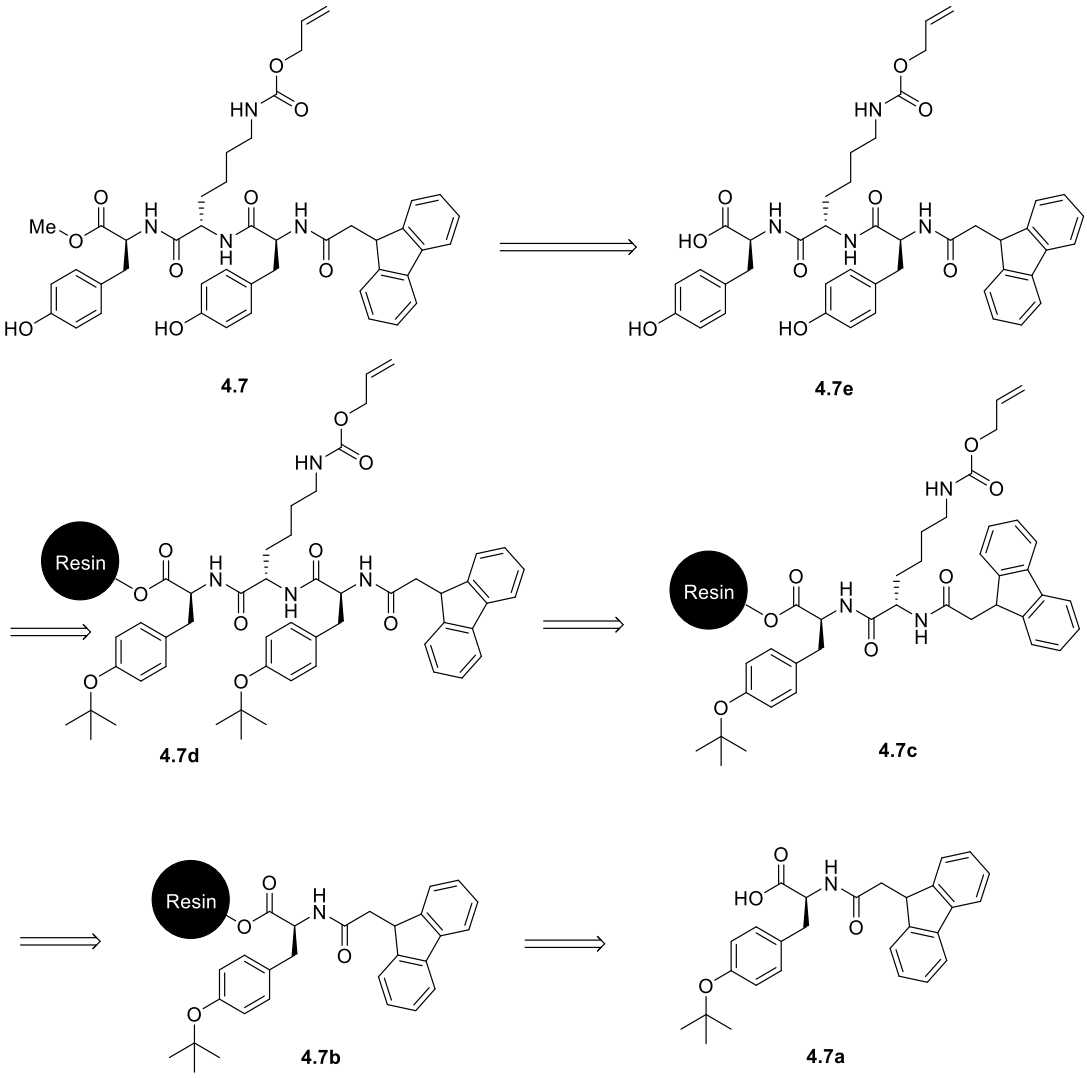

Scheme 4.11 Retrosynthetic analysis of the tripeptide

Synthesis of the Peptide-based Monomer

Following solid phase peptide synthesis involving the sequential addition of Fmoc-*O*-*tert*-butyl-L-tyrosine, N_α-Fmoc-N_ε-Alloc-L-lysine and Fmoc-*O*-*tert*-butyl-L-tyrosine to the Wang Resin, removal from the resin and purification by precipitation. Following the synthesis of the protected peptide, the free carboxylic acid was esterified with a methyl group under general conditions developed by Slaughter group.[170] In toluene:MeOH (3:2), **4.7e** was dissolved under N_2, followed by the dropwise addition of trimethylsilyldiazomethane solution until the yellow color persisted (~1.1 eq.). The reaction was allowed to proceed for 30 min and was monitored by TLC. The reaction mixture was quenched with 10% acetic acid, added dropwise until the color dissipated.

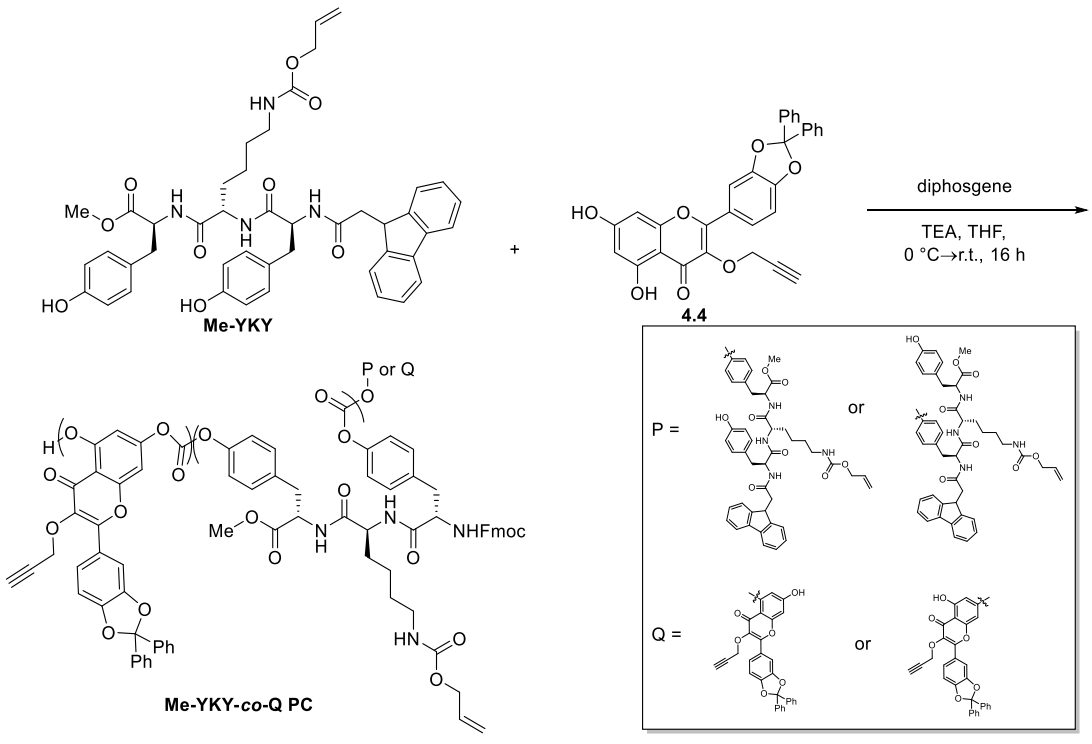

Scheme 4.12 Synthesis of the protected quercetin-peptide polycarbonate

The solvent was removed *in vacuo*, followed by drying *in vacuo* for 2-4 h. The resultant white powder was confirmed as the desired product, **4.7** in good yield.

Initial Copolymerization of the Quercetin and Peptide Monomers

To gain a better understanding of conditions to be used for copolymerization of **4.4** and **4.7**, homopolymerization of **4.7** was attempted. Under basic conditions in DCM, polymerization did not occur, and in pyridine, **4.7** degraded. When the solvent was changed to THF under basic conditions, the polymerization occurred in good yield, affording a polycarbonate with M_n = 20.5 kDa and Đ = 1.5 in 15 h. Utilizing similar conditions, the copolymerization of **4.4** and **4.7** was attempted over 15 h and resulted in a polycarbonate with a M_n = 10.9 kDa and Đ = 1.3. By ^{1}H NMR, comparing the alkene protons of the lysine protecting group and the propargylic protons of the quercetin monomer, the ratio of peptide to quercetin monomer was determined to be *ca.* 4:1. Considering the targeted value of 1:1, the more reactive peptide had a higher incorporation.

4.5 Conclusions and Future Work

The eventual synthesis of quercetin- and peptide-based monomers and copolymerization with a phosgene analog to afford a polycarbonate was described herein. Seven quercetin-based monomers were synthesized, however homopolymerization was unsuccessful. This emergent obstacle led to the design of valuable comonomers, which included a lysine unit within a tripeptide. Evolution of a route in which all four protecting groups were orthogonal and non-participating functional groups were obscured was analyzed. Upon the successful synthesis of the

tripeptide, L-tyrosine-Nε-alloc-L-lysine-Fmoc-L-tyrosine methyl ester, homopolymerization was attempted and a peptide-based polycarbonate resulted. Copolymerization of the tripeptide with 3',4'-diphenylmethylene ketal 3-propargyl quercetin afforded a polycarbonate with a molecular weight of 10.9 kDa. Overall, the synthesis of the protected quercetin-co-tripeptide polycarbonate are the first steps towards a polycarbonate with a free catechol and lysine for the intended application as biomedical adhesives.

Future directions include an increase in molecular weight, followed by the step-wise deprotection of poly(3',4'-diphenylmethylene ketal 3-propargyl quercetin-*co*- L-tyrosine-Nε-alloc-L-lysine-Fmoc-L-tyrosine methyl ester carbonate) to afford poly(3-propargyl quercetin-*co*-L-tyrosine-L-lysine-L-tyrosine methyl ester carbonate). Thermal, mechanical and adhesive properties will then be evaluated for applications towards biomedical applications.

CHAPTER V

SYNTHESIS, CHARACTERIZATION, AND CROSS-LINKING STRATEGY OF A QUERCETIN-BASED EPOXIDIZED MONOMER AS A NATURALLY-DERIVED REPLACEMENT FOR BPA IN EPOXY RESINS[†]

5.1 Overview

The natural polyphenolic compound quercetin was functionalized and cross-linked to afford a robust epoxy network. Quercetin was selectively methylated and functionalized with glycidyl ether moieties using a microwave-assisted reaction on a gram scale to afford the desired monomer (Q). This quercetin-derived monomer was treated with nadic methyl anhydride (NMA) to obtain a cross-linked network (**Q-NMA**). The thermal and mechanical properties of this naturally derived network were compared to those of a conventional diglycidyl ether bisphenol A-derived counterpart (**DGEBA-NMA).** Q-NMA had similar thermal properties [*i.e.*, glass transition (T_g) and decomposition (T_d) temperatures] and comparable mechanical properties (*i.e.*, Young's Modulus, storage modulus) to that of **DGEBA-NMA**. However, it had a lower tensile strength and higher flexural modulus at elevated temperatures. The application of naturally derived, sustainable compounds for the replacement of commercially available petrochemical-based epoxies is of great interest to reduce the environmental impact of

[†] Reprinted with permission from "Synthesis, Characterization, and Cross-Linking Strategy of a Quercetin-Based Epoxidized Monomer as a Naturally-Derived Replacement for BPA in Epoxy Resins" by Kristufek, S. L.; Yang, G.; Link, L. A.; Rohde, B. J.; Robertson, M. L.; Wooley, K. L. 2016 . ChemSusChem, 9, 2135-2142, Copyright 2016 by John Wiley and Sons.

these materials. **Q-NMA** is an attractive candidate for the replacement of bisphenol A-based epoxies in various specialty engineering applications.

5.2 Introduction

Epoxy resins are one of the most widely used thermosetting systems across a vast number of industries including transportation (*e.g.*, automobiles and airplanes), coatings, wind turbine blades and electronics.[108] It has been estimated that the epoxy industry was worth nearly 6 billion USD in 2013 and will grow to more than 9 billion USD by 2019.[175] This enormous industry is one of the many polymer/plastic markets that still largely rely on nonrenewable petrochemicals as starting materials.[110] Replacing these starting materials with sustainable and renewable resources would be beneficial for both environmental and financial reasons.[108] One common industrially used monomer for epoxy resins is the diglycidyl ether of bisphenol A (DGEBA), which provides excellent mechanical and thermal properties. Not only is this monomer derived from nonrenewable petrochemicals, but there have also been several health concerns associated with the precursor, bisphenol A (BPA), including its effect as an estrogen hormone disruptor.[176] A central area of research is devoted to finding a DGEBA replacement that is safe and sustainable without greatly sacrificing the mechanical integrity or thermal properties of the epoxy resin.

There are many ways to introduce sustainability into epoxy resins, such as the addition of natural toughening agents,[177] incorporation of natural cross-linkers or synthesis of naturally derived monomers through epoxidation or glycidyl ether functionalization.[108, 110] A natural-product-based substitute can be selected depending on

the petrochemical-based monomer that needs to be replaced, its properties and the intended application of the material. Currently, natural product derivatives such as itaconic acid, isosorbide and furan derivatives are platform chemicals for the synthesis of epoxy resins.[109] Although the use of natural toughening agents and cross-linkers reduces the petroleum-derived content of epoxy resins, in some systems, harmful BPA still remains as a building block in the DGEBA-based system. As plant-based substitutes of BPA, epoxidized natural products, derived from sources such as plant oils,[178-180] sugars,[181-183] lignin,[184-185] rosin acids[186-189] and many other naturally derived materials,[108, 110] have been explored as epoxy monomers. Alternatively, functional groups inherent to the natural product, such as the hydroxyl groups on tannic acid,[107, 190] have been used for ring opening of epoxides in cross-linked networks. Replacing a commercially available product such as a DGEBA-derived epoxy resin requires the new material to have the desired thermal, mechanical and other properties for the specific applications. It has been proposed that a class of natural polyphenolic compounds may be utilized as the starting materials for monomers in epoxy networks.[108]

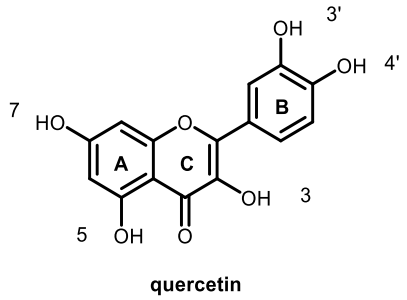

Figure 5.1 The numbering of the hydroxy groups for the selective alkylation of quercetin.

Quercetin is one such natural polyphenol that has the potential to be functionalized and act as a monomer in crosslinked epoxy networks. The first consideration is its wide availability in commonly ingested fruits and vegetables,[132] which has led to numerous studies investigating its health benefits including anti-inflammatory and antioxidant properties.[191-192] Methylated derivatives of quercetin have also been isolated in nature and studied for their biological properties.[193] Quercetin is not as cost efficient as petrochemical-based monomers at current market prices but extraction methods have been investigated as the demand for quercetin has increased over the past decade, in part owing to its numerous therapeutic applications.[194] Isolation methods from various fruits and vegetables have recently been reported.[195] A promising green method has been used to extract quercetin glycosides from onion waste using hot water extraction followed by enzymatic hydrolysis to afford quercetin.[196] Quercetin has been used as a cross-linker in epoxy chemistry in which the hydroxyl groups were reacted with sorbitol polyglycidyl ether and wood flour to form biocomposites.[111] To date, quercetin has not been explored as a replacement for DGEBA in epoxy resins, except as a co-monomer together with sorbitol,[111] or as a cross-linker in an epoxidized

natural rubber/polycaprolactone, both in biocomposites.[197] The rigid tricyclic structure of quercetin is expected to impart desirable thermal and mechanical properties to the resulting epoxy resins. In addition, quercetin undergoes unique chemical reactivity with selective alkylation of the hydroxyl groups in the order 4'>7>3>3'>5 (Figure 5.1),[123-124] allowing for direct functionalization at positions 3' and 5 with glycidyl ether groups, followed by reaction with a cross-linking agent to synthesize networks that have the potential to replace BPA-based epoxy resins.

This research entails the detailed evaluation of natural-product-based alternatives to DGEBA epoxy resins. The synthesis of a novel, quercetin-based monomer, 5,3'-diglycidyl ether-3,7,4'-trimethylquercetin (**5.2**), was explored using traditional and microwave synthesis conditions. This monomer was then crosslinked with nadic methyl anhydride (NMA) to form an epoxy resin (**Q-NMA**), which was characterized thermally and mechanically and compared to a DGEBA-based system prepared with the same cross-linker. The motivation for the synthesis of these quercetin-based materials was to investigate their potential as direct replacements for the BPA-based epoxy resins used in many applications.

5.3 Experimental

Materials and Methods

Quercetin was purchased from Cayman Chemicals. Epichlorohydrin and nadic methyl anhydride (NMA) were purchased from Sigma Aldrich. Sodium hydroxide was purchased from EMD Millipore. Potassium carbonate and tetrabutylammonium iodide were purchased from Alfa Aesar. DER 331 (DGEBA) was received from Dow

Chemical and ANCAMINE K54 (2,4,6-tris(dimethylaminomethyl)phenol) was received from Air Products & Chemicals. All chemicals were used as received without further purification. The monomer was synthesized in a CEM Intellivent Explorer microwave reactor and purified by Medium Pressure Liquid Chromatography (MPLC) using a CombiFlash Rf (Teledyne Isco).

Spectroscopic Characterization

^{1}H (500 MHz) and ^{13}C (125 MHz) NMR spectra were recorded on a Varian 500 spectrometer interfaced to a UNIX computer using VnmrJ software. Chemical shifts were referenced to the solvent proton resonance (DMSO-d_6: 2.50 ppm or $CDCl_3$: 7.26 ppm). IR spectra were obtained on a Shimadzu IR Prestige Attenuated Total Reflectance Fourier-transform Infrared Spectrometer (ATR-FTIR). Spectra were analyzed using IRsolution software package (Shimadzu) and were exported to Origin for analysis. The minimum number of scans was 32 with a minimum resolution of 16 and the apodization was set to SqrTriangle.

Thermal Characterization

Differential scanning calorimetric (DSC) studies were performed on a DSC822^{e} (Mettler-Toledo), with a heating rate of 10 ºC/min to determine the melting point (m.p.) of the monomers, as the peak maximum of the transition. The thermal degradation temperature was analyzed by thermogravimetric analysis (TGA), using a TA Instruments Q500 analyzer. The sample was heated from 30 to 800 °C at a rate of 10 °C/min in an argon environment (the balance argon purge flow was 40 mL/min and the sample purge flow was 60 mL/min). The glass transition temperatures (T_g) and curing protocols were

characterized by a TA Instruments Q2000 differential scanning calorimeter, calibrated with an indium standard, with a nitrogen flow rate of 50 mL/min. The sample was placed in the calorimeter (in a Tzero aluminum pan) and was heated from 40 to 200 °C, cooled back to 40 °C, and subsequently heated to 200 °C, at a rate of 10 °C/min. The value of the T_g was determined at the midpoint of the slope of the second heating using the TA Universal Analysis software.

Mechanical Characterization

Strain-to-failure measurements were carried out on an Instron 5966 tensile tester with a 2 kN load cell at a strain rate of 10 mm/min to obtain tensile strength and elongation at break of both Q-NMA and DGEBA-NMA at room temperature. Test specimens were dog-bone-shaped testing bars (following ASTM D638, bar type 5, thickness 2.0 mm). Pneumatic grips were used to affix the sample in the testing frame at a compressed air pressure of 50 psi. Each measurement was repeated with 5-6 test specimens.

Dynamic mechanical analysis (DMA) was performed on a Mettler Toledo TT-DMA system. Samples with dimensions 3.32 × 2.03 × 5.10 mm for Q-NMA and 3.06 × 1.75 × 5.18 mm for DGEBA-NMA were tested in tension mode. Dynamic measurements were recorded at a frequency of 1 Hz, a dynamic force of 1 N and a static/dynamic force ratio of 1.5 from 25-200 °C at a rate of 3 °C/min with data sampling interval of 10 s. DMA data were obtained from Triton Laboratory software and exported to Origin Pro 9.0 for analysis. Three-point bending tests were performed on bars with dimensions ca. 2.00 × 4.05 × 10 mm. The measurements were recorded at a frequency

of 1 Hz, a dynamic force of 1 N and a static/dynamic force ratio of 1.5 from 0-200 °C at a rate of 3 °C/min with data sampling interval of 10 s.

Synthesis

Synthesis of 3,7,4'-trimethylquercetin, **5.1**

The compound was prepared by a procedure adapted from Moalin et al.[150] A round bottom flask was charged with quercetin (20.0 g, 66.2 mmol), potassium carbonate (20.4 g, 148 mmol), methyl iodide (16.0 mL, 257 mmol) and DMF (500 mL) under nitrogen. The reaction was stirred at room temperature for 24 h and the DMF was then removed *in vacuo*, resulting in a brown solid product. The brown solid was purified by Medium Pressure Liquid Chromatography (MPLC) eluted with a 10% ethyl acetate in chloroform and recrystallized from chloroform to afford a yellow solid, 3,7,4'-trimethylquercetin (9.5 g, 42% yield). ^{1}H NMR (500 MHz, DMSO-d_6, ppm): δ 12.65 (s, 1H, -OH), 9.44 (s, 1H, -OH), 7.59 – 7.55 (m, 2H, Ar), 7.11 (d, J = 8.4 Hz, 1H, Ar), 6.71 (d, J = 2.2 Hz, 1H, Ar), 6.37 (d, J = 2.2 Hz, 1H, Ar), 3.87 (s, 3H, -CH_3), 3.86 (s, 3H, -CH_3), 3.80 (s, 3H, -CH_3). ^{13}C NMR (125 MHz, DMSO-d_6, ppm): δ 178.5, 165.5, 161.3, 156.7, 156.0, 150.7, 146.8, 138.6, 122.9, 120.8, 115.5, 112.2, 105.6, 98.2, 92.6, 60.2, 56.5, 56.1; FTIR (ATR) 3579-3140, 3047-3000, 3000-2847, 1643, 1597, 1196, 918, 895, 818, cm^{-1} HRMS (ESI+, m/z): $[M+H]^{+1}$ calculated for $[C_{18}H_{17}O_7]^+$, 345.0974, found 345.0970. m.p. 175 °C Regiochemistry was confirmed by X-ray analysis (Figure S5.6).

Synthesis of 5,3'-diglycidyl ether-3,7,4'-trimethylquercetin, **5.2**

In an 80-mL microwave vessel, 3,7,4'-trimethylquercetin (2.00 g, 5.81 mmol), sodium hydroxide (460 mg, 11.5 mmol), potassium carbonate (6.40 g, 46.3 mmol), tetrabutylammonium iodide (420 mg, 1.14 mmol), epichlorohydrin (4.80 mL, 61.4 mmol) and ethanol (3.0 mL) were combined along with a stir bar. In the microwave reactor, the solution was heated to 110 °C for 30 min while stirring. The solution was filtered and the solid was washed with ethyl acetate (15 mL). The solvent was removed *in vacuo*. The crude product was purified using MPLC/flash column chromatograph (gradient of 0-100% hexanes/ethyl acetate). The solution was concentrated to a yellow solid and washed with tetrahydrofuran and dried *in vacuo* to afford the desired product as a white solid, 3'5-diglycidyl ether-3,7,4'-trimethylquercetin (1.02 g, 38%). ^{1}H NMR (500 MHz, $CDCl_3$, ppm) δ 7.77-7.70 (m, 2H), 6.98 (app d, J = 8.5 Hz, 1H), 6.52 (app d, J = 2.2 Hz, 1H), 6.38 (app d, J = 2.1 Hz, 1H), 4.38 (dd, J = 11.3, 2.6 Hz, 1H), 4.34 (dd, J = 11.3, 3.4 Hz, 1H), 4.15 (dd, J = 11.3, 4.3 Hz, 1H), 4.09 (dd, J = 11.3, 5.6 Hz, 1H), 3.95 (s, 3H), 3.89 (s, 3H), 3.84 (s, 3H), 3.46-3.41 (m, 2H), 3.19 (m, 1H), 2.94 (m, 2H), 2.80 (m, 1H). ^{13}C NMR (125 MHz, $CDCl_3$, ppm) δ 173.7, 163.7, 159.6, 158.6, 152.5, 151.4, 147.6, 147.5, 141.2, 123.3, 122.7, 113.9, 111.3, 109.7, 97.6, 97.6, 93.3, 93.3, 70.4, 69.0, 59.99, 59.96, 55.99, 55.96, 55.8, 55.8, 50.2, 50.1, 45.1, 45.0. FTIR (ATR) 3105-3009, 2931-2847, 1624, 1607, 1211, 1018, 822 cm^{-1}. HRMS (ESI+, *m/z*): calculated for $[M+H]^+$: $[C_{24}H_{25}O_9]^+$ 457.1499, found 457.1482. m.p. 160 °C Regiochemistry was confirmed by X-ray analysis (Figure S5.7).

Synthesis of 5,3'-diglycidyl ether-3,7,4'-trimethyl quercetin-nadic methyl anhydride, **Q-NMA**

In a glass vial, 5,3'-diglycidyl ether-3,7,4'-trimethylquercetin (**5.2**) (1.50 g, 3.25 mmol) and nadic methyl anhydride (1.17 g, 6.50 mmol) were combined, heated to 160 °C and stirred for 3 min. The mixture was allowed to cool to room temperature (25 °C) and ANCAMINE® K54 (45.0 mg) was added. The mixture was heated to 90 °C, stirred for 3 min and cast into molds preheated to the same temperature (90 °C). The bars were cured for 2 h at 90 °C then at 160 °C for 30 min to afford the **Q-NMA** networks. $T_d^{5\%}$ = 266 °C, $T_d^{10\%}$ = 297 °C, T_g = 134 °C. FTIR (ATR): 3676-3152, 3047-3000, 3000-2808, 1780, 1736, 1623, 1436, 1429, 1349, 1325, 1157, 1108, 1020, 818 cm^{-1}.

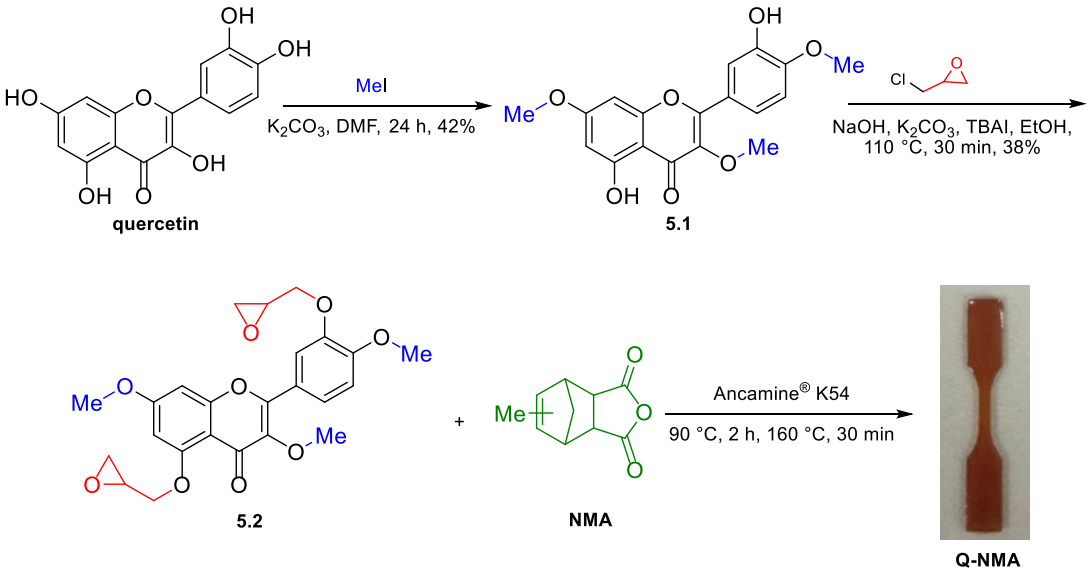

Scheme 5.1 Synthesis of the pre-monomer and monomer used for cross-linking **Q-NMA** networks.

Synthesis of diglycidyl ether of bisphenol A-nadic methyl anhydride, **DGEBA-NMA**

In a round bottom flask, DGEBA (10.0 g, 29.4 mmol), nadic methyl anhydride (10.5 g, 58.8) and ANCAMINE® K54 (300 mg) were combined and heated to 90 °C and stirred for 5 min. The mixture was cast into six molds preheated to 90 °C. The bars were cured for 1 h at 90 °C then at 160 °C for 2 h to afford the **DGEBA-NMA** network. $T_d^{5\%}$ = 284 °C, $T_d^{10\%}$ = 337 °C, T_g = 136 °C. FTIR (ATR) 3645-3124, 3124-3022, 2917-2850, 1737, 1225, 1152, 1106, 1032, 827, cm^{-1}.

5.4 Results and Discussion

Synthesis and Characterization of Epoxy Monomer and Cross-linked Networks

The epoxy monomer was prepared by selective alkylation of the hydroxyl groups in two steps. The regioselectivity of quercetin has been thoroughly studied and has shown to allow good selectivity for alkylation of the 3, 7 and 4' positions over the 5 and 3' hydroxyl groups,[123-124] which provided a convenient route for the stepwise selective methylation and installation of the epoxide-containing glycidyl moieties to form the epoxy monomer (Scheme 5.1). Methylation using methods similar to those reported previously,[150] but on a larger scale, afforded 3,7,4'-trimethylquercetin (**5.1**). Briefly, quercetin was allowed to dissolve in *N*,*N*-dimethylformamide (DMF) at room temperature under an inert atmosphere, and was then treated with potassium carbonate followed by the addition of methyl iodide. The reaction was monitored by TLC and allowed to proceed for 24 h. The resultant mixture contained observable amounts of remaining starting material along with the di-, tri- and tetramethylated quercetin roducts, which were separated by column chromatography and recrystallized to afford the desired

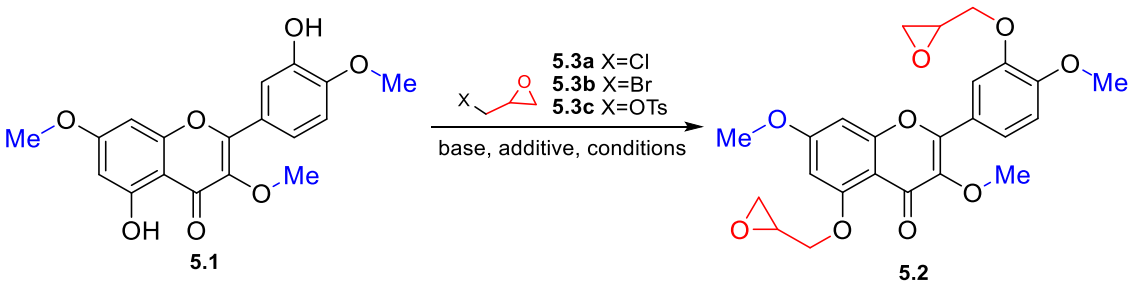

Table 5.1 Selective attempted conditions for the synthesis of the monomer, 3',5-diglycidyl ether-3,7,4'-trimethylquercetin, (**5.2**).

Entries[a]	Reagent	Base + Additive	Solvent	Temperature	Time	Yield
1	**5.3a**	NaH	DMF	0 °C→25 °C	120 h	-
2	**5.3a**	NaOH + TBAB	H_2O	80 °C	120 h	-
3	**5.3a**	K_2CO_3	DMF	80 °C	120 h	-
4	**5.3b**	K_2CO_3	DMF	80 °C	120 h	12%
5[b]	**5.3b**	K_2CO_3	DMF	80 °C	120 h	-
6	**5.3c**	K_2CO_3	DMF	80 °C	120 h	34%
7[b]	**5.3c**	K_2CO_3	DMF	80 °C	120 h	25%
8[c]	**5.3a**	NaOH + K_2CO_3 + TBAI	EtOH	110 °C	0.5 h	49%
9[b,c]	**5.3a**	NaOH + K_2CO_3 + TBAI	EtOH	110 °C	0.5 h	38%

[a]Standard conditions were performed on a 100 mg scale; [b]Performed on a gram scale; [c]Performed under microwave conditions

TBAB: tetrabutylammonium bromide, TBAI: tetrabutylammonium iodide;

tri-methylated product in 42% yield. The product was confirmed using ^{1}H NMR, ^{13}C NMR, IR and ESI-MS (Figure S5.1 and S5.2, Supporting Information). The regioselectivity was confirmed by single crystal X-ray analysis (Figure S5.6). The motivation for this specific selective protection was three-fold. Firstly, **5.1** has previously been extracted as the natural product, ayanin from Croton schiedeanus,[198] a plant found across Central and South America. The bioactivity of this natural product has been studied against several cell lines.[199-201] Secondly, the alkylation of the three hydroxyls leaves the two remaining hydroxy sites on quercetin available for functionalization with glycidyl ether moieties, mimicking the two epoxide functionalities on DGEBA. Finally, limiting the number of free hydroxyl groups present on the monomer would limits the number of reactive functionalities present during the cross-linking reaction and reduces the number of side reactions.

The second step, *O*-alkylation to synthesize the epoxy monomer (**5.2**), was first attempted using traditional synthesis conditions for the addition of an oxirane to a phenol[108] (Table 5.1, entries 1–2) utilizing a strong base (NaH) or an aqueous base solution (NaOH) with a phase transfer catalyst tetrabutylammonium bromide (TBAB); the reactions did not provide the desired product after 5 days, as monitored by TLC, even at elevated temperatures (80 ºC). Subsequently, traditional conditions previously used to functionalize quercetin using K_2CO_3 as a solid base and the solvent, DMF[150, 171] (Table 5.1, entries 3–5) delivered a 12% yield of the desired product using epibromohydrin (**5.3b**). However, when the reaction was scaled up to a gram scale, the only isolated product was the mono-reacted glycidyl ether, 3'-glycidyl ether-3,7,4'-

trimethylquercetin (Table 5.1, entries 4–5). When tosyl (-OTs) was used as the leaving group of the oxirane starting material (**5.3c**), the large-scale reaction proceeded in five days with a poor yield (Table 1, entries 6–7). Additionally, this reaction required the extra step of converting glycidol to the (±)-oxiran-2-ylmethyl 4-methylbenzenesulfonate (**5.3c**) following a literature procedure,[202] which proceeded in excellent yield but increased the overall number of linear steps for the synthesis of **5.2**. A variety of different conventional heating methods for the addition of multiple glycidyl ether functionalities did not allow the reaction to be performed at a large scale to afford sufficient materials for cross-linking in the form of mechanical testing bars.

Considering the two competing mechanisms that can take place to install the epoxide functionality using epichlorohydrin (**5.3a**), 1) the S_N2 reaction with the alkyl halide and **5.2**) the S_N2' reaction, which involves opening of the epoxide followed by reformation of the epoxide to replace the halogen, alternative conditions were found to be effective at directing the reaction towards the desired product. In particular, limiting the opening of the epoxide or accelerating the closing of the ring to reform the epoxide could assist in promoting the forward reaction and increasing the yield. The Pchelka group has demonstrated that it is possible to activate ionic species in the analogous reactions for the preparation of 3-aryloxy-1,2-epoxypropane using microwave-assisted reaction conditions.[203] In conjunction with changing the heating method, potassium carbonate was used in addition to sodium hydroxide to further increase the yield. The conditions used in the studies of the 3-aryloxy-1,2-epoxypropanes were applied to the formation of the quercetin-based monomers.

Although the O-alkylation of simple phenols to afford 3-aryloxy-1,2-epoxypropanes has been studied extensively, the specific conditions for the alkylation of 1 required optimization owing to its unique characteristics. The most significant challenge was the limited reactivity of the 5-OH in quercetin and its analogs owing to hydrogen bonding with the ketone in the C ring (Figure 5.1), which was strongly suggested to be occurring, as shown in the crystal structure of **5.1** (Figure S5.6).[204] Additionally, the 3'-position of **5.1** is sterically affected by the orthomethoxy substituent. By adapting the literature conditions[203] to the current reaction, **5.2** was prepared in reasonable yield in gram-scale quantities (Table 5.1, entry 9, 38%). The conditions were altered by extending the reaction time and increasing the number of equivalents of epichlorohydrin (**5.3a**). TBAB was also replaced with tetrabutylammonium iodide (TBAI). More importantly, this method significantly reduced the reaction time from 120 h to 0.5 h. To further confirm the regioselectivity of the di-substituted product was confirmed by ^{1}H and ^{13}C NMR spectroscopies and high-resolution mass spectrometry (NMR spectra are shown in Figure S5.3 and S5.4). To further confirm the regioselectivity of the final product structure, single crystal X-ray analysis of **5.2** was performed (Figure S5.7).[205] Using the prepared monomer, cross-linked networks were synthesized by allowing the oxirane groups of **5.2** to undergo reaction with nadic methyl anhydride (NMA), a commercially available cross-linker. The catalyst chosen to accelerate the cross-linking reaction was ANCAMINE® K54 (2,4,6-tris(dimethylaminomethyl) phenol) (Figure S5.5) at a concentration of 3 phr (parts per hundred resin). This tertiary amine was used to promote alternating co-

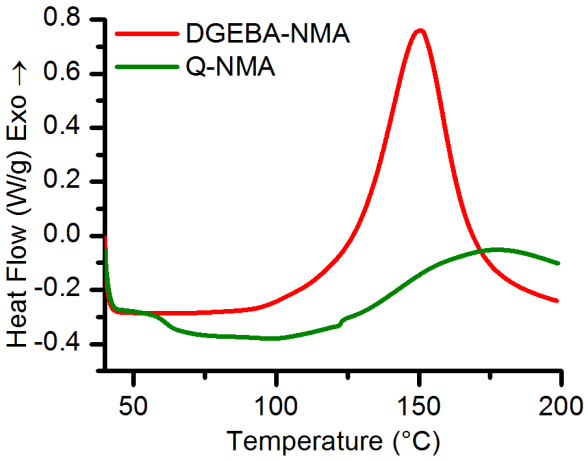

Figure 5.2 Assessment of conditions to cure **5.2** and NMA to produce **Q-NMA**, with evaluation of heat flow *vs*. temperature by DSC.

polymerization of NMA and an epoxy based monomer through chain growth anionic polymerization.[206-207] Side reactions, such as homopolymerization of the oxirane ring and etherification, can occur to further induce cross-linking. Although the natural-based monomer was expected to undergo the same types of reactions as previously studied commercially available monomers, the physical properties of 2 led to a unique curing process. There were several challenges in developing a curing protocol for **Q-NMA**, including the high melting point of the monomer (160 ºC), evaporation of the cross-linker (>90 ºC) (Figure S5.10) and rapid reaction (less than 1 min) of the starting materials in the presence of the catalyst at elevated temperatures. First, to determine an appropriate curing protocol for **Q-NMA**, the reaction kinetics were examined using non-isothermal heating at 10 ºC min^{-1} from 40–200 ºC using differential scanning calorimetry (DSC) (Figure 5.2) and ending at 200 ºC to avoid degradation of the material. The DSC data indicated curing over a broad temperature (~125–200 ºC), with peak reactivity

located at approximately 180 ºC. As the quercetin-based epoxide monomer (**5.2**) was not soluble in NMA at room temperature, the first step in the protocol was the melting of **5.2** (160 ºC) and mixing it with NMA in the absence of the catalyst for 3 min at 160 ºC. Without the K54 catalyst, the mixture did not appear to visibly gel (observed up to 2 h at 160 ºC). After mixing the two monomers at 160 ºC for 3 min, the mass loss was 0.60±0.07% (Figure S5.11). Given the low expected conversion of a thermoset proceeding via chain growth polymerization without the presence of an initiator,[206] it is not anticipated that significant conversion of the monomer during the 3 min mixing time. The mixture was subsequently cooled to room temperature (25 ºC) (during which it remained homogeneous), followed by addition of ANCAMINE® K54 and heating to the desired mixing/curing temperature. Mixing temperatures ranging from 30–90 ºC were tested at 10 ºC increments. At low temperatures, the mixture was too viscous for stirring; therefore, the mixing could only proceed efficiently at 90 ºC to ensure homogeneous distribution of the catalyst. After the addition of ANCAMINE® K54, the mixture was stirred for no longer than 3 min to avoid gelation of the materials in the vials. Following the mixing process, the mixture was cast into molds preheated at 90 ºC to ensure a continuous cross-linking reaction. The networks were allowed to undergo reaction for 2 h at 90 ºC. Thermogravimetric analysis (TGA) confirmed that NMA did not evaporate at this temperature (Figure S5.10). The curing time was determined by measuring the glass transition temperature (T_g) of the bar every 30 min during the curing at 90 ºC until the T_g was constant. Subsequently, the resin was post-cured at a temperature higher than the network T_g and at the melting point of the monomer to help

drive the reaction to completion. The post-curing time was also determined by monitoring the T_g as the resin was held at the post-curing temperature, until no noticeable changes occurred (Figure S5.8). The required post-curing time was 30 min at 160 ºC. In summary, the final curing protocol chosen for **Q-NMA** included a heated mixing step followed by a two-stage curing that involved an initial curing step at 90 ºC for 2 h and a post-curing at 160 ºC for 30 min. The quercetin-network was characterized by IR spectroscopy (Figure 5.3). The IR spectrum of NMA (Figure 5.3b) shows peaks at 1852 cm^{-1} (asymmetrical C=O stretch) and at 1775 cm^{-1} (symmetrical C=O stretch), each of which disappeared upon formation of **Q-NMA** (Figure 5.3c), indicating the consumption of the anhydride functionality. The anhydride absorbances were replaced by a characteristic ester peak at 1736 cm^{-1} (C=O stretch) indicating the formation of the ring-opened product. The **Q-NMA** spectrum also contained a strong ester peak at 1157 cm^{-1} (C=O stretch) for the C=O stretching vibration and broad, albeit weak peak at 3675–3152 cm^{-1} (O-H stretch) indicating the presence of the -OH group of the unreacted chain ends. The combination of the IR peaks indicates that the reaction proceeded and cross-linking of the **Q-NMA** network occurred to afford the desired cross-linked materials.

To directly compare **Q-NMA** and DGEBA cross-linked with NMA (**DGEBA-NMA**), the **DGEBA-NMA** network was optimized by applying the same catalyst loading (3 phr) and curing temperatures. The reaction time was optimized for each monomer. Although the **DGEBA-NMA** curing kinetics have been previously reported,[208-209] the trace for the mixture curing is shown in Figure 5.2 for a comparison

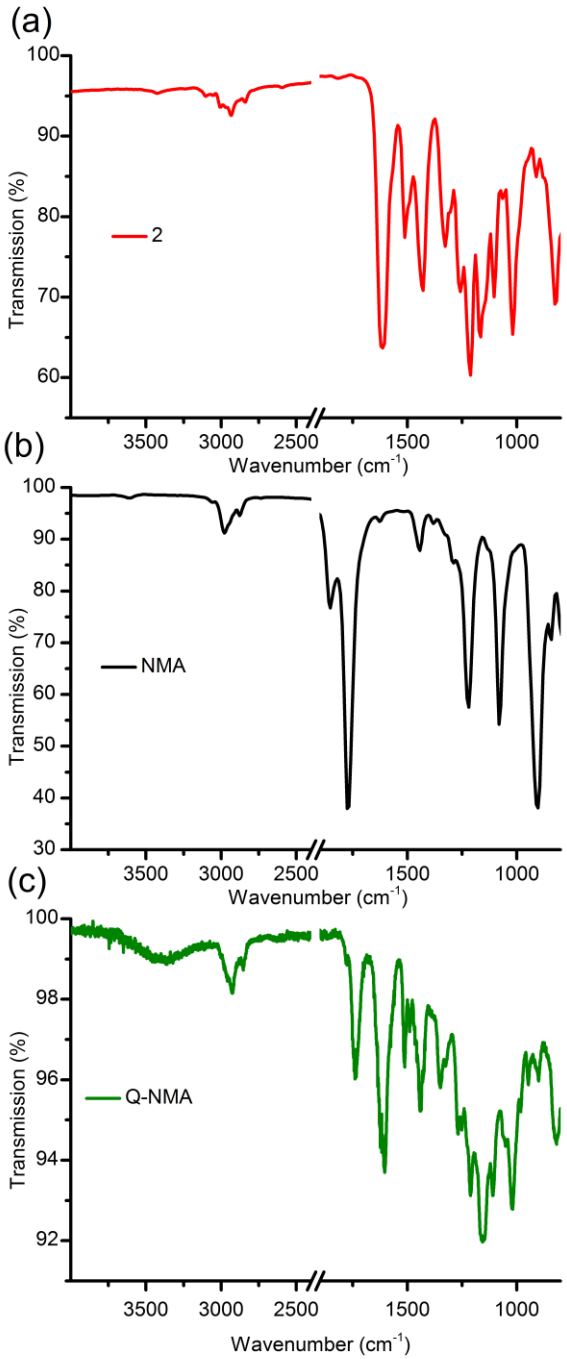

Figure 5.3 IR spectra of (a) monomer **5.2**, (b) cross-linker (NMA) and (c) cured network (**Q-NMA**).

to the quercetin-based network (Scheme S5.1). The same process was applied to optimize the curing protocol times for the **DGEBA-NMA** network. In this case, the DGEBA monomer was a liquid at room temperature, therefore, there was no need for a complex mixing process.

The DGEBA/NMA/K54 mixture was stirred at 90 ºC for 5 min to ensure a homogeneous mixture before casting into the hot molds heated to 90 ºC. The optimal conditions for the DGEBA-NMA reaction were determined to be curing for 1 h at 90 ºC followed by 2 h at 160 ºC, by monitoring the change in T_g during the second step. IR spectroscopy confirmed the presence of a cross-linked network, with the appearance of an ester peak at 1737 cm^{-1} (C=O stretch) and a strong ester peak at 1152 cm^{-1} (C=O stretch) as well as the disappearance of the anhydride peaks from NMA. The faint peak at 3645–3140 cm^{-1} (-O-H stretch) is indicative of the hydroxyl group of the ring-opened side reaction, similar to the one that appears in the **Q-NMA** system. The IR peaks of **DGEBA-NMA** were similar to those for **Q-NMA**, with the appearance of the hydroxyl and ester peaks and the disappearance of the anhydride peak (Figure S5.13). Following confirmation of the synthesis of the epoxy resins, the thermal and mechanical properties of the two systems were measured and compared.

*Thermal Properties of the **Q-NMA** and **DGEBA-NMA** Networks*

The two systems had thermal similar properties. The decomposition temperatures (T_d) of Q-NMA and DGEBA-NMA were 266 and 284 ºC, respectively, measured at the 5% mass loss by TGA (Table 5.2). The glass transition temperatures, T_g, of Q-NMA and DGEBA-NMA measured by DSC were 134 ºC and 137 ºC,

respectively (Table 5.2). Using dynamic mechanical analysis (DMA) in tensile mode, the temperatures at which the maximum tan d occurred (which are proportional to T_g), were determined to be 170 ºC and 171 ºC for **Q-NMA** and **DGEBA-NMA**, respectively. Given that the two epoxy resins have similar thermal properties, it is expected that replacement of **DGEBA-NMA** with **Q-NMA** could occur in applications covering a wide range of temperatures. High T_g values of the systems tend to correlate with high tensile strength and modulus, which was later explored.

Table 5.2 Thermal and mechanical properties of the cross-linked networks **Q-NMA** and **DGEBA-NMA**.

Property	Q-NMA	DGEBA-NMA
T_g (°C)[a]	134	**137**
$T_{d5\%}$ (°C)	266	**284**
Tensile Strength (MPa)[b]	37 ± 8	**66 ± 15**
% Elongation at Break[b]	1.3 ± 0.4	**2.8 ± 0.9**
Young's Modulus (GPa)[b]	3.5 ± 0.2	**3.0 ± 0.2**
Storage Modulus (GPa)[b]	1.72	**1.75**
Flexural Modulus (GPa) [b]	3.49	**3.48**
Storage Modulus, ε' (MPa)[c]	7.7	**14.0**
v_c (mol/cm^3)	6.67×10^{-4}	**1.21×10^{-3}**

[a]Measured by DSC; [b]Storage Modulus, Flexural Modulus, Tensile Strength, % elongation at break and Young's Modulus measured at 25 °C; [c]Storage Modulus measured at 190 °C.

*Mechanical Properties of the **Q-NMA** and **DGEBA-NMA** Networks*

The dynamic moduli were measured for each system in tension and in three-point-bending mode using DMA (Figure 5.4A and 5.4B). The tensile storage modulus

behavior with respect to temperature for the two systems was similar. Under tension, the temperature range at which the network is expected to behave as a glassy solid ($T<T_g$) and the temperature range at which the network is expected to behave as a rubbery solid ($T_g<T<T_d$) are equivalent for the two systems. Conversely, under flexural stress, **DGEBA-NMA** began to transition to its rubbery state at approximately 70 ºC, a lower temperature than the **Q-NMA** transition (~120 ºC). From approximately 70–170 ºC, **Q-NMA** exhibited a flexural modulus which was greater than that of **DGEBA-NMA**. At 130 ºC, **Q-NMA** exhibited a flexural modulus which was two orders of magnitude greater than that of **DGEBA-NMA**. Therefore, for elevated temperature applications (50–150 ºC), **Q-NMA** is expected to be more resistant to bending (flexural stress/strain) compared to **DGEBA-NMA**. Using the theory of rubber elasticity, the cross-link density (υ_c) defined as the number of moles of elastically effective network chains per cubic centimeter of sample, can be calculated using the following equation:

$$\upsilon_c = \varepsilon'/3RT \quad \text{(equation 5.1)}$$

where R is the gas constant, T is the temperature and ε' is the rubbery modulus at 190 ºC measured using DMA in tension mode.[210] **DGEBA-NMA** has a higher cross-link density than that of the natural-product-based counterpart. Although there is a considerable difference in cross-link density between the different networks, the T_g, flexural modulus and storage modulus are similar, which is possibly owing to the rigidness of quercetin.

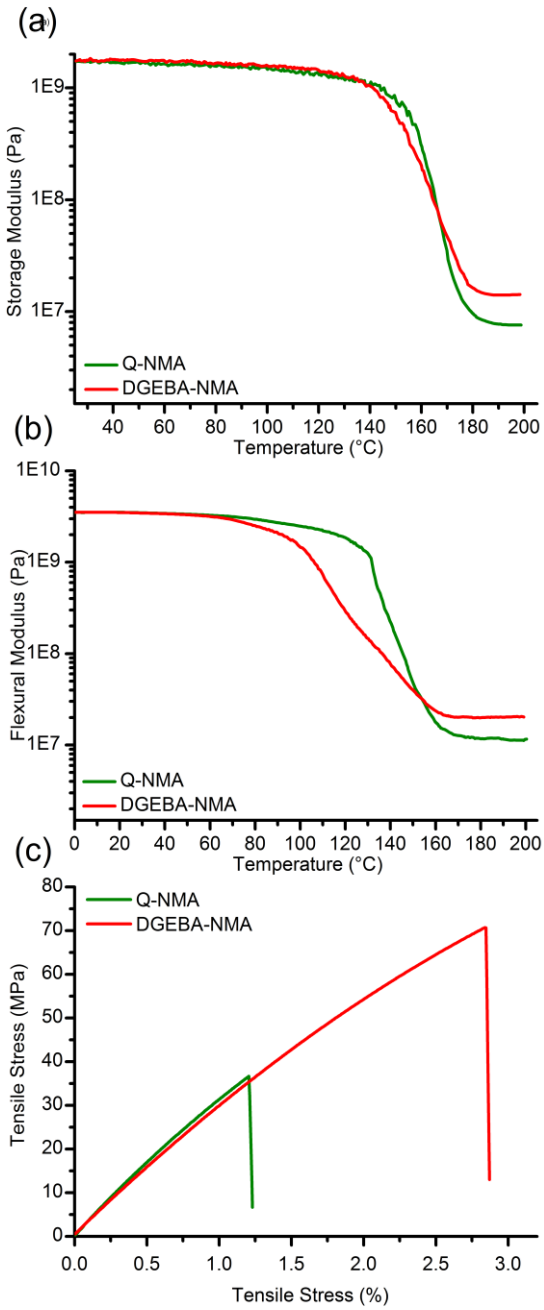

Figure 5.4 (a) Tensile storage modulus as a function of temperature. (b) Flexural modulus as a function of temperature. (c) Representative stress-strain behavior (n). = 5-6.

The tensile stress/strain behavior of the **Q-NMA** and **DGEBA-NMA** networks measured through tensile testing at 25 ºC is shown in Figure 4c and relevant parameters are reported in Table 5.2. The average tensile strength, or maximum stress, was 37.8 and 66.15 MPa for **Q-NMA** and **DGEBA-NMA**, respectively. Both materials exhibited brittle fracture at less than 3% elongation. The Young's modulus, calculated from the linear portion of the stress–strain curve was 3.5±0.2 and 3.0±0.2 GPa for Q-NMA and DGEBA-NMA, respectively (Table 5.2, Figure 5.4C). Overall, the mechanical properties of Q-NMA, such as Young's Modulus, storage modulus and flexural modulus, are comparable to that of DGEBA-NMA, indicating the quercetin-based epoxy monomer is appropriate for the replacement of DGEBA in many epoxy resin applications.

5.5 Conclusions

A novel monomer from a natural polyphenolic starting material was synthesized in two steps. The monomer has the potential to replace the diglycidyl ether of bisphenol A (DGEBA) and, therefore, to eliminate the use of bisphenol A (BPA) in epoxy networks. The functionalization of the monomer with diglycidyl ether groups was performed using microwave synthesis conditions, which led to an increase in the yield and the scale, as well as a greatly reduced reaction time. The quercetin-based monomer was cross-linked with nadic methyl anhydride (NMA) to afford the cross-linked network (**Q-NMA**). The thermal and mechanical properties of **Q-NMA** were compared to that of DGEBA cross-linked with NMA (**DGEBA-NMA**), at optimized curing conditions. The two systems have similar decomposition and glass transition temperatures and many

comparable mechanical properties including Young's modulus, flexural modulus and storage modulus at 25 ºC. At elevated temperatures, **Q-NMA** exhibited a flexural modulus which was greater (by two orders of magnitude at 130 ºC) than that of **DGEBA-NMA**. This naturally derived monomer shows tremendous potential to replace BPA in practical applications.

CHAPTER VI

CONCLUSIONS AND FUTURE WORK FOR QUERCETIN-BASED POLYMERIC MATERIALS

Overall, described herein were the design and synthesis of four quercetin-based polymeric systems applied towards a wide variety of applications. First, described was the general overview and outlook for natural product-based polymeric materials with a focus on polymers with an aromatic backbone followed by the assessment of quercetin-based monomers for incorporation into polymeric materials and an overview of their applications.

Chapter II highlighted the fundamental study of the synthesis of quercetin-based polycarbonates and their aggregation-induced emission properties. Quercetin was selectively triprotected with benzyl group followed by the copolymerization with a phosgene analogue. The resultant polycarbonates were 8 and 13 kDa. Unexpectedly, the polycarbonates exhibited a bright fluorescence post-polymerization. To probe this property, model compounds were synthesized followed by extensive fluorescence studies. Upon exploration of conditions for aggregation-induced emission, the emission increased *ca.* 2-4 times. Molecular modeling was used to support the aggregation induced emission rationalizing the exhibited fluorescence. The synthesized polycarbonates were designed from the natural product quercetin and presented a broad band fluorescence that has the potential to be utilized in advanced engineering applications.

Further extension of the project will be to further probe the fluorescence through exploration of common AIE applications such as explosive detection and/or chemo/bio sensors. Additionally, the deprotection of the benzyl groups will be explored. Upon the synthesis of poly (quercetin carbonate) (Figure 6.1), a degradation study will be performed to assess the byproducts. The deprotected polycarbonate will also be assessed for fluorescence properties and various applications.

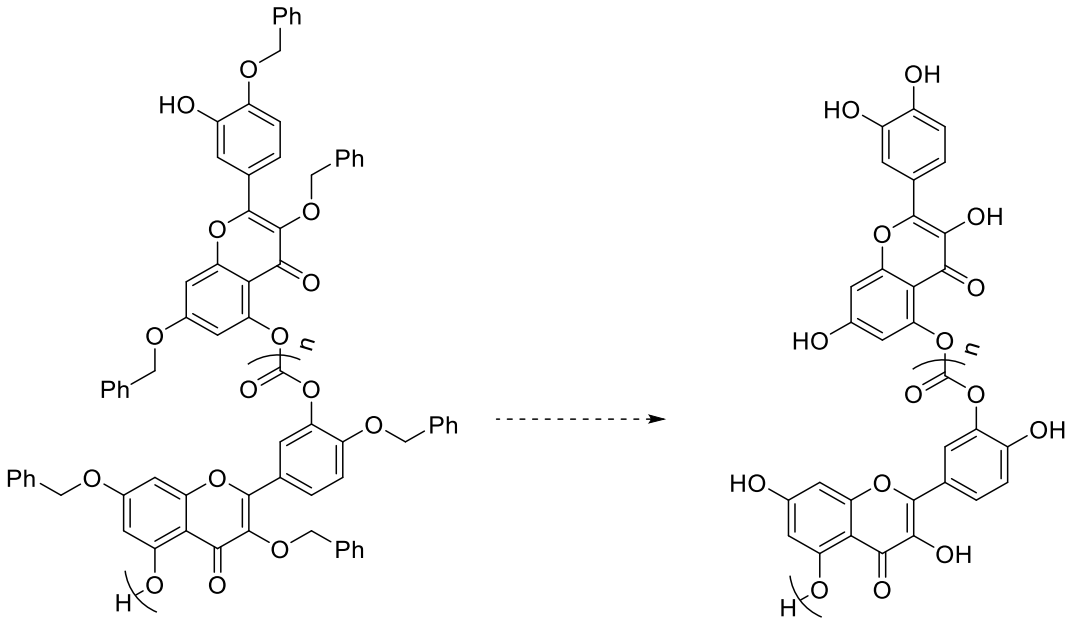

Figure 6.1 Proposed deprotection of poly(3,7,4'-tribenzylquercetin carbonate).

Building upon the discovered AIE properties, Chapter III explored quercetin polycarbonates towards a drug delivery system as micellular structures with inherent fluorescent properties. A copolycarbonate of 3,7,4'-tribenzylquercetin and 3,7,4'-tripropargylquercetin was synthesized using a phosgene analogue. The inserted

propargyl groups were utilized to “click” on multiple grafting percentages of N_3-PEG-OMe with respect to the number of functional groups. Varying the number of PEG units on the polycarbonate backbone resulted in changing micelle properties such as size and fluorescence. The quercetin-based micelles have the potential to be used for a drug delivery system. The quercetin-based micelles will next be studied for loading and releasing of a drug such as paclitaxel. The micelles fluorescence properties will also be studied among cells to analyze if the AIE fluorescence contrasts well against cells.

The final set of polycarbonates synthesized from quercetin were described in Chapter IV. A series of catechol-moiety protected quercetin monomers were designed and attempted to be polymerized. Upon the failure of all syntheses of free catechol quercetin polycarbonates, a comonomer was introduced. The design and synthesis of a tripeptide containing lysine were explored. The successful copolymerization of the quercetin- and peptide-based monomers with a phosgene analogue produced a polycarbonate with a molecular weight of 10.9 kDa. Continuing this work, attempts towards a higher molecular weight polymer is first proposed. With the polycarbonates in hand, cleavage of the remaining protecting groups will allow for an exploration of the desired adhesive properties. After full characterization of the thermal, mechanical and adhesive properties, biomedical applications will be explored.

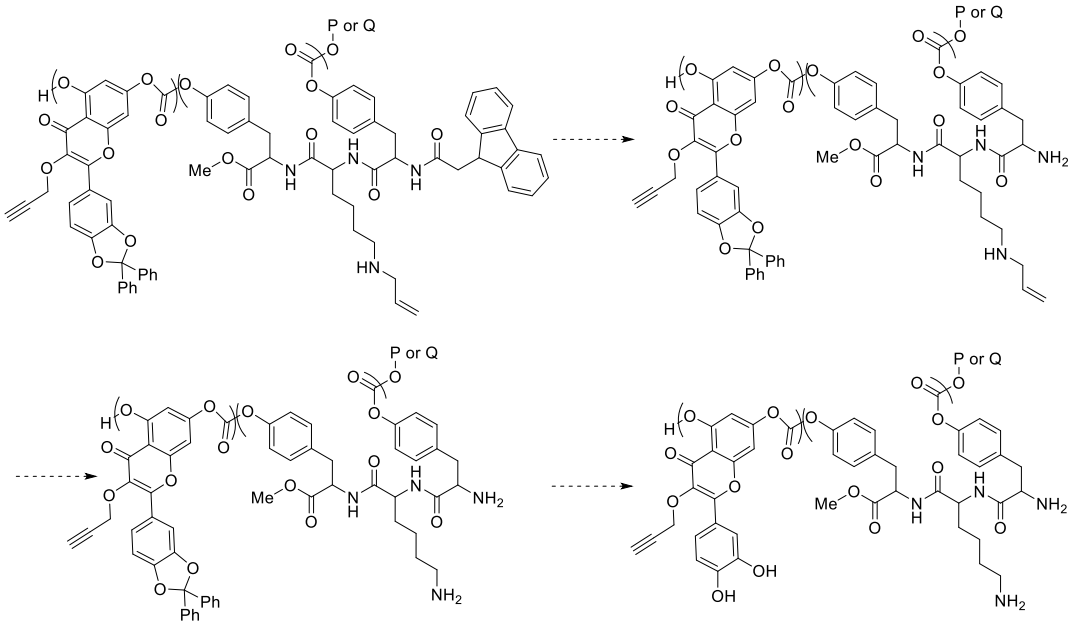

Figure 6.2 Proposed deprotection route for the removal of the three-remaining protection group on the quercetin-peptide polycarbonate.

In Chapter V, a cross-linked network based on quercetin was explored rather than a linear polycarbonate. Quercetin was transformed into a bi-functional monomer for epoxy resins in two synthetic steps. Cross-linking with the commercially-available, nadic methyl anhydride (NMA) afforded the epoxy resin, Q-NMA. The quercetin-based networks were compared thermally and mechanically to DGEBA-NMA. The natural product-based epoxy had similar thermal properties [*i.e.*, glass transition (T_g) and decomposition (T_d) temperatures] and comparable mechanical properties (*i.e.*, Young's Modulus, storage modulus). The flexural modulus at increased temperature was greater for **Q-NMA** than **DGEBA-NMA** but the tensile modulus was lower. The quercetin-based networks have the potential of replacing **DGEBA-NMA** in some applications.

Future work on quercetin-based epoxy resins includes increasing the percentage of natural product content within the epoxy resin. First, it will be essential to replace the petrochemical based cross-linkers such as NMA. Utilizing natural products and their derivatives with alcohol functionalities such as isosorbide, 1,4-butanediol and/or quercetin (Figure 6.3). Another direction for future work would be to reduce the number of synthetic steps and special equipment needed for the synthesis of a quercetin-based monomer. Rather than the initial methylation step that was performed in Chapter V, future work could include the addition of the oxirane functional handle on quercetin utilizing two, three or four equivalents of epichlorohydrin to afford the bi-, tri- or tetra reacted product. All new synthesized quercetin-based epoxy resins would be tested thermally and mechanically then compared to the appropriate commercially available epoxy resins.

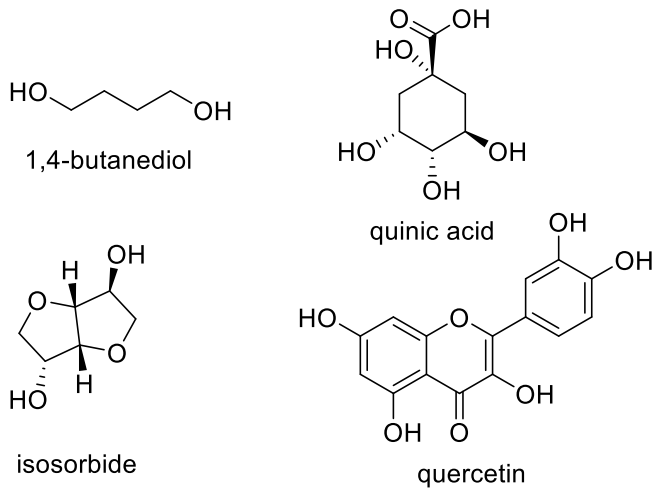

Figure 6.3 Examples of natural products proposed a natural cross-linkers for epoxy resins.

REFERENCES

1. Kuttruff, C. A.; Eastgate, M. D.; Baran, P. S., *Nat. Prod. Rep.* **2014,** *31* (4), 419-432.

2. Erdmenger, T.; Guerrero-Sanchez, C.; Vitz, J.; Hoogenboom, R.; Schubert, U. S., *Chem. Soc. Rev.* **2010,** *39* (8), 3317-3333.

3. Shoda, S.-i.; Uyama, H.; Kadokawa, J.-i.; Kimura, S.; Kobayashi, S., *Chem. Rev.* **2016,** *116* (4), 2307-2413.

4. Darensbourg, D. J., *Personal Adventures in the Synthesis of Copolymers from Carbon Dioxide and Cyclic Ethers*. 2014; Vol. 66, p 1-23.

5. Niaounakis, M., *Biopolymers: Processing and Products*. William Andrew: 2014.

6. Recyclable PET Plastic Partially Made from Plants. http://www.coca-colacompany.com/our-company/plantbottle (accessed September 2016).

7. Bomgardner, M. M., *Chemical & Engineering News* **2015,** *93* (14), 15.

8. Pehere, A. D.; Xu, S.; Thompson, S. K.; Hillmyer, M. A.; Hoye, T. R., *Org. Lett.* **2016,** *18* (11), 2584-2587.

9. Mikami, K.; Lonnecker, A. T.; Gustafson, T. P.; Zinnel, N. F.; Pai, P.-J.; Russell, D. H.; Wooley, K. L., *J. Am. Chem. Soc.* **2013,** *135* (18), 6826-6829.

10. Gustafson, T. P.; Lonnecker, A. T.; Heo, G. S.; Zhang, S. Y.; Dove, A. P.; Wooley, K. L., *Biomacromolecules* **2013,** *14* (9), 3346-3353.

11. Lonnecker, A. T.; Lim, Y. H.; Felder, S. E.; Besset, C. J.; Wooley, K. L., *Macromolecules* **2016,** *49* (20), 7857-7867.

12. Kristufek, T. S.; Kristufek, S. L.; Link, L. A.; Weems, A. C.; Khan, S.; Lim, S.-M.; Lonnecker, A. T.; Raymond, J. E.; Maitland, D. J.; Wooley, K. L., *Polym. Chem.* **2016,** *7* (15), 2639-2644.

13. Besset, C. l. J.; Lonnecker, A. T.; Streff, J. M.; Wooley, K. L., *Biomacromolecules* **2011,** *12* (7), 2512-2517.

14. Link, L. A.; Lonnecker, A. T.; Hearon, K.; Maher, C. A.; Raymond, J. E.; Wooley, K. L., *ACS Appl. Mater. Interfaces* **2014,** *6* (20), 17370-17375.

15. Wacker, K. T.; Kristufek, S. L.; Lim, S.-M.; Kahn, S.; Wooley, K. L., *RSC Adv.* **2016,** *6* (85), 81672-81679.

16. Noel, A.; Borguet, Y. P.; Raymond, J. E.; Wooley, K. L., *Macromolecules* **2014,** *47* (9), 2974-2983.

17. Noel, A.; Borguet, Y. P.; Raymond, J. E.; Wooley, K. L., *Macromolecules* **2014,** *47* (20), 7109-7117.

18. Noel, A.; Borguet, Y. P.; Wooley, K. L., *ACS Macro Lett.* **2015,** *4* (6), 645-650.

19. He, X.; Fan, J.; Zou, J.; Wooley, K. L., *Chem. Commun.* **2016,** *52* (54), 8455-8458.

20. He, X.; Fan, J.; Wooley, K. L., *Chem. Asian J.* **2016,** *11* (4), 437-447.

21. He, X.; Fan, J.; Zhang, F.; Li, R.; Pollack, K. A.; Raymond, J. E.; Zou, J.; Wooley, K. L., *J. Mater. Chem. B* **2014,** *2* (46), 8123-8130.

22. Zou, J.; He, X.; Fan, J.; Raymond, J. E.; Wooley, K. L., *Chem. Eur. J.* **2014,** *20* (29), 8842-8847.

23. Fan, J.; Li, R.; He, X.; Seetho, K.; Zhang, F.; Zou, J.; Wooley, K. L., *Polym. Chem.* **2014,** *5* (13), 3977-3981.

24. Fan, J.; Zou, J.; He, X.; Zhang, F.; Zhang, S.; Raymond, J. E.; Wooley, K. L., *Chem. Sci.* **2014,** *5* (2).

25. Zou, J.; Fan, J.; He, X.; Zhang, S.; Wang, H.; Wooley, K. L., *Macromolecules* **2013,** *46* (10), 4223-4226.

26. Holmberg, A. L.; Reno, K. H.; Wool, R. P.; Epps III, T. H., *Soft Matt.* **2014,** *10* (38), 7405-7424.

27. Yao, K. J.; Tang, C. B., *Macromolecules* **2013,** *46* (5), 1689-1712.

28. Gandini, A.; Lacerda, T. M., *Prog. Polym. Sci.* **2015,** *48*, 1-39.

29. Gandini, A.; Lacerda, T. M.; Carvalho, A. J.; Trovatti, E., *Chem. Rev.* **2016,** *116* (3), 1637-1669.

30. Ricapito, N. G.; Ghobril, C.; Zhang, H.; Grinstaff, M. W.; Putnam, D., *Chem. Rev.* **2016,** *116* (4), 2664-2704.

31. Kristufek, S. L.; Wacker, K. T.; Tsao, Y.-Y. T.; Su, L.; Wooley, K. L., *Nat. Prod. Rep.* **Submitted**.

32. Vandenberg, L. N.; Hauser, R.; Marcus, M.; Olea, N.; Welshons, W. V., *Reprod. Toxicol.* **2007,** *24* (2), 139-177.

33. Thompson, R. C.; Moore, C. J.; vom Saal, F. S.; Swan, S. H., *Phil. Trans. R. Soc. B* **2009,** *364* (1526), 2153-2166.

34. Thompson, R. C.; Olsen, Y.; Mitchell, R. P.; Davis, A.; Rowland, S. J.; John, A. W. G.; McGonigle, D.; Russell, A. E., *Science* **2004,** *304* (5672), 838.

35. *Lignin and Lignans: Advances in Chemistry*. 2010.

36. Xu, C.; Arancon, R. A.; Labidi, J.; Luque, R., *Chem. Soc. Rev.* **2014,** *43* (22), 7485-7500.

37. Ragauskas, A. J.; Beckham, G. T.; Biddy, M. J.; Chandra, R.; Chen, F.; Davis, M. F.; Davison, B. H.; Dixon, R. A.; Gilna, P.; Keller, M.; Langan, P.; Naskar, A. K.; Saddler, J. N.; Tschaplinski, T. J.; Tuskan, G. A.; Wyman, C. E., *Science* **2014,** *344* (6185), 1246843-1246841 - 1246843-1246810.

38. Azadi, P.; Inderwildi, O. R.; Farnood, R.; King, D. A., *Renew. Sust. Energy Rev.* **2013,** *21*, 506-523.

39. Galkin, M. V.; Samec, J. S. M., *ChemSusChem* **2016,** *9* (13), 1544-1558.

40. Pandey, K. K., *J. Appl. Polym. Sci.* **1999,** *71* (12), 1969-1975.

41. Thakur, V. K.; Thakur, M. K.; Raghavan, P.; Kessler, M. R., *ACS Sustainable Chem. Eng.* **2014,** *2* (5), 1072-1092.

42. Raquez, J. M.; Deléglise, M.; Lacrampe, M. F.; Krawczak, P., *Prog. Polym. Sci.* **2010,** *35* (4), 487-509.

43. Upton, B. M.; Kasko, A. M., *Chem. Rev.* **2016,** *116* (4), 2275-2306.

44. Luo, J.; Xie, Z.; Lam, J. W.; Cheng, L.; Chen, H.; Qiu, C.; Kwok, H. S.; Zhan, X.; Liu, Y.; Zhu, D.; Tang, B. Z., *Chem. Commun.* **2001,** (18), 1740-1741.

45. Mei, J.; Hong, Y. N.; Lam, J. W. Y.; Qin, A. J.; Tang, Y. H.; Tang, B. Z., *Adv. Mater.* **2014,** *26* (31), 5429-5479.

46. Hong, Y.; Lam, J. W.; Tang, B. Z., *Chem. Soc. Rev.* **2011,** *40* (11), 5361-5388.

47. Li, Y.; Xu, L.; Su, B., *Chem. Commun.* **2012,** *48* (34), 4109-4111.

48. Jin, X.; Dong, L.; Di, X.; Huang, H.; Liu, J.; Sun, X.; Zhang, X.; Zhu, H., *RSC Adv.* **2015,** *5* (106), 87306-87310.

49. Xu, L.; Li, Y.; Li, S.; Hu, R.; Qin, A.; Tang, B. Z.; Su, B., *Analyst* **2014,** *139* (10), 2332-2335.

50. Zhang, W.; Liu, W.; Li, P.; Huang, F.; Wang, H.; Tang, B., *Anal. Chem.* **2015,** *87* (19), 9825-9828.

51. Jiang, Y.; Chen, Y.; Alrashdi, M.; Luo, W.; Tang, B. Z.; Zhang, J.; Qin, J.; Tang, Y., *RSC Adv.* **2016,** *6* (102), 100318-100325.

52. Shyamal, M.; Mazumdar, P.; Maity, S.; Samanta, S.; Sahoo, G. P.; Misra, A., *ACS Sensors* **2016,** *1* (6), 739-747.

53. Mei, J.; Leung, N. L.; Kwok, R. T.; Lam, J. W.; Tang, B. Z., *Chem. Rev.* **2015,** *115* (21), 11718-11940.

54. Chan, C. Y. K.; Lam, J. W. Y.; Deng, C. M.; Chen, X. J.; Wong, K. S.; Tang, B., *Macromolecules* **2015,** *48* (4), 1038-1047.

55. Zhou, H.; Wang, X.; Lin, T. T.; Song, J.; Tang, B. Z.; Xu, J., *Polym. Chem.* **2016,** *7* (41), 6309-6317.

56. Chua, M. H.; Zhou, H.; Lin, T. T.; Wu, J.; Xu, J. W., *J. Polym. Sci. A Polym. Chem.* **2016**.

57. Chen, Y.; Han, H.; Tong, H.; Chen, T.; Wang, H.; Ji, J.; Jin, Q., *ACS Appl. Mater. Interfaces* **2016,** *8* (33), 21185-21192.

58. Zhao, Y. M.; Zhu, W.; Ren, L. X.; Zhang, K., *Polym. Chem.* **2016,** *7* (34), 5386-5395.

59. Yahia-Ammar, A.; Sierra, D.; Merola, F.; Hildebrandt, N.; Le Guevel, X., *ACS Nano* **2016,** *10* (2), 2591-2599.

60. Hu, R.; Leung, N. L.; Tang, B. Z., *Chem. Soc. Rev.* **2014,** *43* (13), 4494-4562.

61. Elsabahy, M.; Heo, G. S.; Lim, S. M.; Sun, G.; Wooley, K. L., *Chem. Rev.* **2015,** *115* (19), 10967-11011.

62. Verduzco, R.; Li, X.; Pesek, S. L.; Stein, G. E., *Chem. Soc. Rev.* **2015,** *44* (8), 2405-2420.

63. Thipparaboina, R.; Chavan, R. B.; Kumar, D.; Modugula, S.; Shastri, N. R., *Colloids Surf., B* **2015,** *135*, 291-308.

64. Moughton, A. O.; Hillmyer, M. A.; Lodge, T. P., *Macromolecules* **2012,** *45* (1), 2-19.

65. Richardson, J. J.; Cui, J.; Bjornmalm, M.; Braunger, J. A.; Ejima, H.; Caruso, F., *Chem. Rev.* **2016,** *116* (23), 14828-14867.

66. Reisch, A.; Klymchenko, A. S., *Small* **2016,** *12* (15), 1968-1992.

67. Huang, H.; Lovell, J. F., *Adv. Funct. Mater.* **2016**.

68. Zhang, S.; Zou, J.; Zhang, F.; Elsabahy, M.; Felder, S. E.; Zhu, J.; Pochan, D. J.; Wooley, K. L., *J. Am. Chem. Soc.* **2012,** *134* (44), 18467-18474.

69. Zhang, S.; Zou, J.; Elsabahy, M.; Karwa, A.; Li, A.; Moore, D. A.; Dorshow, R. B.; Wooley, K. L., *Chem. Sci.* **2013,** *4* (5), 2122-2126.

70. Lim, Y. H.; Tiemann, K. M.; Heo, G. S.; Wagers, P. O.; Rezenom, Y. H.; Zhang, S.; Zhang, F.; Youngs, W. J.; Hunstad, D. A.; Wooley, K. L., *ACS Nano* **2015,** *9* (2), 1995-2008.

71. Zhang, F.; Zhang, S.; Pollack, S. F.; Li, R.; Gonzalez, A. M.; Fan, J.; Zou, J.; Leininger, S. E.; Pavía-Sanders, A.; Johnson, R.; Nelson, L. D.; Raymond, J. E.; Elsabahy, M.; Hughes, D. M. P.; Lenox, M. W.; Gustafson, T. P.; Wooley, K. L., *J. Am. Chem. Soc.* **2015,** *137* (5), 2056-2066.

72. Gustafson, T. P.; Lonnecker, A. T.; Heo, G. S.; Zhang, S.; Dove, A. P.; Wooley, K. L., *Biomacromolecules* **2013,** *14* (9), 3346-3353.

73. Cho, S.; Heo, G. S.; Khan, S.; Gonzalez, A. M.; Elsabahy, M.; Wooley, K. L., *Macromolecules* **2015,** *48* (24), 8797-8805.

74. Gustafson, T. P.; Lim, Y. H.; Flores, J. A.; Heo, G. S.; Zhang, F.; Zhang, S.; Samarajeewa, S.; Raymond, J. E.; Wooley, K. L., *Langmuir* **2014,** *30* (2), 631-641.

75. Zhang, X.; Wang, K.; Liu, M.; Zhang, X.; Tao, L.; Chen, Y.; Wei, Y., *Nanoscale* **2015,** *7* (27), 11486-11508.

76. Xue, X.; Xu, J.; Wang, P. C.; Liang, X.-J., *J. Mater. Chem. C* **2016,** *4* (14), 2719-2730.

77. Chen, S.; Wang, H.; Hong, Y.; Tang, B. Z., *Mater. Horiz.* **2016,** *3* (4), 283-293.

78. Huang, Y.; Zhang, P. S.; Gao, M.; Zeng, F.; Qin, A. J.; Wu, S. Z.; Tang, B. Z., *Chem. Comm.* **2016,** *52* (45), 7288-7291.

79. Wang, X.; Hu, J.; Zhang, G.; Liu, S., *J. Am. Chem. Soc.* **2014,** *136* (28), 9890-9893.

80. Wang, X.; Gao, Z. C.; Zhu, J. L.; Gao, Z.; Wang, F., *Polym. Chem.* **2016,** *7* (33), 5217-5220.

81. Li, C. Y.; Liu, X. L.; He, S. S.; Huang, Y. B.; Cui, D. M., *Polym. Chem.* **2016,** *7* (5), 1121-1128.

82. Long, Z.; Liu, M.; Mao, L.; Zeng, G.; Wan, Q.; Xu, D.; Deng, F.; Huang, H.; Zhang, X.; Wei, Y., *Colloids Surf., B* **2016,** *150*, 114-120.

83. Wang, X.; Yang, Y.; Zhuang, Y.; Gao, P.; Yang, F.; Shen, H.; Guo, H.; Wu, D., *Biomacromolecules* **2016,** *17* (9), 2920-2929.

84. Scognamiglio, F.; Travan, A.; Rustighi, I.; Tarchi, P.; Palmisano, S.; Marsich, E.; Borgogna, M.; Donati, I.; de Manzini, N.; Paoletti, S., *J. Biomed. Mater. Res. Part B* **2016,** *104* (3), 626-639.

85. Ghobril, C.; Grinstaff, M. W., *Chem. Soc. Rev.* **2015,** *44* (7), 1820-1835.

86. Kwon, I. S.; Kim, Y. J.; Klosterman, L.; Forssell, M.; Fedder, G. K.; Bettinger, C. J., *J. Mater. Chem. B* **2016,** *4* (18), 3031-3036.

87. Garcia Cerda, D.; Ballester, A. M.; Aliena-Valero, A.; Caraben-Redano, A.; Lloris, J. M., *Surg. Today* **2015,** *45* (8), 939-956.

88. McNichol, L.; Lund, C.; Rosen, T.; Gray, M., *J. Wound Ostomy Continence Nurs.* **2013,** *40* (4), 365-380; quiz E361-362.

89. Lee, B. P.; Messersmith, P. B.; Israelachvili, J. N.; Waite, J. H., *Annu. Rev. Mater. Res.* **2011,** *41*, 99-132.

90. Sedo, J.; Saiz-Poseu, J.; Busque, F.; Ruiz-Molina, D., *Adv. Mater.* **2013,** *25* (5), 653-701.

91. Kord Forooshani, P.; Lee, B. P., *J. Polym. Sci. A Polym. Chem.* **2017,** *55* (1), 9-33.

92. Waite, J. H.; Tanzer, M. L., *Science* **1981,** *212* (4498), 1038-1040.

93. Faure, E.; Falentin-Daudré, C.; Jérôme, C.; Lyskawa, J.; Fournier, D.; Woisel, P.; Detrembleur, C., *Prog. Polym. Sci.* **2013,** *38* (1), 236-270.

94. Lee, H.; Dellatore, S. M.; Miller, W. M.; Messersmith, P. B., *Science* **2007,** *318* (5849), 426-430.

95. Maier, G. P.; Rapp, M. V.; Waite, J. H.; Israelachvili, J. N.; Butler, A., *Science* **2015,** *349* (6248), 628-632.

96. Rapp, M. V.; Maier, G. P.; Dobbs, H. A.; Higdon, N. J.; Waite, J. H.; Butler, A.; Israelachvili, J. N., *J. Am. Chem. Soc.* **2016,** *138* (29), 9013-9016.

97. Jin, F.-L.; Li, X.; Park, S.-J., *J. Ind. Eng. Chem.* **2015,** *29*, 1-11.

98. *Chemistry and Technology of Epoxy Resins*. 1st ed.; 1993.

99. *Epoxy Polymers: New Materials and Innovations*. 2010.

100. Seachrist, D. D.; Bonk, K. W.; Ho, S. M.; Prins, G. S.; Soto, A. M.; Keri, R. A., *Reprod. Toxicol.* **2016,** *59*, 167-182.

101. Stojanoska, M. M.; Milosevic, N.; Milic, N.; Abenavoli, L., *Endocrine* **2016**.

102. Im, J.; Loffler, F. E., *Environ. Sci. Technol.* **2016,** *50* (16), 8403-8416.

103. Cox, K. H., *Endocrinology* **2016,** *157* (2), 449-451.

104. Chen, D.; Kannan, K.; Tan, H.; Zheng, Z.; Feng, Y. L.; Wu, Y.; Widelka, M., *Environ. Sci. Technol.* **2016,** *50* (11), 5438-5453.

105. Baroncini, E. A.; Yadav, S. K.; Palmese, G. R.; Stanzione, J. F., *J. Appl. Polym. Sci.* **2016,** *133* (45).

106. Raquez, J. M.; Deleglise, M.; Lacrampe, M. F.; Krawczak, P., *Prog. Polym. Sci.* **2010,** *35* (4), 487-509.

107. Shibata, M.; Nakai, K., *J. Polym. Sci. B Pol. Phys.* **2010,** *48* (4), 425-433.

108. Auvergne, R.; Caillol, S.; David, G.; Boutevin, B.; Pascault, J. P., *Chem. Rev.* **2014,** *114* (2), 1082-1115.

109. Ma, S.; Li, T.; Liu, X.; Zhu, J., *Polym. Int.* **2016,** *65* (2), 164-173.

110. Ding, C.; Matharu, A. S., *ACS Sustainable Chem. Eng.* **2014,** *2* (10), 2217-2236.

111. Shibata, M.; Yoshihara, S.; Yashiro, M.; Ohno, Y., *J. Appl. Polym. Sci.* **2013,** *128* (5), 2753-2758.

112. Gupta, P.; Authimoolam, S. P.; Hilt, J. Z.; Dziubla, T. D., *Acta Biomater.* **2015,** *27*, 194-204.

113. Dasgupta, F. Biocompatible and biodegradable polymers from renewable natural polyphenols. 2013.

114. Zhang, K. D.; Matile, S., *Angew. Chem. Int. Ed.* **2015,** *54* (31), 8980-8983.

115. Puoci, F.; Morelli, C.; Cirillo, G.; Curcio, M.; Parisi, O. I.; Maris, P.; Sisci, D.; Picci, N., *Anticancer Res.* **2012,** *32* (7), 2843-2847.

116. Song, X. L.; Li, J. H.; Wang, J. T.; Chen, L. X., *Talanta* **2009,** *80* (2), 694-702.

117. Xia, Y.-q.; Guo, T.-y.; Song, M.-d.; Zhang, B.-h.; Zhang, B.-l., *React. Funct. Polym.* **2006,** *66* (12), 1734-1740.

118. Liu, S.; Pan, J.; Zhu, H.; Pan, G.; Qiu, F.; Meng, M.; Yao, J.; Yuan, D., *Chem. Eng. J.* **2016,** *290*, 220-231.

119. El-Gogary, R. I.; Rubio, N.; Wang, J. T.; Al-Jamal, W. T.; Bourgognon, M.; Kafa, H.; Naeem, M.; Klippstein, R.; Abbate, V.; Leroux, F.; Bals, S.; Van Tendeloo, G.; Kamel, A. O.; Awad, G. A.; Mortada, N. D.; Al-Jamal, K. T., *ACS Nano* **2014,** *8* (2), 1384-1401.

120. Mashhadi Malekzadeh, A.; Ramazani, A.; Tabatabaei Rezaei, S. J.; Niknejad, H., *J. Colloid Interface Sci.* **2016,** *490*, 64-73.

121. Song, X.; Zhao, Y.; Hou, S.; Xu, F.; Zhao, R.; He, J.; Cai, Z.; Li, Y.; Chen, Q., *Eur. J. Pharm. Biopharm.* **2008,** *69* (2), 445-453.

122. Russo, M.; Spagnuolo, C.; Tedesco, I.; Bilotto, S.; Russo, G. L., *Biochem. Pharmacol.* **2012,** *83* (1), 6-15.

123. Jurd, L., *J. Am. Chem. Soc.* **1958,** *80* (20), 5531-5536.

124. Jurd, L., *J. Org. Chem.* **1962,** *27* (4), 1294-1297.

125. Meier, M. A. R.; Metzger, J. O.; Schubert, U. S., *Chem. Soc. Rev.* **2007,** *36* (11), 1788-1802.

126. Samarajeewa, S.; Shrestha, R.; Li, Y.; Wooley, K. L., *J. Am. Chem. Soc.* **2012,** *134* (2), 1235-1248.

127. Petzetakis, N.; Robin, M. P.; Patterson, J. P.; Kelley, E. G.; Cotanda, P.; Bomans, P. H. H.; Sommerdijk, N. A. J. M.; Dove, A. P.; Epps, T. H.; O'Reilly, R. K., *ACS Nano* **2013,** *7* (2), 1120-1128.

128. Gustafson, T. P.; Lonnecker, A. T.; Heo, G. S.; Zhang, S.; Dover, A. P.; Wooley, K. L., *Biomacromolecules* **2013,** *ASAP*.

129. Azechi, M.; Matsumoto, K.; Endo, T., *J. Polym. Sci. A Polym. Chem.* **2013,** *51* (7), 1651-1655.

130. Shen, Y.; Chen, X.; Gross, R. A., *Macromolecules* **1999,** *32* (8), 2799-2802.

131. Li, Q.; Wenxiang, Z.; Li, C.; Guan, G.; Zhang, D.; Xiao, Y.; Zheng, L., *J. Polym. Sci. Part A: Polym. Chem.* **2013,** *51* (6), 1387-1397.

132. Miean, K. H.; Mohamed, S., *J. Agric. Food Chem.* **2001,** *49* (6), 3106-3112.

133. Chirumbolo, S., *Inflamm Allergy Drug Targets* **2010,** *9* (4), 263-285.

134. Chirumbolo, S., *Integr Cancer Ther* **2013,** *12* (2), 97-102.

135. Heo, H. J.; Lee, C. Y., *J. Agric. Food Chem.* **2004,** *52* (25), 7514-7517.

136. Manach, C.; Morand, C.; Crespy, V.; Demigné, C.; Texier, O.; Régérat, F.; Rémésy, C., *FEBS Lett.* **1998,** *426* (3), 331-336.

137. Zhang, Y.; Hays, A.; Noblett, A.; Thapa, M.; Hua, D. H.; Hagenbuch, B., *J. Nat. Prod.* **2013,** *76* (3), 368-373.

138. Graefe, E., *Int. J. Clin. Pharm. Th.* **1999,** *37* (5), 219.

139. Moon, Y. J.; Morris, M. E., *Mol. Pharmaceutics* **2007,** *4* (6), 865-872.

140. Bury, K.; Du Prez, F.; Neugebauer, D., *Macromol. Biosci.* **2013,** *ASAP*.

141. Puoci, F.; Morelli, C.; Cirillo, G.; Curcio, M.; Parisi, O. I.; Maris, P.; Sisci, D.; Picci, N., *Anticancer Res.* **2012,** *32*, 2843-2848.

142. Li, C.; Liu, X.; He, S.; Huang, Y.; Cui, D., *Polym. Chem.* **2016,** *7* (5), 1121-1128.

143. Cao, Z. H.; Liang, X. Q.; Chen, H. N.; Gao, M.; Zhao, Z. J.; Chen, X. L.; Xu, C.; Qu, G.; Qi, D. M.; Tang, B. Z., *Polym. Chem.* **2016,** *7* (35), 5571-5578.

144. He, L.; Liu, X.; Liang, J.; Cong, Y.; Weng, Z.; Bu, W., *Chem. Commun.* **2015,** *51* (33), 7148-7151.

145. Huang, Z. F.; Zhang, X. Q.; Zhang, X. Y.; Yang, B.; Zhang, Y. L.; Wang, K.; Yuan, J. Y.; Tao, L.; Wei, Y., *Polym. Chem.* **2015,** *6* (11), 2133-2138.

146. Taniguchi, R.; Yamada, T.; Sada, K.; Kokado, K., *Macromolecules* **2014,** *47* (18), 6382-6388.

147. Roy, D.; Brooks, W. L. A.; Sumerlin, B. S., *Chem. Soc. Rev.* **2013,** *42* (17), 7214-7243.

148. Theato, P.; Sumerlin, B. S.; O'Reilly, R. K.; Epps, T. H., *Chem. Soc. Rev.* **2013,** *42* (17), 7055-7056.

149. Thapa, M.; Kim, Y.; Desper, J.; Chang, K.-O.; Hua, D. H., *Bioorg. Med. Chem. Lett.* **2012,** *22* (1), 353-356.

150. Moalin, M.; van Strijdonck, G. P. F.; Beckers, M.; Hagemen, G. J.; Borm, P. J.; Bast, A.; Haenen, G. R. M. M., *Molecules* **2011,** *16* (11), 9636-9650.

151. Kristufek, S. L.; Yang, G.; Link, L. A.; Rohde, B. J.; Robertson, M. L.; Wooley, K. L., *ChemSusChem* **2016,** *9* (16), 2135-2142.

152. Zhou, J.; Wang, L.-f.; Wang, J.-y.; Tang, N., *J. Inorg. Biochem.* **2001,** *83* (1), 41-48.

153. Tang, Z.; He, C.; Tian, H.; Ding, J.; Hsiao, B. S.; Chu, B.; Chen, X., *Prog. Polym. Sci.* **2016,** *60*, 86-128.

154. Shukla, S. K.; Shukla, S. K.; Govender, P. P.; Giri, N. G., *RSC Adv.* **2016,** *6* (97), 94325-94351.

155. Wurm, F. R.; Weiss, C. K., *Front Chem* **2014,** *2*, 49.

156. Palivan, C. G.; Goers, R.; Najer, A.; Zhang, X.; Car, A.; Meier, W., *Chem. Soc. Rev.* **2016,** *45* (2), 377-411.

157. Sizovs, A.; Xue, L.; Tolstyka, Z. P.; Ingle, N. P.; Wu, Y.; Cortez, M.; Reineke, T. M., *J. Am. Chem. Soc.* **2013,** *135* (41), 15417-15424.

158. Dhande, Y. K.; Wagh, B. S.; Hall, B. C.; Sprouse, D.; Hackett, P. B.; Reineke, T. M., *Biomacromolecules* **2016,** *17* (3), 830-840.

159. Zhang, X.; Zhang, X.; Tao, L.; Chi, Z.; Xu, J.; Wei, Y., *J. Mater. Chem. B* **2014,** *2* (28), 4398.

160. Liu, Y.; Ai, K.; Lu, L., *Chem. Rev.* **2014,** *114* (9), 5057-5115.

161. Seo, S.; Das, S.; Zalicki, P. J.; Mirshafian, R.; Eisenbach, C. D.; Israelachvili, J. N.; Waite, J. H.; Ahn, B. K., *J. Am. Chem. Soc.* **2015,** *137* (29), 9214-9217.

162. Mehdizadeh, M.; Weng, H.; Gyawali, D.; Tang, L.; Yang, J., *Biomaterials* **2012,** *33* (32), 7972-7983.

163. Ahn, B. K.; Das, S.; Linstadt, R.; Kaufman, Y.; Martinez-Rodriguez, N. R.; Mirshafian, R.; Kesselman, E.; Talmon, Y.; Lipshutz, B. H.; Israelachvili, J. N.; Waite, J. H., *Nat Commun* **2015,** *6*, 8663.

164. Madhurakkat Perikamana, S. K.; Lee, J.; Lee, Y. B.; Shin, Y. M.; Lee, E. J.; Mikos, A. G.; Shin, H., *Biomacromolecules* **2015,** *16* (9), 2541-2555.

165. Zhou, J.; Defante, A. P.; Lin, F.; Xu, Y.; Yu, J.; Gao, Y.; Childers, E.; Dhinojwala, A.; Becker, M. L., *Biomacromolecules* **2015,** *16* (1), 266-274.

166. Brubaker, C. E.; Messersmith, P. B., *Biomacromolecules* **2011,** *12* (12), 4326-4334.

167. Dong, J.; Zhang, Q.; Cui, Q.; Huang, G.; Pan, X.; Li, S., *ChemMedChem* **2016,** *11* (19), 2102-2118.

168. Rice-Evans, C. A.; Miller, N. J.; Paganga, G., *Free Radic Biol Med* **1996,** *20* (7), 933-956.

169. Chan, W. C.; White, P. D., *Fmoc solid phase peptide synthesis: A Practical Approach*.

170. Kuhnel, E.; Laffan, D. D.; Lloyd-Jones, G. C.; Martinez Del Campo, T.; Shepperson, I. R.; Slaughter, J. L., *Angew. Chem. Int. Ed.* **2007,** *46* (37), 7075-7078.

171. Bouktaib, M.; Lebrun, S.; Atmani, A.; Rolando, C., *Tetrahedron* **2002,** *58* (50), 10001-10009.

172. Yao, L. H.; Datta, N.; Tomas-Barberan, F. A.; Ferreres, F.; Martos, I.; Singanusong, R., *Food Chem.* **2003,** *81* (2), 159-168.

173. Diaz, L.; Bujons, J.; Casas, J.; Llebaria, A.; Delgado, A., *J Med Chem* **2010,** *53* (14), 5248-5255.

174. Martin, E. H.; Brittain, W. J., *Polym Bull* **2002,** *47* (6), 517-520.

175. *Epoxy Resin Market by Application (Paints & Coating, Wind Turbine, Composites, Construction, Electrical & Electronics, Adhesives) and Geography - Trends & forecasts to 2019*; MarketsandMarkets, 2/2/16, 2014.

176. Vandenberg, L. N.; Maffini, M. V.; Sonnenschein, C.; Rubin, B. S.; Soto, A. M., *Endocr. Rev.* **2009,** *30* (1), 75-95.

177. Liu, W.; Zhou, R.; Goh, H. L. S.; Huang, S.; Lu, X., *ACS Appl. Mater. Interfaces* **2014,** *6* (8), 5810-5817.

178. Pin, J. M.; Guigo, N.; Vincent, L.; Sbirrazzuoli, N.; Mija, A., *ChemSusChem* **2015,** *8* (24), 4149-4161.

179. Pin, J. M.; Sbirrazzuoli, N.; Mija, A., *ChemSusChem* **2015,** *8* (7), 1232-1243.

180. Yang, G.; Rohde, B. J.; Robertson, M. L., *Green Mater.* **2013,** *1* (2), 125-134.

181. Kovash, C. S., Jr.; Pavlacky, E.; Selvakumar, S.; Sibi, M. P.; Webster, D. C., *ChemSusChem* **2014,** *7* (8), 2289-2294.

182. Rapi, Z.; Szolnoki, B.; Bakó, P.; Niedermann, P.; Toldy, A.; Bodzay, B.; Keglevich, G.; Marosi, G., *Eur. Polym. J.* **2015,** *67* (0), 375-382.

183. Hong, J.; Radojcic, D.; Ionescu, M.; Petrovic, Z. S.; Eastwood, E., *Polym. Chem.* **2014,** *5* (18), 5360-5368.

184. Zhao, S.; Abu-Omar, M. M., *Biomacromolecules* **2015,** *16* (7), 2025-2031.

185. Llevot, A.; Grau, E.; Carlotti, S.; Grelier, S.; Cramail, H., *Macromol. Rapid Commun.* **2016,** *37*, 9-28.

186. Mantzaridis, C.; Brocas, A. L.; Llevot, A.; Cendejas, G.; Auvergne, R.; Caillol, S.; Carlotti, S.; Cramail, H., *Green Chem.* **2013,** *15* (11), 3091-3098.

187. Brocas, A. L.; Llevot, A.; Mantzaridis, C.; Cendejas, G.; Auvergne, R.; Caillol, S.; Carlotti, S.; Cramail, H., *Des. Monomers Polym.* **2014,** *17* (4), 301-310.

188. Ma, Q. Q.; Liu, X. Q.; Zhang, R. Y.; Zhu, J.; Jiang, Y. H., *Green Chem.* **2013,** *15* (5), 1300-1310.

189. Wang, H. H.; Liu, X. Q.; Liu, B.; Zhang, J. W.; Xian, M., *Polym. Int.* **2009,** *58* (12), 1435-1441.

190. Shibata, M.; Teramoto, N.; Makino, K., *J. Appl. Polym. Sci.* **2011,** *120* (1), 273-278.

191. Formica, J. V.; Regelson, W., *Food Chem. Toxicol.* **1995,** *33* (12), 1061-1080.

192. Boots, A. W.; Haenen, G. R. M. M.; Bast, A., *Eur. J. Pharmacol.* **2008,** *585* (2–3), 325-337.

193. Matsuda, H.; Morikawa, T.; Yoshikawa, M., *Pure Appl. Chem.* **2002,** *74* (7), 1301-1308.

194. D'Andrea, G., *Fitoterapia* **2015,** *106*, 256-271.

195. Dmitrienko, S. G.; Kudrinskaya, V. A.; Apyari, V. V., *J. Anal. Chem.* **2012,** *67* (4), 299-311.

196. Turner, C.; Turner, P.; Jacobson, G.; Almgren, K.; Waldebäck, M.; Sjöberg, P.; Karlsson, E. N.; Markides, K. E., *Green Chem.* **2006,** *8* (11), 949-959.

197. Masek, A.; Zaborski, M., *C. R. Chim.* **2014,** *17* (9), 944-951.

198. Puebla, P.; López, J. L.; Guerrero, M.; Carrón, R.; Martìn, M. L.; San Román, L.; San Feliciano, A., *Phytochemistry* **2003,** *62* (4), 551-555.

199. Kaulich, M.; Streicher, F.; Mayer, R.; Müller, I.; Müller, C. E., *Drug Dev. Res.* **2003,** *59* (1), 72-81.

200. Shi, Z.-H.; Li, N.-G.; Tang, Y.-P.; Wei, L.; Lian, Y.; Yang, J.-P.; Hao, T.; Duan, J.-A., *Eur. J. Med. Chem.* **2012,** *54* (0), 210-222.

201. Wang, Y.; Hamburger, M.; Gueho, J.; Hostettmann, K., *Phytochemistry* **1989,** *28* (9), 2323-2327.

202. Toelle, N.; Weinstabl, H.; Gaich, T.; Mulzer, J., *Angew. Chem. Int. Ed.* **2014,** *53* (15), 3859-3862.

203. Pchelka, B. K.; Loupy, A.; Petit, A., *Tetrahedron* **2006,** *62* (47), 10968-10979.

204. CCDC 1451608 contains the supplementary crystallographic data for this paper. These data can be obtained free of charge from The Cambridge Crystallographic Data Centre.

205. CCDC 1451607 contains the supplementary crystallographic data for this paper. These data can be obtained free of charge from The Cambridge Crystallographic Data Centre.

206. Tanaka, Y.; Kakiuchi, H., *J. Polym. Sci. A Polym. Chem.* **1964,** *2* (8), 3405-3430.

207. Leukel, J.; Burchard, W.; Krüger, R.-P.; Much, H.; Schulz, G., *Macromol. Rapid Commun.* **1996,** *17* (5), 359-366.

208. Rohde, B. J.; Robertson, M. L.; Krishnamoorti, R., *Polymer* **2015,** *69*, 204-214.

209. Antoon, M. K.; Koenig, J. L., *J. Polym. Sci. A Polym. Chem.* **1981,** *19* (2), 549-570.

210. Hill, L. W., *Prog. Org. Coat.* **1997,** *31* (3), 235-243.

211. Iwata, T., *Angew. Chem. Int. Ed.* **2015,** *54* (11), 3210-3215.

212. Miller, S. A., *Polym. Chem.* **2014,** *5* (9), 3117-3118.

213. Miller, S. A., *ACS Macro Lett.* **2013,** *2* (6), 550-554.

214. Fenouillot, F.; Rousseau, A.; Colomines, G.; Saint-Loup, R.; Pascault, J. P., *Prog. Polym. Sci.* **2010,** *35* (5), 578-622.

215. Rose, M.; Palkovits, R., *ChemSusChem* **2012,** *5* (1), 167-176.

216. Chatti, S.; Schwarz, G.; Kricheldorf, H. R., *Macromolecules* **2006,** *39* (26), 9064-9070.

217. Yokoe, M.; Aoi, K.; Okada, M., *J. Polym. Sci. A Polym. Chem.* **2003,** *41* (15), 2312-2321.

218. Gallagher, J. J.; Hillmyer, M. A.; Reineke, T. M., *ACS Sustainable Chem. Eng.* **2015,** *3* (4), 662-667.

219. Sadler, J. M.; Nguyen, A.-P. T.; Toulan, F. R.; Szabo, J. P.; Palmese, G. R.; Scheck, C.; Lutgen, S.; La Scala, J. J., *J. Mater. Chem. A* **2013,** *1* (40), 12579-12586.

220. Gallagher, J. J.; Hillmyer, M. A.; Reineke, T. M., *Macromolecules* **2014,** *47* (2), 498-505.

221. Juais, D.; Naves, A. F.; Li, C.; Gross, R. A.; Catalani, L. H., *Macromolecules* **2010,** *43* (24), 10315-10319.

222. Shearouse, W. C.; Lillie, L. M.; Reineke, T. M.; Tolman, W. B., *ACS Macro Lett.* **2015,** *4* (3), 284-288.

223. Kang, H.; Li, X.; Xue, J.; Zhang, L.; Liu, L.; Xu, R.; Guo, B., *RSC Adv.* **2014,** *4* (37), 19462-19471.

224. Okada, M.; Aoi, K., *Current Trends in Polymer Science* **2002,** *7*, 57-70.

225. Oulame, M. Z.; Pion, F.; Allauddin, S.; Raju, K. V. S. N.; Ducrot, P.-H.; Allais, F., *Eur. Polym. J.* **2015,** *63*, 186-193.

226. Lorenzini, C.; Haider, A.; Kang, I.-K.; Sangermano, M.; Abbad-Andalloussi, S.; Mazeran, P.-E.; Lalevée, J.; Renard, E.; Langlois, V.; Versace, D.-L., *Biomacromolecules* **2015,** *16* (3), 683-694.

227. Ortiz, R. A.; Martinez, A. Y. R.; Valdez, A. E. G., *J. Biobased Mater. Bio.* **2012,** *6* (1), 36-41.

228. Lorenzini, C.; Versace, D. L.; Gaillet, C.; Lorthioir, C.; Boileau, S.; Renard, E.; Langlois, V., *Polymer* **2014,** *55* (17), 4432-4440.

229. Renard, E.; Modjinou, T.; Versace, D.-L.; Abbad-Andaloussi, S.; Bousserrhine, N.; Babinot, J.; Langlois, V., *ACS Sustainable Chem. Eng.* **ASAP**, DOI: 10.1021/acssuschemeng.1025b00018.

230. Artham, T.; Doble, M., *Macromol Biosci* **2008,** *8* (1), 14-24.

231. Albertsson, A.-C.; Eklund, M., *J. Appl. Polym. Sci.* **1995,** *57* (1), 87-103.

232. Liu, Q. Y.; Jiang, L.; Shi, R.; Zhang, L. Q., *Prog. Polym. Sci.* **2012,** *37* (5), 715-765.

233. Lörcks, J., *Polymer Degradation and Stability* **1998,** *59* (1-3), 245-249.

234. Lin, Q.; Pasatta, J.; Long, T. E., *J. Polym. Sci. A Polym. Chem.* **2003,** *41* (16), 2512-2520.

235. Yokoe, M.; Aoi, K.; Okada, M., *J. Appl. Polym. Sci.* **2005,** *98* (4), 1679-1687.

236. Dondoni, A., *Angew. Chem. Int. Ed.* **2008,** *47* (47), 8995-8997.

237. Kolb, H. C.; Finn, M. G.; Sharpless, K. B., *Angew. Chem. Int. Ed.* **2001,** *40* (11), 2004-2021.

238. Killops, K. L.; Campos, L. M.; Hawker, C. J., *J. Am. Chem. Soc.* **2008,** *130* (15), 5062-5064.

239. Rydholm, A. E.; Bowman, C. N.; Anseth, K. S., *Biomaterials* **2005,** *26* (22), 4495-4506.

240. Kasprzak, S. E.; Martin, B.; Raj, T.; Gall, K., *Polymer* **2009,** *50* (23), 5549-5558.

241. Shin, J.; Nazarenko, S.; Hoyle, C. E., *Macromolecules* **2008,** *41* (18), 6741-6746.

242. Imbesi, P. M.; Raymond, J. E.; Tucker, B. S.; Wooley, K. L., *J. Mater. Chem.* **2012,** *22* (37), 19462-19473.

243. Olofsson, K.; Malkoch, M.; Hult, A., *RSC Adv.* **2014,** *4* (57), 30118.

APPENDIX I

RAPIDLY-CURED ISOSORBIDE-BASED CROSS-LINKED POLYCARBONATE ELASTOMERS[‡]

A.1 Overview

The rapid synthesis of an optically-transparent, flexible elastomer was performed utilizing the naturally-derived source, isosorbide. A novel monomer based on isosorbide (isosorbide dialloc, IDA) was prepared by installing carbonate functionalities along with external olefins for use in thiol-ene click chemistry. Cross-linked networks were created using the commercially-available cross-linker, trimethylolpropane tris(3-mercaptopropionate) (TMPTMP) and resulted in IDA-*co*-TMPTMP, an optically-transparent elastomer. Systematically, IDA-*co*-TMPTMP networks were synthesized using a photoinitiator, a UV cure time of one minute and varied post cure times (0-24 h, 125 mm Hg) at 100 °C to observe effects on mechanical, thermal and surface alterations. The mechanical properties also had limited changes with post cure time, including a modulus at 25 °C of 1.9-2.8 MPa and an elongation of 220-344%. The thermal decomposition temperatures of the networks were consistent, *ca.* 320°C, while the glass transition temperature remained below room temperature for all samples. A cell viability assay and fluorescence imaging with adherent cells are also reported in this

[‡] Reprinted with permission from "Rapidly-cured isosorbide-based cross-linked polycarbonate elastomers" by Kristufek, T. S.; Kristufek, S. L.; Link, L. A.; Weems, A. C.; Khan, S.; Lim, S.-M.; Lonnecker, A. T.; Raymond, J. E.; Maitland, D. J.; Wooley, K. L. 2016. Polymer Chemistry, 7, 2639-2644, Copyright 2016 by The Royal Society of Chemistry.

study to show the potential of the material as a biomedical substrate. A degradation study for 60 days resulted in 8.3 ± 3.5% and 97.7 ± 0.3% mass remaining under accelerated (1M NaOH, 60 °C) and biological conditions (pH 7.4 PBS at 37 °C), respectively. This quickly-synthesized material has the potential to hydrolytically degrade into biologically-benign and environmentally-friendly by-products and may be utilized in renewable plastics and/or bioelastomer applications.

A.2 Introduction

The use of safe, natural products is one avenue to introduce sustainability and utility into materials. Specifically, by adopting renewable resources, there is a decrease in the reliance on petrochemicals that are inherently unsustainable in their current state. Considering easily mass produced, inexpensive starting materials from natural products would allow for natural material to begin to rival petrochemicals as a source for monomers.[28, 211-213] Derived from sugars, 1,4:3,6-dianhydrohexitols (*e.g.* isosorbide, isomannide and isoidide), especially isosorbide, have served as attractive renewable starting materials, contributing to a large assortment of bio-based/inspired polymers due to both the rigidity of their fused ring systems and the easily-modifiable dual-hydroxyl functionalities.[214] 1,4:3,6-Dianhydro-D-sorbitol, isosorbide is readily available in a few steps from biomass sources.[215] Mass production of this material has been utilized by Mitsubishi Chemical through the incorporation of isosorbide into what they call "the world's first high performance bio-based polycarbonatediol."[7] Isosorbide has also been incorporated into other polycarbonates,[216-217] polymethacrylates,[218-220] polyesters[221-223] and other polymers.[214, 224-225]

Although there has been a large amount of industrial and academic research focused on isosorbide-based materials, one area that has had limited exploration utilizing isosorbide is elastomers formed by thiol-ene click chemistry to produce cross-linked networks.[226-229] Specifically, isosorbide was functionalized with allyl ether moieties and subsequently copolymerized with a tri-functional mercaptopropionate. The resulting bio-based elastomers exhibited T_g values ranging -10 to -2 °C and have the potential to hydrolytically degrade through the ester linkages.[226-227, 229] One previously-reported strategy to induce degradability is to functionalize hydroxyl groups to create carbonate linkages. This strategy was employed to produce degradable poly(thioether-*co*-carbonate) networks derived from the natural product quinic acid.[14] In contrast to esters, which produce acids upon hydrolysis, carbonates are converted to carbon dioxide and hydroxyl-containing compounds upon degradation.[230-231] By including carbonate linkages at the hydroxyl sites, it is possible to design a material from isosorbide that has the potential to also produce isosorbide as it degrades. The goal of this work is to produce rapidly-photo-cross-linked isosorbide-based elastomers *via* thiol-ene chemistry that also have the potential to hydrolytically break down into their original natural building blocks. These materials can have applications similar to other bioelastomers including scaffolding materials or soft tissue engineering.[232] or starch-based biopolymers including renewable plastics.[233]

Herein is described the synthesis of a novel isosorbide-based monomer, isosorbide dialloc, (IDA) (Scheme 1). IDA contains terminal olefins capable of thiol-ene cross-linking *via* radical addition of a thiol across the alkene. Copolymerization of

IDA and commercially-available, trimethylolpropane *tris*(3-mercaptopropionate) (TMPTMP) in the presence of a photoinitiator was achieved by mixing IDA and TMPTMP based on equal molar functional groups and exposing to UV light (365 nm) for 1 minute. Crosslinking was confirmed by consumption of the alkene (1650 cm^{-1}) and thiol (2570 cm^{-1}) groups in both FTIR and Raman spectra. Networks were subjected to a post-cure at an elevated temperature and under reduced pressure (100 °C, 125 mm Hg) for times ranging from 0-24 h. The effect of post-cure time was evaluated by examining the surface chemistry (contact angle, Raman and IR spectroscopy) as well as the thermal (DSC/TGA) and mechanical (DMA and stain-to-failure measurements) properties to understand if the application of heat after the photo-reaction is necessary to give the optimal properties of the synthesized materials.

A.3 Experimental

Materials

Isosoribe (98%), allyl chloroformate (97%), 2,2-dimethoxy-2-phenylacetophenone (DMPA, 99%) and trimethylolpropane tris(3-mercaptopropionate) (TMPTMP, ≥95%) were purchased from Sigma Aldrich. *N*,*N*,*N*′,*N*′-Tetramethylethylenediamine (TMEDA, 99%) was purchased from Alfa Aesar. Anhydrous solvents were purchased from Fisher Scientific and further dried and degassed using a SciMatCo solvent purification system. All other reagents were used as received.

Characterization

^{1}H and ^{13}C NMR spectra were recorded on a Varian 500 spectrometer interfaced to a UNIX computer using Mercury software. The monomer was purified by Medium Pressure Liquid Chromatography (MPLC) using a CombiFlash R_f (Teledyne Isco) (80:20 hexanes:ethylacetate). Chemical shifts were referenced to the solvent nuclei resonances. IR spectra were obtained on a Shimadzu IR Prestige Attenuated Total Reflectance Fourier-transform Infrared Spectrometer (ATR-FTIR). Spectra were analysed using IRsolution software package (Shimadzu). Raman Spectroscopy was recorded using the B&W Tek iRaman system operating at 785 nm over the range of 700 to 3400 cm^{-1} and were analyzed by BW Spec 3.27 software.

Differential scanning calorimetric (DSC) studies were performed on a DSC822^{e} (Mettler-Toledo), with a heating rate of 10 ºC/min to determine the glass transition (T_g) of the thermosets. The T_g was taken as the midpoint of the inflection tangent upon the third heating scan. Thermogravimetric analysis was performed under Ar atmosphere using a model TGA/DSC 1 Star^{e} system (Mettler-Toledo), with a heating rate of 10 ºC/min measured at the onset. Measurements were analyzed using Star^{e} software version 10.00d (Mettler-Toledo).

Static Water Contact Angle Measurements

Contact angles were measured as static contact angles using the sessile drop technique with an Attension Theta optical tensiometer (Biolin Scientific). Drops were fitted with a Young–Laplace formula to calculate the static contact angle in the Theta software (Biolin Scientific). Each measurement was performed five times with reported

value being the average of these runs and was taken 3 seconds from the time that the drop was placed on the thermoset. After each run, the sample was picked up by a set of tongs and the surface was dried with a Kimwipe.

Mechanical Measurements

Dynamic mechanical analysis (DMA) was performed on a Mettler Toledo TT-DMA system. Samples were *ca.* 7 x 5 x 0.6 mm. DMA data were obtained from Triton Laboratory software and exported to Origin Pro 9.0 for analysis. Dynamic mechanical analysis (Mettler-Toledo TT-DMA, Columbus, OH) was measured in tension via thermal scan (3 °/min) from -80 to 120 °C, under a dynamic force of 1 N, a static/dynamic force ratio of 1.5, and a frequency of 1 Hz.

To determine toughness values, ultimate tensile strengths, and failure strains, tensile testing experiments were conducted to failure on ASTM D638 type IV, with a thickness of 0.60 mm ± 0.05 mm. dog bone samples (n = 5) using a dual-column Instron model 5965 tensile tester with a 500 N load cell, 1000 N high temperature pneumatic grips, and a temperature chamber thermally controlled by forced convection heating. Tests were run at a speed of 5 mm/min to obtain elastic modulus, tensile strength and elongation at break at room temperature. The dog bone samples were cut with a 40 W Gravograph LS100 CO_2 laser and edges were smoothed with 180 grit sandpaper.

Pneumatic grips were used to affix the sample in the testing frame at a compressed air pressure of 50 psi. Each measurement was repeated with 5 test specimens minimum, with each sample examined after testing to ensure the break occurred in the neck segment.

Cell Culture

MC3T3 cells were purchased from the American Type Culture Collection (ATCC, Manassas, VA) and subcultured according to ATCC protocol. Briefly, cells were cultured in MEM-alpha medium supplemented with 10% fetal bovine serum (Sigma-Aldrich, St. Louis, MO) and 1% antibiotic (Lonza, Walkersville, MD). Confluent cells were treated with Trypsin:EDTA (Sigma-Aldrich, St. Louis, MO) and counted with a Countess II cell counter (ThermoFisher Scientific, Waltham, MA). Prior to plating cells on glass-bottomed cell culture dishes and incubated at 37 °C with 5 % CO_2. Polymer-coated dishes were sterilized under UV in the biosafety cabinet and washed with sterile DPBS (Life Technologies, Carlsbad, CA) before plating cells on them.

Fixation and Immunofluorescence

Cells were fixed after 24 h from cell plating with 2% paraformaldehyde (Electron microscopy sciences, Hatfield, PA) and co-stained with Phalloidin-Alexa488 (Life Technologies, Carlsbad, CA) and anti-vinculin antibody (Sigma-Aldrich, St. Louis, MO) followed by secondary antibody conjugated with Alexa 647 (Life Technologies, Carlsbad, CA).

Confocal Imaging

Fluorescence images were acquired with a laser scanning confocal microscope (Olympus, Japan) with default excitation and emission filter settings for each fluorophore. Overall cell population was identified from large filter view with 10x objective (image size 1271.81 x 1271.81 μm). Details of cell morphology were

investigated from the images acquired with 20x objective with 2x zoom (image size 317.44 x 317.44 μm).

Cytotoxicity Assays

IDA-*co*-TMPTMP film polymer was plated with MC3T3-E1 mouse preosteoblast cells (5 x 103 cells/well) in 96-well plate in MEMα medium (10% fetal bovine serum and 1% penicillin/streptomycin). Cells with films were incubated at 37 ºC in a humidified atmosphere containing 5% CO_2 for 72 h. MTS combined reagent (20 μL) was added to each well (Cell Titer 96® Aqueous Non-Radioactive Cell Proliferation Assay, Promega Co., Madison, WI). The cells were incubated with the reagent for 2 h at 37 °C in a humidified atmosphere containing 5% CO_2 protected from light. Absorbance was measured at 490 nm using SpectraMax M5 (Molecular Devices Co., Sunnyvale, CA). The cell viability was calculated based on the relative absorbance to the control-untreated cells.

Synthetic Procedure

<u>Monomer Synthesis, isosorbide dialloc, IDA.</u>

In a 500-mL round bottom flask, oven dried (100 °C for ~1 h) under N_2 (degassing by vacuuming and back filling with N_2 4 times at room temperature) and in an ice bath above a stir plate (*c.a*. 500 rpm) isosorbide (10.0 g, 68.4 mmol), dry CH_2Cl_2 (250 mL) and TMEDA (24.0 mL, 150 mmol) were combined and cooled to 0 °C. Allyl chloroformate (25.0 mL, 235 mmol) was added via syringe pump at a rate of 20 mL/h. The reaction was allowed to warm to room temperature and proceed over the following 24 h. The solution was washed with water (250 mL x 3), 0.5 M HCl (250 mL x 2),

saturated solution of sodium bicarbonate (250 mL x 2) and brine (250 mL x 2). The organic phase was dried over anhydrous $MgSO_4$ and concentrated in vacuo to a slightly viscous pale yellow oil. The crude oil was purified by an automatic flash column chromatography system eluded with a gradient of ethyl acetate in hexanes (0 to 20%) and concentrated to afford a clear oil (18.5 g, 86.1% yield, isosorbide dialloc, IDA). R_f = 0.7 ^{1}H-NMR (500 MHz, $CDCl_3$): δ 5.99-5.91 (m, 2H, H9, H9'), 5.39 (m, 2H, H10-trans, H10'-trans), 5.31 (m, 2H, H10-cis, H10'-cis), 5.13 (d, *J* = 3.4 Hz, 1H, H2), 5.10 (app q, *J* = 5.4 Hz, 1H, H5), 4.92 (app t, *J* = 5.2 Hz, 1H, H4), 4.68-4.65 (m, 4H, H8, H8'), 4.57 (app d, *J* = 4.8 Hz, 1H, H1), 4.11 (d, *J* = 11.1 Hz, 1H, H6), 4.05 (dd, *J* = 11.0, 3.4 Hz, 1H, H3'), 3.94-3.92 (m, 2H, H3 and H6'); ^{13}C NMR (125 MHz, $CDCl_3$): δ 154.3 (C7 or C7'), 154.0 (C7' or C7), 131.30 (C9 or C9'), 131.17 (C9' or C9), 119.3 (C10 or C10'), 119.0 (C10' or C10), 85.9 (C1), 81.3 (C2), 80.9 (C4), 76.8 (C5), 73.2 (C6 or C3), 70.5 (C3 or C6), 68.82 (C8 or C8'), 68.79 (C8' or C8); FTIR (ATR) 3060-2860, 1740, 1650, 1450, 1430, 1370, 1350, 1290, 1240, 1170, 1100, 1050, 1000, 970, 940 cm^{-1}; HRMS (ESI^+, m/z): $[M+Li]^{+1}$ calculated for $C_{14}H_{18}O_8Li$, 321.1162, found 321.1163.

Thermoset Synthesis, IDA-*co*-TMPTMP.

In a vial wrapped in aluminum foil (to protect from undesired UV radiation), IDA (1.26 g, 4.00 mmol) and trimethylolpropane tris(3-mercaptopropionate) (TMPTMP) (1.07 g, 2.67 mmol) were combined in reactive end functionality stoichiometric ratio along with DMPA (0.0236 g, 1 wt%), stirred for 10 minutes over a stir plate, placed on the vortex for 2 minutes then sonicated for 10 minutes. Immediately, the mixture was pipetted between two glass slides in-between three glass cover slips and placed under a

365 nm light for 1 minute. Post cross-linking the sample was placed in a vacuum oven at 100 °C and 125 mm Hg for various times (0, 6, 12, 18 or 24 h) to afford the desired product, IDA-*co*-TMPTMP as a transparent, colorless film. FTIR (ATR) 3050-2810, 1740, 1730, 1250, 1140, 1000, 970 cm^{-1}.

A.4 Results and Discussion

The monomer IDA was prepared in one step by functionalizing 1,4:3,6-dianhydro-D-sorbitol, isosorbide, with two alloc functionalities using allyl chloroformate under conditions as described previously (Scheme 1).[14] Briefly, to install the alloc

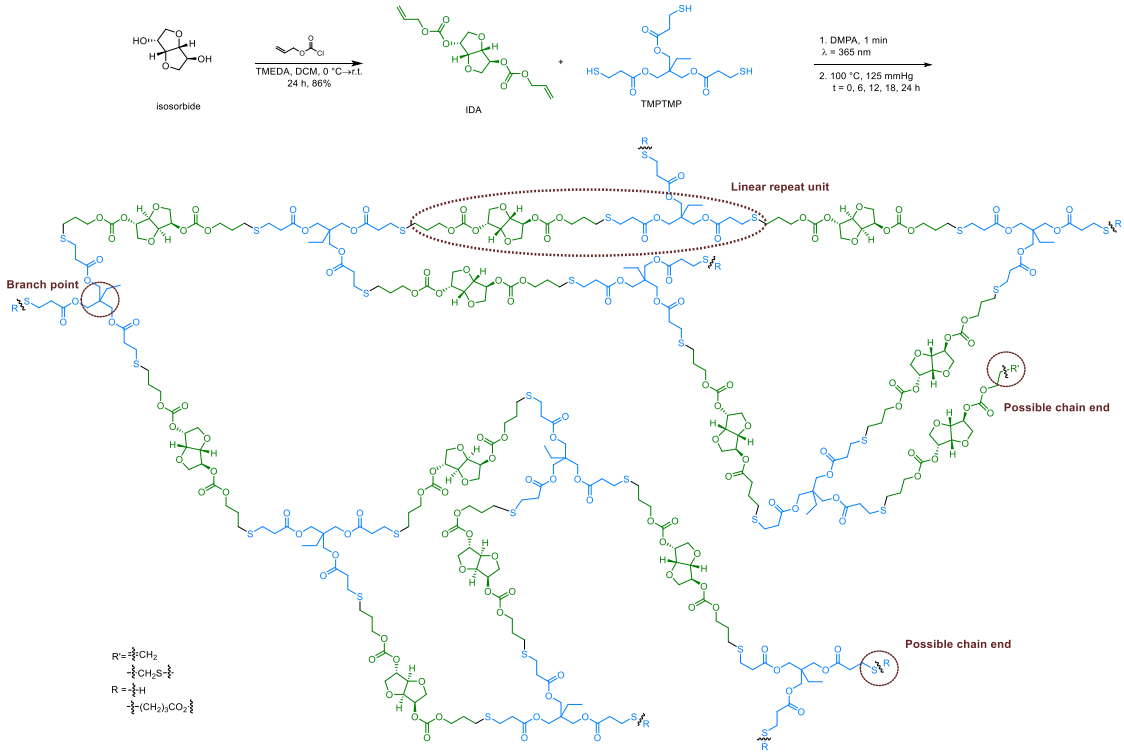

Scheme A1. Synthesis of the monomer IDA and the cross-linked network, IDA-*co*-TMPTMP.

groups *N,N,N′,N′*-tetramethylethylenediamine was added to isosorbide dissolved in dichloromethane and cooled to 0 °C. Allyl chloroformate was added dropwise at 0 °C and the reaction mixture was allowed to warm to room temperature overnight to deliver a purified yield of 86% as a lightly viscous, colourless oil. The synthesis of the monomer was confirmed by ^{1}H NMR, ^{13}C NMR, COSY, ATR-FTIR and ESI-MS (SI Figures 1-4).

Polycarbonates derived from the natural product isosorbide were designed with several attractive features. Isosorbide includes a fused-ring system that is non-toxic and chiral, both of which are beneficial to the final material.[214, 234] Functionalizing isosorbide *via* installation of allyl carbonates served two purposes. First, the carbonate functionality allows for potential degradation back to isosorbide and CO_2, resulting in an environmentally/biologically-friendly product. Various carbonate-based co-polymers have been shown to be degradable in other cross-linked networks.[235] Secondly, the alkene was introduced for polymerization and/or cross-linking by thiol-ene click chemistry. Click chemistry has become a widely used, simple, prominent concept in organic synthesis, polymerizations, and materials chemistry due to multiple factors: no/low solvent systems, limited excess material, high efficiency, low catalyst loading under ambient conditions, and insensitivity to the presence of moisture.[236-238] In these studies, focus was upon cross-linked network formation, involving reaction of commercially-available trimethylolpropane *tris*(3-mercaptopropionate) (TMPTMP) with IDA to afford an optically-transparent, flexible material, IDA-*co*-TMPTMP. Besides the thiol functionalities that were used for cross-linking, TMPTMP also has ester linkages,

which may act other potential degradation sites.[239] With degradation as the intention of these types of materials, TMPTMP has been previously been studied *in vivo* for toxicity and found to be a good candidate for these types of materials.[239] Ester cross-linkers are well known to have flexible and elastomeric properties[240] that, when combined with the rigid structure of IDA, are expected to yield a tough yet ductile material. The cross-linker is trifunctional, so by combining it with the difunctional IDA, three-dimensional cross-linked networks with moderate crosslink density can be achieved.

In all experiments, IDA and TMPTMP were mixed in an equal molar ratio based on functional groups, with variation in the curing conditions. Full reaction of the TMPTMP thiol was observed at 1 minute UV curing (λ = 365 nm) and no post-cure heating. This result displays that at least at the surface level,

the network can be synthesized quickly under mild conditions including no solvent and limited catalyst loading (*e.g.* 1 wt%).

Thiol consumption was confirmed by Raman and IR spectroscopies with the disappearance of the thiol bands observed at *ca*. 2570 cm^{-1} in parallel with an apparent increase in alkane functionality (2800-2980 cm^{-1}) (SI Figure 4A and 4B).

To understand whether post-cure heating would exert effects on multiple properties, such as T_g, decomposition temperature (T_d), elongation and storage modulus of the IDA-co-TMPTMP films, the post-cure time at 100 °C under vacuum was altered and tested systematically over the range of 0-24 h. The extent of cross-linking reaction was monitored by IR and Raman spectroscopies (Figure 4A and 4B) by following the alkane growth and thiol disappearance. Static water contact angle measurements were

taken at five different points on each film and averaged (SI Figure 5). Slight changes in the contact angle occurred with the addition of a post-cure. From a post-cure time 0 h temperature for the 1 min UV cure until 18 h the water contact angle steadily increased from 72 ° to 81 ° followed by a decrease from 18 h to 24 h, where it returned to 72 °. The trend might indicate relaxation of the chains upon application of heat to the material which can induce reorder depending on the time and temperature used during the post-cure process.[241] While there was a change in the surface properties overall, the material remained relatively hydrophobic under all tested conditions. Although the reaction was complete on the surface at one minute of UV irradiation, post-cure heating conditions has the potential to enable vaporization of remaining small molecules, vulcanization of any residual thiols[242] and network relaxation.[241]

Table A1. Observed thermal properties of IDA-*co*-TMPTMP networks.

Time (h)	**T_d (°C)**	**T_g (°C)**
0	317	16.5 ± 0.2
6	320	18.4 ± 0.6
12	322	15.8 ± 0.1
18	322	14.1 ± 0.5
24	322	14.4 ± 0.2

The surface morphology, thermal and mechanical properties were, therefore, monitored with the addition of a thermal post-cure at elevated temperature and reduced pressure. The T_d of the networks was measured by thermogravimetic analysis (TGA) and remained nearly constant around 320 °C with the addition of a post-cure (Table 1). The T_g of the networks was measured using differential scanning calorimetry (DSC) and reported the average of three runs. The T_g remained below room temperature in the range from 14 to 18 °C for different post-cure times (Table 1). The thermo-mechanical behaviour of the networks was determined by dynamic mechanical analysis (DMA), run in tension. The storage modulus as a function of temperature of each network is shown in Figure 1. These traces are indicative of amorphous cross-linked networks. Three regions of the differing mechanical response were observed with changing temperature. At low temperatures, there was a glassy modulus plateau on the order of 1 GPa. The glass transition region is recognized by the drastic decrease in modulus with increasing temperature. Beyond the glass transition region, the rubbery modulus plateau was constant or slightly increasing with increasing temperature and, in accordance with the rubber elasticity theory, is proportional to the crosslink density of the network. The storage modulus at 25 °C increased from 79 to 550 MPa with the application of a post-cure for at least 18 h. This trend is similar to the trend in hydrophobicity determined by contact angle measurements, which could be due to microstructuring and relaxation of the network as more energy is added to the system. With the exception of the sample that received no post-cure, the rubbery modulus of the networks increased with increasing post-cure time, from 5.8 MPa at 6 h to 7.1 MPa at 24 h, showing a slight

increase in crosslink density as a result of additional crosslinking reactions occurring, including the vulcanization of residual thiols and the stiffening of the network as a result of matrix relaxation. The reduction in rubbery modulus from 6.5 MPa at 0 h to 5.8 MPa at 6 h under post-cure conditions is not unusual and may be due to entanglement relaxation. Using the theory of rubber elasticity, the cross-link density (ν_c) defined as the number of moles of elastically effective network chains per cubic centimeter of sample can be calculated with the following equation:

$$\nu_c = \frac{\varepsilon'}{3RT} \ (equation\ 1)$$

where R is the gas constant, T is the temperature and ε' is the rubbery modulus at 50 °C.[210] Values (Table 1) can be compared to the ideal cross-linked network density of 1.98 x 10^{-3} mol/cm^3. The difference between the theoretical and calculated ν_c is characteristic of a network with incomplete conversion of all functional groups. The cross-link density can be used to calculate the molecular weight between crosslinks defined as total sample weight that contains one mole of elastically effective network chains (M_c) using the following equation:

$$M_c = \frac{\rho}{\nu_c} \ (equation\ 2)$$

where ρ is the density of the film.[210] The density was measured to be 1.2 g/cm^3 and the theoretical M_c was calculated to be 606 g/mol. The measured values are *ca.* 2.5x greater than the calculated values indicative of a non-ideal crosslinked network. The values have limited changes with the application of heat showing the networks are crosslinked to the fullest extent permitted by the chemical structure within the confined space of the reaction.

Table A2. Thermal and mechanical properties of various thermally cured IDA-*co*-TMPTMP networks.

Time (h)	***Storage Modulus [a] (MPa)***	***E_r* (MPa)[b]**	***Modulus (MPa)***	***Elongation at break(%)***	***Tensile Strength (MPa)***	***Toughness ($MJ*m^{-3}$)***	***ν_c (mol/cm^3)***	**M_c (g/mol)**
0	79	6.5	1.9 ± 0.2	250 ± 40	3.7 ± 0.5	4.9 ± 0.5	8.06×10^{-4}	1488
6	280	5.8	2.8 ± 0.2	280 ± 50	6.6 ± 1.0	9.5 ± 3.0	7.20×10^{-4}	1668
12	430	6.2	2.4 ± 0.2	340 ± 50	7.8 ± 1.0	13.4 ± 3.6	7.69×10^{-4}	1560
18	550	6.9	2.5 ± 0.4	260 ± 40	4.6 ± 1.3	7.2 ± 1.9	8.56×10^{-4}	1402
24	350	7.1	2.8 ± 0.2	220 ± 30	4.6 ± 0.7	5.3 ± 0.2	8.81×10^{-4}	1362

[a]Storage modulus measured by DMA at 25 °C [b]Rubbery modulus measured at 50 °C.

To further characterize the mechanical properties of IDA-*co*-TMPTMP, ASTM type V dog-bone samples were prepared, by laser cutting sheets of the material, and subjected to strain-to-failure measurements (five of each sample species); representative curves are shown in Figure 1. The average % elongation, tensile strengths and moduli are shown in Table 1. Consistent with thermal, surfacial and other mechanical data,

there were limited changes in the stain-to-failure properties. The modulus increased slightly from 1.9 to 2.8 MPa with the addition of 6 h post-cure, but beyond 6 h, changes were negligible. The % elongation at break ranged from 220-340% and showed no significant change with the addition of a post-cure. The ultimate tensile strength ranged from 3.7-7.8 MPa and was maximized at 12 h post-cure.

Degradation Study

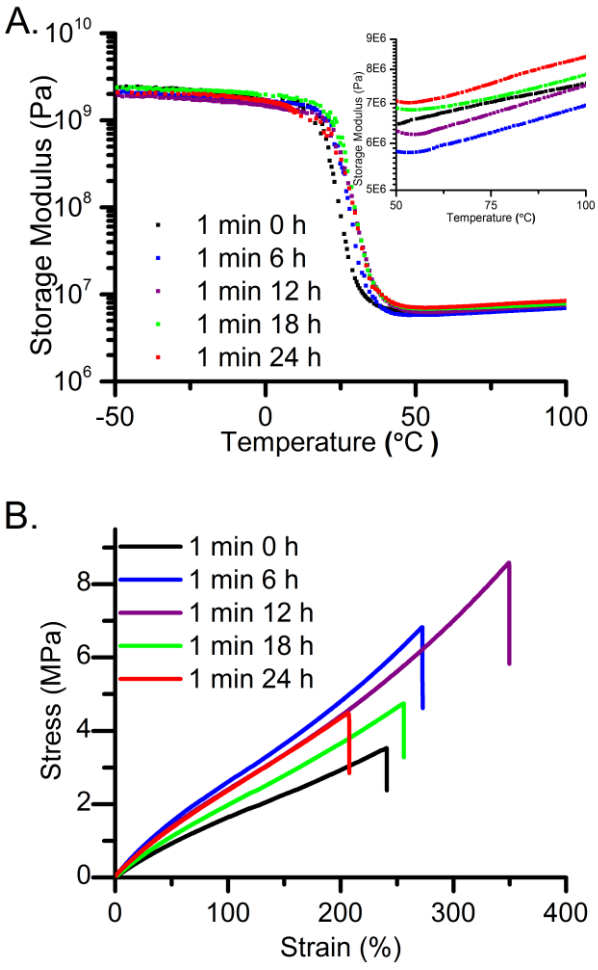

Figure A1. A. Storage modulus as a function of increasing series with inset zoomed in on the rubbery modulus. B. Representative stain-to-failure curves of IDA-*co*-TMPTMP.

With the goal of rapidly UV-cured materials, the bulk materials were subjected to a degradation study under both accelerated and biological conditions. Pellets were formed by casting a mixture of IDA and TMPTMP into moulds and cured then removed from the moulds and cured on the other side (1 min irradiation each side). In the accelerated study, pellets were initially massed dry then submerged into a solution of 1 M NaOH (2.0 mL). Each solution with a pellet was heated to 60 °C with 120 rpm stirring. After two days, the samples were removed from solution, washed with DI water and blotted dry with a Kimwipe. The mass was measured to obtain the wet mass (x_{wet}). The pellets were then dried at 100 °C under vacuum for 2 h. The dry pellets were massed again followed by submersion into a fresh solution of 1 M NaOH and heated to 60 °C. This process was repeated for 60 days. After being submerged in solution, the pellets were translucent (Figure 2, bottom, left), but after drying, the pellets returned to being transparent (Figure 2, bottom, right). Degradation occurred at a closely linear trend for the duration of the study. On day 60, 8.3 ± 3.5% mass remained. The swelling ratio (SR) was calculated using the following equation:

$$SR = \frac{x_{wet} - x_{dry}}{x_{dry}} \times 100\% \ (equation\ 3)$$

where x_{wet} and x_{dry} are the mass of the wet (after blotting) and dry (after vacuum) materials, respectively. This material had limited swelling over the length of the study with a slight increase in swelling with time (Figure 2) and a swelling ratio of 4.9 ± 1.1 on day 60. The linear decrease in degradation of the mass with time while maintaining the shape (Figure 2, bottom) suggests surface erosion of the polymer networks.

Under biological conditions, PBS buffer at 37 °C and pH = 7.4, three pellets were submerged for the same duration as the accelerated study, and were found to show 97.7 ± 0.3% mass remaining on day 60. Under these biological conditions, the swelling ratio increased slightly over time and was 2.1 ± 0.3 on day 60. IDA-*co*-TMPTMP will degrade under biological conditions, but at a slower rate when compared to the accelerated basic conditions.

Cell Viability and Fluorescence Microscopy

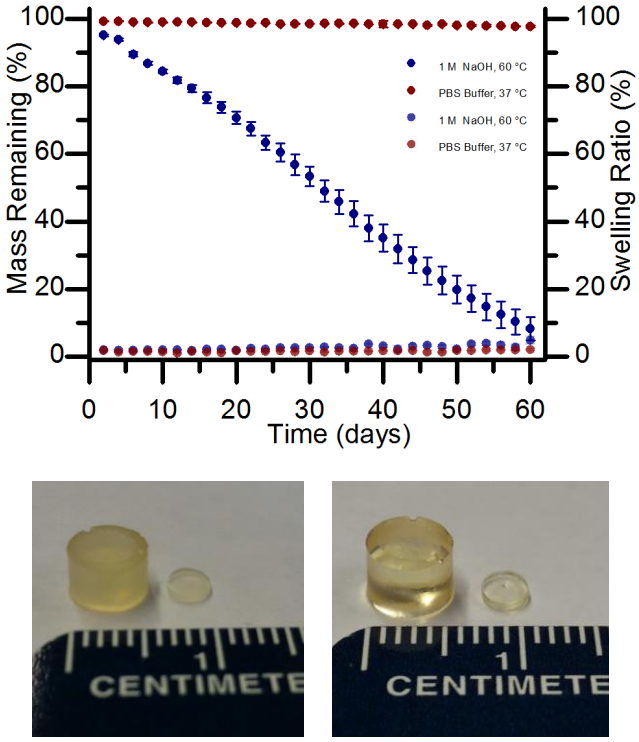

Figure A2. Degradation study in NaOH, 60 °C (blue) and PBS buffer, pH = 7.4, 37 °C (red). Samples from the degradation study before drying (bottom, left) and after drying (bottom, right).

IDA-*co*-TMPTMP was tested for the potential for biomedical application by monitoring stable attachment and cytoskeletal development from adherent preosteoblast

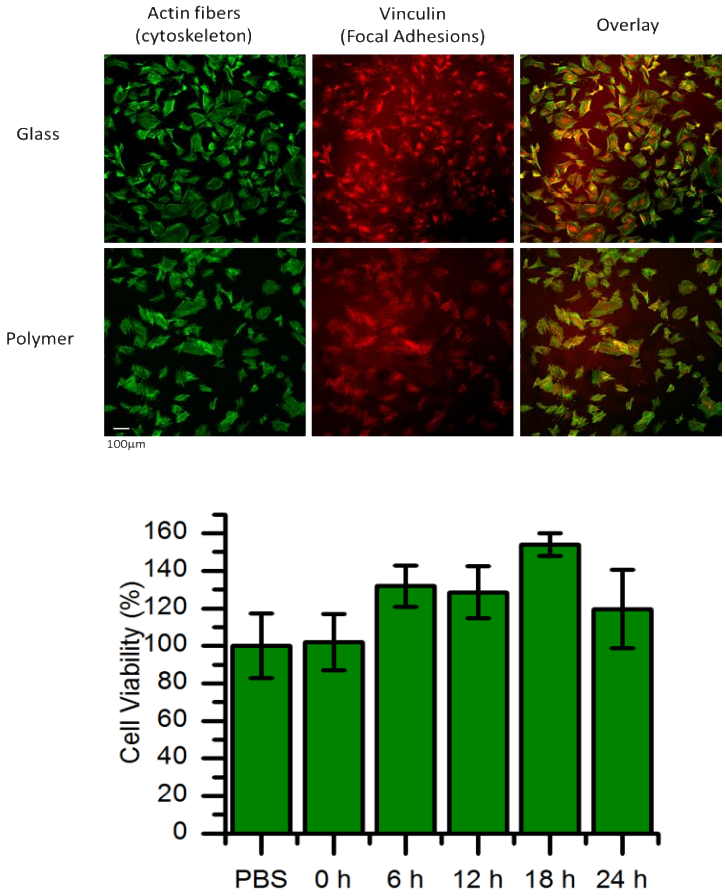

Figure A3. MC3T3 cells on IDA-*co*-TMPTMP-coated glass bottom dishes (top). Viability of MC3T3 E1 mouse preosteoblast cells of IDA-*co*-TMPTMP polymer at timed intervals with an incubation time of 72 h (bottom)

(MC3T3) cells. Cells were fixed with 2% paraformaldehyde and co-stained with phalloidin-Alexa488 to visualize actin in cytoskeleton and with anti-vinculin and anti-mouse-Alexa647 antibodies to visualize focal adhesions. Cytoskeleton and focal adhesions are dynamic structures and sensitive to the substrate on which the cells reside. Stained cells were imaged with a laser scanning confocal microscope (Olympus FV 1000) with 10x objective. Fluorescence images of cells on the IDA-*co*-TMPTMP-

coated glass bottom dishes showed matured cytoskeleton (green) and focal adhesions (red), as observed from cells on a glass surface (Figure 3), therefore, it is clear that the newly-developed material has potential to be used as a biomedical substance. The cytotoxicity of IDA-*co*-TMPTMP was evaluated against MC3T3 E1 mouse preosteoblast cells, however, IC_{50} values of the copolymers could not be determined because high cell-viabilities were observed.

A.5 Conclusions

Overall, a novel cross-linked network system was synthesized using a naturally-derived monomer, isosorbide dialloc (IDA) and cross-linked with TMPTMP. The optically- transparent, flexible cross-linked networks, IDA-*co*-TMPTMP, were synthesized with environmentally-friendly methods including solvent-free conditions, low catalyst loading and UV irradiation. A study of a constant UV cure time (1 minute) and variation of the thermal curing times led to the conclusion that the material is near its optimal thermal and mechanical properties without requiring post-cure heating. The T_d remained *ca*. 320 °C and the T_g remained below room temperature, in a narrow range. The elastomeric material had a % elongation of 220-340%. The hydrolytic degradation of the material (1 min UV cure, no post cure) was evaluated, and found to afford 8.3 ± 3.5% and 97.7 ± 0.3% mass remaining after 60 days under accelerated aqueous basic and physiological neutral buffer conditions, respectively. MC3T3 cells deposited on IDA-*co*-TMPTMP-coatings showed matured cytoskeletons and focal adhesions as well as high cell-viability. Overall, this novel material has properties that could be useful in biomedical applications or as environmentally friendly materials.

A.6 Supplemental Information

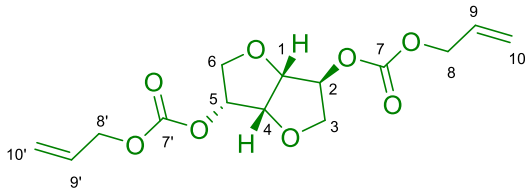

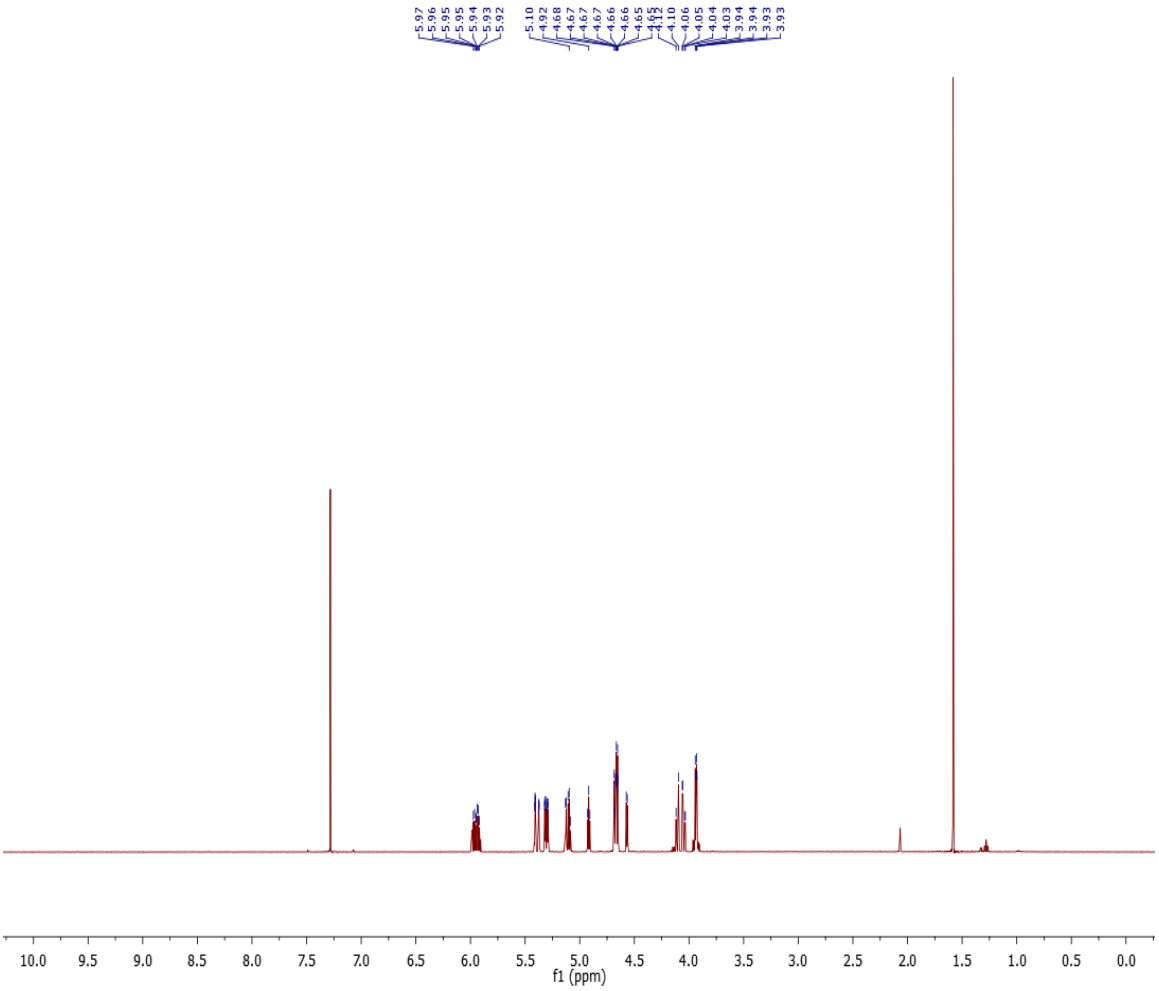

Figure S1. ^{1}H NMR spectrum (500 MHz, $CDCl_3$) of IDA.

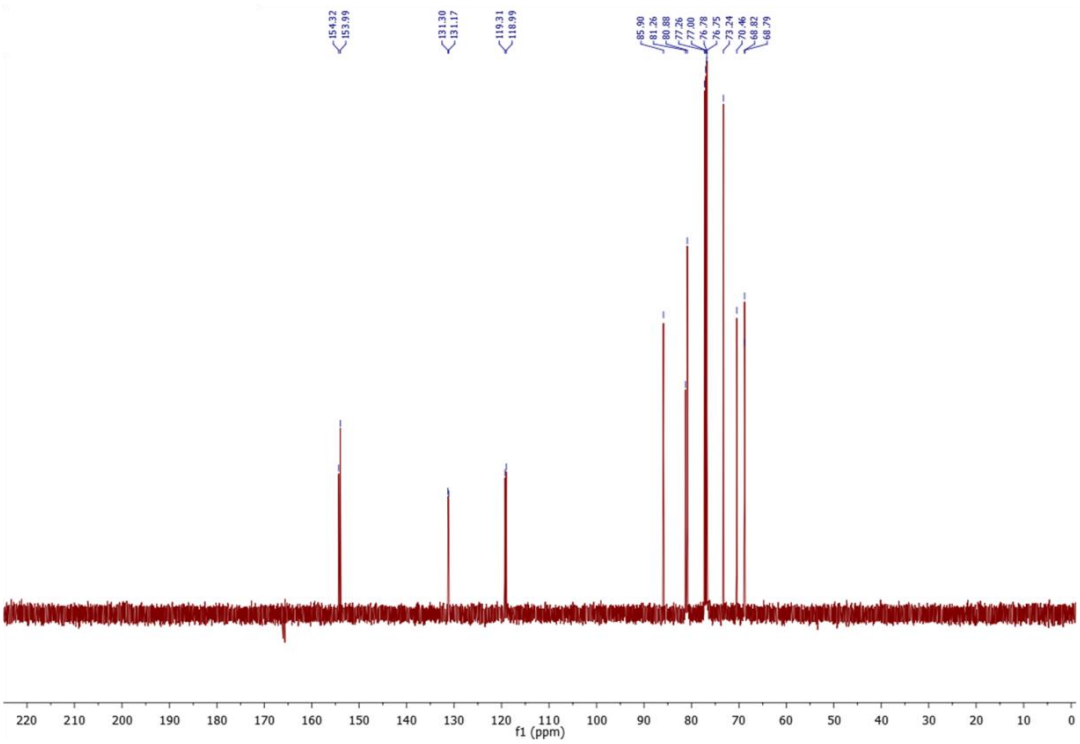

Figure S2. ^{13}C NMR spectrum (125 MHz, $CDCl_3$) of IDA.

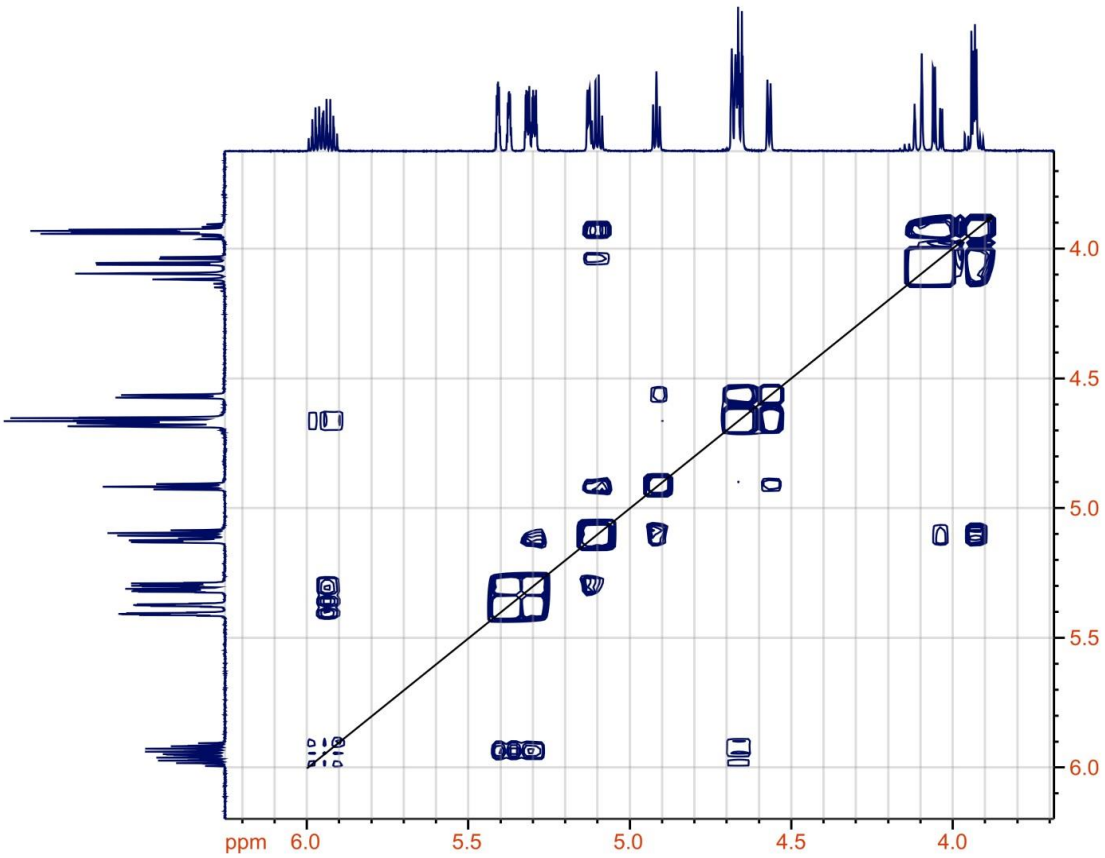

Figure S3. COSY Spectrum for IDA.

A.

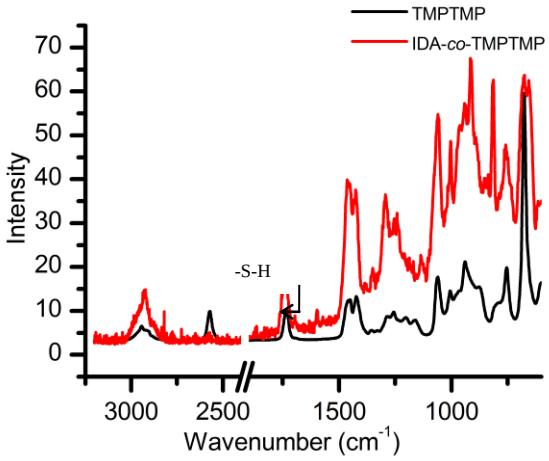

B.

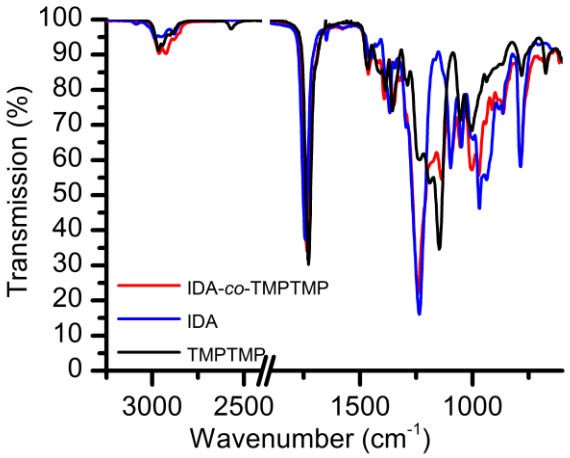

Figure S4. Raman (A) and IR (B) spectra of starting materials and films (IDA-*co*-TMPTMP) with no post-cure.

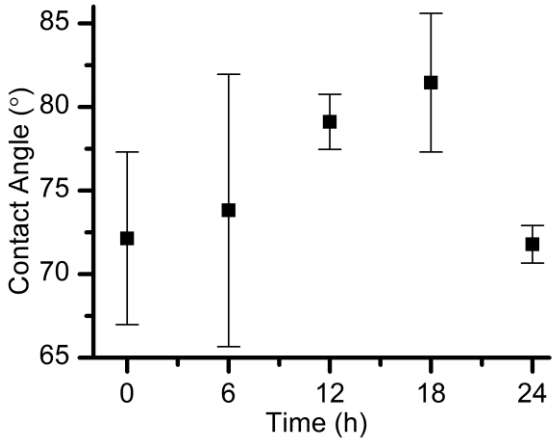

Figure S5. Water contact angle values of films with 1 minute UV curing time and various post-cure heating times.

Table S1. Storage moduli at various temperatures.

Time	**E' @ 0 °C (MPa)**	**E' @ 25 °C (MPa)**	**E'*@ 50* °C (MPa)**	**E'' 0°C (MPa)**	**E'' @ 50 °C (MPa)**
0 h	1700	79	6.5	120	0.6
6 h	1700	280	5.8	90	1.1
12 h	1500	430	6.2	67	1.3
18 h	2000	550	6.9	130	1.1
24 h	1700	350	7.1	110	1.2

A.

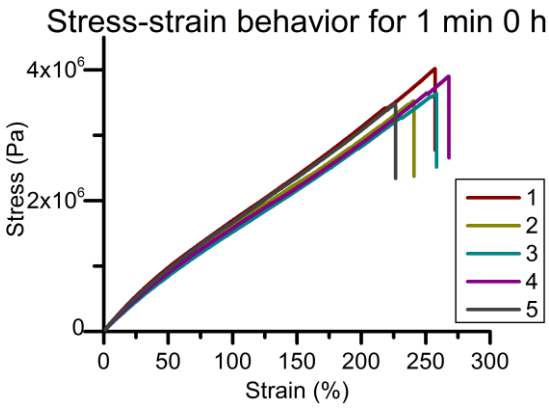

D.

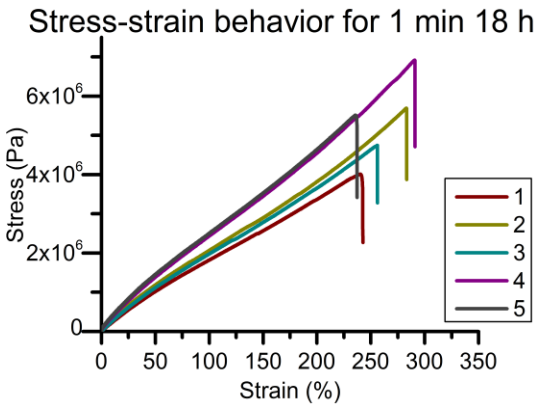

B.

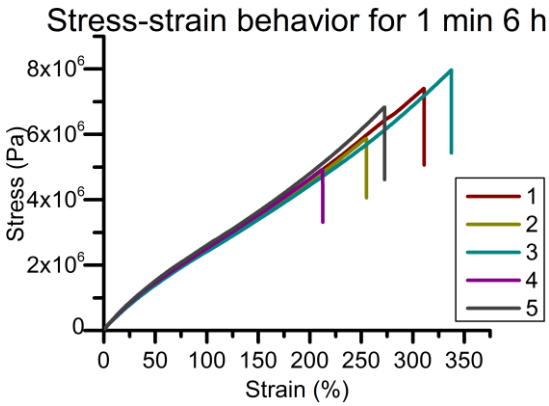

E

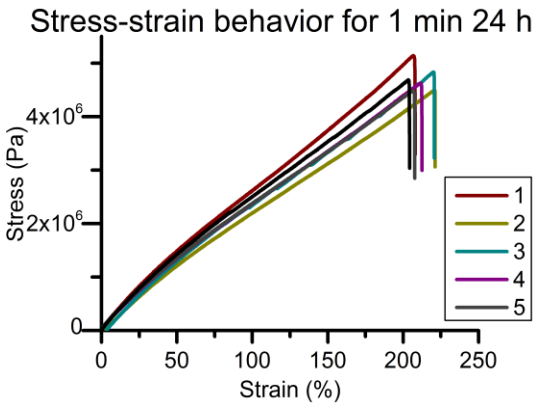

C.

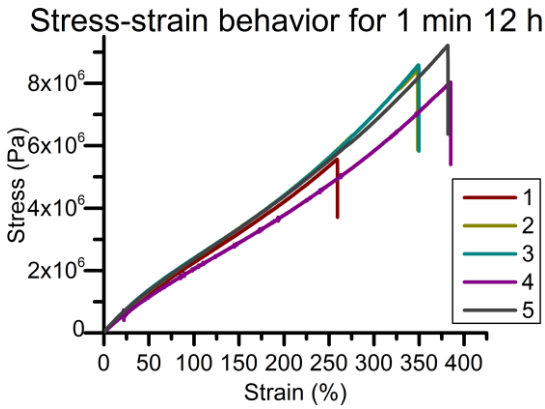

Figure S6. Stress-strain curves for all trials of each IDA-*co*-TMPTMP, following 1 min UV-irradiation and various post-cure heating times, as noted in the headings.

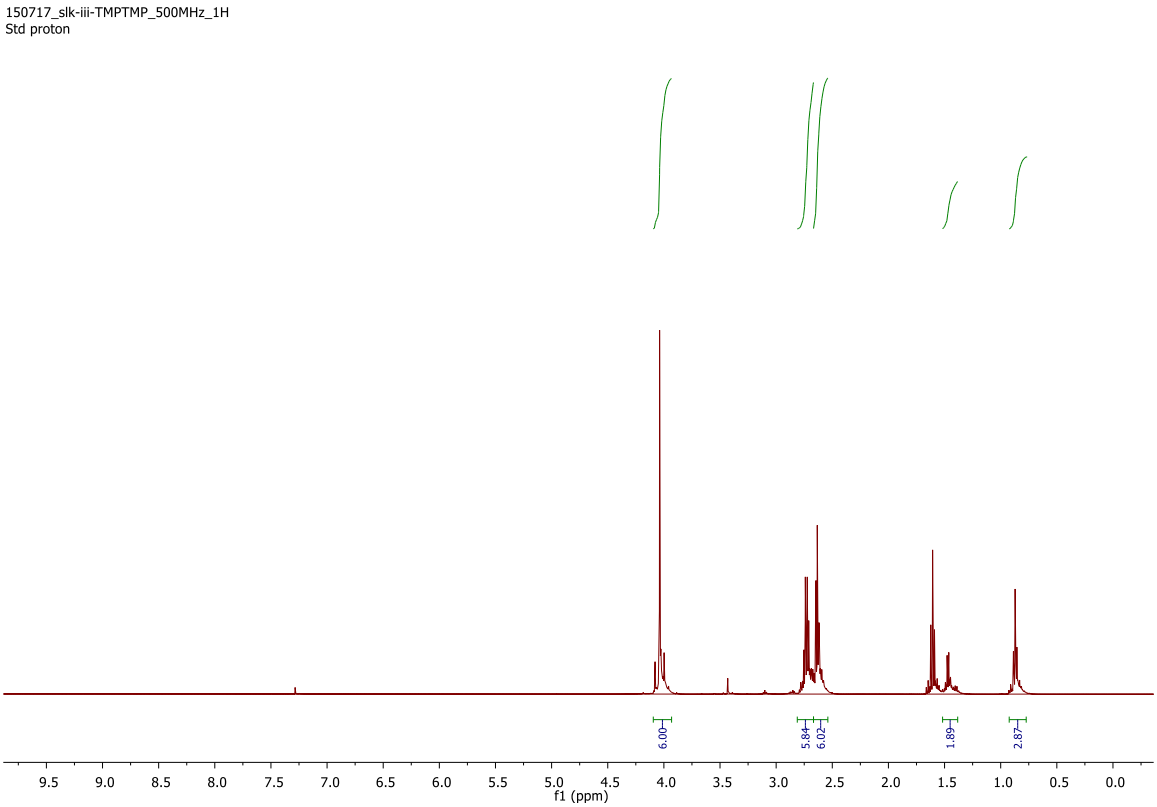

Figure S7. ^{1}H NMR of the commercially available starting material, TMPTMP. Spectra agrees with literature.[243]

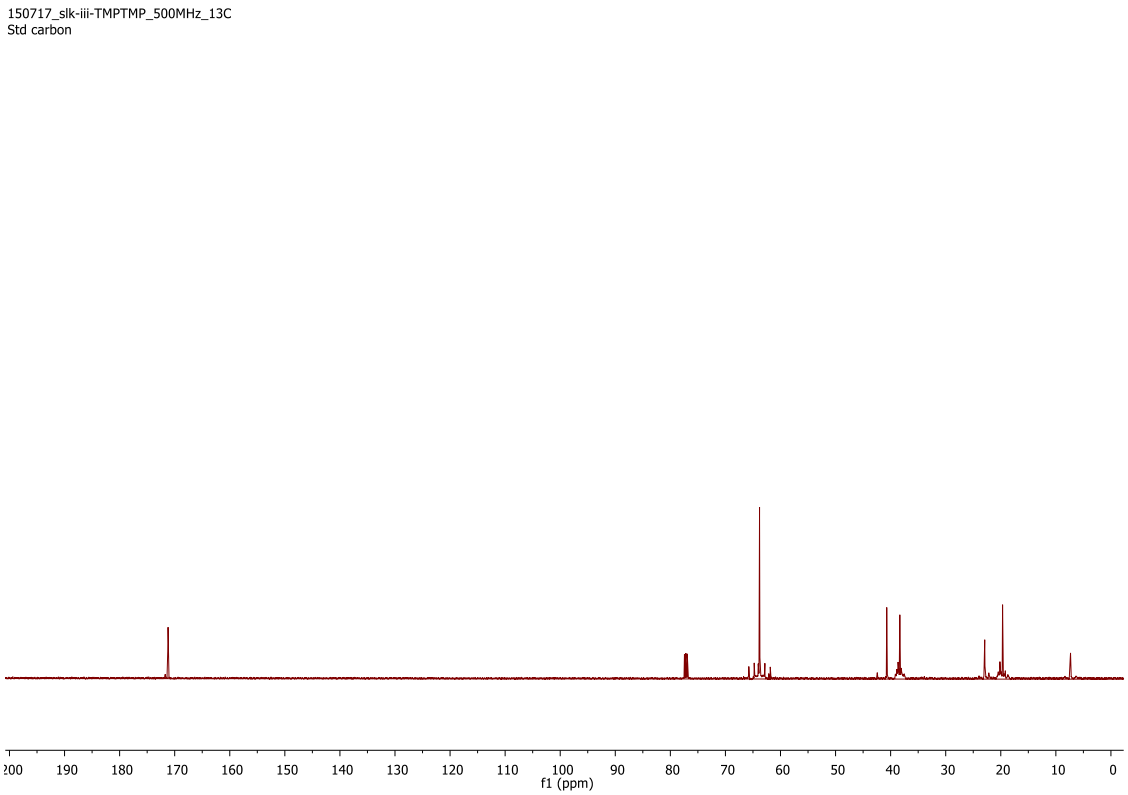

Figure S8. ^{13}C NMR of the commercially available starting material, TMPTMP. Spectra agrees with literature.[243]

APPENDIX II

SUPPLEMENTAL INFORMATION FOR AGGREGATION-INDUCED EMISSION PROPERTIES OF A POLYCARBONATE DESIGNED FROM THE RENEWABLE RESOURCE QUERCETIN

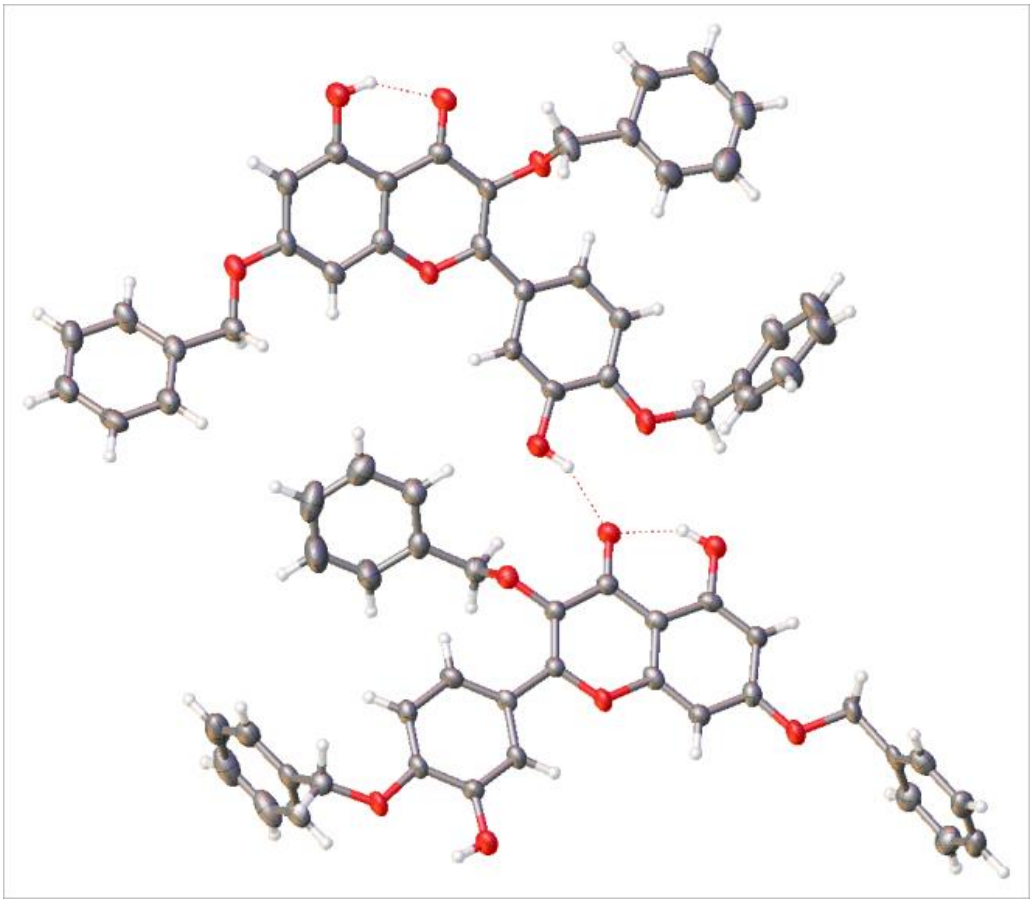

Figure S 6.1 Crystal structure of 3,4',7-tribenzylquercetin, **2.1.**

Table S 6.1 Crystal data and structure refinement for **2.1.**

Identification code	**2.1**
Empirical formula	$C_{36}H_{28}O_7$
Formula weight	572.58
Temperature/K	110.0
Crystal system	triclinic
Space group	P-1
a/Å	4.9612(10)
b/Å	19.172(5)
c/Å	29.275(6)
α/°	93.971(13)
β/°	94.692(12)
γ/°	94.067(13)
Volume/Å^3	2760.4(10)
Z	4
ρ_{calc}mg/mm^3	1.378
m/mm^{-1}	0.780
F(000)	1200.0
Crystal size/mm^3	0.36 × 0.07 × 0.01
Radiation	CuKα (λ = 1.54178)
2Θ range for data collection	3.036 to 128.19°
Index ranges	$-5 \leq h \leq 5$, $-22 \leq k \leq 21$, $-32 \leq l \leq 33$
Reflections collected	15502
Independent reflections	8026[R(int) = 0.0769]
Data/restraints/parameters	8026/0/779
Goodness-of-fit on F^2	1.043
Final R indexes [I>=2σ (I)]	R_1 = 0.0642, wR_2 = 0.1368
Final R indexes [all data]	R_1 = 0.1219, wR_2 = 0.1568
Largest diff. peak/hole / e Å^{-3}	0.26/-0.28

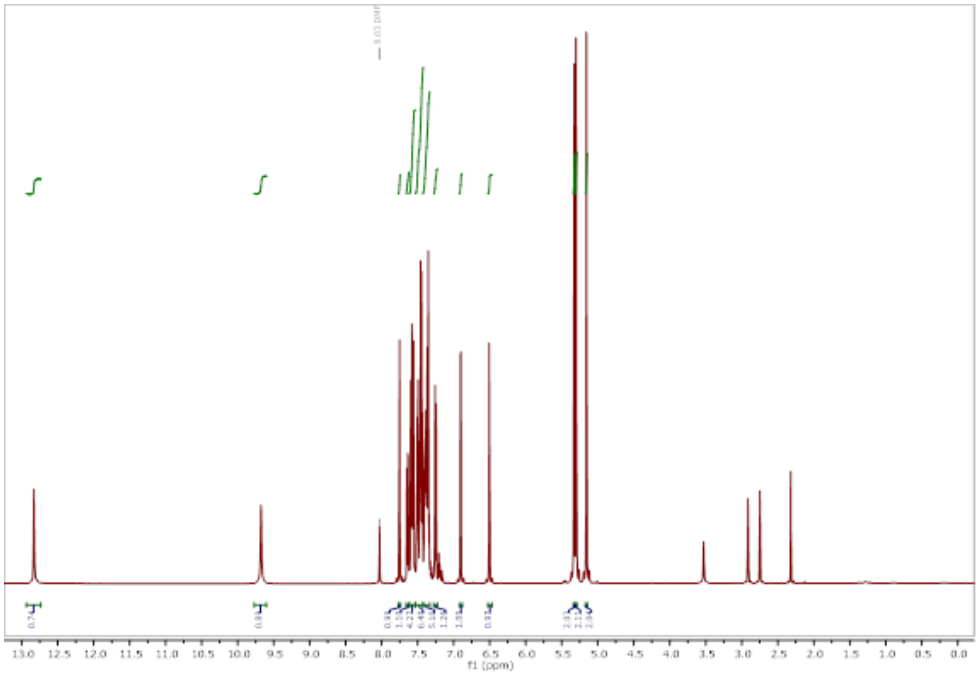

Figure S 6.2 ^{1}H NMR of **2.1.**

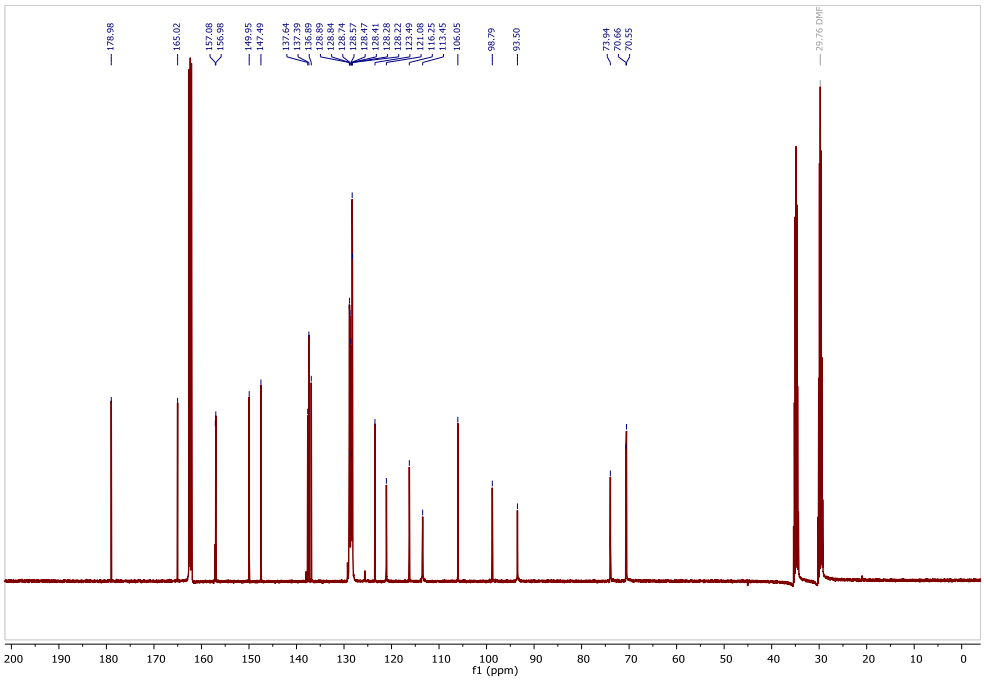

Figure S 6.3 ^{13}C NMR of **2.1**

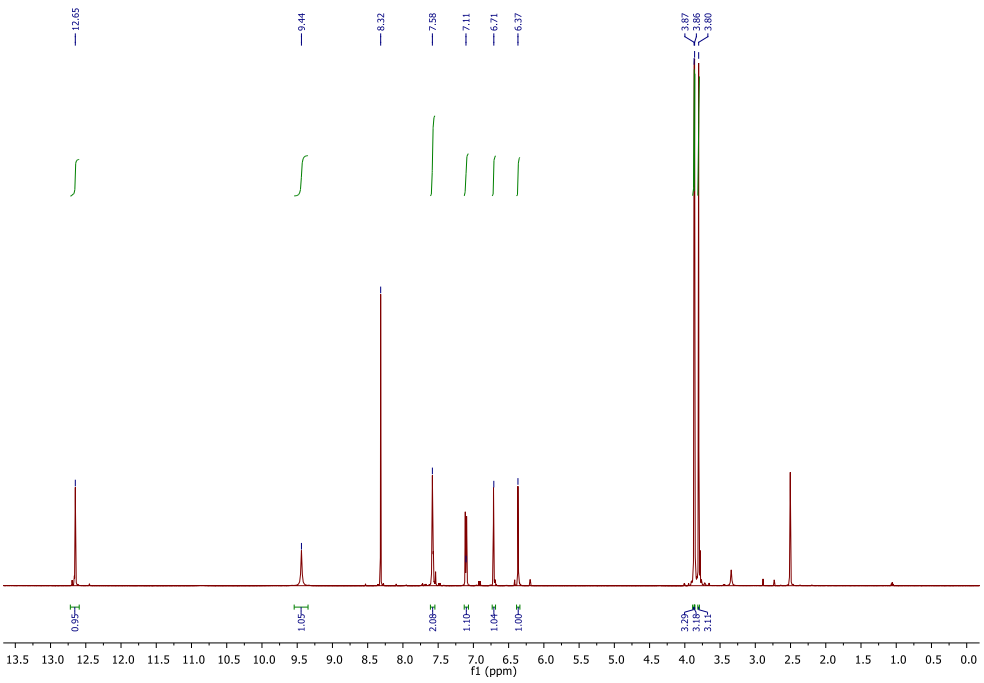

Figure S 6.4 ^{1}H NMR spectrum (500 MHz, DMSO-d_6) of **2.4**.

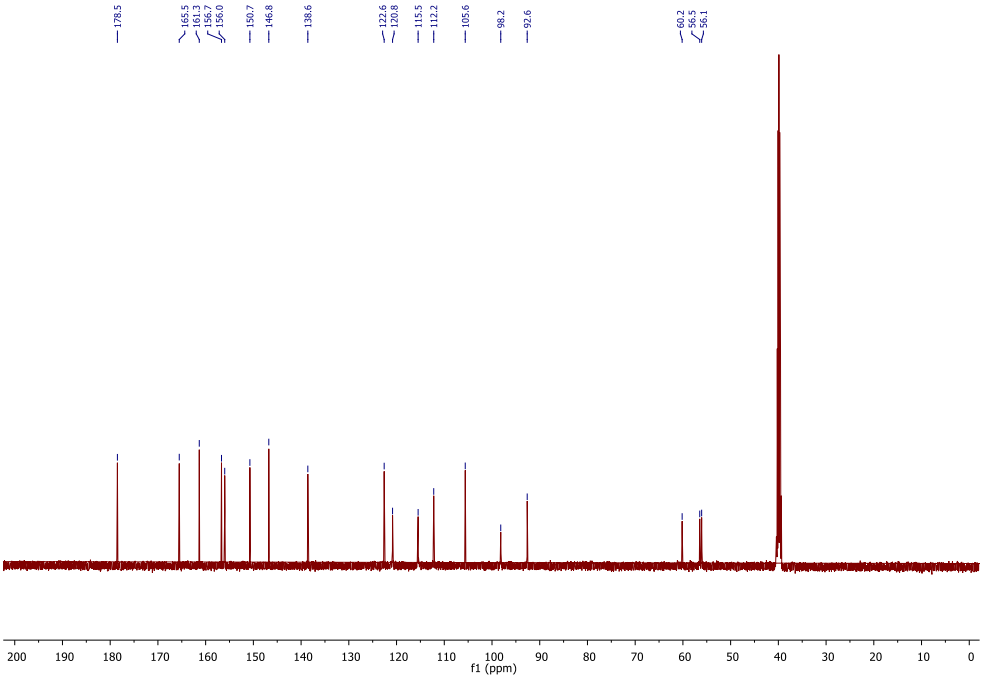

Figure S 6.5 ^{13}C NMR spectrum (125 MHz, DMSO-d_6) of **2.4**

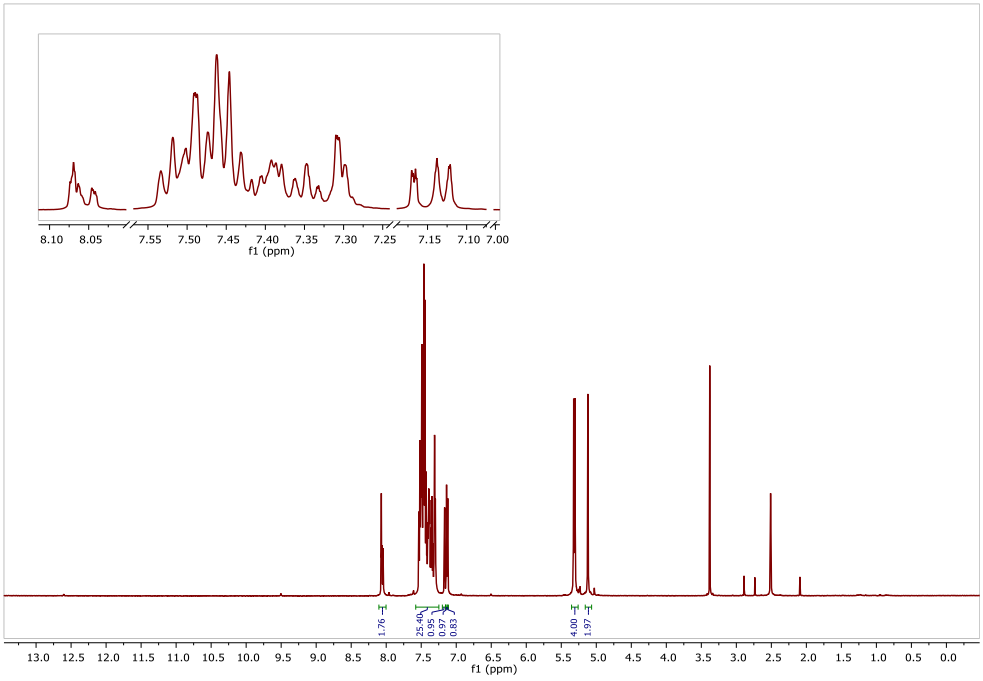

Figure S 6.6 ^{1}H NMR of **2.6**

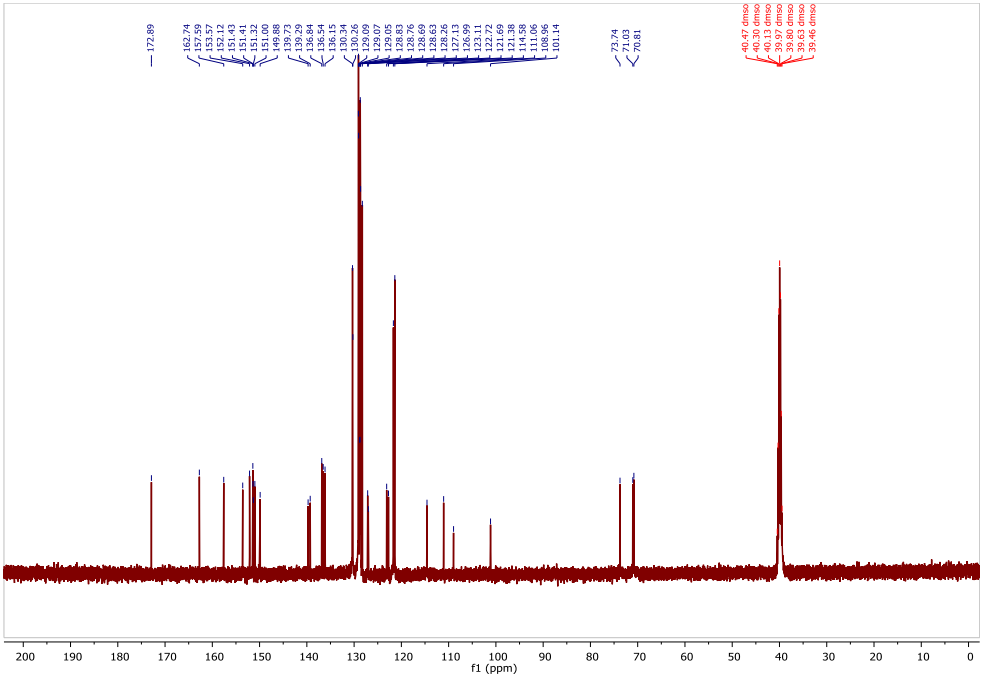

Figure S 6.7 ^{13}C NMR of **2.6**

APPENDIX III

SUPPLEMENTAL INFORMATION FOR FLAVONOID-BASED POLYCARBONATES APPLIED TOWARDS SELF-REPORTING, FLUORESCENT NANOSTRUCTURES FROM THE NATURAL PRODUCT QUERCETIN

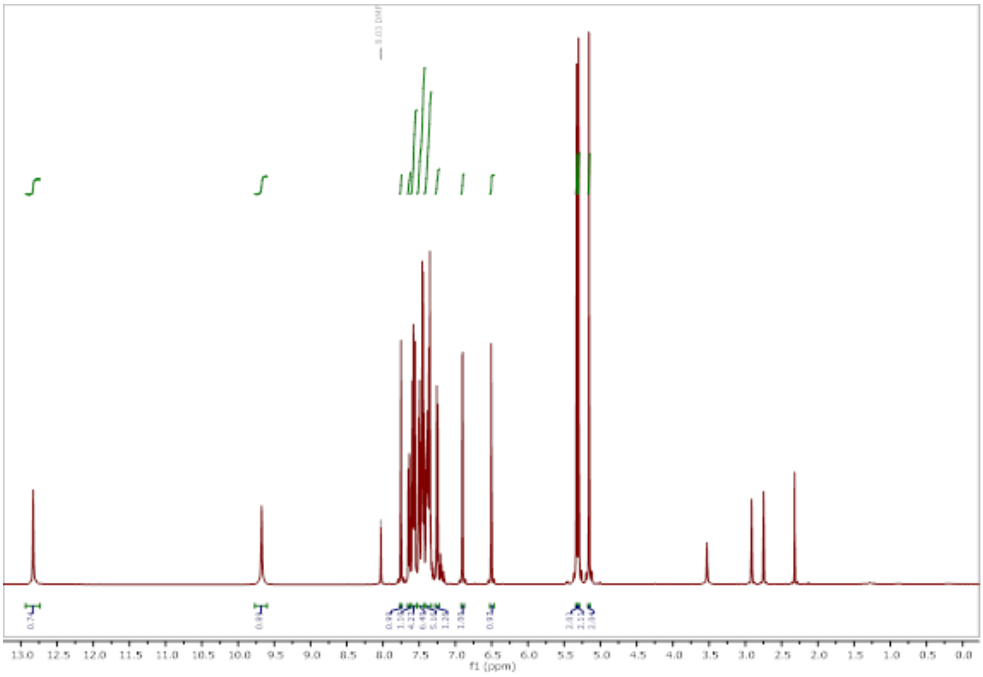

Figure S 6.8 ^{1}H NMR of **3.1.**

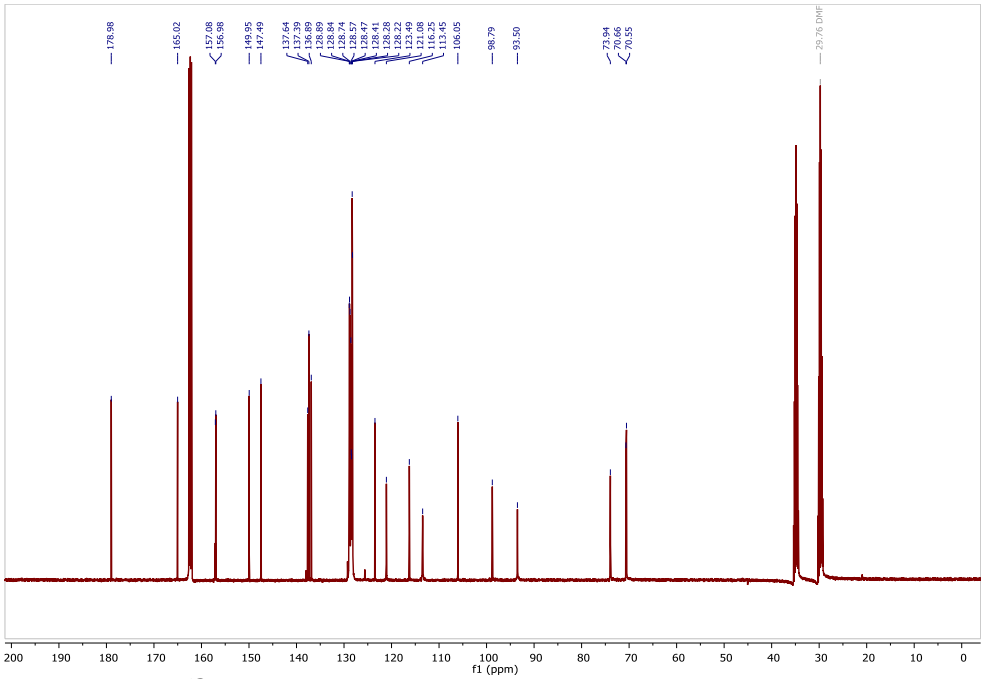

Figure S 6.9 ^{13}C NMR of **3.1.**

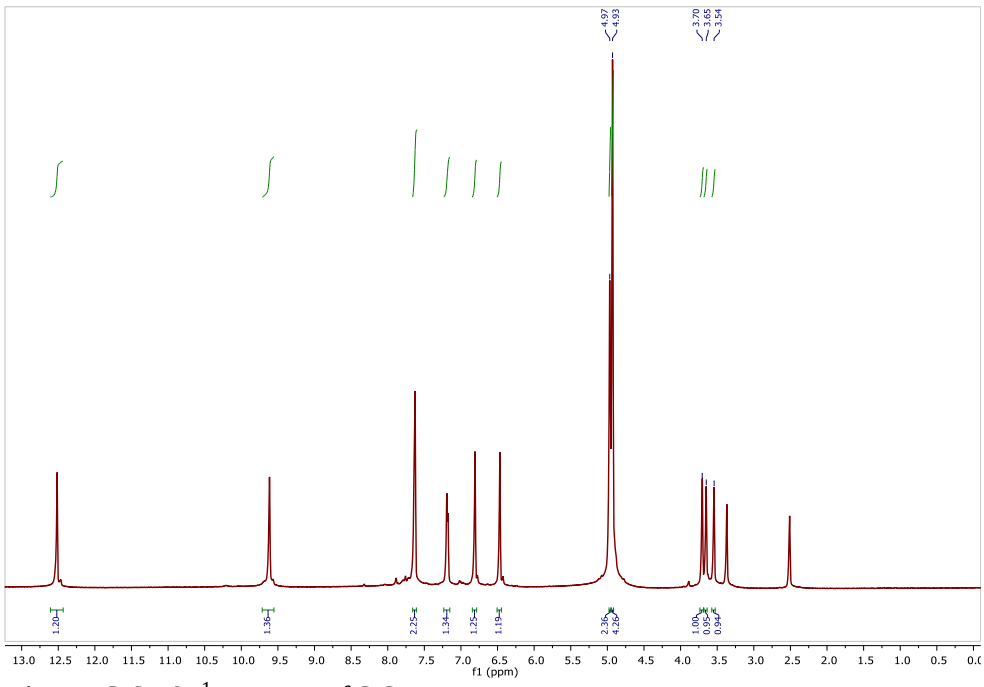

Figure S 6.10 ^{1}H NMR of **3.2.**

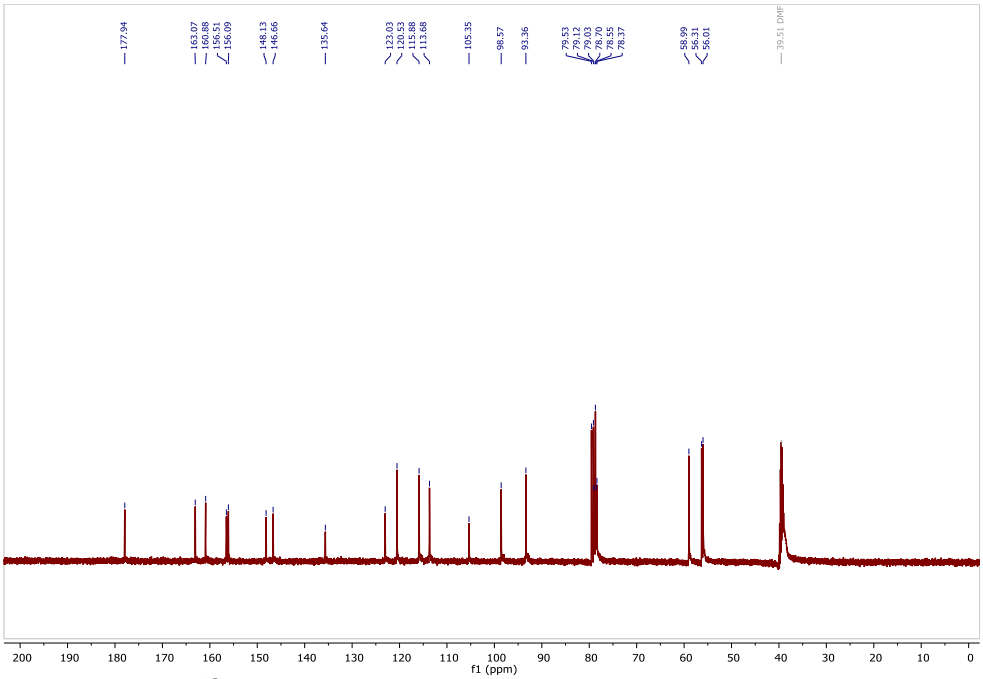

Figure S 6.11 ^{13}C NMR of **3.2.**

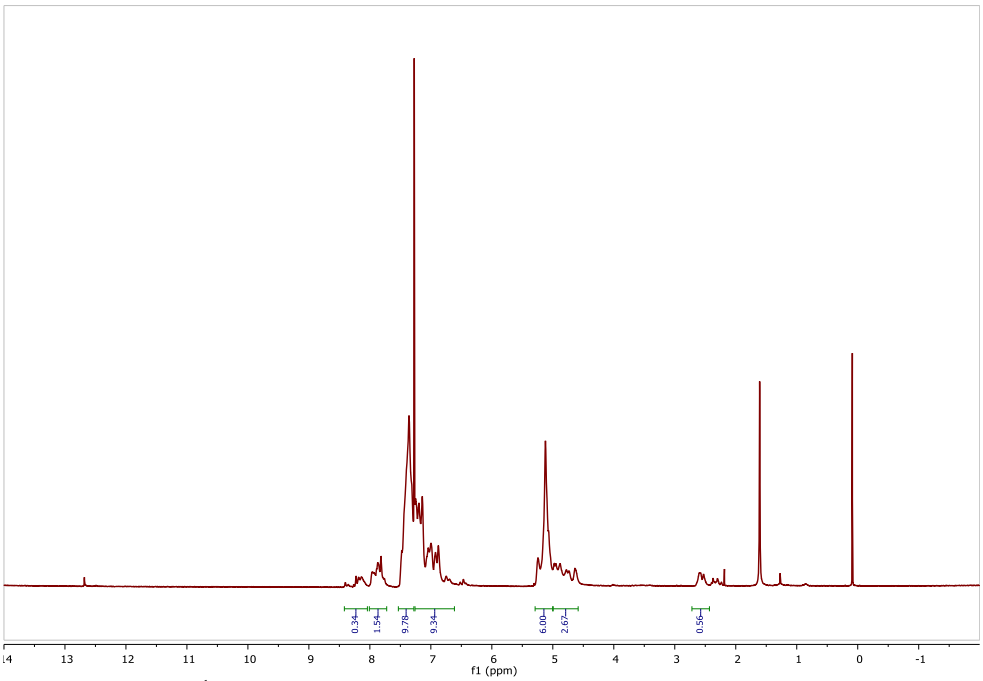

Figure S 6.12 ^{1}H NMR of **Q-PC**.

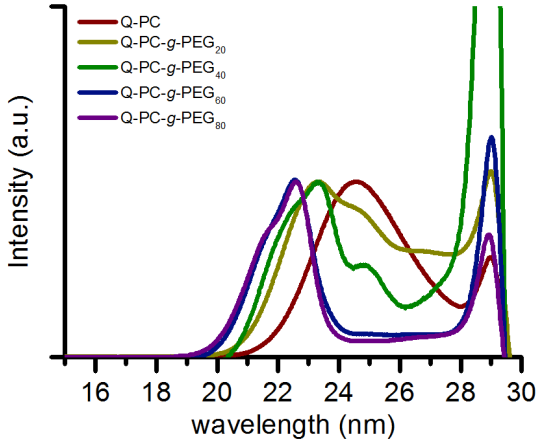

Figure S 6.13 SEC traces of the **Q-PC-*g*-PEG$_x$** series.

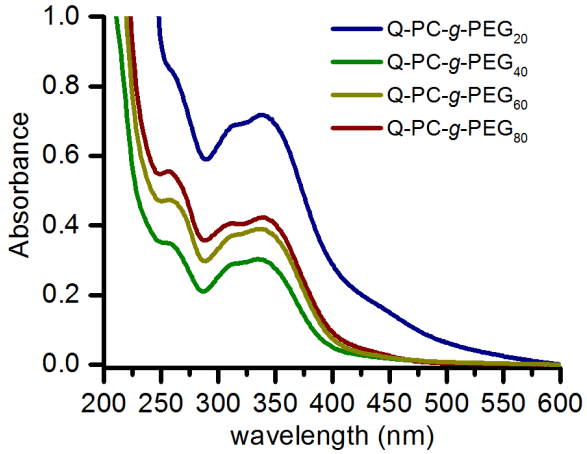

Figure S 6.14 UV/Vis traces of the **Q-PC-*g*-PEG$_x$** series

APPENDIX IV

SUPPLEMENTAL INFORMATION FOR PROGRESS TOWARDS NATURAL PRODUCT-BASED, PLANT-DERIVED, MUSSEL-INSPIRED POLYCARBONATES FROM QUERCETIN AND LYSINE

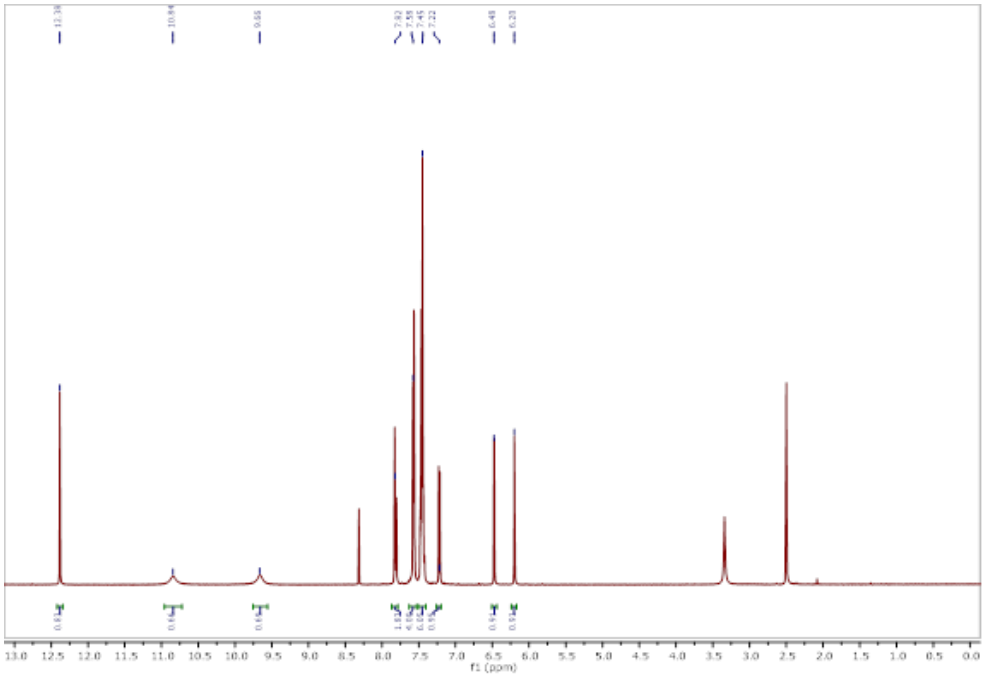

Figure S 6.15 ^{1}H NMR of **4.1.**

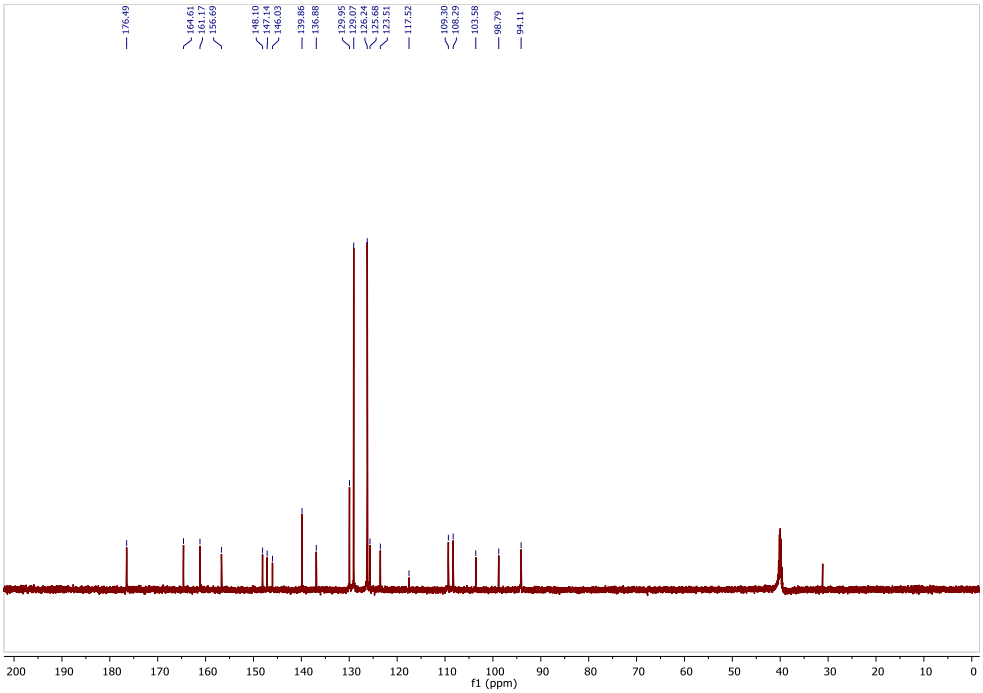

Figure S 6.16 ^{13}C NMR of **4.1.**

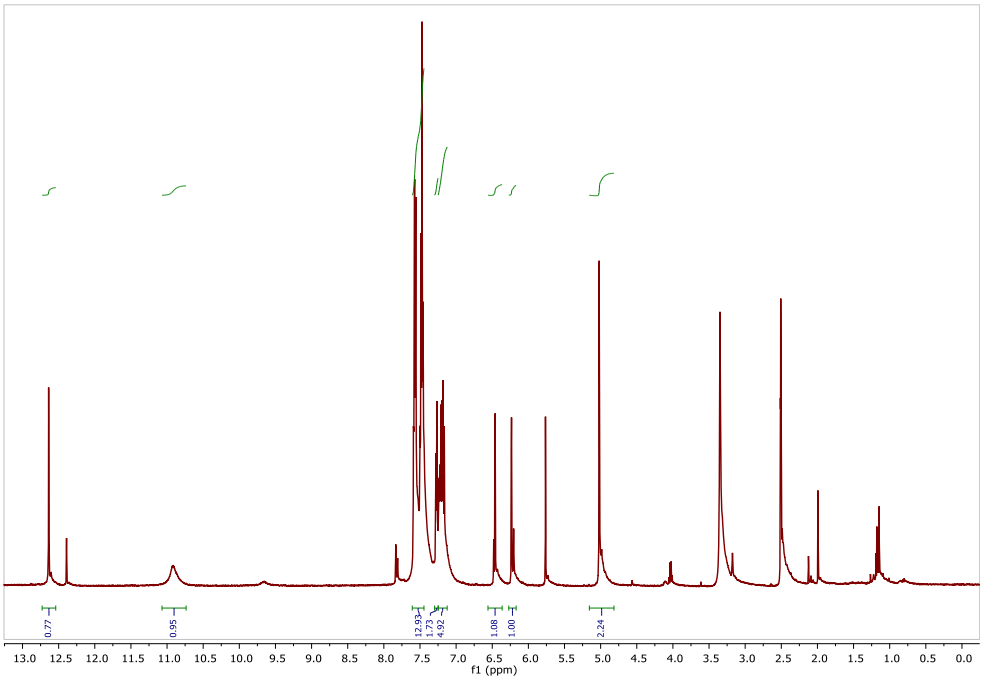

Figure S 6.17 ^{1}H NMR of **4.2.**

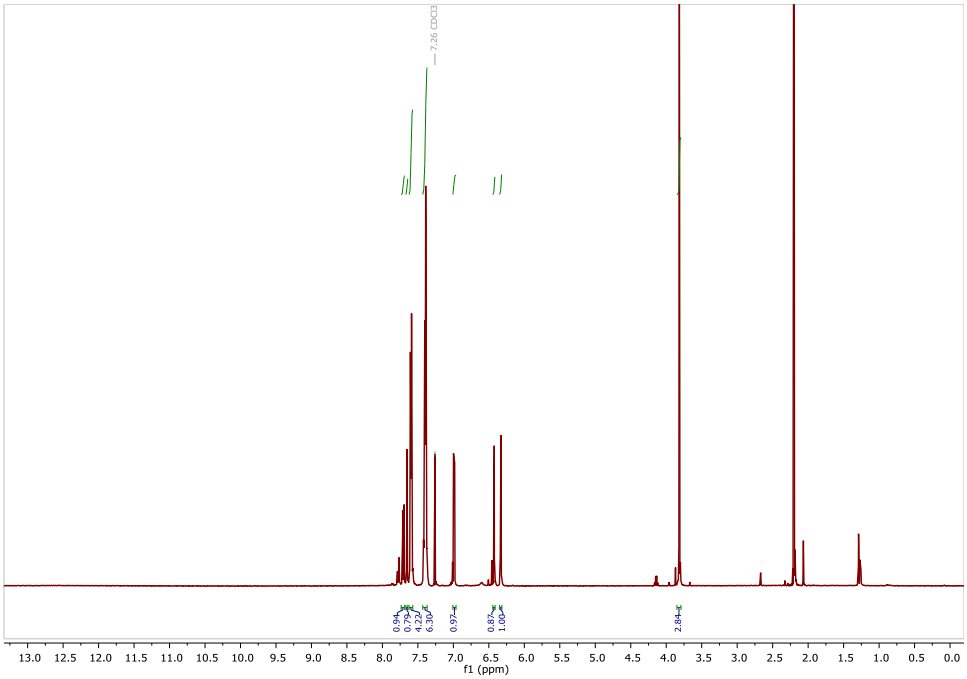

Figure S 6.18 ^{1}H NMR of **4.3.**

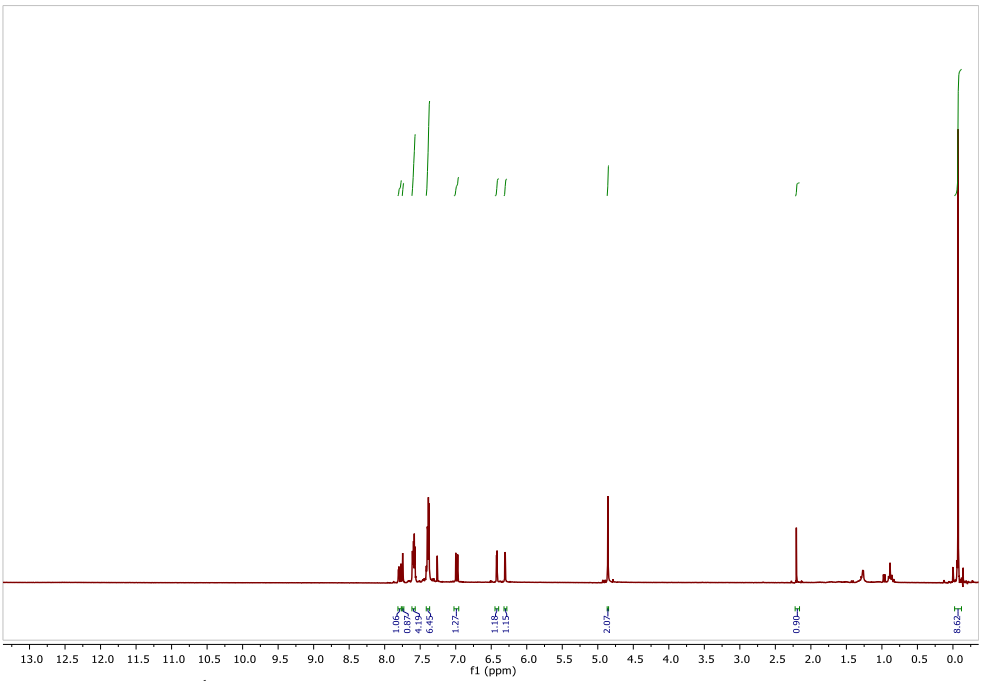

Figure S 6.19 ^{1}H NMR of **4.4.**

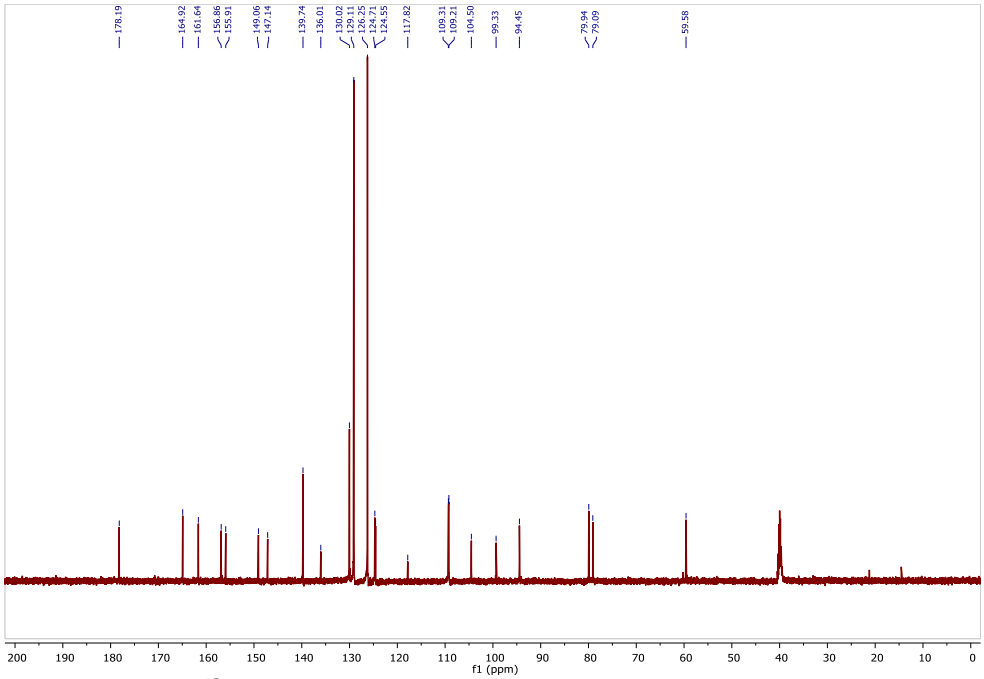

Figure S 6.20 ^{13}C NMR of **4.4**.

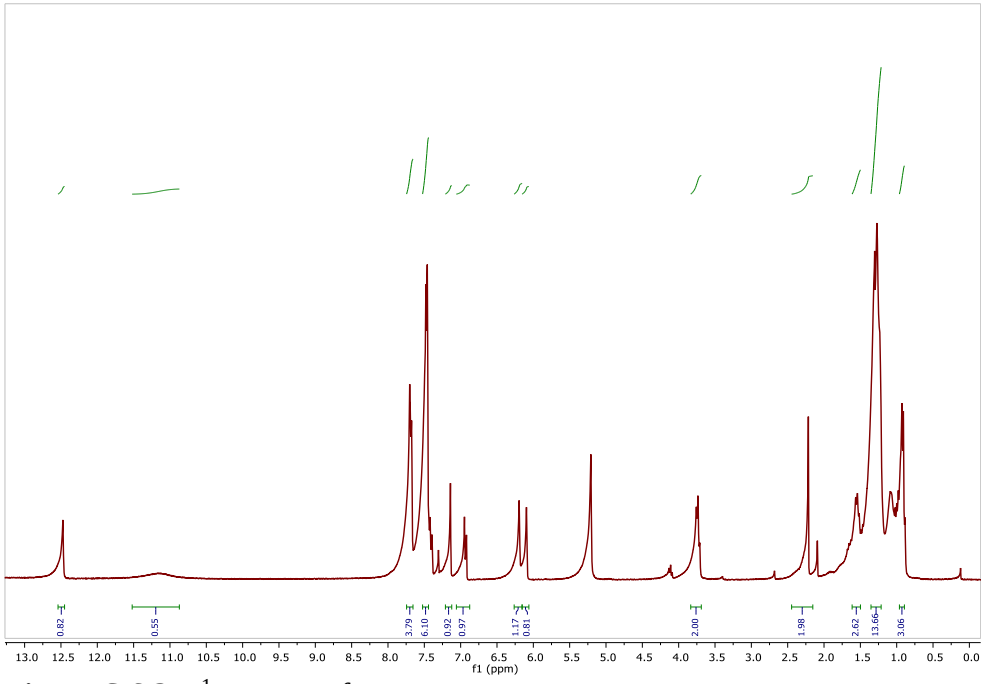

Figure S 6.21 ^{1}H NMR of **4.5.**

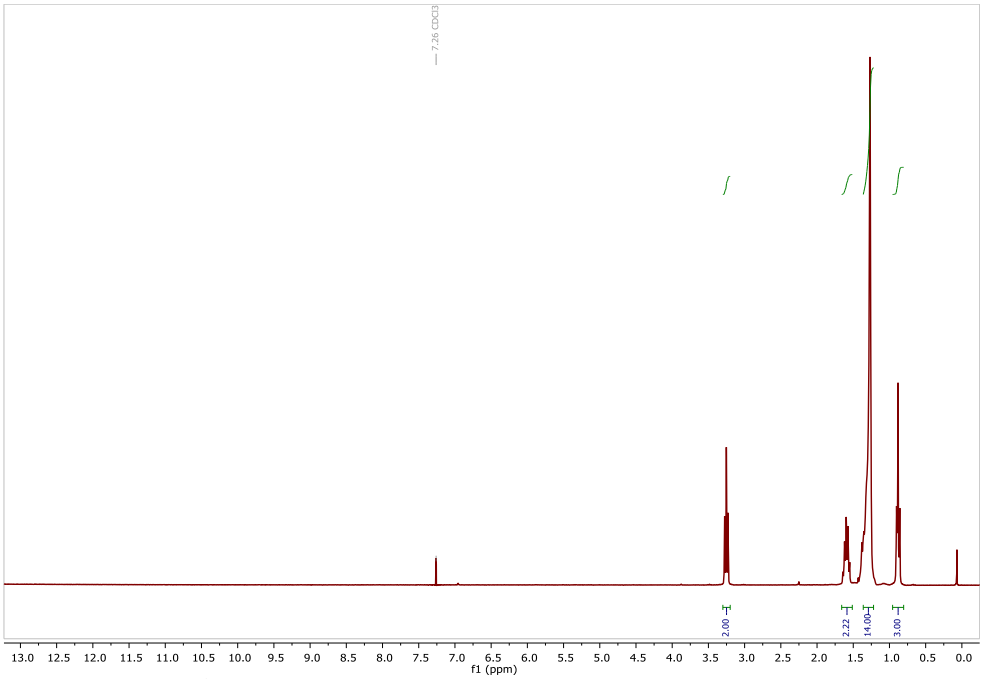

Figure S 6.22 ^{1}H NMR of azidodecane**.**

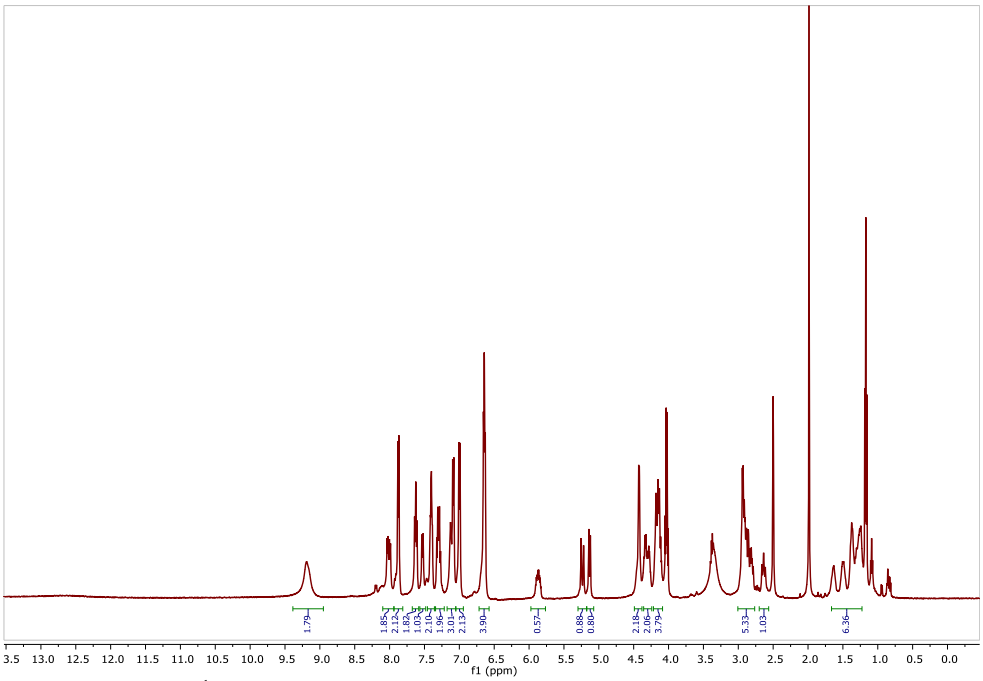

Figure S 6.23 ^{1}H NMR of **4.7e**

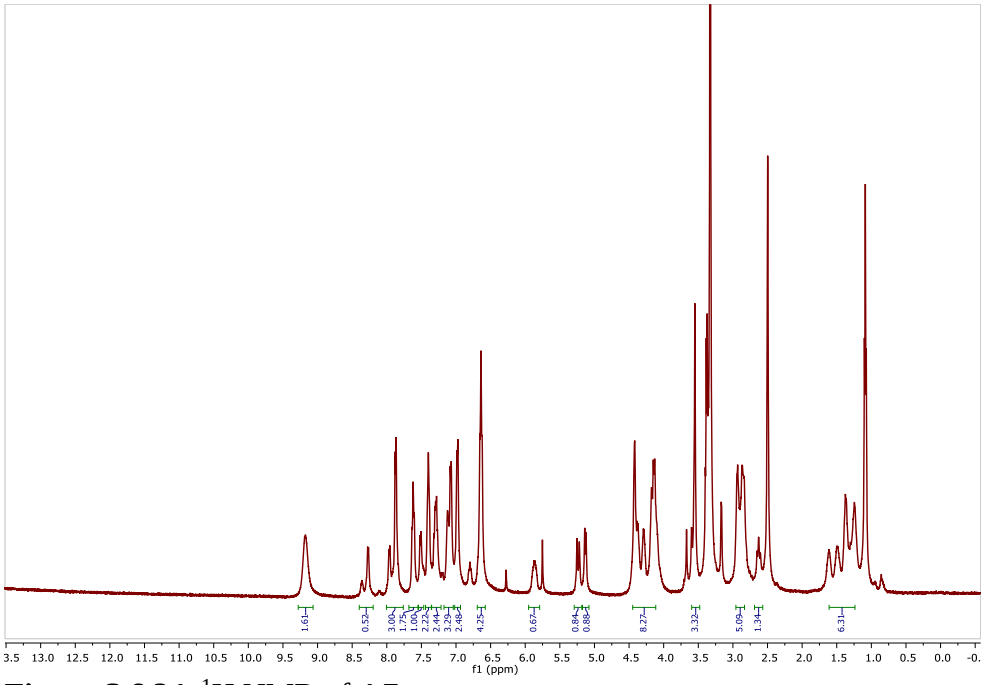

Figure S 6.24 ^{1}H NMR of **4.7.**

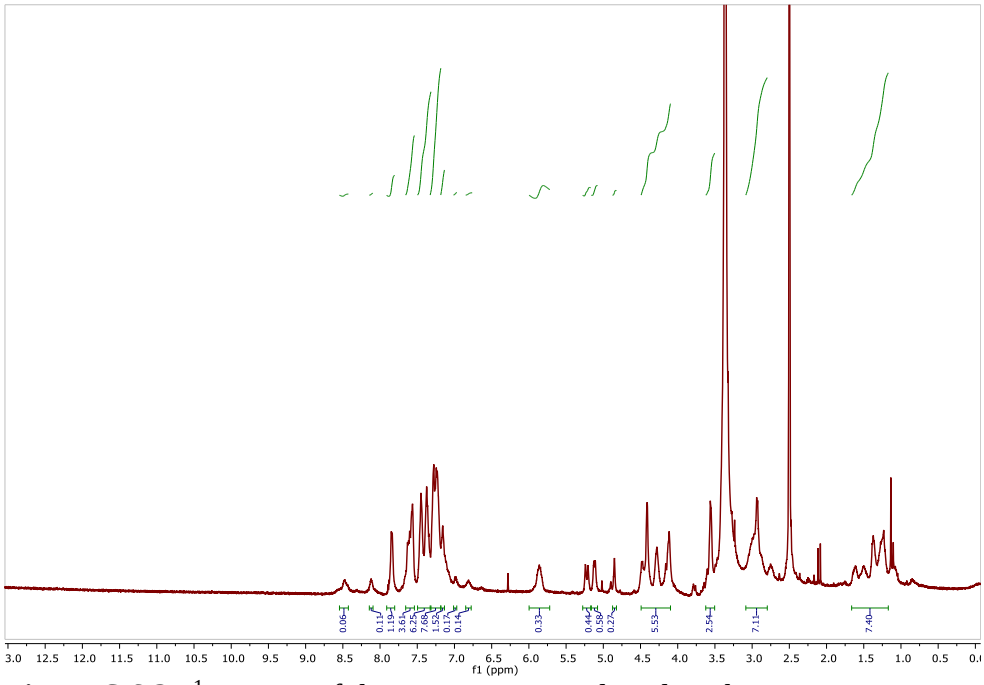

Figure S 6.25 ^{1}H NMR of the quercetin-peptide polycarbonate

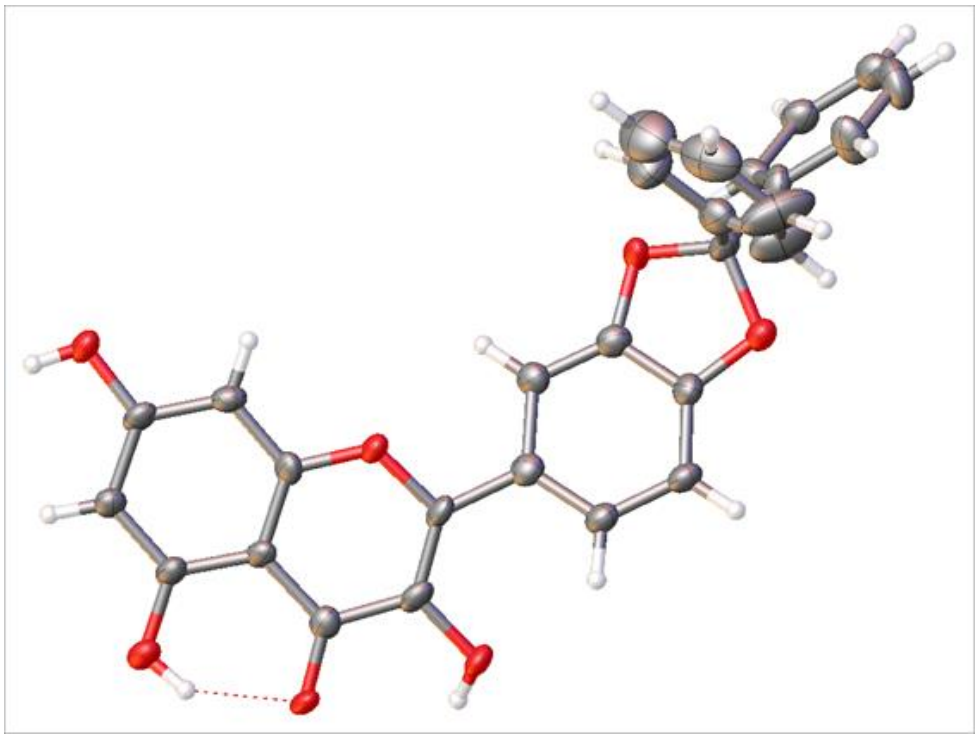

Figure S 6.26 Crystal structure of **4.1**.

Table S 6.2 Crystal data and structure refinement for **4.1**.

Identification code	**4.1**
Empirical formula	$C_{28}H_{18}O_7$
Formula weight	466.42
Temperature/K	110.0
Crystal system	monoclinic
Space group	$P2_1/c$
a/Å	16.628(2)
b/Å	9.6759(13)
c/Å	14.2693(19)
α/°	90
β/°	112.872(7)
γ/°	90
Volume/Å^3	2115.3(5)
Z	4
ρ_{calc}g/cm^3	1.465
μ/mm^{-1}	0.881
F(000)	968.0
Crystal size/mm^3	0.1 × 0.1 × 0.01
Radiation	CuKα (λ = 1.54178)
2Θ range for data collection/°	5.768 to 128.062
Index ranges	$-19 \leq h \leq 19$, $-11 \leq k \leq 11$, $-16 \leq l \leq 16$
Reflections collected	26591
Independent reflections	3352 [R_{int} = 0.1103, R_{sigma} = 0.0784]
Data/restraints/parameters	3352/0/320
Goodness-of-fit on F^2	1.059
Final R indexes [I>=2σ (I)]	R_1 = 0.1153, wR_2 = 0.2858
Final R indexes [all data]	R_1 = 0.1369, wR_2 = 0.3024
Largest diff. peak/hole / e Å^{-3}	0.79/-0.38

APPENDIX V

SUPPLEMENTAL INFORMATION FOR PROGRESS TOWARDS NATURAL PRODUCT-BASED, PLANT-DERIVED, MUSSEL-INSPIRED POLYCARBONATES FROM QUERCETIN AND LYSINE

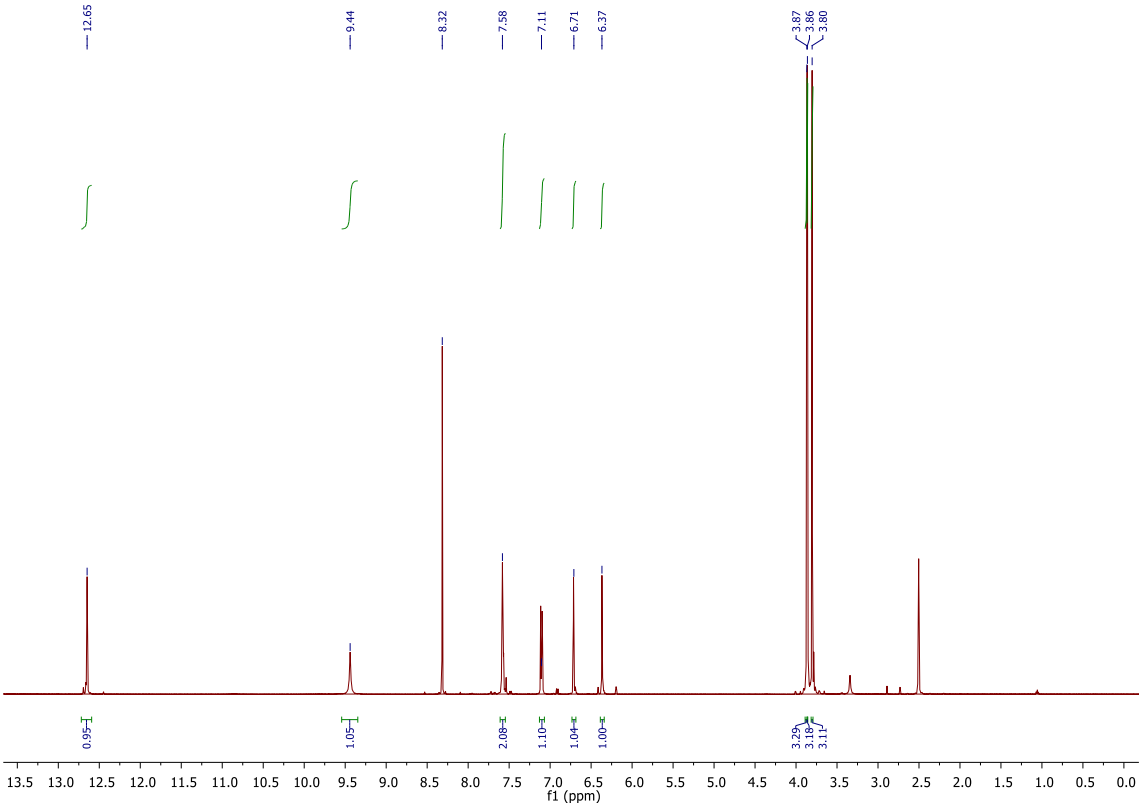

Figure S 6.27 ^{1}H NMR spectrum (500 MHz, DMSO-d_6) of **5.1**.

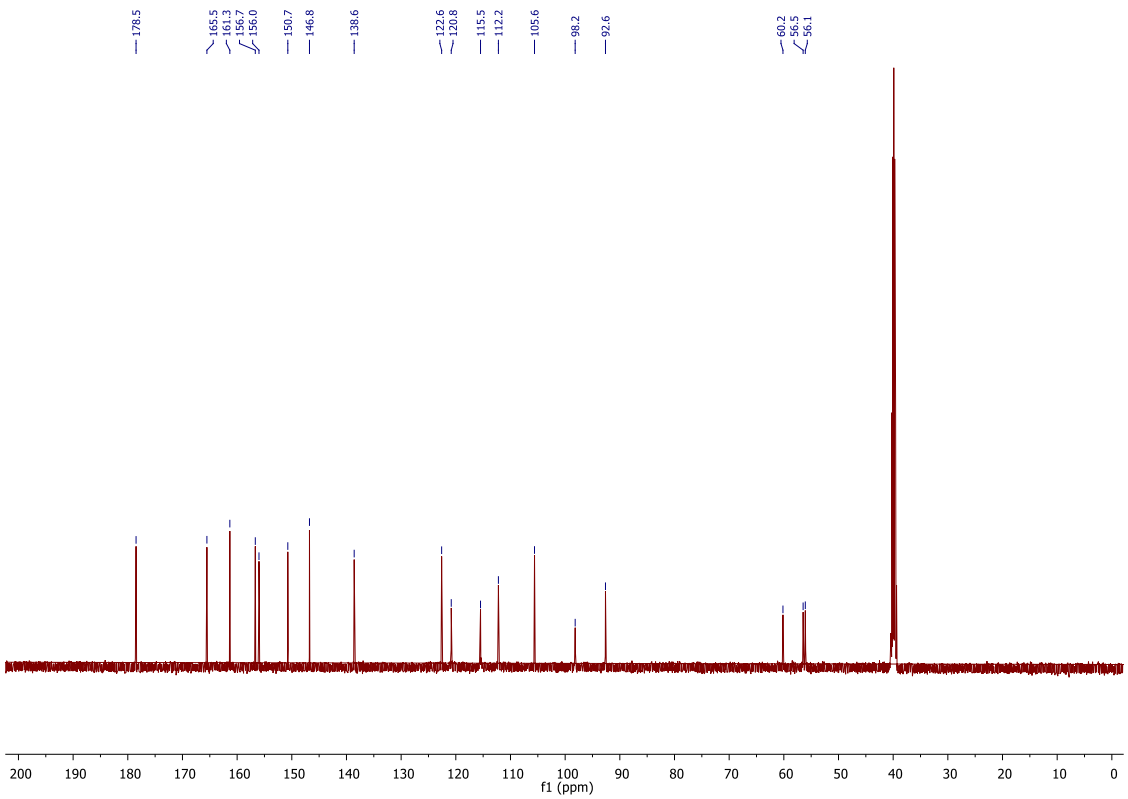

Figure S 6.28 ^{13}C NMR spectrum (125 MHz, DMSO-d_6) of **5.1**.

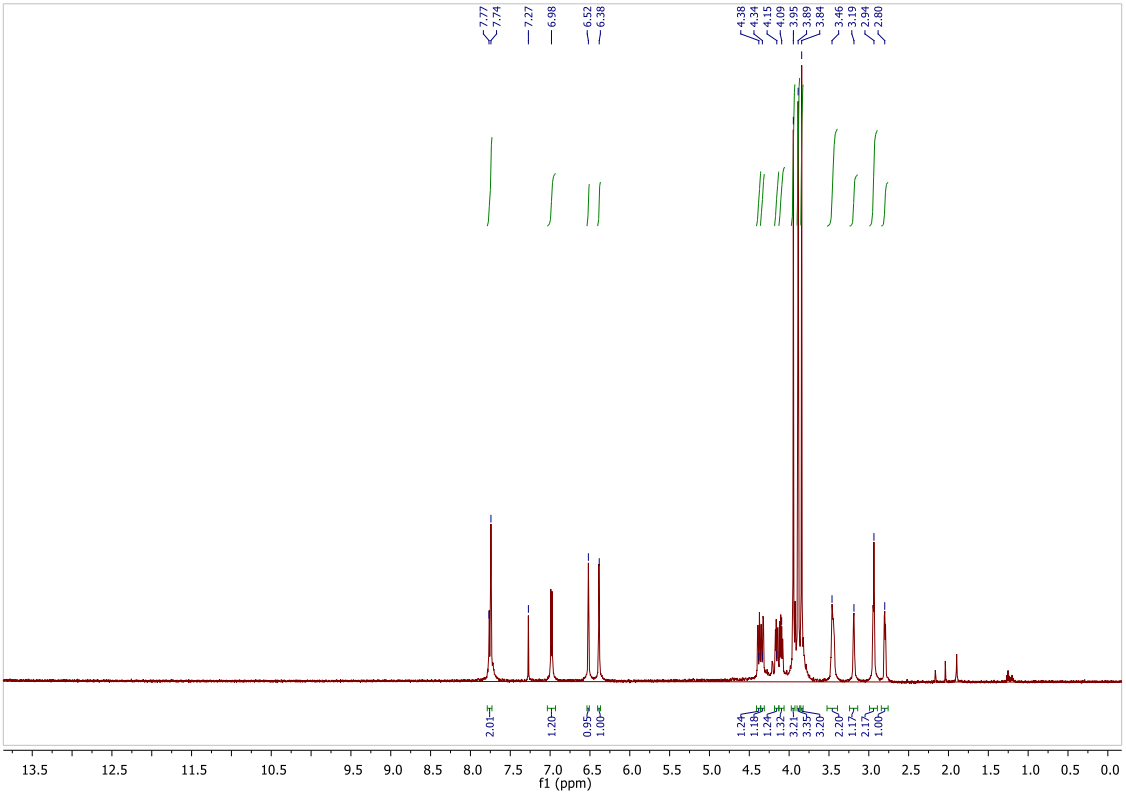

Figure S 6.29 ^{1}H NMR spectrum (500 MHz, $CDCl_3$) of **5.2**.

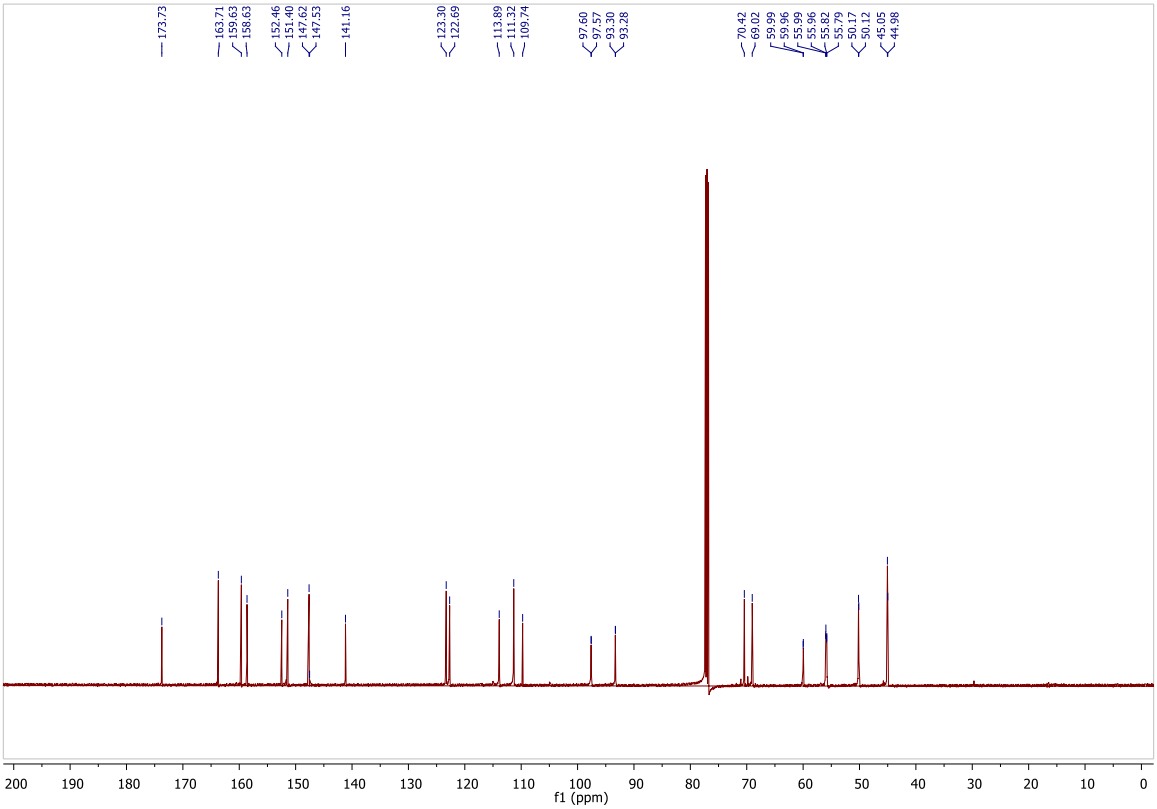

Figure S 6.30 ^{13}C NMR spectrum (125 MHz, $CDCl_3$) of **5.2**.

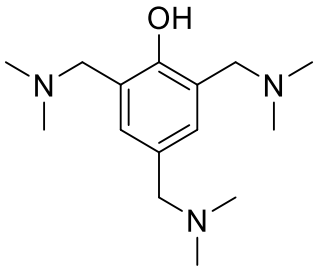

Figure S 6.31 Structure of ANCAMINE® K54.

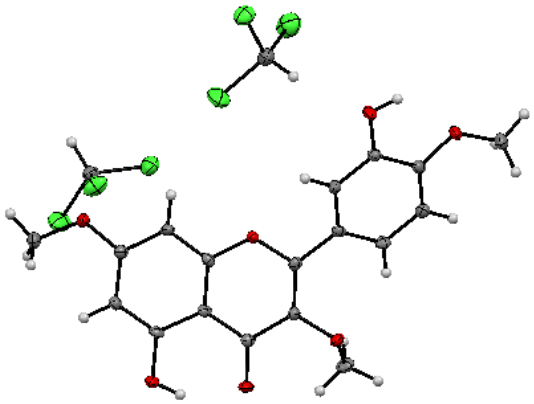

Figure S 6.32 X-ray structure of compound **5.1**.

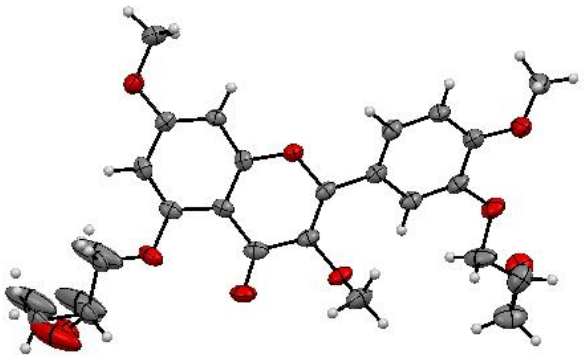

Figure S 6.33 X-ray structure of compound **5.2.**

Q/NMA/3%K54

- small piece of sample in oven
- 90 °C for 2 h, then varied heating time at 160 °C
- DSC T_g measurements (heating scan from 40-200 °C)
- 30 min: curing peak observed

0.5 h: T_g = 135 °C
1 h: T_g = 135 °C
2 h: T_g = 135 °C

Conclusion: Heating protocol of 2 h at 90 °C and 0.5 h at 160 °C.

Figure S 6.34 Optimization of curing values for **Q-NMA**.

DGEBA/NMA/3%K54

- small piece of sample in oven
- 90 °C for 1 h, then varied heating time at 160 °C
- DSC T_g measurements (heating scan from 40 °C-200 °C)
- 30 min: curing peak observed

1h: T_g = 129 °C
2h: T_g = 132 °C
3h: T_g = 133 °C
4h: T_g = 134 °C
5h: T_g = 133 °C

Conclusion: Heating protocol of 1 h at 90 °C and 2 h at 160 °C.

Figure S 6.35 Optimization of curing values for **DGEBA-NMA**.

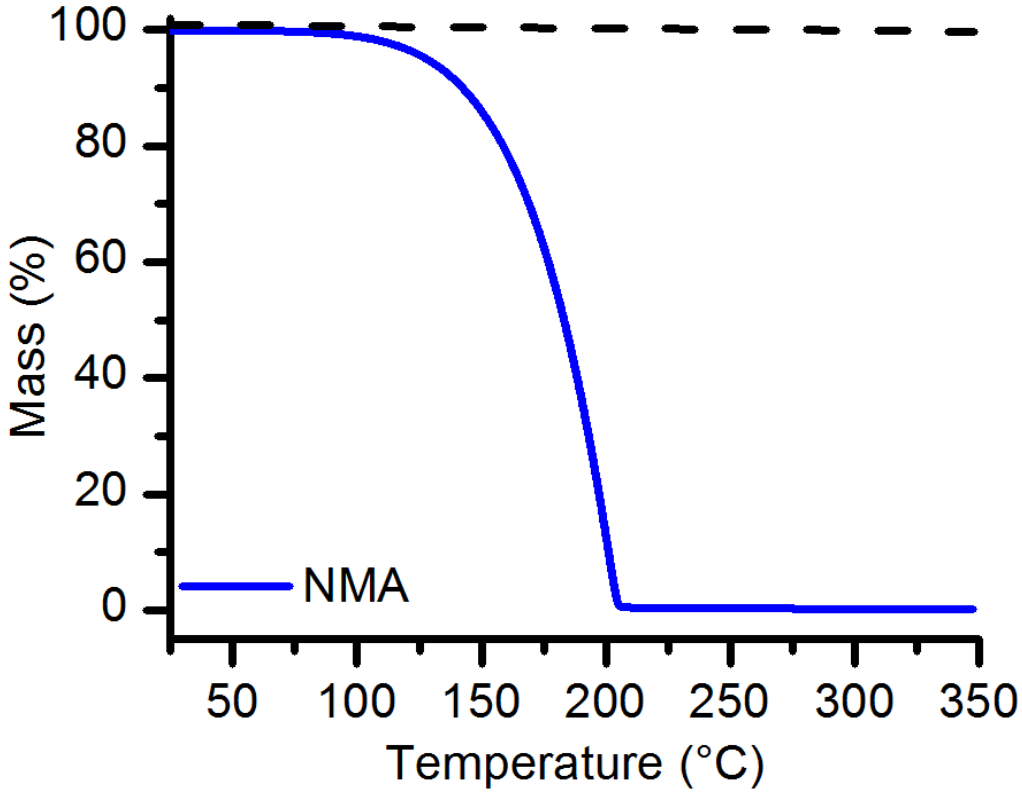

Figure S 6.36 TGA trace of **NMA** curing agent.

Figure S 6.37 Mass loss curing experiment.

Intial Mass (mg)	Mass after Mixing (mg)	Mass loss (%)
1.85006	1.83774	0.66592
1.83177	1.82016	0.63381
1.77562	1.76650	0.51362
1.80090	1.79130	0.53307
1.77303	1.76188	0.62887

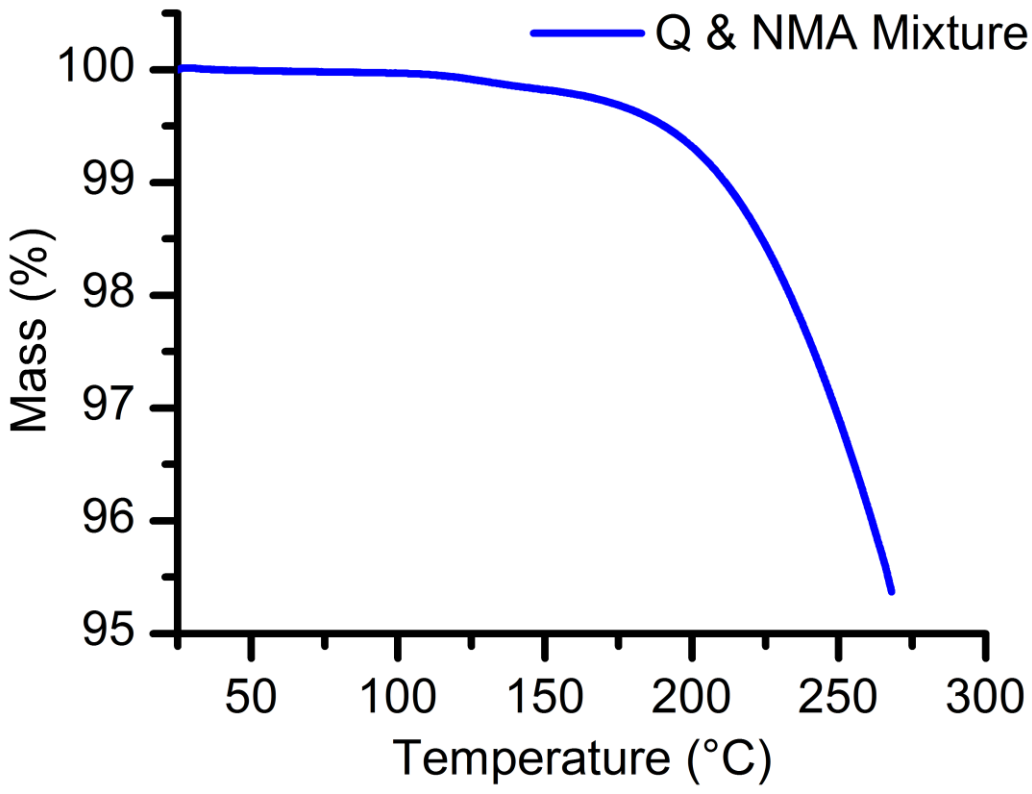

Figure S 6.38 TGA trace of the monomer and NMA after mixing at 160 °C.

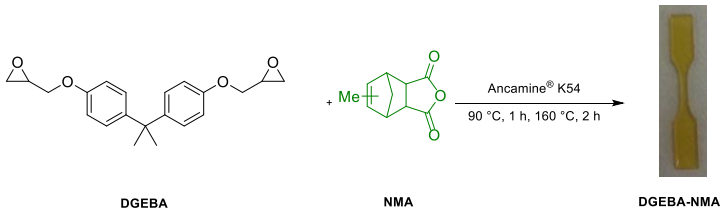

Scheme S 5.1 Synthesis of **DGEBA-NMA.**

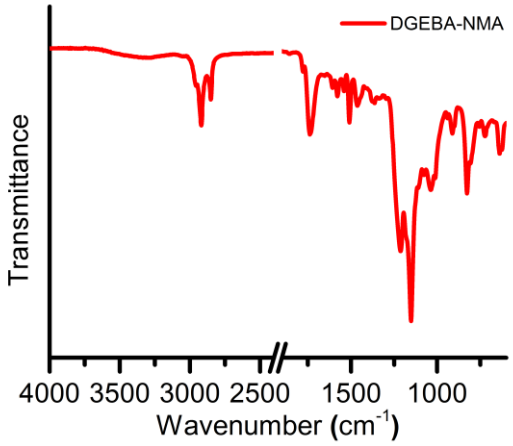

Figure S 6.39 IR spectrum of **DGEBA-NMA**.

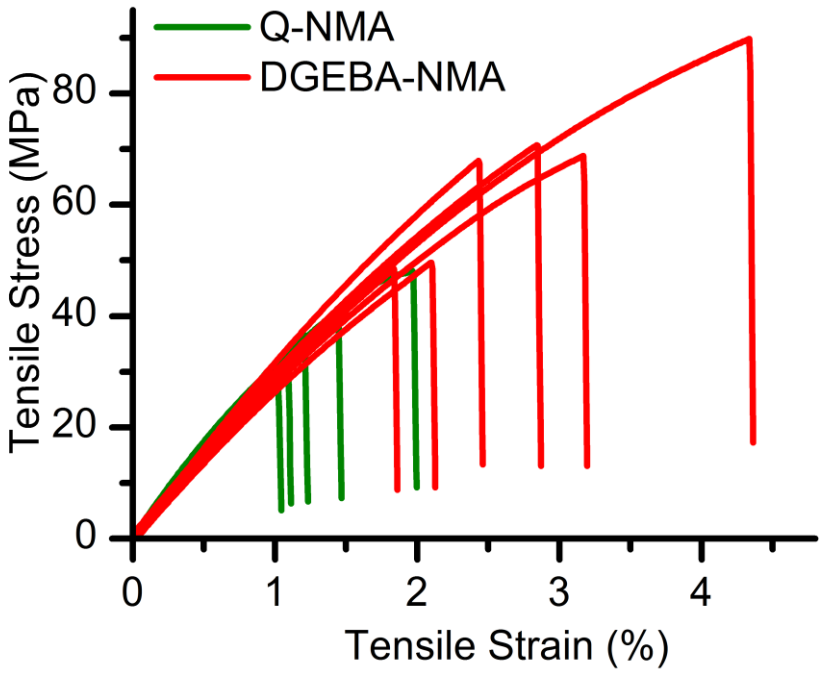

Figure S 6.40 Strain-to-failure data for each run of **Q-NMA** and **DGEBA-NMA**.

Figure S 6.41 Raw strain-to-failure data for **Q-NMA**.

	1	2	3	4	5	Mean	S.D.
Thickness (mm)	2.16	2.11	1.85	2.11	1.94	2.03	0.13
Width (mm)	3.18	3.18	3.18	3.18	3.18	3.18	0
Area Under curve (N/m)	8,010	5,990	14,380	4,880	3,890	7,400	4100
Modulus (Secant 1 %) (MPa)	3,010	3,140	3,110	3,140	2,720	3,000	200
Modulus (MPa)	3,330	3,560	3,640	3,670	3,340	3,500	200
Elongation at Break (%)	1.44	1.21	1.97	1.09	1.02	1.35	0.39
Tensile Strength at Break (MPa)	40.4	36.6	48.1	33.7	27.7	37	8
Elongation at Yield (%)	1.44	1.21	1.97	1.09	1.02	1.35	0.38
Tensile Strength at Yield (MPa)	40.4	36.6	48.1	33.7	27.7	37	8
Tensile Strength (MP)	40.4	36.6	48.1	33.7	27.7	37	8

Figure S 6.42 Raw strain-to-failure data for **DGEBA-NMA**.

	1	2	3	4	5	6	Mean	S.D.
Thickness (mm)	1.73	1.89	1.74	1.72	1.73	1.93	1.79	0.09
Width (mm)	3.18	3.18	3.18	3.18	3.18	3.18	3.18	0
Area under curve (N/m)	31,390	28,170	22,520	58,040	12,070	14,090	27,700	16,700
Modulus (Secant 1 %) (MPa)	2,770	2,990	3,160	2,910	2,870	2,640	2,90	200
Modulus (MPa)	2,940	3,090	3,380	2,920	3,020	2,870	3,000	200
Elongation at Break (%)	3.17	2.84	2.43	4.34	1.84	2.1	2.78	0.90
Tensile Strength at Break (MPa)	68.8	70.7	67.9	89.8	48.5	49.6	66	15
Elongation at Yield (%)	3.17	2.84	2.43	4.34	1.84	2.10	2.78	0.90
Tensile Strength at Yield (MPa)	68.8	70.7	67.9	89.8	48.5	49.6	66	15
Tensile Strength (MPa)	68.8	70.7	67.9	89.8	48.5	49.6	66	15

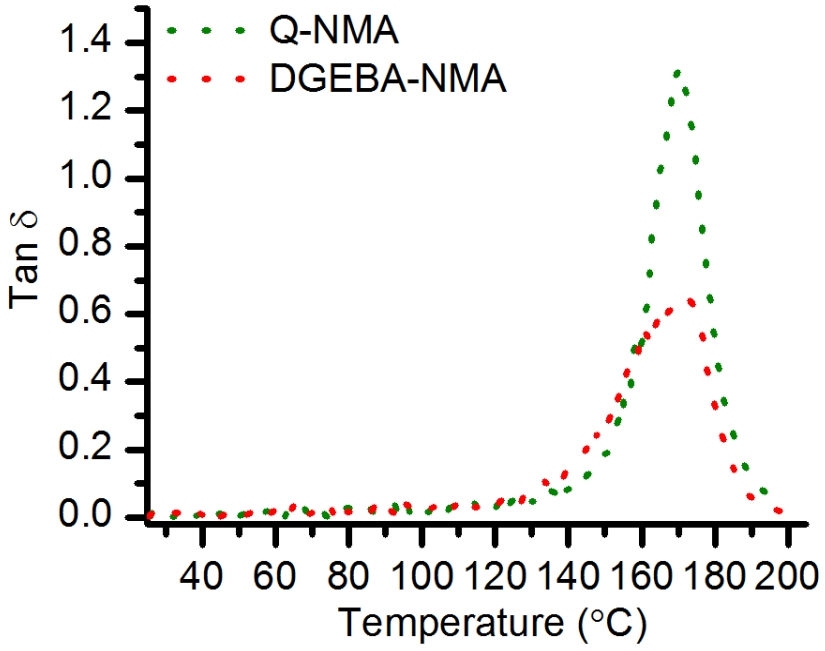

Figure S 6.43 Tan δ curve for **Q-NMA** and **DGEBA-NMA**.

Crystal and Molecular Structure Determination for **5.1**.

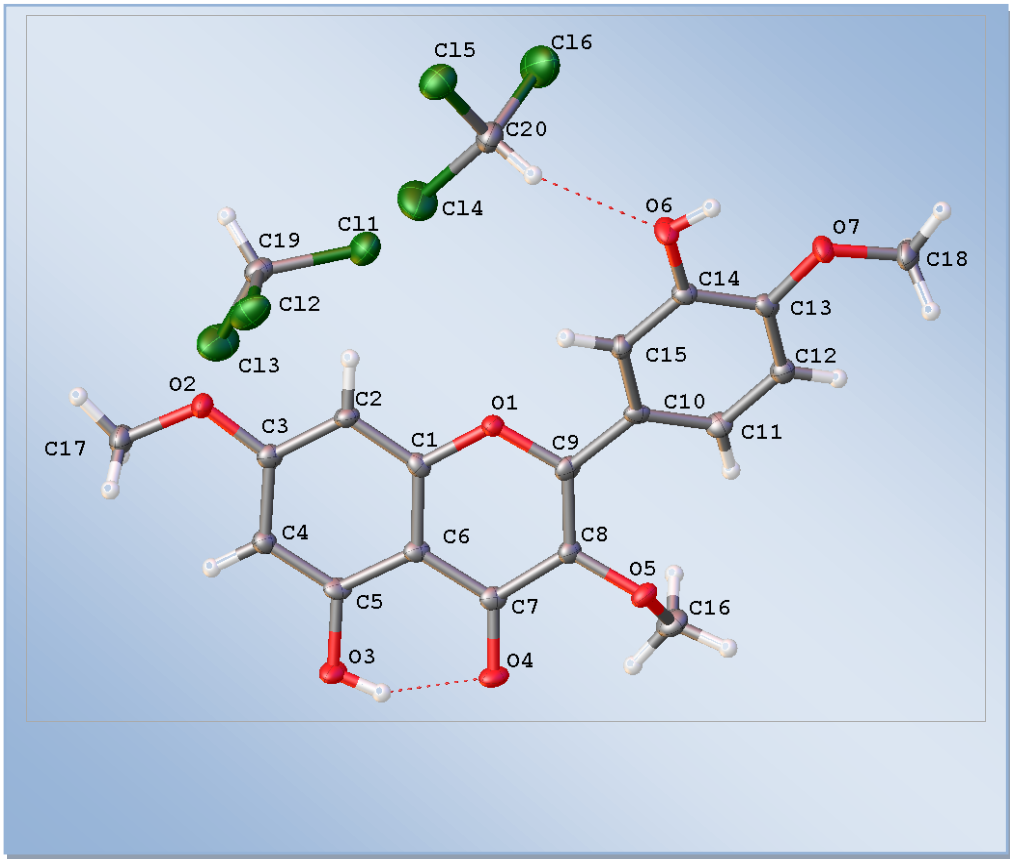

Experimental

A single crystal of $C_{20}H_{18}Cl_6O_7$ was selected and mounted on a **Bruker_GADDS** diffractometer. The crystal was kept at 110.0 K during data collection. Using Olex2[1], the structure was solved with the XT[2] structure solution program using Direct Methods and refined with the ShelXL [2] refinement package using Least Squares minimization.

O.V. Dolomanov, L.J. Bourhis, R.J. Gildea, J.A.K. Howard, and H. Puschmn, *J. Appl. Cryst*. **2009**, *42*, 339-341.

G.M. Sheldrick, *Acta Cryst.* **2008**, *A64*, 112-122.

Crystal structure determination of **5.1**

Crystal Data for $C_{20}H_{18}Cl_6O_7$ (*M* =583.04): monoclinic, space group C2/c (no. 15), *a* = 22.298(4) Å, *b* = 9.7054(19) Å, *c* = 22.247(4) Å, *β* = 90.166(11)°, *V* = 4814.4(15) $Å^3$, *Z* = 8, *T* = 110.0 K, μ(CuKα) = 6.876 mm^{-1}, *Dcalc* = 1.609 g/mm^3, 48647 reflections measured ($7.93 \leq 2\Theta \leq 128.912$), 3982 unique ($R_{int}$ = 0.0807, R_{sigma} = 0.0305) which were used in all calculations. The final R_1 was 0.0488 ($I > 2\sigma(I)$) and wR_2 was 0.1374 (all data).

Table S 6.3 Crystal data and structure refinement for **5.1**

Identification code	**5.1**
Empirical formula	$C_{20}H_{18}Cl_6O_7$
Formula weight	583.04
Temperature/K	110.0
Crystal system	monoclinic
Space group	C2/c
a/Å	22.298(4)
b/Å	9.7054(19)
c/Å	22.247(4)
α/°	90
β/°	90.166(11)
γ/°	90
Volume/Å^3	4814.4(15)
Z	8
ρ_{calc}mg/mm^3	1.609
m/mm^{-1}	6.876
F(000)	2368.0
Crystal size/mm^3	0.7 × 0.1 × 0.06
Radiation	CuKα (λ = 1.54178)
2Θ range for data collection	7.93 to 128.912°
Index ranges	$-25 \leq h \leq 25$, $-10 \leq k \leq 11$, $-25 \leq l \leq 25$
Reflections collected	48647
Independent reflections	3982 [R_{int} = 0.0807, R_{sigma} = 0.0305]
Data/restraints/parameters	3982/0/304
Goodness-of-fit on F^2	1.130
Final R indexes [I>=2σ (I)]	R_1 = 0.0488, wR_2 = 0.1280
Final R indexes [all data]	R_1 = 0.0540, wR_2 = 0.1374
Largest diff. peak/hole / e Å^{-3}	0.56/-0.67

Table S 6.4 Fractional atomic coordinates (×104) and equivalent isotropic displacement parameters (Å2×103) for **2.1** Ueq is defined as 1/3 of the trace of the orthogonalised UIJ tensor.

Atom	*x*	*y*	*z*	U(eq)
O1	2833.5(7)	91.9(19)	220.5(7)	14.5(4)
O2	2170.5(8)	-3092.7(19)	1634.5(8)	18.6(4)
O3	1027.1(8)	-2421(2)	-167.2(8)	22.2(5)
O4	1435.5(8)	-647(2)	-920.5(8)	20.2(4)
O5	2316.2(8)	1226.8(19)	-1246.4(8)	16.9(4)
O6	4896.4(8)	1601(2)	84.1(9)	23.1(5)
O7	4906.8(8)	3898.6(19)	-574.9(8)	19.5(4)
C1	2407.6(11)	-843(3)	384.8(12)	14.5(6)
C2	2486.1(11)	-1502(3)	925.9(11)	15.8(5)
C3	2058.8(11)	-2472(3)	1100.8(11)	15.9(6)
C4	1559.1(11)	-2773(3)	739.1(11)	15.9(6)
C5	1497.2(11)	-2107(3)	196.0(11)	15.5(6)
C6	1917.2(11)	-1106(3)	6.8(11)	14.5(6)
C7	1859.2(11)	-398(3)	-558.9(11)	14.7(6)
C8	2323.6(11)	593(3)	-694.5(11)	14.0(5)
C9	2795.4(11)	794(3)	-313.5(11)	15.0(5)
C10	3328.5(11)	1660(3)	-401.7(11)	14.3(5)
C11	3322.9(11)	2844(3)	-751.5(12)	16.5(6)
C12	3838.8(11)	3637(3)	-815.6(12)	16.4(6)
C13	4367.7(11)	3238(3)	-536.5(11)	16.4(6)
C14	4379.6(11)	2039(3)	-184.4(11)	15.3(5)
C15	3867.3(11)	1260(3)	-115.4(11)	15.2(5)
C16	1841.1(12)	2228(3)	-1324.9(13)	22.8(6)
C17	1723.2(12)	-4014(3)	1866.6(13)	23.1(6)
C18	4925.7(12)	5159(3)	-910.1(13)	22.9(6)
Cl1	1755.1(3)	2569.2(8)	2371.5(3)	32.2(2)
Cl2	1850.4(4)	-380.1(8)	2268.7(3)	35.6(3)
Cl3	737.6(3)	857.7(11)	2657.8(4)	45.8(3)
C19	1527.4(12)	985(3)	2674.9(12)	21.4(6)
Cl4	4079.9(4)	-457.1(11)	1499.1(4)	49.9(3)
Cl5	5341.4(3)	-939.3(8)	1703.0(3)	33.6(3)
Cl6	4882.1(5)	1841.1(9)	1670.2(4)	48.4(3)

C20	4811.6(13)	171(3)	1376.6(13)	27.3(7)

Table S 6.5 Anisotropic displacement parameters ($Å^2 \times 10^3$) for **2.1**. The anisotropic displacement factor exponent takes the form: $-2\pi^2[h^2a^{*2}U_{11}+2hka^*b^*U_{12}+\ldots]$.

Atom	U_{11}	U_{22}	U_{33}	U_{23}	U_{13}	U_{12}
O1	11.3(9)	19.8(10)	12.3(9)	1.4(7)	-0.4(7)	-3.5(7)
O2	17.1(9)	24.6(11)	13.9(9)	5.4(8)	-1.5(7)	-5.2(7)
O3	12.5(9)	36.1(12)	18(1)	6.3(8)	-4.4(7)	-7.7(8)
O4	11.6(9)	34.7(12)	14.2(10)	1.0(8)	-3.6(7)	-3.2(8)
O5	14.4(9)	24.6(11)	11.8(9)	3.2(7)	-1.1(7)	1.1(7)
O6	11.4(9)	30.3(12)	27.5(11)	11.9(9)	-5.0(8)	-6.1(8)
O7	13.7(9)	21.2(11)	23.6(10)	7.3(8)	-0.8(7)	-6.3(7)
C1	10.3(12)	16.0(14)	17.2(13)	-2.2(10)	3.3(10)	-0.9(10)
C2	13.2(12)	22.3(14)	11.9(12)	-1.1(10)	-2.2(9)	-1.4(10)
C3	12.5(12)	22.5(15)	12.8(13)	-2(1)	2.2(10)	0.3(10)
C4	12.0(12)	20.6(14)	15.1(13)	-0.5(10)	1.6(10)	-1.9(10)
C5	7.3(11)	23.1(15)	16.0(13)	-2.9(11)	0.5(9)	0.1(10)
C6	8.6(12)	22.3(15)	12.6(13)	-2.3(10)	1.5(9)	0.8(10)
C7	10.4(12)	21.1(15)	12.4(12)	-2.7(10)	2.3(9)	2.1(10)
C8	12.7(12)	17.6(14)	11.9(12)	0.3(10)	1.6(9)	-0.6(10)
C9	14.3(13)	20.0(14)	10.7(12)	-1.3(10)	2.9(9)	1.6(10)
C10	12.3(12)	19.7(14)	10.8(12)	-4.1(10)	0.2(9)	-1(1)
C11	12.7(12)	19.9(15)	16.9(13)	-0.5(10)	-1.3(10)	2.9(10)
C12	17.1(13)	16.8(14)	15.4(13)	0.7(10)	0.5(10)	0.4(10)
C13	12.6(12)	23.1(15)	13.6(12)	-2.1(10)	1.6(9)	-3.3(10)
C14	12.3(12)	19.1(14)	14.5(13)	-0.7(10)	-0.3(9)	-0.8(10)
C15	14.2(13)	17.8(14)	13.5(12)	2.4(10)	-0.2(10)	-0.5(10)
C16	19.8(14)	27.6(16)	20.9(14)	3.3(12)	-4.9(11)	5.3(11)
C17	20.3(14)	29.1(17)	19.8(15)	6.6(12)	1.8(11)	-4.8(11)
C18	18.3(14)	27.7(16)	22.7(15)	7.6(12)	2.0(11)	-5.7(11)
Cl1	36.6(4)	32.2(5)	27.8(4)	6.3(3)	-4.9(3)	-1.1(3)
Cl2	47.3(5)	34.2(5)	25.3(4)	-6.4(3)	-3.4(3)	12.0(3)
Cl3	19.7(4)	79.1(7)	38.5(5)	4.7(4)	0.5(3)	-6.4(4)
C19	18.0(14)	30.4(17)	15.9(14)	0.4(11)	-0.6(11)	0.4(11)
Cl4	24.3(4)	67.5(7)	57.9(6)	16.0(5)	-8.1(4)	-11.5(4)
Cl5	27.9(4)	41.4(5)	31.3(4)	2.3(3)	-0.8(3)	6.4(3)
Cl6	66.3(6)	32.1(5)	46.7(6)	3.8(4)	-8.9(4)	0.7(4)
C20	26.9(16)	32.3(18)	22.8(15)	7.4(13)	-2.1(12)	-4.6(13)

Table S 6.6 Bond lengths for **5.1**.

Atom	Atom	Length/Å
O1	C1	1.364(3)
O1	C9	1.372(3)
O2	C3	1.354(3)
O2	C17	1.437(3)
O3	C5	1.356(3)
O4	C7	1.262(3)
O5	C8	1.373(3)
O5	C16	1.448(3)
O6	C14	1.364(3)
O7	C13	1.365(3)
O7	C18	1.433(3)
C1	C2	1.374(4)
C1	C6	1.401(4)
C2	C3	1.396(4)
C3	C4	1.403(4)
C4	C5	1.377(4)
C5	C6	1.414(4)
C6	C7	1.439(4)
C7	C8	1.446(4)
C8	C9	1.363(4)
C9	C10	1.469(4)
C10	C11	1.388(4)
C10	C15	1.413(4)
C11	C12	1.392(4)
C12	C13	1.386(4)
C13	C14	1.403(4)
C14	C15	1.379(4)
Cl1	C19	1.755(3)
Cl2	C19	1.759(3)
Cl3	C19	1.766(3)
Cl4	C20	1.764(3)
Cl5	C20	1.755(3)
Cl6	C20	1.754(3)

Table S 6.7 Bond angles for **5.1**.

Atom	Atom	Atom	Angle/°
C1	O1	C9	121.4(2)
C3	O2	C17	117.8(2)
C8	O5	C16	114.54(19)
C13	O7	C18	117.4(2)
O1	C1	C2	117.2(2)
O1	C1	C6	120.2(2)
C2	C1	C6	122.6(2)
C1	C2	C3	118.2(2)
O2	C3	C2	114.9(2)
O2	C3	C4	123.7(2)
C2	C3	C4	121.5(2)
C5	C4	C3	118.9(2)
O3	C5	C4	119.5(2)
O3	C5	C6	119.2(2)
C4	C5	C6	121.3(2)
C1	C6	C5	117.6(2)
C1	C6	C7	120.4(2)
C5	C6	C7	122.0(2)
O4	C7	C6	122.1(2)
O4	C7	C8	122.0(2)
C6	C7	C8	115.9(2)
O5	C8	C7	118.5(2)
C9	C8	O5	119.9(2)
C9	C8	C7	121.2(2)
O1	C9	C10	110.6(2)
C8	C9	O1	120.8(2)
C8	C9	C10	128.5(2)
C11	C10	C9	122.8(2)
C11	C10	C15	119.1(2)
C15	C10	C9	118.1(2)
C10	C11	C12	120.6(2)
C13	C12	C11	120.1(2)
O7	C13	C12	126.1(2)
O7	C13	C14	114.1(2)
C12	C13	C14	119.8(2)
O6	C14	C13	121.2(2)
O6	C14	C15	118.6(2)
C15	C14	C13	120.2(2)
C14	C15	C10	120.2(2)
Cl1	C19	Cl2	110.06(15)
Cl1	C19	Cl3	110.06(16)

Cl2	C19	Cl3	110.24(16)
Cl5	C20	Cl4	110.22(17)
Cl5	C20	Cl6	110.72(16)
Cl6	C20	Cl4	110.12(18)

Table S 6.8 Hydrogen bonds for **5.1**.

D	H	A	d(D-H)/Å	d(H-A)/Å	d(D-A)/Å	D-H-A/°
O3	H3	O4	0.84	1.82	2.571(3)	148.6
O6	H6	O3[1]	0.84	1.96	2.753(2)	156.0
O6	H6	O7	0.84	2.22	2.669(3)	114.0
C20	H20	O6	1.00	2.32	3.199(3)	145.6

[1]1/2+X,1/2+Y,+Z

Table S 6.9 Torsion angles for **5.1.**

A	B	C	D	Angle/°
O1	C1	C2	C3	-179.4(2)
O1	C1	C6	C5	178.7(2)
O1	C1	C6	C7	0.3(4)
O1	C9	C10	C11	-153.9(2)
O1	C9	C10	C15	26.0(3)
O2	C3	C4	C5	-178.3(2)
O3	C5	C6	C1	-177.9(2)
O3	C5	C6	C7	0.5(4)
O4	C7	C8	O5	-3.3(4)
O4	C7	C8	C9	-176.4(2)
O5	C8	C9	O1	-175.1(2)
O5	C8	C9	C10	1.2(4)
O6	C14	C15	C10	-178.1(2)
O7	C13	C14	O6	-0.6(4)
O7	C13	C14	C15	-179.0(2)
C1	O1	C9	C8	1.0(4)
C1	O1	C9	C10	-176.0(2)
C1	C2	C3	O2	179.1(2)
C1	C2	C3	C4	-0.2(4)
C1	C6	C7	O4	177.3(2)
C1	C6	C7	C8	-1.3(4)
C2	C1	C6	C5	-0.9(4)
C2	C1	C6	C7	-179.3(2)
C2	C3	C4	C5	1.0(4)
C3	C4	C5	O3	177.8(2)
C3	C4	C5	C6	-1.7(4)
C4	C5	C6	C1	1.7(4)
C4	C5	C6	C7	-179.9(2)
C5	C6	C7	O4	-1.0(4)
C5	C6	C7	C8	-179.7(2)
C6	C1	C2	C3	0.2(4)
C6	C7	C8	O5	175.3(2)
C6	C7	C8	C9	2.2(4)
C7	C8	C9	O1	-2.1(4)
C7	C8	C9	C10	174.2(2)
C8	C9	C10	C11	29.4(4)
C8	C9	C10	C15	-150.7(3)

C9	O1	C1	C2	179.6(2)
C9	O1	C1	C6	0.0(4)
C9	C10	C11	C12	179.3(2)
C9	C10	C15	C14	-180.0(2)
C10	C11	C12	C13	1.0(4)
C11	C10	C15	C14	0.0(4)
C11	C12	C13	O7	178.2(2)
C11	C12	C13	C14	-0.6(4)
C12	C13	C14	O6	178.4(2)
C12	C13	C14	C15	-0.1(4)
C13	C14	C15	C10	0.4(4)
C15	C10	C11	C12	-0.6(4)
C16	O5	C8	C7	71.7(3)
C16	O5	C8	C9	-115.1(3)
C17	O2	C3	C2	174.7(2)
C17	O2	C3	C4	-6.0(4)
C18	O7	C13	C12	3.2(4)
C18	O7	C13	C14	-177.9(2)

Table S 6.10 Hydrogen atom coordinates (Å×104) and isotropic displacement parameters (Å2×103) for **5.1.**

Atom	*x*	*y*	*z*	**U(eq)**
H3	1045	-1943	-482	33
H6	5183	2100	-27	35
H2	2822	-1302	1174	19
H4	1268	-3426	867	19
H11	2964	3115	-949	20
H12	3829	4454	-1051	20
H15	3877	452	125	18
H16A	1888	2690	-1713	34
H16B	1861	2911	-1001	34
H16C	1452	1759	-1313	34
H17A	1656	-4765	1580	35
H17B	1348	-3509	1928	35
H17C	1861	-4396	2251	35
H18A	4810	4979	-1328	34
H18B	5333	5536	-898	34
H18C	4646	5824	-733	34
H19	1666	931	3102	26
H20	4885	209	934	33

Refinement model description
Number of restraints - 0, number of constraints - unknown.
Details:
1. Fixed Uiso
 At 1.2 times of:
  All C(H) groups
 At 1.5 times of:
  All C(H,H,H) groups, All O(H) groups
2.a Ternary CH refined with riding coordinates:
 C19(H19), C20(H20)
2.b Aromatic/amide H refined with riding coordinates:
 C2(H2), C4(H4), C11(H11), C12(H12), C15(H15)
2.c Idealised Me refined as rotating group:
 C16(H16A,H16B,H16C), C17(H17A,H17B,H17C), C18(H18A,H18B,H18C)
2.d Idealised tetrahedral OH refined as rotating group:
 O3(H3), O6(H6)

Crystal and Molecular Structure Determination for **5.2**.

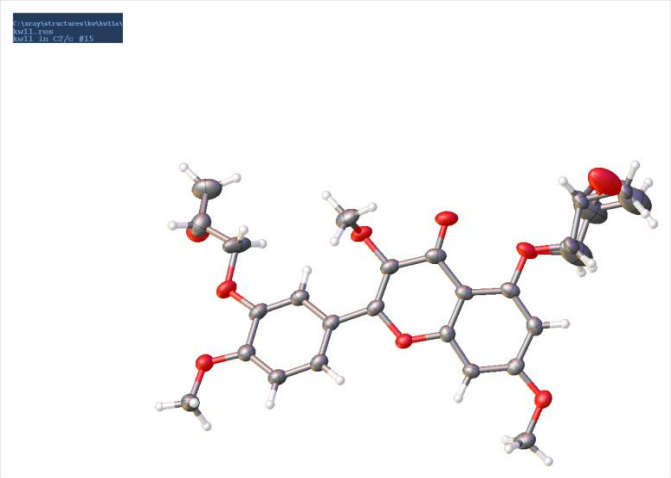

Note : The structure has a high r-value due to crystal quality and disorder. The connectivity is correct.

Data Collection

A Leica MZ 75 microscope was used to identify a suitable colorless multi-faceted crystal with very well defined faces with dimensions (max, intermediate, and min) 0.1 mm x 0.2 mm x 0.4 mm from a representative sample of crystals of the same habit. The crystal mounted on a nylon loop was then placed in a cold nitrogen stream maintained at 110 K.

An APEXII BRUKER X-ray (three-circle) diffractometer was employed for crystal screening, unit cell determination, and data collection. The goniometer was controlled using the APEX2 software suite[1]. The sample was optically centered with the aid of a video camera such that no translations were observed as the crystal was rotated through all positions. The detector was set at 6.0 cm from the crystal sample. The X-ray

radiation employed was generated from a Mo sealed X-ray tube (K_α = 0.70173Å with a potential of 40 kV and a current of 40 mA) fitted with a graphite monochromator in the parallel mode (175 mm collimator with 0.5 mm pinholes).

Sixty data frames were taken at widths of 0.5° with an exposure time of 30 seconds. These reflections were used in the auto-indexing procedure to determine the unit cell. A suitable cell was found and refined by nonlinear least squares and Bravais lattice procedures. The unit cell was verified by examination of the *h k l* overlays on several frames of data. No super-cell or erroneous reflections were observed.

After careful examination of the unit cell, a standard data collection procedure was initiated using omega scans. Each frame was exposed for 30 sec and contrasted against a 30 sec. dark current exposure.

Data Reduction, Structure Solution, and Refinement

Integrated intensity information for each reflection was obtained by reduction of the data frames with the program APEX2.[1] The integration method employed a three dimensional profiling algorithm and all data were corrected for Lorentz and polarization factors, as well as for crystal decay effects.[1] Finally the data was merged and scaled to produce a suitable data set. The absorption correction program SADABS[2] was employed to correct the data for absorption effects.

Systematic reflection conditions and statistical tests for the data suggested the space group *C2/c*. A solution was obtained readily using SHELXTL (SHELXT).[3] All non-hydrogen atoms were refined with anisotropic thermal parameters. The Hydrogen atoms bound to carbon were placed in idealized positions [C–H = 0.96 Å, U_{iso}(H) = 1.2

x U_{iso}(C)]. The structure was refined (weighted least squares refinement on F^2) to convergence.[3] OLEX-2 was employed for the final data presentation and structure plots.[4]

[1] APEX2 "Program for Data Collection on Area Detectors" BRUKER AXS Inc., 5465 East Cheryl Parkway, Madison, WI 53711-5373 USA

[2] SADABS, Sheldrick, G.M. "Program for Absorption Correction of Area Detector Frames", BRUKER AXS Inc., 5465 East Cheryl Parkway, Madison, WI 53711-5373 USA

[3] SHELXTL, G.M. Sheldrick, *Acta Cryst*. **2008**, *A64*, 112-122

[4] O.V. Dolomanov, L.J. Bourhis, R.J. Gildea, J.A.K. Howard and H. J. Puschmann, Appl. Cryst. 2009, 42, 339-341.

Table S 6.11 Crystal data and structure refinement for **5.2.**

Identification code	2
Empirical formula	$C_{24}H_{24}O_9$
Formula weight	456.43
Temperature/K	110
Crystal system	monoclinic
Space group	C2/c
a/Å	28.5129(13)
b/Å	10.6108(5)
c/Å	14.2365(7)
α/°	90
β/°	95.167(3)
γ/°	90
Volume/Å^3	4289.7(4)
Z	8
ρ_{calc}g/cm^3	1.413
μ/mm^{-1}	0.109
F(000)	1920.0
Crystal size/mm^3	0.421 × 0.188 × 0.096
Radiation	MoKα (λ = 0.71073)
2Θ range for data collection/°	4.098 to 49.998
Index ranges	$-33 \leq h \leq 33$, $-12 \leq k \leq 12$, $-16 \leq l \leq 16$
Reflections collected	33791
Independent reflections	3693 [R_{int} = 0.0427, R_{sigma} = 0.0213]
Data/restraints/parameters	3693/71/338
Goodness-of-fit on F^2	1.042
Final R indexes [I>=2σ (I)]	R_1 = 0.0992, wR_2 = 0.2380
Final R indexes [all data]	R_1 = 0.1105, wR_2 = 0.2493
Largest diff. peak/hole / e Å^{-3}	1.49/-0.68

Table S 6.12 Fractional atomic coordinates (×104) and equivalent isotropic displacement parameters (Å2×103) for **5.2**. Ueq is defined as 1/3 of the trace of the orthogonalised UIJ tensor.

Atom	*x*	*y*	*z*	U(eq)
O1	4618.4(10)	3806(3)	6082.0(19)	28.2(7)
O2	2832.2(11)	2025(3)	4016(2)	41.7(8)
O3	2374.2(13)	2945(4)	2068(2)	48.3(9)
O4	3043.0(11)	-115(3)	4810(2)	39.8(8)
O5	3573.3(10)	5661(3)	5466(2)	37.4(8)
O6	4208.0(12)	7474(3)	6005(2)	45.7(9)
O7	5127.6(13)	8079(3)	6379(2)	44.9(9)
O9	6226.3(10)	4775(3)	6764(2)	35.0(7)
C1	4159.8(14)	4117(4)	5806(3)	29.1(9)
C2	4027.2(15)	5351(4)	5776(3)	31.0(9)
C3	4353.7(16)	6391(4)	6009(3)	33.6(10)
C4	4843.3(15)	5999(4)	6232(3)	27.2(9)
C5	5231.7(16)	6831(4)	6422(3)	30.3(9)
C6	5676.6(16)	6385(4)	6618(3)	31.2(10)
C7	5768.5(14)	5084(4)	6613(3)	28.5(9)
C8	5403.4(14)	4249(4)	6455(3)	26.7(9)
C9	4952.6(14)	4717(4)	6262(3)	26.5(9)
C10	3871.5(14)	2998(4)	5584(3)	29.0(9)
C11	3478.1(14)	3068(4)	4910(3)	31.5(10)
C12	3217.0(14)	2029(5)	4667(3)	33.3(10)
C13	3334.0(15)	837(4)	5089(3)	32.9(10)
C14	3717.0(15)	778(4)	5757(3)	31.9(10)
C15	3984.7(15)	1836(4)	5994(3)	32.3(10)
C16	2662(2)	3259(6)	3714(4)	58.2(16)
C17	2262.1(19)	3134(6)	3022(4)	54.1(14)
C18	2152(2)	4099(6)	2320(4)	60.8(16)
C19	3129.2(18)	-1321(5)	5246(4)	44.8(12)
C20	3268.8(17)	5796(5)	6201(4)	46.5(12)
C24	6344.5(16)	3472(5)	6692(3)	39.2(11)
C21_1	5491(4)	8968(8)	6649(7)	41(2)
O8_1	5387(2)	10944(6)	5658(4)	47.9(18)
C22_1	5291(3)	10226(8)	6474(6)	41.9(18)

C23_1	5625(4)	11117(8)	6601(7)	42.3(19)
C21_2	5552(12)	8860(13)	6416(15)	128(6)
O8_2	5394(7)	11164(12)	6765(9)	128(6)
C22_2	5417(7)	10138(12)	6116(11)	129(6)
C23_2	5805(6)	10851(14)	6272(13)	131(6)

Table S 6.13 Anisotropic displacement parameters (Å2×103) for **5.2**. The anisotropic displacement factor exponent takes the form: -2π2[h2a*2U11+2hka*b*U12+…].

Atom	**U_{11}**	**U_{22}**	**U_{33}**	**U_{23}**	**U_{13}**	**U_{12}**
O1	26.8(14)	28.3(15)	29.4(15)	1.2(12)	2.0(11)	4.0(12)
O2	34.3(17)	50(2)	38.4(17)	1.9(15)	-11.7(13)	8.6(15)
O3	56(2)	60(2)	28.3(17)	4.4(15)	3.4(15)	2.9(18)
O4	34.8(17)	36.7(18)	45.8(19)	-4.3(14)	-8.8(14)	3.3(14)
O5	30.0(16)	47(2)	34.0(16)	7.7(14)	-2.2(13)	13.0(14)
O6	48(2)	34.8(18)	52(2)	0.4(16)	-8.3(16)	15.9(15)
O7	62(2)	22.8(16)	46(2)	-2.3(14)	-13.5(16)	3.1(15)
O9	28.8(15)	37.8(18)	38.5(17)	-2.0(14)	3.4(12)	-0.1(13)
C1	25(2)	40(2)	22.8(19)	3.8(17)	1.5(15)	4.9(18)
C2	30(2)	38(2)	25(2)	3.4(18)	0.2(16)	8.1(18)
C3	43(2)	34(2)	23(2)	1.1(17)	-1.2(17)	11(2)
C4	37(2)	25(2)	20.1(19)	-0.9(15)	1.4(16)	3.5(17)
C5	43(2)	26(2)	22(2)	3.0(16)	3.5(17)	3.8(18)
C6	39(2)	31(2)	23(2)	-1.3(17)	2.7(17)	-7.7(18)
C7	28(2)	37(2)	20.8(19)	-0.3(17)	5.0(15)	2.7(18)
C8	32(2)	25(2)	23.1(19)	-0.4(16)	3.3(16)	4.1(17)
C9	30(2)	29(2)	20.5(18)	-1.4(16)	2.0(15)	-2.6(17)
C10	26(2)	38(2)	23.0(19)	2.4(17)	2.8(16)	4.2(18)
C11	31(2)	36(2)	27(2)	7.2(18)	2.7(17)	5.5(18)
C12	25(2)	46(3)	27(2)	1.1(19)	-2.7(16)	7.0(19)
C13	30(2)	35(2)	34(2)	0.4(19)	2.2(17)	3.2(19)
C14	31(2)	34(2)	30(2)	3.2(18)	-0.6(17)	5.8(18)
C15	30(2)	41(3)	25(2)	2.7(18)	-1.8(16)	2.0(19)
C16	66(4)	59(4)	45(3)	-10(3)	-22(3)	30(3)
C17	43(3)	71(4)	48(3)	2(3)	1(2)	-2(3)
C18	74(4)	65(4)	44(3)	20(3)	6(3)	19(3)
C19	41(3)	32(3)	59(3)	1(2)	-8(2)	-1(2)

C20	34(2)	59(3)	47(3)	10(2)	8(2)	12(2)
C24	35(2)	43(3)	40(2)	2(2)	5.6(19)	10(2)
C21_1	52(4)	24(3)	43(4)	-10(3)	-15(3)	-6(3)
O8_1	64(3)	32(3)	46(3)	-7(2)	-5(2)	-6(2)
C22_1	56(3)	26(3)	41(3)	-12(2)	-6(2)	-4(2)
C23_1	57(3)	25(3)	43(3)	-14(2)	-4(3)	-3(2)
C21_2	246(16)	52(6)	68(7)	-32(5)	-76(8)	49(7)
O8_2	247(15)	51(6)	71(7)	-30(5)	-76(8)	51(7)
C22_2	248(15)	53(6)	71(7)	-31(5)	-75(8)	48(7)
C23_2	248(16)	56(6)	73(7)	-29(5)	-74(8)	47(7)

Table S 6.14 Bond lengths for **5.2.**

Atom	Atom	Length/Å
O1	C1	1.371(5)
O1	C9	1.365(5)
O2	C12	1.371(5)
O2	C16	1.448(6)
O3	C17	1.437(6)
O3	C18	1.438(7)
O4	C13	1.344(5)
O4	C19	1.433(6)
O5	C2	1.369(5)
O5	C20	1.426(6)
O6	C3	1.222(5)
O7	C5	1.358(5)
O7	C21_1	1.428(10)
O7	C21_2	1.46(3)
O9	C7	1.344(5)
O9	C24	1.429(6)
C1	C2	1.362(6)
C1	C10	1.462(6)
C2	C3	1.463(7)
C3	C4	1.464(6)
C4	C5	1.423(6)
C4	C9	1.395(6)
C5	C6	1.359(6)
C6	C7	1.405(6)
C7	C8	1.370(6)
C8	C9	1.382(6)
C10	C11	1.411(6)
C10	C15	1.389(6)
C11	C12	1.358(6)
C12	C13	1.427(6)
C13	C14	1.384(6)
C14	C15	1.382(6)
C16	C17	1.444(7)
C17	C18	1.445(8)
C21_1	C22_1	1.464(9)

O8_1	C22_1	1.436(9)
O8_1	C23_1	1.460(11)
C22_1	C23_1	1.343(11)
C21_2	C22_2	1.462(9)
O8_2	C22_2	1.434(10)
O8_2	C23_2	1.459(11)
C22_2	C23_2	1.341(11)

Table S 6.15 Bond angles for **5.2**.

Atom	**Atom**	**Atom**	**Angle/°**
C9	O1	C1	121.0(3)
C12	O2	C16	115.1(4)
C17	O3	C18	60.3(4)
C13	O4	C19	117.7(3)
C2	O5	C20	114.1(3)
C5	O7	C21_1	118.8(5)
C5	O7	C21_2	112.0(8)
C7	O9	C24	117.2(3)
O1	C1	C10	111.7(4)
C2	C1	O1	119.7(4)
C2	C1	C10	128.6(4)
O5	C2	C3	117.1(4)
C1	C2	O5	119.5(4)
C1	C2	C3	123.3(4)
O6	C3	C2	120.0(4)
O6	C3	C4	125.8(4)
C2	C3	C4	114.2(4)
C5	C4	C3	125.1(4)
C9	C4	C3	119.3(4)
C9	C4	C5	115.5(4)
O7	C5	C4	115.7(4)
O7	C5	C6	123.0(4)
C6	C5	C4	121.3(4)
C5	C6	C7	120.8(4)
O9	C7	C6	114.7(4)
O9	C7	C8	125.5(4)
C8	C7	C6	119.8(4)
C7	C8	C9	118.6(4)
O1	C9	C4	122.3(4)
O1	C9	C8	113.8(4)

C8	C9	C4	123.9(4)
C11	C10	C1	120.1(4)
C15	C10	C1	121.7(4)
C15	C10	C11	118.2(4)
C12	C11	C10	121.0(4)
O2	C12	C13	115.1(4)
C11	C12	O2	124.2(4)
C11	C12	C13	120.7(4)
O4	C13	C12	115.3(4)
O4	C13	C14	126.7(4)
C14	C13	C12	118.0(4)
C15	C14	C13	121.0(4)
C14	C15	C10	121.1(4)
C17	C16	O2	110.0(5)
O3	C17	C16	115.4(5)
O3	C17	C18	59.9(4)
C16	C17	C18	121.0(6)
O3	C18	C17	59.8(4)
O7	C21_1	C22_1	107.1(7)
C22_1	O8_1	C23_1	55.2(5)
O8_1	C22_1	C21_1	121.4(8)
C23_1	C22_1	C21_1	111.0(8)
C23_1	C22_1	O8_1	63.3(6)
C22_1	C23_1	O8_1	61.5(6)
C22_2	C21_2	O7	108.7(19)
C22_2	O8_2	C23_2	55.2(5)
O8_2	C22_2	C21_2	122.8(14)
C23_2	C22_2	C21_2	106.5(16)
C23_2	C22_2	O8_2	63.3(6)
C22_2	C23_2	O8_2	61.4(6)

Table S 6.16 Torsion angles for **5.2.**

A	B	C	D	Angle/°	A	B	C	D	Angle/°
O1	C1	C2	O5	177.6(3)	C5	C6	C7	O9	176.4(4)
O1	C1	C2	C3	1.2(6)	C5	C6	C7	C8	-3.1(6)
O1	C1	C10	C11	-150.8(4)	C6	C7	C8	C9	2.7(6)
O1	C1	C10	C15	26.5(5)	C7	C8	C9	O1	177.8(3)
O2	C12	C13	O4	-1.8(6)	C7	C8	C9	C4	-1.0(6)
O2	C12	C13	C14	-179.5(4)	C9	O1	C1	C2	-4.8(5)
O2	C16	C17	O3	-84.0(6)	C9	O1	C1	C10	175.7(3)
O2	C16	C17	C18	-152.7(5)	C9	C4	C5	O7	179.0(3)
O4	C13	C14	C15	-178.9(4)	C9	C4	C5	C6	0.0(6)
O5	C2	C3	O6	6.5(6)	C10	C1	C2	O5	-3.1(7)
O5	C2	C3	C4	-173.5(3)	C10	C1	C2	C3	-179.5(4)
O6	C3	C4	C5	-4.2(7)	C10	C11	C12	O2	-179.7(4)
O6	C3	C4	C9	176.2(4)	C10	C11	C12	C13	0.1(6)
O7	C5	C6	C7	-177.2(4)	C11	C10	C15	C14	-0.7(6)
O7	C21_1	C22_1	O8_1	-101.9(9)	C11	C12	C13	O4	178.4(4)
O7	C21_1	C22_1	C23_1	-172.6(9)	C11	C12	C13	C14	0.6(6)
O7	C21_2	C22_2	O8_2	104.0(16)	C12	O2	C16	C17	179.1(4)
O7	C21_2	C22_2	C23_2	172.5(14)	C12	C13	C14	C15	-1.4(6)
O9	C7	C8	C9	-176.7(4)	C13	C14	C15	C10	1.5(7)
C1	O1	C9	C4	4.0(5)	C15	C10	C11	C12	-0.1(6)
C1	O1	C9	C8	-174.8(3)	C16	O2	C12	C11	-10.8(6)
C1	C2	C3	O6	-177.0(4)	C16	O2	C12	C13	169.3(4)
C1	C2	C3	C4	3.0(6)	C16	C17	C18	O3	103.3(6)
C1	C10	C11	C12	177.3(4)	C18	O3	C17	C16	-112.5(7)
C1	C10	C15	C14	-178.1(4)	C19	O4	C13	C12	-176.9(4)
C2	C1	C10	C11	29.8(6)	C19	O4	C13	C14	0.6(7)
C2	C1	C10	C15	-152.9(4)	C20	O5	C2	C1	94.2(5)
C2	C3	C4	C5	175.8(4)	C20	O5	C2	C3	-89.2(5)
C2	C3	C4	C9	-3.7(5)	C24	O9	C7	C6	-175.0(3)
C3	C4	C5	O7	-0.6(6)	C24	O9	C7	C8	4.4(6)
C3	C4	C5	C6	-179.5(4)	C21_1	O7	C5	C4	174.1(6)
C3	C4	C9	O1	0.5(6)	C21_1	O7	C5	C6	-6.9(8)
C3	C4	C9	C8	179.2(4)	C21_1	C22_1	C23_1	O8_1	115.6(8)
C4	C5	C6	C7	1.7(6)	C23_1	O8_1	C22_1	C21_1	-99.3(9)
C5	O7	C21_1	C22_1	176.3(5)	C21_2	O7	C5	C4	-169.8(10)
C5	O7	C21_2	C22_2	164.9(11)	C21_2	O7	C5	C6	9.1(10)
C5	C4	C9	O1	-179.1(3)	C21_2	C22_2	C23_2	O8_2	-118.9(16)
C5	C4	C9	C8	-0.3(6)	C23_2	O8_2	C22_2	C21_2	93(2)

Table S 6.17 Hydrogen atom coordinates (Å×104) and isotropic displacement parameters (Å2×103) for **5.2**.

Atom	*x*	*y*	*z*	U(eq)
H6	5923	6948	6756	37
H8	5458	3385	6476	32
H11	3396	3838	4629	38
H14	3796	14	6052	38
H15	4245	1769	6434	39
H16A	2571	3730	4253	70
H16B	2911	3721	3444	70
H17	1994	2651	3218	65
H18A	1824	4223	2096	73
H18B	2342	4859	2358	73
H19A	2908	-1923	4966	67
H19B	3094	-1256	5909	67
H19C	3443	-1590	5156	67
H20A	2954	5966	5931	70
H20B	3376	6482	6605	70
H20C	3271	5032	6562	70
H24A	6223	3158	6085	59
H24B	6209	3006	7178	59
H24C	6681	3377	6763	59
H21A_1	5757	8841	6280	49
H21B_1	5598	8870	7311	49
H22_1	4992	10401	6738	50
H23A_1	5950	10840	6708	51
H23B_1	5551	11869	6945	51
H21A_2	5703	8876	7054	153
H21B_2	5772	8513	6004	153
H22_2	5237	10226	5500	155
H23A_2	5884	11410	5771	157
H23B_2	6074	10484	6639	157

Table S 6.18 Atomic occupancy for **5.2.**

Atom	*Occupancy*
C21_1	0.571(11)
O8_1	0.571(11)
C23_1	0.571(11)
C21_2	0.429(11)
O8_2	0.429(11)
C23_2	0.429(11)
H21A_1	0.571(11)
C22_1	0.571(11)
H23A_1	0.571(11)
H21A_2	0.429(11)
C22_2	0.429(11)
H23A_2	0.429(11)
H21B_1	0.571(11)
H22_1	0.571(11)
H23B_1	0.571(11)
H21B_2	0.429(11)
H22_2	0.429(11)
H23B_2	0.429(11)

Crystal structure determination of 5.2

Crystal Data for $C_{24}H_{24}O_9$ (M =456.43 g/mol): monoclinic, space group C2/c (no. 15), a = 28.5129(13) Å, b = 10.6108(5) Å, c = 14.2365(7) Å, β = 95.167(3)°, V = 4289.7(4) Å^3, Z = 8, T = 110 K, μ(MoKα) = 0.109 mm^{-1}, *Dcalc* = 1.413 g/cm^3, 33791 reflections measured (4.098° ≤ 2Θ ≤ 49.998°), 3693 unique (R_{int} = 0.0427, R_{sigma} = 0.0213) which were used in all calculations. The final R_1 was 0.0992 (I > 2σ(I)) and wR_2 was 0.2493 (all data).

Refinement model description

Number of restraints - 71, number of constraints - unknown.

Details:

1. Fixed Uiso

At 1.2 times of:

All C(H) groups, All C(H,H) groups

At 1.5 times of:

All C(H,H,H) groups

2. Rigid bond restraints

C21_1, O8_1, C22_1, C23_1
C21_2, O8_2, C22_2, C23_2
with sigma for 1-2 distances of 0.003 and sigma for 1-3 distances of 0.003
3. Uiso/Uaniso restraints and constraints
C21_1 ≈ O8_1 ≈ C22_1 ≈ C23_1 ≈ C21_2 ≈ O8_2 ≈ C22_2
≈ C23_2: within 1.7A with sigma of 0.003 and sigma for terminal atoms of
0.006
4. Same fragment restrains
[C21_2, O8_2, C22_2, C23_2]
as
[C21_1, O8_1, C22_1, C23_1] sigma for 1-2: 0.003 1-3: 0.04
5. Others

Sof(C21)=Sof(H21A)=Sof(H21B)=Sof(O8)=Sof(C22)=Sof(H22)=Sof(C23)=Sof(H23A)
=
Sof(H23B)=1-FVAR(1)

Sof(C21)=Sof(H21A)=Sof(H21B)=Sof(O8)=Sof(C22)=Sof(H22)=Sof(C23)=Sof(H23A)
=
Sof(H23B)=FVAR(1)
6.a Ternary CH refined with riding coordinates:
C17(H17), C22(H22), C22(H22)
6.b Secondary CH2 refined with riding coordinates:
C16(H16A,H16B), C18(H18A,H18B), C21(H21A,H21B), C23(H23A,H23B),
C21(H21A,
H21B), C23(H23A,H23B)
6.c Aromatic/amide H refined with riding coordinates:
C6(H6), C8(H8), C11(H11), C14(H14), C15(H15)
6.d Idealised Me refined as rotating group:
C19(H19A,H19B,H19C), C20(H20A,H20B,H20C), C24(H24A,H24B,H24C)